**Title**
Modeling the Acute Effects of Exercise on Insulin-Glucose Dynamics



**Author**
Frank, Spencer Troy

**Publication Date**
2017

Peer reviewed|Thesis/dissertation

**Modeling the Acute Effects of Exercise on Insulin-Glucose Dynamics**

by

Spencer Frank

A dissertation submitted in partial satisfaction of the

requirements for the degree of

Doctor of Philosophy

in

Engineering - Mechanical Engineering

in the

Graduate Division

of the

University of California, Berkeley

Committee in charge:

Professor Andrew Szeri, Chair
Professor Shawn Shadden
Professor Per-Olof Persson
Professor Dorian Liepmann

Fall 2017

**Modeling the Acute Effects of Exercise on Insulin-Glucose Dynamics**

## Abstract

Modeling the Acute Effects of Exercise on Insulin-Glucose Dynamics

by

Spencer Frank

Doctor of Philosophy in Engineering - Mechanical Engineering

University of California, Berkeley

Professor Andrew Szeri, Chair

Only four grams of glucose are present in an adult's blood stream at any moment in time. This amount of glucose can be burned up in only 10 minutes during exercise. To maintain glucose homeostasis, the human body has an outstanding control system that utilizes several hormones, mainly insulin. Unfortunately, in type 1 diabetes (T1D), this control system is faulty because the pancreas no longer secretes insulin. Those with T1D must manually dose and inject insulin to survive. Exercise drastically changes the needed insulin dose, and an overdose can be fatal. An artificial pancreas that can autonomously and safely adjust the insulin dose would greatly improve the lives of those with T1D.

This dissertation focuses on the development of a novel pharmacokinetics model of insulin-glucose dynamics that is specifically designed to include the effects of exercise. We model five primary glucoregulatory phenomena that are sensitive to exercise. To validate the model we compare predictions to data from four cohorts of human subjects studied during controlled clinical exercise trials. We also carry out several test cases to demonstrate the effects of exercise intensity and duration on blood glucose levels. The model provides insight into insulin dosing during exercise and can be used to improve model predictive control algorithms in the artificial pancreas.

To my family and my skateboard.

Mom and Dad, you supported me 100 %. My skateboard, you taught me perseverance.

# Contents

# List of Figures

# List of Tables

## Acknowledgments

I say, without reservation, that this work would not have been possible without the full endorsement and guidance of my Ph.D. adviser, Professor Andrew Szeri. Not only did he encourage my initial foray into the new territory that would become my dissertation project, but he also pushed me throughout the project to be patient and to focus on the learning, not the results. The additional tidbits of knowledge he provided will forever stay with me - "sushi should be served."

My labmates Abdulrahman Jbaily, Claire Funke, and Prashanth Selvaraj made the journey intellectually stimulating, fun, and frequently delicious. Lots of cake was involved. Without them our lab would have been just another grey and windowless room in Etcheverry Hall.

The mechanical engineering staff, specifically Yawo Akpawu, Shareena Samson, Donna Craig, and Isabel Blanco, make our department run smoothly. More importantly, they make all the students feel welcome and cared for, no matter the political or university climate.

My dissertation committee, Professors Shawn Shadden, Per-Olof Persson, and Dorian Liepmann, were a pleasure to work with. They provided insight and constructive criticism when needed, and were always kind and helpful. Also, Professor Morris taught me the importance of rigor (and non-dimensionalization) in research.

My collaborators at the Mayo Clinic, Dr. Ananda Basu, Dr. Rita Basu, Dr. Ling Hinshaw, and Dr. Matthew Johnson not only provided loads of high quality clinical data for use in model validation, but also provided helpful insight on research questions and grant applications. They also ensured that I was well-fed and well-trained during a visit to the Mayo Clinic in 2015.

Countless family and friends supported this journey. Most importantly, my Mom and Dad always gave me their ear whenever I was frustrated with research or needed to boast about a small achievement. An incomplete list of supportive friends/colleagues: Alison Garcia Kellar, Louis Malito, Vivek Mishra, Chris Warner, Rachael Hager, David Fernández-Gutiérrez, Shanti Corrigan, and Maribel Jaquez. And of course Ari had an enormous impact on everything that got me to the point of writing this acknowledgements section.

For financial acknowledgment: The National Science Foundation Graduate Research Fellowship (thanks Obama!), Berkeley Graduate Division Block Grant Award for Academic Excellence, and Graduate Student Instruction opportunities (ME 106, ME 167, ME 107, and E 296MA).

# Nomenclature

| | |
|---|---|
| $\bar{c}$ | average concentration of insulin in the interstitial fluid |
| $\check{\rho}$ | non-dimensional radial coordinate of cylindrical capillary |
| $\check{b}$ | non-dimensional concentration of insulin in the capillary domain |
| $\check{c}$ | non-dimensional concentration of insulin in the interstitial fluid domain |
| $\check{q}$ | non-dimensional wall flux |
| $\check{x}$ | non-dimensional axial coordinate of cylindrical capillary |
| $\dot{\mathcal{C}}_a$ | absorption mass flow rate by capillaries in the subcutaneous domain |
| $\dot{\mathcal{G}}_{cl}$ | glucose clearance mass flow rate from the circulatory system domain |
| $\dot{\mathcal{G}}_{in_d}$ | glucose mass flow returning to the CS from the SM delivering capillaries |
| $\dot{\mathcal{G}}_{in_d}$ | mass flow rate of glucose into the circulatory system domain from the delivering capillaries |
| $\dot{\mathcal{G}}_{in}$ | glucose mass flow into the circulatory system domain |
| $\dot{\mathcal{G}}_{out_d}$ | mass flow rate of glucose out of the circulatory system domain entering the delivering capillaries |
| $\dot{\mathcal{G}}_{out}$ | glucose mass flow out of the circulatory system domain |
| $\dot{\mathcal{H}}_{cl}$ | clearance mass flow rate of glucose from the skeletal muscle domain |
| $\dot{\mathcal{H}}_d$ | delivery mass flow rate of glucose to skeletal muscle domain |
| $\dot{\mathcal{H}}_{in}$ | mass flow rate of glucose moving into the skeletal muscle domain |
| $\dot{\mathcal{H}}_{out}$ | mass flow rate of glucose moving out of the skeletal muscle domain |
| $\dot{\mathcal{I}}_{cl}$ | mass flow rate of insulin being cleared from the circulatory system by the liver and kidneys |

$\dot{\mathcal{I}}_{in}$ mass flow rate of insulin entering the circulatory system domain from the subcutaneous domain by convection

$\dot{\mathcal{I}}_{out}$ mass flow rate of insulin leaving the circulatory system domain to the skeletal muscle domain by convection

$\dot{\mathcal{S}}_d$ insulin delivery mass flow rate in skeletal muscle

$\dot{\mathcal{S}}_{cl}$ insulin mass flow rate due to clearance from the skeletal muscle domain

$\dot{m}$ mass flow rate

$\dot{m}_a$ absorption mass flow rate by capillaries

$\eta$ maximum exercise-action on endogenous glucose production

$\mathcal{C}$ mass of insulin in subcutaneous domain (a.k.a. insulin-on-board)

$\mathcal{G}$ mass of glucose in the circulatory system domain

$\mathcal{H}$ mass of glucose in the skeletal muscle domain

$\mathcal{I}$ mass of insulin in the circulatory system domain

$\mathcal{S}$ mass of insulin in the skeletal muscle domain

$\mathcal{U}$ insulin infusion rate into the subcutaneous domain

r metabolic clearance rate

$\mathrm{r}^I_{tot}$ total metabolic clearance rate of insulin

$\mathrm{r}^G$ glucose metabolic clearance rate

$\mathrm{r}^G_{SM_0}$ glucose uptake at zero insulin

$\mathrm{r}^G_{SM_{exr}}$ glucose uptake exercise sensitivity (proportionality factor between glucose uptake and exercise intensity)

$\mathrm{r}^G_{SM_{ins}}$ glucose uptake insulin sensitivity (proportionality factor between glucose uptake and insulin concentration)

$\mathrm{r}^I_{CS_N}$ normalized clearance rate of insulin from circulatory system domain

$\mathrm{r}^I_{CS}$ clearance rate of insulin from circulatory system domain

$\mathrm{r}^I_{SM_N}$ normalized clearance rate of insulin from skeletal muscle domain

$\mathrm{r}^I_{SM}$ clearance rate of insulin from skeletal muscle domain

| | |
|---|---|
| $\rho$ | radial coordinate of cylindrical capillary |
| $\tau_{EGP}$ | time-constant for endogenous glucose production |
| $\tau_{liv}$ | time-constant for liver glucose uptake |
| $_N$ | normalized parameter |
| $A$ | area |
| $a$ | isotopic abundance |
| $a_N$ | isotopic abundance at natural level |
| $AR$ | aspect ratio |
| $b$ | concentration of insulin in a capillary |
| $c$ | concentration of insulin in the subcutaneous domain interstitial fluid |
| $D_b$ | diffusion coefficient of insulin in blood |
| $D_g$ | diffusion coefficient of glucose in blood |
| $E$ | exercise intensity |
| $e$ | isotopic enrichment |
| $e_{inf}$ | enrichment of infused tracer |
| $e_{meal}$ | enrichment of meal tracer |
| $ef$ | extraction fraction |
| $EGP$ | endogenous glucose production |
| $F$ | infusion rate of tracer |
| $F_{^3H}$ | Infusion rate of $G[^3H]$ |
| $G$ | glucose concentration in plasma |
| $G[^2H]$ | glucose molecule labeled with deuterium ($^2H$) |
| $G[^3H]$ | glucose molecule labeled with tritium ($^3H$) |
| $G[^{12}C]$ | glucose molecule labeled with carbon-12 ($^{12}C$) |
| $G[^{13}C]$ | glucose molecule labeled with carbon-13 ($^{13}C$) |

$G_b$ basal glucose concentration in plasma

$g_d$ concentration of glucose in a delivering capillary

$G_{nat_{EGP}}$ natural glucose from endogenous sources

$G_{nat_{meal}}$ natural glucose from the meal

$G_{Q_I}$ glucose concentration of isotopic species $I$ in tracee $Q$

$G_{q_I}$ glucose concentration of isotopic species $I$ in tracer $q$

$G_{Q_{II}}$ glucose concentration of isotopic species $II$ in tracee $Q$

$G_{q_{II}}$ glucose concentration of isotopic species $II$ in tracer $q$

$G_Q$ glucose concentration of tracee

$G_q$ glucose concentration of tracer

$GU$ glucose uptake

$H$ concentration of glucose in the interstitial fluid of the skeletal muscle domain

$H_{cell}$ glucose concentration inside of cell

$I$ insulin concentration in plasma

$I_b$ basal insulin concentration in plasma

$ICD$ intercapillary distance

$k_d^G$ rate of glucose delivery

$L$ exercise-action factor on endogenous glucose production

$L$ length of capillary

$M$ multiplicative factor for liver glucose uptake

$m$ mass of glucose in a system

$m_Q$ mass of tracee in a system

$m_q$ mass of tracer in a system

$m_{Q_I}$ mass of isotopic species $I$ in tracee $Q$

$m_{q_I}$ mass of isotopic species $I$ in tracer $q$

$m_{Q_{II}}$ mass of isotopic species $II$ in tracee $Q$

$m_{q_{II}}$ mass of isotopic species $II$ in tracer $q$

$P$ permeability of capillary

$p$ pool-fraction of volume of distribution of glucose

$P_{cell}$ permeability of the cell membrane to glucose

$PS$ capillary permeability surface area

$Pu_{inf}$ purity of infusate tracer

$Pu_{meal}$ purity of meal tracer

$Q$ tracee

$q$ tracer

$q$ wall flux

$Q_d$ tissue perfusion rate

$R$ radius of capillary

$r$ isotopic ratio

$r$ radial coordinate of the subcutaneous domain

$R_a$ rate of appearance

$R_d$ rate of disappearance

$R_{a_{exo}}$ rate of appearance of glucose from exogenous sources

$Ra_{meal}$ rate of meal appearance

$Ra_{tot}$ total rate of appearance of glucose from all sources

$RGU$ rate of glucose uptake

$RGU_{CS_{fix}}$ rate of glucose uptake 'fixed' constant uptake tissues

$RGU_{CS_{liv}}$ rate of glucose uptake by the liver

$RGU_{SM_{exr}}$ exercise-induced glucose uptake from skeletal muscle domain

$RGU_{SM_{ins}}$ insulin-dependent glucose uptake from skeletal muscle domain

$RGU_{SM_{TOT}}$ total glucose uptake from skeletal muscle domain

$S_G$ glucose effectiveness

$sa$ specific activity

$sa_{meal_{2T}}$ specific activity for tracing meal glucose in the dual tracer method

$sa_{tot_{2T}}$ specific activity for tracing total glucose in the dual tracer method

$SI$ insulin sensitivity

$t$ time

$ttr_{inf}$ tracer to tracee ratio in the infusate prior to infusion

$ttr_{meal}$ tracer to tracee ratio in the meal prior to ingestion

$U$ velocity of blood in capillary

$u$ insulin pump infusion rate per unit volume

$V$ volume of distribution

$V^G$ glucose volume of distribution

$V^I$ insulin volume of distribution

$V^I_{CS_N}$ normalized volume of distribution of insulin in the circulatory system domain

$V^I_{SM_N}$ normalized volume of distribution of insulin in the skeletal muscle domain

$V^{tiss}$ volume of tissue

$V^{tiss}_{SC}$ volume of subcutaneous tissue in the vicinity of the injection site

$V^I_{CS}$ volume of distribution of insulin in the circulatory system domain

$V^I_{SM}$ volume of distribution of insulin in the skeletal muscle domain

$w$ mass-fraction

$w_Q$ mass-fraction of tracee

$w_q$ mass-fraction of tracer

$X$ insulin action

$x$ axial coordinate of capillary

$z$ tracer to tracee ratio

$z_{EGP_{3T}}$ tracer to tracee ratio for tracing endogenous glucose in the triple tracer method

1-MX 1-methylxanthine

ADA American Diabetes Association

AP artificial pancreas

AR capillary aspect ratio

ATBF adipose tissue blood flow

BG blood glucose concentration

BVP boundary value problem

BW body weight

CGM continuous glucose monitor

CHO carbohydrate

CLC closed loop control

CO cardiac output

CS circulatory system

CSII continuous subcutaneous insulin infusion

DKA diabetic ketoacidosis

FSBG finger-stick blood glucose

GI gastrointestinal tract

GIM Glucose Insulin Model of Cobelli and Dalla Man

IOB insulin-on-board

ISF interstitial fluid

LBF leg blood flow

LGU leg glucose uptake

LHS left hand side of equation

MBV microvascular blood volume

MDI multiple daily injections

MMTT mixed-meal tolerance test

MPC model predictive control

ODE ordinary differential equation

OMM Oral Minimal Model of Bergman and Cobelli

PBPK physiology-based pharmacokinetics

PDE partial differential equation

Pe Péclet number in capillary

PKPD pharmacokinetic/pharmacodynamic

PT pump therapy

RBC red blood cell

RHS right hand side of equation

SA specific activity

SAP sensor-augmented pump therapy

SC subcutaneous tissue

SM skeletal muscle

T1D type 1 diabetes

T1DE cohort of type 1 diabetes with exercise

T1DR cohort of type 1 diabetes at rest

U units (of insulin)

$V0_{2_{max}}$ maximum volume of oxygen consumed per unit time

$V0_2$ volume of oxygen consumed per unit time

# Chapter 1

# Introduction to Type 1 Diabetes and Insulin-Glucose Dynamics

## Overview

Only four grams of glucose exist in an adult's blood stream at any moment in time. This amount of glucose can be burned up in only 10 minutes during exercise. To prevent glucose levels from falling too low, causing dizziness and fainting, the human body has an outstanding control system that utilizes several hormones to signal the liver to replenish the body with stored glucose in order to maintain glucose homeostasis. Unfortunately, in type 1 diabetes (T1D), this control system is faulty because the pancreas is damaged by an autoimmune response and it can no longer produce the most important regulatory hormone, insulin. Consequently, subjects with T1D must inject insulin to survive. Unfortunately, even with careful insulin dosing, glucose control is often erratic, causing adverse health effects. A panacea for persons with T1D would be a machine that can rigorously calculate the correct insulin dose and infuse it automatically. This machine is known as the *artificial pancreas*.

One of the great challenges in the development of the artificial pancreas is how the controller should respond to exercise [1, 2]. Exercise causes significant changes to insulin-glucose dynamics, seen schematically in Figure 1.1. These exercise-induced changes confound insulin-dosing because there is a significant time-lag associated with the control input - injected insulin. The ramifications are significant - if a dose is given prior to exercise, without accounting for the exercise-induced changes to insulin-glucose dynamics, the dose could be fatal. This makes safe dosing calculations a critical component of a robust and safe artificial pancreas.

**Dissertation Objective:** To include the acute effects of exercise in a model of insulin-glucose dynamics. This model will provide insight into insulin-dosing during exercise and can be used to inform model predictive control (MPC) algorithms for the artificial pancreas.

This introductory chapter gives the requisite background information for understanding the context, challenges, and contributions of the insulin-glucose modeling work that makes up

this dissertation. In Section 1.1 we will introduce the disease and provide information about disease demographics, treatment methods, and complications. Next, Section 1.2 explains the challenges of exercising with T1D. Then, Section 1.3 will go over some of the fundamental concepts that govern insulin-glucose dynamics. Section 1.4 will go over tracer methods for measuring glucose metabolism, which are important for obtaining model inputs. Next, Section 1.5 will summarize previous mathematical models that describe insulin-glucose dynamics. Finally, Section 1.6 will conclude by summarizing how the modeling work presented in this dissertation addresses the insulin dosing challenges associated with acute exercise.

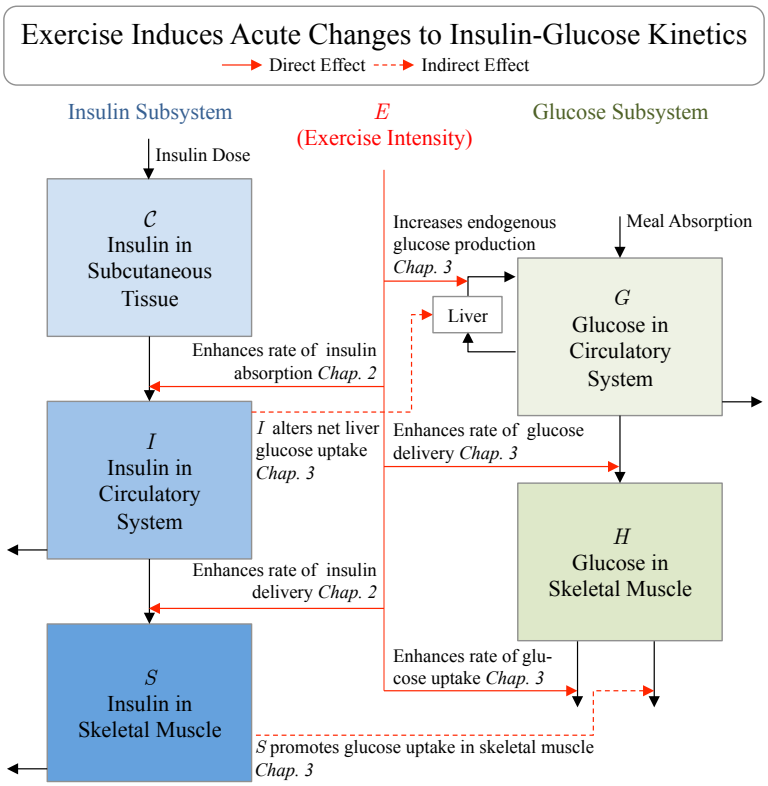


Figure 1.1: Block diagram showing the primary effects of exercise on insulin and glucose dynamics. The insulin subsystem model will be derived in Chapter 2 and the Glucose subsystem model will be derived in Chapter 3. Red arrows indicate the phenomena that are dependent on exercise intensity $E$.

## 1.1 Background on Type 1 Diabetes

Type 1 Diabetes (T1D) affects all segments of the population, the youth to the elderly and across all demographics and ethnicities. According to the Center for Disease Control (CDC)[3] and the Juvenile Diabetes Research Foundation (JDRF)[4]:

- 1.25 million Americans are living with T1D

- 40,000 people are diagnosed with T1D each year in the U.S.
- 5 million people in the U.S. are expected to have T1D by 2050.
- $14 billion T1D-associated annual healthcare costs in the U.S.
- T1D is associated with an estimate loss of life-expectancy of up to 13 years

Persons with T1D are characterized mainly by one thing - an inability of the pancreas to produce insulin. T1D is an autoimmune disease, meaning that the afflicted person's own immune system attacks the pancreas' insulin-producing beta cells. With functional beta cells almost completely destroyed within a year of diagnosis, a diabetic can no longer produce insulin. This is problematic because insulin is the hormone that allows the human body to utilize glucose. Without insulin, a person will slowly whither, losing all the fat on the body, and producing potentially fatal ketone toxicity known as diabetic ketoacidosis (DKA). To survive, persons with T1D must inject insulin to replace the insulin that would normally be produced by the pancreas.

Treatment of T1D revolves mainly around one thing - dosing insulin correctly. However, insulin dosing is multi-factorial. Persons with T1D often report insulin doses changing moderately day to day depending on stress levels [5], time of day [6, 7], activity levels [2, 8–11], food type, and even altitude (the author, who also struggles with T1D, recalls insulin requirement reduced by 50% on a day spent in the Sierra Nevada Mountains in Lake Tahoe, CA at 8000 ft elevation). The problem with dosing variability is that dosing incorrectly has very significant acute short term and long term health effects. These manifest themselves into three main groups of complications:

- Hypoglycemia - Hypoglycemia is an acute condition of low concentration of glucose in the blood, $< 70$ [mg/dL]. This condition typically occurs when a diabetic subject has injected too much insulin and as a result, the cells in the body absorb too much glucose from the blood, thereby reducing concentrations to levels too low for the body to operate normally. The condition can also result from high levels of physical exertion, where CHOs are burned more rapidly than they are replaced by endogenous glucose sources. Early warning signs of hypoglycemia are dizziness, shakiness, and cold sweats. Untreated hypoglycemia can lead to seizure and loss of consciousness. In rare extreme cases it can be fatal. If caught early, treating hypoglycemia is as easy as drinking a sugary beverage or eating glucose tablets. At later stages, a patient may lose consciousness and one of the only ways to raise glucose levels is by injection of the hormone glucagon, signaling the liver to release stored glucose and rapidly raise BG concentrations.
- Hyperglycemia - Hyperglycemia is the condition of high concentration of glucose in the blood, $> 190$ [mg/dL]. This conditions is common in people with diabetes and is typically caused by eating foods that contain high levels of carbohydrates (CHO) (sugars, starches) and not taking enough insulin to metabolize the ingested CHO. Chronic

hyperglycemia, if left untreated, can lead to many long term comorbidities such as kidney, neural, and cardiovascular complications[12]. In T1D patients, Hyperglycemia is treated by administering insulin.

- Diabetic Ketoacidosis (DKA) - Extreme hyperglycemia can lead to an acute life threatening condition called Diabetic Ketoacidosis. DKA is a serious complication that occurs when your body no longer produces enough insulin, and results in very high levels of blood acids called ketones. A lack of insulin causes this condition because without insulin many cells cannot absorb glucose to use as energy. Without the ability to utilize glucose, the body instead burns fat for fuel, of which ketones are a byproduct. If the fat burning rate is rapid enough the result is a high level of ketones in the blood, which can cause ketoacidosis. Symptoms of DKA are frequent urination, extreme thirst, weight loss, nausea, and fatigue. Untreated ketoacidosis can cause diabetic coma, which can be fatal [12]. Replacement of insulin is the only way to avoid and treat DKA.

### Glucose Variability

In principle, diabetes seems easy to treat - inject the right amount of insulin so that glucose can stay in normal ranges (euglycemia). This avoids hyperglycemia, DKA, and hypoglycemia. However, in practice, this is an extremely difficult task because (1) the acute effects of exercise on insulin-glucose dynamics and (2) the long time-lag of injected insulin. Any person with T1D can attest that controlling BG levels with insulin injections is extremely difficult, frustrating, and sometimes seems hopeless. To demonstrate the difficultly it is illustrative to look at BG levels for a non-diabetic and a person with T1D on insulin therapy. Figure 1.2 shows the typical BG levels over the course of a day.

The light red shading represents the hyperglycemic (>190 [mg/dL]) and the hypoglycemia(<70 [mg/dL]) regions. The green shading shows the safe region between 70 and 190 [mg/dL]. At first look, it is obvious that the T1D subject averages a much higher BG level than the nondiabetic subject. It is common for T1D subjects to average BG of 200 [mg/dL]. The average BG for a nondiabetic is around 100 [mg/dL].

Consider the individual glucose traces for each case. The BG of the nondiabetic subject (blue line) rises with the ingestion of breakfast at 7:00 AM, peaks around 250 [mg/dL], and then decreases quickly to the green region. Two more noticeable bumps can be seen for lunch and dinner, but these are short lived. At nighttime the BG levels are remarkably stable.

In comparison, the T1D subject (red line) has very large swings in BG throughout the day. The subject starts the day already in the red region at 200 [mg/dL]. Blood glucose continues to rise until about an hour after breakfast. This rise is a common occurrence in T1D subjects called the 'dawn phenomenon.' The day's first large bolus of insulin is given around 8:30 AM and kicks in at 9:00 AM, rapidly decreasing BG levels from 10:00 AM to 12:00 PM. Then, approaching hypoglycemia around noon, the subject ingests lunch, and the BG levels rise from 70 to 300 [mg/dL] in only one hour and then slowly reduce until settling around 180 [mg/dL]. Around 6:00 PM the subject eats dinner, resulting in a

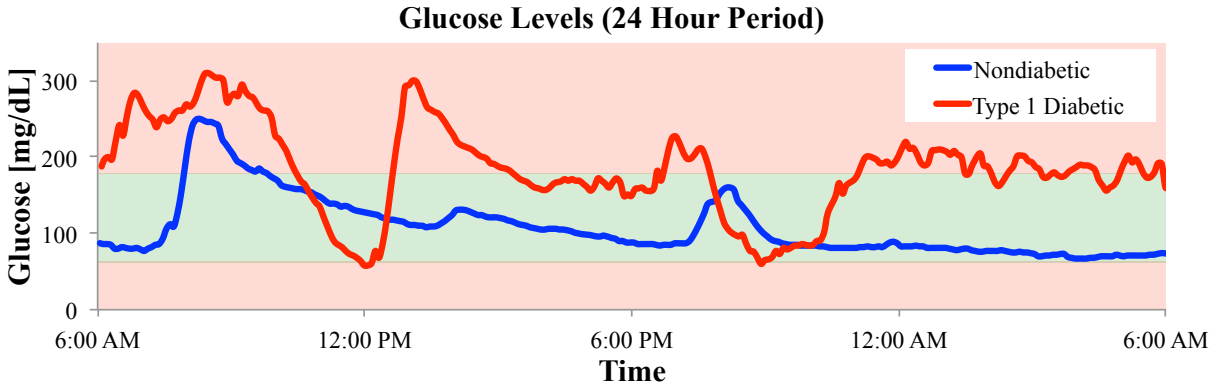


Figure 1.2: Comparison of blood glucose levels for a non-diabetic and diabetic subject. The BG of the nondiabetic subject (blue line) rises with the ingestion of breakfast at 7:00 AM, peaks around 250 [mg/dL], and then decreases quickly to the green region. Two more noticeable bumps can be seen for lunch and dinner, but these are short lived. In comparison, the T1D subject (red line), has very large swings in BG throughout the day, averaging 200 [mg/dL] and experiencing two mild hypoglycemia episodes at 12:00 PM and and 9:00 PM.

small spike up to 210 [mg/dL], followed by a rapid fall in BG from 7:00 PM to 9:00 PM, culminating in a mild hypoglycemic event with BG of 60 [mg/dL]. The subject then recovers from the hypoglycemic event with a small snack of CHO. Around 10:00 PM, the BG rapidly rises again, probably as a result of the glucose in the dinner becoming available 4 hours after ingestion (if the meal contained a high level of fat, this is not uncommon). The BG stabilizes at midnight at a high level of 200 [mg/dL] and the subject stays in the red range the remainder of the night.

The BG comparison paints a very unsettling picture for the diabetic subject. In one day there were two hypoglycemic events and the average BG level still ended up around 200 [mg/dL]. This level is far too high. If these high levels continue over many years complications such as neuropathy, retinopathy, kidney disease, and a host of other cardiovascular problems are imminent. This exemplifies the type of unpredictability that diabetic subjects must deal with on a daily basis. To prevent each day from looking like this, diabetics must eat right, dose insulin correctly, and exercise. Unfortunately, even the most diligent diabetics often have days like that depicted in Figure 1.2. It is for this reason that technology for improving treatment for type 1 diabetes continues to be a hot topic of research.

### Insulin Therapy

There are generally two methods of treatment for administering insulin: Multiple Daily Injection (MDI) therapy and continuous subcutaneous insulin infusion (CSII, a.k.a insulin-pump therapy (PT)).

With MDI therapy, the subject often administers several doses of insulin daily through

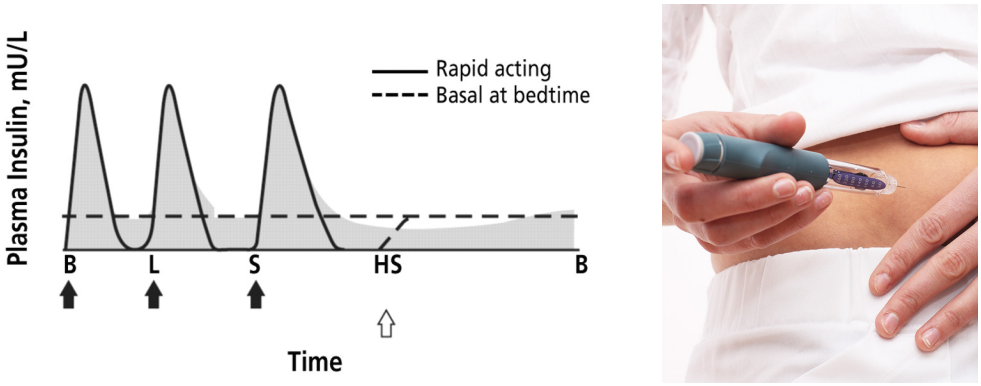


Figure 1.3: (left) Typical insulin concentration profile that results from multiple daily injections. Ideally, four doses would be given per day: one for breakfast (B), one for lunch (L), one for supper (S) and one long acting insulin dose given at bedtime (HS, *Hora Somni*) to provide basal insulin. Adapted from [13], without permission. (right) Typical pen injection. From [14], used without permission

subcutaneous injections. Usually a patient administers an additional dose of long acting insulin once a day that lasts for 24 hours. This long-acting insulin provides a background or *basal* level of insulin that ideally keeps a subject at a stable euglycemic glucose level during fasting conditions. Euglycemic means at a normal level of glucose, generally about 90-100 [mg/dL].

On top of *basal* insulin, the subject administers a rapid-acting *bolus* of insulin to metabolize the glucose contained in a meals and snacks. The combination of the *basal* and *bolus* injections typically results in insulin concentrations like those shown in Figure 1.3. Note that the insulin concentration depicted is highly idealized, and correction insulin doses are frequently given between meals to bring glucose levels closer to normal. *It is not uncommon for T1D subjects to administer a total of 8-10 injections per day.*

The other popular treatment methodology is continuous subcutaneous insulin infusion (CSII, a.k.a pump therapy (PT)). PT involves wearing an insulin pump 24 hours a day so that insulin can be continuously infused. However, PT still requires the patient to make all dosing decisions, and is not automated. PT insulin is infused in the subcutaneous tissue through an 'infusion set' that typically lasts three days.

One advantage of existing PT is that only one type of insulin is infused, rapid-acting insulin. Small background infusion rates provide the *basal* insulin. Then at mealtime, the user informs the pump of the number of CHO being ingested and the pump suggests an insulin bolus based on simple calculations. After confirming the calculations the user directs the pump to infuse the insulin. A typical daily pump infusion profile is shown in Figure 1.4.

Certain pump features are available that allow the user more freedom in the way the insulin is infused. For example all the insulin does not need to be given given upfront at mealtime, it can be spread out over a longer 'extended wave' (Figure 1.4), where part of the insulin is given at meal time and part is given a few hours later. This gives the user more freedom to change the infusion profiles for different types of meals. For example, pizza, due

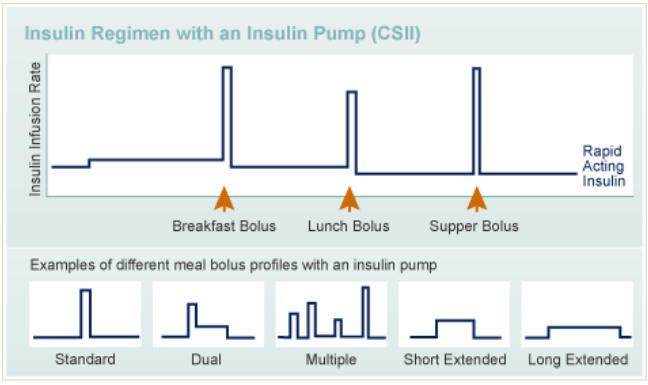


Figure 1.4: (left) Typical infusion profiles for continuous subcutaneous insulin infusion (CSII, a.k.a. pump therapy (PT)). Notice that the basal levels are adjusted throughout the day, giving the patient more flexibility to achieve optimal background insulin concentrations. In the bottom frame different types of bolus infusion profiles are shown. A 'standard' profile gives an entire meal bolus up front, while an 'long extended' profile gives the insulin over an extended period, when a meal contains significant fat that tales longer to digest [15], used without permission. (right) Typical insulin pump with subcutaneous infusion set. The infusion set contains a small cannula that sits about 0.5-1 inch below the skin. From [16], used without permission

to high fat content, can take up to eight hours to digest. Insulin works over only four hours, so to account for the mismatch of insulin availability in blood and digestion rates the user can direct the pump to give 50% of insulin now, and 50% four hours later, so that insulin will continuously work the entire eight hours that the pizza is being digested. Some examples of different pump bolus profiles are shown in Figure 1.4

Insulin pumps are gradually becoming more popular, especially with the recent advances in diabetes technology that have incorporated continuous glucose monitoring (CGM) into insulin pumps, displaying glucose measurements every 5 minutes on the pump screen. This combination of therapy is called sensor augmented pump (SAP) therapy and has been shown to be superior to MDI and CSII [17]. This integration of continuous glucose measurements into the pump has also made closing the loop possible, where insulin is dosed automatically in response to glucose excursions. The first partially automated insulin pump (a.k.a. artificial pancreas) reached the market in spring of 2017. It called the Medtronic 670G and is a hybrid-closed loop system that can automatically adjust basal insulin rates, though meal boluses are still manually inputted by the user. More details on the artificial pancreas will be given in the next section.

### Glucose Monitoring

Accurate glucose monitoring is critically important to diabetes management. The correct dose of insulin is based not just on the amount of CHO being ingested, but also on the current BG level. Before dosing insulin at mealtime, a subject needs to check BG levels to determine whether they should give a larger dose (if BG is higher than normal) or a lower dose (if BG is lower than normal). Even a 10 % error in the insulin dose amount can lead to


Figure 1.5: Examples of the tools for measuring BG. (left) Urine glucose test strips. (center) Finger-stick BG (FSBG) meter. (right) Continuous glucose monitor (CGM). The CGM consists of a sensor (white patch), a transmitter (round and grey), and a receiver (blue device placed in pocket). Urine test strips for BG measurement have been replaced by FSBG meters. FSBG meters may suffer a similar demise as CGMs become more comfortable, more accurate, and more affordable. Newer CGMs no longer require calibration with FSBG meters. Images from [18–20], used without permission.

unsafe glucose levels. Having an accurate glucose measurement makes a dosing calculation much easier.

Glucose monitoring technology has advanced at a steady pace over the past four decades. Only 40 years ago, urine test strips were the standard method to of BG measurement. This technology was very crude by today's standard. A patient would urinate on a test strip, then compare the color to the spectrum printed on the packaging. This would give an estimate of what the BG levels were a few hours prior. An example of a urine test strip is shown in Figure 1.5 (left).

In the early 1980s, the first in-home finger-stick BG (FSBG) test strips were introduced, revolutionizing treatment for patients with T1D. The technology has steadily improved to today's sleek, tiny, and reliable FSBG meters. An example of a FSBG monitor is shown in Figure 1.5 (middle). A finger-stick BG meter involves pricking the finger with a needle, obtaining a drop of blood, and placing it on a test strip that is inserted into a small electronic reader. These meters are fairly accurate, with errors required to be less than 20% according to the International Organization for Standardization. For most all practical situations, 20% error is sufficiently accurate for persons with T1D to make treatment decisions. A person with T1D can take up to 10 readings daily.

Recently, a revolutionary new technology has come to fruition - the continuous glucose monitor (CGM). This technology uses an implantable wire to continuously measure glucose levels, providing a reading every 5 minutes. An example of a CGM is shown in Figure 1.5. CGMs have revolutionized treatment for persons with T1D. With a CGM, BG readings are reported on a receiver (or smartphone) every 5 minutes, 24 hours a day. This feature provides information that can warn a person with T1D of impending hypoglycemia, or wake up a patient if they experience a nighttime low. The frequent sampling of CGM has also, for the first time, enabled users to make dosing decisions based not just on current values of BG, but also recent trends in BG (is BG rising or falling at the moment?). A typical CGM readout is shown in Figure 1.6.


Figure 1.6: Two typical CGM readouts as seen in the Dexcom application on the iPhone. The left shows the case where a CGM reading is high. The right shows the case where a CGM reading is low. Measurements are reported in 5 minute increments. CGM has revolutionized treatment for T1D, and has been shown to significantly improve treatment outcomes[21, 22].

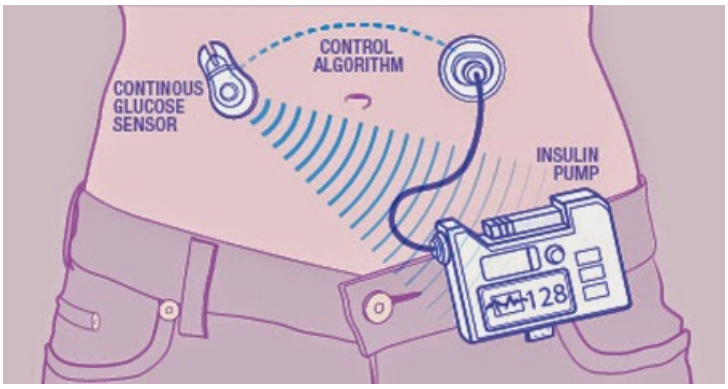


Figure 1.7: The three main components of an artificial pancreas are a continuous glucose monitor, an insulin pump, and a control algorithm. These three components work together to close the loop, allowing for automated insulin delivery that effectively replaces the pancreas. Images from [23], used without permission.

### The Future of Treatment - The Artificial Pancreas

Insulin pumps are becoming more reliable, and continuous glucose monitors more accurate. The natural next step is to close the loop by using real-time glucose measurements to make dosing decisions so that insulin can be infused automatically. This closed loop system is known as the artificial pancreas (AP). The system consists of three main components: a CGM, an insulin pump, and a control algorithm. A schematic of an AP system is shown in Figure 1.7.

An AP system would work by continuously dosing insulin based on a CGM reading. In a perfect world, where insulin works immediately upon injection and CGM readings are 100% accurate, the AP would be a relatively easy single-input (insulin) and a single output (BG

concentration) control problem. However, as is always the case in the real world, the problem is never that simple. There are various limitations and challenges of the AP. Some of the main challenges are:

- *Insulin time-lag.* Subcutaneously injected insulin does not reach the bloodstream until 20-30 minutes after administration. After injection it works in the body for 3-4 hours. In this time, glucose levels can change, food can be ingested, or exercise can happen - all which affect what the optimal prior insulin dose should have been.

- *Insulin sensitivity is highly variable.* How much insulin to inject changes day-to-day and hour-to-hour depending on exercise, stress, and food type.

- *Exercise.* Physical activity can rapidly lower BG levels potentially causing dangerous hypoglycemia. Because of this people with T1D need to be extremely careful both during exercise [2, 24] and in the several hour period following exercise [9].

- *Mechanical Failures.* Like all mechanical devices, parts sometimes fail. The insulin infusion cannula can become clogged, the tubing can kink, the insulin pump itself can malfunction, and the insulin can deteriorate. Any of these failures can be life threatening for a person that depends on an AP to keep them alive, and hence even with a fully automated AP system, the patient would need to remain vigilant.

Despite the many challenges, significant progress has been made over the past two decades in the medical community. Recently, the world's first partially automated insulin pump was released, the Medtronic 670g [25].

Some of the most important research work being done to develop the AP is by Kovatchev [26], Damiano [27], Hovorka [28], Doyle [29] as well as many other dedicated researchers. The potential benefits of an AP system are tremendous. Already, clinical study after clinical study have shown significant improvements to glucose control, and reduction in hypoglycemia [26, 27, 29].

However, despite the significant progress, there are still many challenges to the development of a fully autonomous system. Many of these challenges have to do with the acute effects of exercise on glucose metabolism [24].

## 1.2 Exercise and Type 1 Diabetes

Exercise poses significant challenges for people with T1D. On one hand, exercise has been shown to improve glucose control and overall health, and thus it is recommended for T1D by the American Diabetes Association (ADA) [30]. On the other hand, exercise can cause dangerous hypoglycemia, which in some rare cases has caused death [2, 31].

The ability to control glucose concentrations during and after exercise is considered a major hurdle to closed-loop control (CLC) [24]. This is because the control system needs to administer robustly an appropriate amount of insulin before, during, and following exercise.

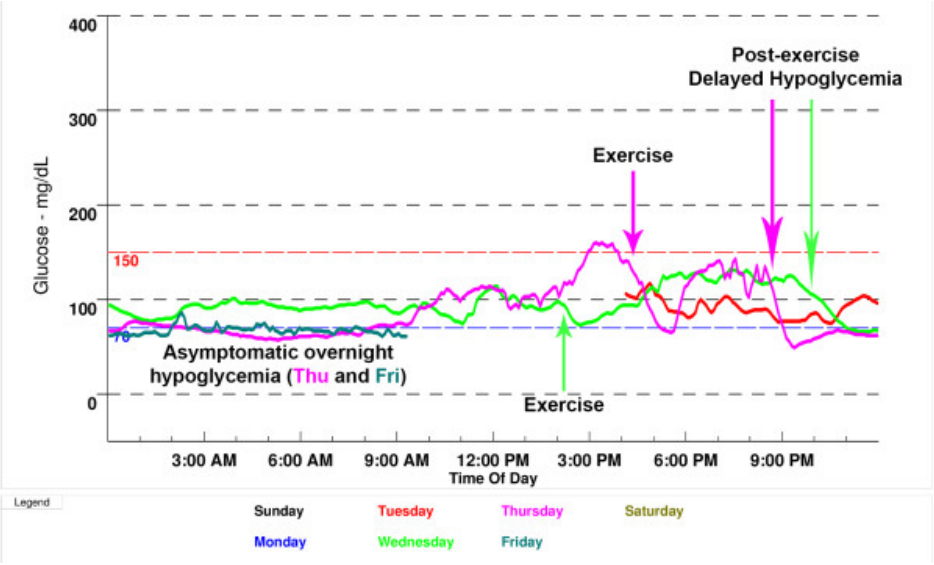


Figure 1.8: Glucose traces from several days of CGM measurements show the prolonged and acute effects of exercise on hypoglycemia. On Wednesday (green) and Thursday (magenta) the subject exercised in the late afternoon (2:00 PM and 4:00 PM, respectively). The *acute* effects of exercise caused mild hypoglycemia during exercise on both days, reaching a nadir near 70 [mg/dL] about 30 minutes after the commencement of exercise(around 3:00 PM and 6:00 PM). Glucose levels rebounded because of a snack and then due to the *prolonged* effects of exercise began to drop again, reaching hypoglycemic levels around 11:00 PM (Thursday) and 9:00 PM (Wednesday). Image from [17], used without permission.

The 'appropriate' amount of insulin, however, is not always clear. Even if carbohydrates are counted correctly and insulin is scaled back in anticipation of exercise, the glucose response can be highly variable, often resulting in hypoglycemia. As a result, to avoid hypoglycemia diabetics typically need to ingest carbohydrates during and after exercise as well as adjust their basal insulin levels. Still, even if great care is taken, hypoglycemia is common and often occurs during exercise and/or several hours afterwards while the subject is asleep [32, 33].

This inability to determine accurately the correct dose of insulin when exercise is involved stems from the observation that exercise significantly alters several metabolic processes in the body. These effects can be roughly broken into two groups: *prolonged* and *acute* exercise effects. Figure 1.8 demonstrates hypoglycemia episodes that are caused by both the *acute* effects of exercise (sharp drop in glucose during exercise) and the *prolonged* effects of exercise (post-exercise delayed hypoglycemia). See Figure 1.8 caption for detailed explanation.

### Prolonged Effects of Exercise in Type 1 Diabetes

Prolonged exercise effects can cause hypoglycemia up to 48 hours following exercise [2, 9]. This is made clear by the observation that insulin sensitivity ($SI$), a measure of the ability of insulin to stimulate the uptake of glucose and suppress endogenous glucose production, is

greatly enhanced due to a bout of exercise, increasing two-fold in healthy subjects undergoing moderate exercise [10]. This means that if a person with T1D vigorously exercises late in the day, and neglects to scale back their insulin basal rates prior to bedtime, they may fall into severe hypoglycemia [17] while asleep.

Fortunately, these prolonged effects can be readily handled in the AP because the system can automatically scale back insulin based on feedback from a continuous glucose monitor. In fact, one of the main benefits of the recently released Medtronic 670G hybrid-closed loop system is its ability to use effectively CGM measurement feedback to prevent nighttime hypoglycemia and hyperglycemia [34].

### Acute Effects of Exercise in Type 1 Diabetes

The acute effects of exercise on glucose kinetics are much harder to control than the prolonged effects. This is because insulin injected through the subcutaneous route experiences a significant time-lag before it acts to lower glucose levels. Rapid-acting insulin (the typical insulin used in a insulin pump) takes 20-30 minutes to start promoting glucose uptake and remains in the system for 3-4 hours. The problem is that if a person with T1D exercises only an hour after injection then glucose will be taken up due to the exercise itself *and* the insulin that is present in the body. The combination of the two glucose-lowering effects can rapidly lead to dangerous hypoglycemia. This presents a major problem for effective and safe CLC during exercise.

There are several acute effects of exercise on glucose metabolism. Each effect is shown schematically in Figure 1.1. There are three *direct* effects (solid red lines), two direct effects on insulin (solid red lines) which cause two *indirect* effects (dotted red lines) on glucose metabolism. The effects are said to be indirect because they alter insulin kinetics, which then in-turn alters glucose kinetics. These five main effects are:

1. *Exercise increases endogenous glucose production (EGP).* To keep up with glucose demand, the rate that the liver releases glucose increases [35, 36].

2. *Exercise enhances the rate of glucose delivery to skeletal muscle.* To keep up with glucose demand in skeletal muscle, capillaries dilate and blood flow increases, so glucose can be delivered to muscle at a higher rate [37, 38].

3. *Exercise enhances the rate of glucose uptake in skeletal muscle.* Glucose is one of the primary sources of fuel during exercise and is rapidly oxidized in skeletal muscle [35, 39, 40].

4. *Exercise causes capillary vasodilation which enhances the rate of insulin absorption from the subcutaneous injection site* [41, 42]. This causes an increase in plasma insulin concentration altering glucose uptake in the liver, muscle and other insulin-sensitive tissues.

5. *Exercise causes capillary vasodilation and enhances the rate of insulin delivery to skeletal muscle* [43]. This causes the insulin concentration in skeletal muscle to rise, promoting glucose uptake [44].

## 1.3 The Physiology of Insulin-Glucose Dynamics

Glucose metabolism is a complex process in the human body. Glucose enters the circulatory system either by absorption through the digestive tract, or when fasting or exercising, by release from endogenous storage, mainly the liver. Through the circulatory system glucose is delivered throughout the body, where its fate is determined by tissue demand and hormonal signaling. Figure 1.9 illustrates the complex network that governs glucose control in the human body.

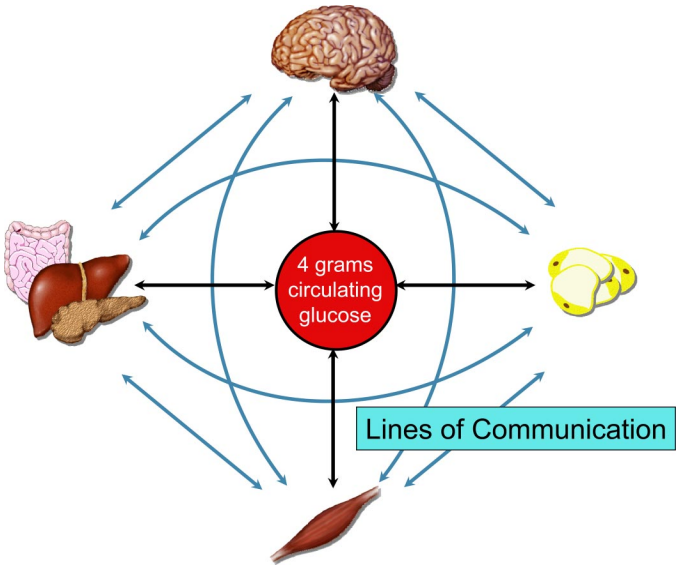


Figure 1.9: Glucose is controlled by a complex network involving the brain, muscle, digestive tract, and fatty tissue. Image taken from [36], used without permission.

The circulatory system in an adult contains roughly four grams of glucose at any moment in time [36]. Under fasting and resting conditions the whole-body rate of glucose uptake is 155 [mg/min] in an average person. This means that 4 grams of glucose turns over every 25 minutes. Figure 1.10 shows the size of a 4 gram glucose tablet and the respective contributions of different tissue groups. Of the 155 [mg/min] of glucose uptake, about 45 % goes to the brain, 30 % to the skeletal muscle and periphery, 20 % to the liver and kidneys, and the remaining 5 % to other organs [45]. Because of the constant uptake, blood glucose must be continuously replenished via endogenous sources (liver glucose release) or exogenous sources (meal ingestion).

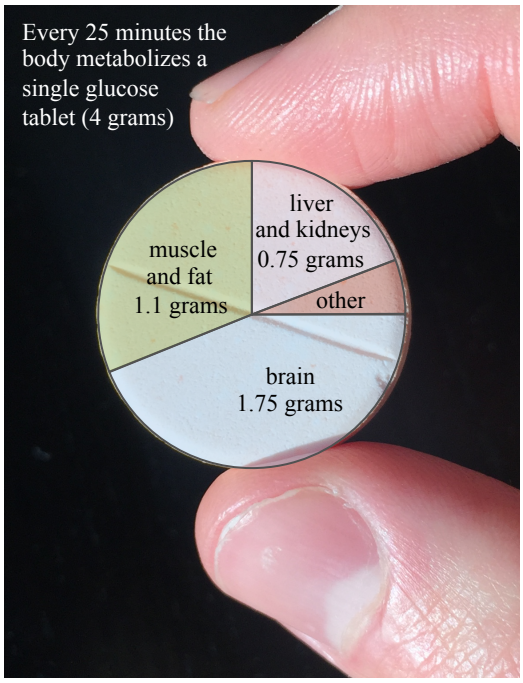


Figure 1.10: As basal glucose levels, roughly four grams of glucose are in your circulatory system [36]. Under fasting and resting conditions four grams (equivalent of one glucose tablet) is taken up by the body every 25 minutes. Each organ has different glucose requirements. Numbers taken from [45].

Because glucose is such an important fuel in the body, it must be continuously supplied to organs at a high concentration, typically about 90-100 [mg/dL]. Glucose is judiciously regulated through a complex hormonal system. The two primary hormones are insulin, which promotes glucose uptake, and glucagon, which promotes glucose production (release into bloodstream). These counter-regulatory hormones are both secreted from the pancreas.

With respect to insulin, tissues fall into two groups: *insulin-sensitive* and *insulin-independent* tissues. The main *insulin-sensitive* tissues are the liver and the peripheral tissue (skeletal muscle and fat). The glucose uptake in these tissues is dependent on the insulin concentration in the tissue. Glucose uptake in *insulin-independent* tissues, such as the brain, is largely insensitive to insulin concentration. Thus different tissues types are independently affected by hormones. A model of glucose uptake in the body must model insulin-independent and insulin-dependent tissues independently.

The variation in the digestion rate of ingested glucose adds another layer of complexity. Fatty foods are generally digested at a slower rate than foods made up of simple carbohydrates. This makes estimation of the ingested glucose absorption rate (i.e. rate of meal appearance $Ra_{meal}$) difficult to predict. Without an accurate estimation of $Ra_{meal}$, glucose levels in the postprandial state are difficult to predict. Isotopic tracers may be employed in a clinical environment to to estimate $Ra_{meal}$, as will be shown in Section 1.4 [46–53].

Considering the individual behavior of many tissue types, the number of hormones, the

variation in digestion rate, and the non-linear nature of many metabolic processes, it may seem like an intractable problem to model insulin-glucose dynamics quantitatively. We thus ease into modeling all the complexities by starting with the simplest possible model, the one compartment model of glucose metabolism.

### 1.3.1 The One Compartment Model of Glucose Metabolism

The one compartment model of glucose metabolism is a single compartment of constant volume representing the circulatory system. In actuality glucose occupies more than one compartment [51], but the one compartment assumption is valid under certain circumstances (i.e. steady state) and allows for the simplest possible mathematical representation.

**Assumption 1 (One compartment)** *Glucose occupies a single compartment with a fixed volume (usually taken to be the plasma volume of the circulatory system). Once a glucose molecule leaves the compartment it never re-enters.*

The single compartment model contains a mass of glucose $m$ that is directly proportional (through the volume $V$) to the glucose concentration in the system $G$

$$m = V \cdot G. \tag{1.1}$$

In the one compartment model we assume that the system is well-mixed.

**Assumption 2 (Well-mixed)** *A compartment is considered well mixed when the concentration of a material does not vary spatially throughout the compartment (i.e. no spatial derivatives). This means that no matter where the blood is sampled the concentration of glucose will be the same.*

This assumption is valid when the rate of species transport and dispersion throughout the system is fast in comparison to the time-scale of a species leaving the system. For example an intravenous injection of a drug distributes throughout the circulatory system in a matter of minutes but is typically present in plasma for hours. The implication is that if we wish to study the overall metabolism of the drug it is probably not important to consider the short-term spatial variation of drug concentration that is present after the initial injection. Indeed the well-mixed assumption is made out of convenience - we only need one time derivative to describe the rate of change of the system and do not need to account for spatial derivatives. The fluxes in the compartment are called rate of appearance $R_a$ and rate of disappearance $R_d$.

The one compartment description can be written mathematically as

$$\frac{dm}{dt} = R_a - R_d. \tag{1.2}$$

In words, 1.2 says that the change in the mass of glucose in the compartment is equal to the rate glucose enters the compartment minus the rate glucose leaves the compartment. Using

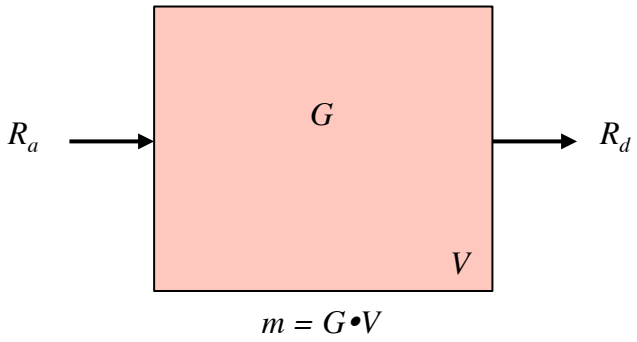


Figure 1.11: The one compartment model of glucose represents the conservation of mass of glucose in the circulatory system. $m$ is the total mass of glucose in the system, $G$ is the total concentration of glucose in the system, $V$ is the volume of distribution of glucose in blood plasma, $R_a$ the total rate of appearance of glucose into the bloodstream, and $R_d$ is the total rate of disappearance of glucose out of the bloodstream.

the relation 1.1, and assuming that volume is fixed in time we can rewrite 1.2 as

$$V\frac{dG}{dt} = R_a - R_d \tag{1.3}$$

which is the general one compartment model governing the concentration of glucose in the bloodstream.

Equation 1.3 can be given more granularity, also more physiological meaning, by accounting for the specific sources and sinks that are contained within $R_a$. Specifically, the human body has two sources of glucose: *exogenous glucose* which includes the rate of appearance of orally ingested glucose in the circulation $Ra_{meal}$ and (in certain experiments in diabetes research) infused glucose $F$ which typically comes from an intravenous infusion. Endogenous glucose comes from sources within the body - primarily the liver and of secondary importance the kidneys [53]. Endogenous glucose is usually written as $EGP$ for Endogenous Glucose Production. Written mathematically Equation 1.3 becomes

$$V\frac{dG}{dt} = Ra_{meal} + F + EGP - R_d. \tag{1.4}$$

In most cases the infused glucose $F$ is a tracer and is small compared to other sources (only about 2% of $R_a$) and therefore is neglected in most calculations.

With Equation 1.4 we have a basic model of glucose metabolism. With this model we can study the effects that insulin, demographics, and other physiological signals have on glucose metabolism, in particular $R_d$. However, to make these inferences we need to be able to measure the other terms in the model: $G$, $Ra_{meal}$, $EGP$. Measuring $G$ can be achieved through the use of readily available glucose measurement devices, but measurement of $Ra_{meal}$ and $EGP$ is much more involved because these fluxes cannot be measured directly. Rather, we can indirectly measure these fluxes using isotopic tracers. These methodologies are outlined in the next section.

## 1.4 Measurement of Glucose Flux using Isotopic Tracers

### 1.4.1 Glucose Flux Measurements Guide Model Development

In order to develop a model of glucose dynamics, it is important to have measurements of glucose fluxes. These measurements allow for the estimation of model parameters such as the distribution volume $V$ and metabolic clearance rates r. Measurements can also be used as direct inputs to candidate models to provide predictions that can be directly compared with measured outputs. Typically, in the development of glucose models the measured rate of ingested meal absorption (i.e. rate of meal appearance $Ra_{meal}$) is given as an input. The model then predicts the glucose concentration in blood plasma $G$ for direct comparison with concentration measurements. The degree to which the predicted concentration agrees with the measured concentration is an indication of model accuracy.

To evaluate the models that will be developed in this dissertation we need measurements of glucose inputs and outputs. This section summarizes the theory of isotopic tracers, the most popular and accurate measurement methodology for studying glucose dynamics.

### 1.4.2 Theory of Isotopic Tracers

Consider a glucose molecule: it enters the bloodstream at some unknown time, it is present in the bloodstream for a finite (but unknown) amount of time, and eventually it leaves the bloodstream at an unknown time. By measuring the concentration of glucose in the bloodstream, $G$, we are only made aware of how many glucose molecules are in the bloodstream at a given time, but we still have no idea how many molecules are entering or exiting the bloodstream at that time - we are unaware of the flux.

Now consider a special glucose molecule, a *tracer*. We send these special molecules into the bloodstream and they move around just like all the other glucose molecules: they circulate at the same rate, exit the bloodstream at the same rate, and are converted to energy at the same rate. In scientific terms these tracers are *metabolically identical* to all the other glucose molecules. What makes these *tracers* special is that they are slightly heavier (by molecular weight) and/or radioactive. Because of this small (but measurable) difference we are able

to detect their numbers among the entire glucose population. Moreover, if we specify how quickly they are infused into the bloodstream then we can calculate how quickly they leave the bloodstream by using mass conservation. Then, finally, because they are metabolically identical to the entire glucose population, we can leverage the information they provide to learn about all the other glucose molecules. This is the essence of a tracer.

**Definition 1 (Tracer, $q$)** *A substance that is externally introduced into the system at a known rate, $F$, and can provide quantitative information about the system as a whole. In our case the tracer is a glucose molecule that has a heavier and/or radioactive carbon atom. Its concentration is denoted $G_q$.*

**Definition 2 (Tracee, $Q$)** *A substance that is naturally occurring in the system. It is the substance that we wish to learn about by extrapolating information gathered from the tracer. In our case, this is the naturally occurring glucose. Its concentration is denoted $G_Q$.*

In order for a substance to be considered a tracer it must have the following properties [52, Ch. 2]

**Property 1 (Tracer properties)**

1. *It is detectable by an observer*
2. *Its introduction into the system does not perturb the system being studied*
3. *It is indistinguishable with respect to the properties of the tracee being studied (i.e. metabolically identical [49])*

To clarify how we can utilize tracers to quantify glucose metabolism, consider the one compartment model described by Equation 1.3. We may apply this model to the tracer and tracee systems separately to obtain two ODEs

$$V\frac{dG_q}{dt} = F - R_{d_q} \tag{1.5}$$

$$V\frac{dG_Q}{dt} = R_{a_Q} - R_{d_Q}. \tag{1.6}$$

The two equations are shown schematically in Figure 1.12. $V$ is the same for each system because they both occupy the same circulatory system. The subscripts represent the tracer $q$ or tracee $Q$ system. $F$ is the imposed infusion rate of the tracer $q$ and has replaced the rate of appearance of the tracer $R_{a_q}$ .

Our two equations describing the tracer and tracee system still have three unknowns: $R_{d_q}$, $R_{a_q}$, and $R_{d_Q}$. Thus we need one more equation to complete the system. The missing

equation relates the mass in the system to the flux in the system. We define the mass fraction of our tracer and tracee to be

$$w_q = \frac{m_q}{m_Q + m_q} = \frac{G_q}{G_Q + G_q} \tag{1.7}$$

$$w_Q = \frac{m_Q}{m_Q + m_q} = \frac{G_Q}{G_Q + G_q}. \tag{1.8}$$

Note that

$$1 = w_q + w_Q \tag{1.9}$$

$$m = m_q + m_Q \tag{1.10}$$

$$G = G_q + G_Q. \tag{1.11}$$

Now, if we continue with the well mixed assumption and further assume that the tracer is metabolically identical to the tracee, then the mass leaving the system of each species (tracer and tracee) is simply the mass fraction times the total mass leaving the system $\dot{m}$

$$R_{d_q} = w_q \dot{m} \tag{1.12}$$

$$R_{d_Q} = w_Q \dot{m} \tag{1.13}$$

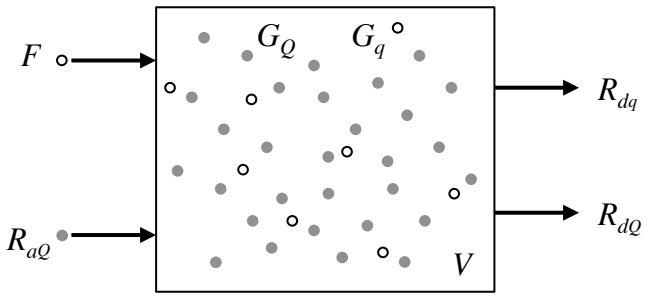


Figure 1.12: The tracer($q$ open circles) and tracee($Q$ closed circles) system. Both species occupy the same volume. Note that both the tracer and tracee particles are evenly distributed per the model well-mixed assumption.

eliminating $\dot{m}$ we have

$$R_{d_Q} = \frac{w_Q}{w_q} R_{d_q} \tag{1.14}$$

Equation 1.14 is called the tracer indistinguishably assumption. It can stated equivalently as a probability [52, pp. 19]:

**Assumption 3 (Isotopic indistinguishably a.k.a. metabolically identical)** *The probability that a particle that leaves the system is a tracer is equal to the probability that a particle in the system is a tracer. Mathematically this is stated as*

$$\frac{R_{d_q}}{R_{d_q} + R_{d_Q}} = \frac{m_q}{m_q + m_Q} \tag{1.15}$$

To get our desired expression, that is to calculate $R_{d_Q}$, we substitute Equation 1.14 and 1.5 into 1.6. After some manipulations, and defining the tracer to tracee ratio as $z = \frac{G_q}{G_Q}$ we obtain the well-known Steele Equation [51]

$$R_{a_Q} = \frac{F}{z} - V\frac{G_Q}{z}\frac{dz}{dt}. \tag{1.16}$$

Equation 1.16 gives a way to calculate $R_{a_Q}$ directly under the assumptions of a well mixed, metabolically identical, single pool model of glucose. This is the model that is used throughout the vast literature of isotopic tracers in order to elucidate information about many metabolites [7, 46, 50, 54].

In order to utilize Equation 1.16 a researcher needs to be able to measure $G_q$, $G_Q$, and $V$ for a given input $F$. Typically $V$ is assumed to have a certain value measured from previous studies. However, this is problematic for two reasons: (1) there is large patient variability of V and (2) glucose in fact occupies more than one compartment which is contrary to our model assumption [51]. This assumption is almost always problematic when one hopes to quantify $R_{a_Q}$ accurately from Equation 1.16 and sometimes leads to large errors. A "pool-fraction" $p$ is sometimes used to correct for this one-compartment assumption [46], so $V$ would be replaced by $pV$, effectively decreasing the volume of distribution to decrease error. However the value of $p$ is difficult to measure and changes with time. These problems are largely overcome by *clamping* $z$. This means that the tracers are infused in a manner such that $z$ is nearly constant. This causes the second term in 1.16 to drop out. The process of clamping $z$ will be discussed in the coming sections.

### 1.4.3 Tracer Measurements and Methodologies

In the previous section it was explained how a researcher with a measurement for the tracer to tracee ratio $z$ can calculate $R_{a_Q}$ using Equation 1.16. However, no mention was made about how to obtain a measurement for $z$. This section is devoted to explaining how these

measurements are obtained. For the purposes of this discussion, we will limit ourselves to only glucose tracers. For the curious reader, many important details on tracer methodologies can be found in [46, 49, 52, 53].

Glucose contains three elements: hydrogen, carbon, and oxygen. In its natural form glucose contains two isotopes of carbon, $G[^{12}C]$ and $G[^{13}C]$ with natural abundances of 98.9% and 1.1%, respectively. Other carbon isotopes may exist in a glucose molecule, however these are in very small quantities. In addition to carbon isotopes, other elements can be used to as labels for tracers: deuterium $G[^{2}H]$ and tritium $G[^{3}H]$ are commonly used. For the purposes of this discussion we will limit ourselves to the three isotopes that are most commonly utilized for glucose tracers: two stable forms of glucose ($G[^{13}C]$ and $G[^{2}H]$) and one radioactive form ($G[^{3}H]$).

#### Stable isotopic tracers, $G[^{13}C]$, $G[^{2}H]$

Because the abundance of $G[^{12}C]$ is so high relative to $G[^{13}C]$, it is possible to create an *enriched* quantity of glucose that has a much higher abundance of $G[^{13}C]$ than naturally occurs. This enriched quantity of glucose is used as the tracer. Another commonly used stable isotopic tracer is the $G[^{2}H]$, a.k.a. deuterium. This tracer is typically introduced in the use of the triple tracer technique [46]. A mass spectrometer is used to measure the abundances of $G[^{13}C]$ and $G[^{2}H]$. With these measurements we can calculate the tracer to tracee ratio $z$ so that we may obtain $R_{a_Q}$ from Equation 1.16.

#### Radioactive isotopic tracers, $G[^{3}H]$

Radioactive glucose isotopes only occur naturally in minute quantities. It is for this reason that they make excellent tracers, as their mass does not need to be taken into account when calculating enrichment. The concentration of $G[^{3}H]$ in the bloodstream is found by using a scintillation counter.

### 1.4.4 Tracer Variables

There are several commonly used tracer variables. Which variable is the sensible choice to use depends on whether the tracer is stable or radioactive and specifically which measurements are available.

For stable tracers the tracer to tracee ratio $z$ is used. For radioactive tracers the specific activity $sa$ is used. Each of these variables aim to quantify the same thing, namely they are some measurement of the ratio of tracer to tracee in the system. Once $z$ or $sa$ is obtained, it is input into Equation 1.16 to estimate the glucose flux.

Typically, $z$ and $sa$ are not directly measurable and are rather derived from directly measurable quantities such as the isotopic ratio $r$, isotopic abundance $a$, or enrichment $e$.

**Definition 3 (Tracer to tracee ratio, $z$)** *The ratio of the mass of the tracer to the mass of the tracee in a system*

$$z = \frac{m_q(t)}{m_Q(t)} = \frac{G_q(t)}{G_Q(t)}. \tag{1.17}$$

$z$ is the most useful way to describe stable isotope data because it is the direct input for Equation 1.16. $z$ is time dependent and is measured in the blood plasma. There are two other variables that are identical to $z$ in their mathematical definition, but instead are used to describe the ratios in the meal and the infused tracer (the latter is only relevant if the tracer is not 100% pure).

**Definition 4 (Tracer to tracee ratio of the meal, $ttr_{meal}$)** *The ratio of the mass of the tracer to the mass of the tracee, in the meal prior to ingestion*

$$ttr_{meal} = \frac{m_{q_{meal}}}{m_{Q_{meal}}}. \tag{1.18}$$

**Definition 5 (Tracer to tracee ratio of the infused tracer, $ttr_{inf}$)** *The ratio of the mass of the tracer to the mass of the tracee, in the prepared infusate*

$$ttr_{inf} = \frac{m_{q_{inf}}}{m_{Q_{inf}}}. \tag{1.19}$$

Since $z$ cannot be directly measured it is derived from a mass-spectrometer measurement of the isotopic ratio $r$, isotopic abundance $a$, or in some cases the isotopic enrichment $e$. These related variables are defined as

**Definition 6 (Isotopic ratio, $r$)** *The ratio of the mass of one isotopic species ($I$) to another species ($II$)*

$$r = \frac{m_{q_I} + m_{Q_I}}{m_{q_{II}} + m_{Q_{II}}} = \frac{G_{q_I} + G_{Q_I}}{G_{q_{II}} + G_{Q_{II}}} \tag{1.20}$$

Where $I$ and $II$ denote two distinct isotopic species, each present in both the tracer $q$ and the tracee $Q$, i.e. $G_{q_I}$ is the glucose concentration of the isotopic species $I$ in the tracer $q$. The reason why it is necessary to define both $z$ and $r$ is because there is always a finite amount of each isotope $I$ and $II$ that naturally occurs in the tracee and the tracer (a tracer is never 100% pure). Even if $z$ is zero because there is no tracer present, $r$ would not be because of naturally occurring isotope. For example, natural glucose is 98.9% $G[^{12}C]$ and 1.1%$G[^{13}C]$. So the isotopic ratio in this case would be $r_N = 1.1/98.9 = 0.01112$, but because there is no tracer present $z = 0$. Another way of expressing an isotopic measurement is through the isotopic abundance $a$. $a$ is a nearly identical measurement to the isotopic ratio except that it is the ratio of one isotopic species to the total mass, rather than the ratio of one isotopic species to another.

**Definition 7 (Isotopic abundance, $a$)** *The ratio of the mass of one isotopic species to the total mass of the system*

$$a = \frac{m_{q_I} + m_{Q_I}}{m} = \frac{G_{q_I} + G_{Q_I}}{G}, \tag{1.21}$$

*or alternatively*

$$a = \frac{r}{1+r}. \tag{1.22}$$

A very commonly used derivative of $r$ and $a$ is called the enrichment of a substance $e$

**Definition 8 (Isotopic enrichment, $e$)** *The abundance of an isotopic species above its natural level*

$$e = a - a_N = \frac{r}{1+r} - \frac{r_N}{1+r_N}. \tag{1.23}$$

Enrichment is the most commonly used measurement for expressing stable isotope data [52]. Meal enrichment, $e_{meal}$, and infusate enrichment, $e_{inf}$, can also be defined.

It is necessary to convert a measurement of $e$ to $z$ in order to calculate the tracer flux from Equation 1.16. To do this the following equation can be used [52, Chap. 2, pg. 33] with either $Pu_{inf}$ or $Pu_{meal}$

$$z = \frac{e}{Pu_{inf} - e} \tag{1.24}$$

Where $Pu_{inf}$ is the purity of the infusate tracer, defined as the actual mass of tracer divided by the tracer sample mass (between 0 and 1, usually very close to 1). This formula can also be used for the tracer in the meal by replacing $Pu_{inf}$ by $Pu_{meal}$. Additionally, it can be used to convert between $ttr_{meal}$ or $ttr_{inf}$ and $e_{meal}$ or $e_{inf}$.

$z$ and $e$ are used for stable isotopes. When radioactive isotopes are used a similar variable to $z$ is defined, known as specific activity $sa$

**Definition 9 (Specific activity, $sa$)** *Radioactivity per unit total mass*

$$sa = \frac{\nu m_q}{m} = \frac{\nu G_q}{G} = \frac{measured\ dpm}{G} \tag{1.25}$$

The units of $sa$ are typically disintegrations per minute (dpm) per mass, which is the number of atomic disintegrations a scintillation counter measures in a minute divided by the total mass of the sample. Given a particular radioactive tracer the dpm only depends on the total mass of the tracer. Hence the mass of a tracer is related to the measured number of dpm by a simple proportionality constant $\nu$. This relationship is $measured\ dpm = \nu m_q$.

$sa$ is typically used in an identical way as $z$ because $sa \approx z$ due to the mass of the radioactive tracer being very small in comparison to the tracee. For this reason $z$ in Equation 1.16 can be replaced by $sa$ with negligible error

$$R_{a_Q} = \frac{F}{sa} - V\frac{G_Q}{sa}\frac{d(sa)}{dt}. \tag{1.26}$$

Equation 1.16 should be used for stable tracers and Equation 1.26 should be used for radioactive tracers.

For a more complete discussion of each of the aforementioned tracer variables see [52, Ch. 2].

### 1.4.5 State of the Art in Tracer Methodology

Various methodologies have been developed to assess glucose metabolism quantitatively. The single tracer methodology is rather limited due to its inability to differentiate between exogenous and endogenous sources of glucose. The dual-tracer and triple-tracer methods give the experimenter more control over $z$ (or $sa$) reducing errors as well as allowing for the differentiation of endogenous and exogenous glucose. Hence these latter methods are the most popular.

#### Single Tracer Methodology

The single tracer methodology is typically employed under non-physiological conditions when glucose is not ingested orally, but rather infused intravenously; unlabeled natural glucose $G_Q$ is infused intravenously at a specified rate $R_{a_{exo}}$, the rate of appearance from exogenous sources. During this type of test $R_{a_{exo}}$ replaces $Ra_{meal}$ because the subject is in a fasting state. Thus, the only other source of natural glucose is EGP. By mass conservation $R_{a_Q}$, the rate of appearance of the tracee, is then

$$R_{a_Q} = R_{a_{exo}} + EGP \tag{1.27}$$

Now a tracer, for instance radioactive $G[^3H]$, is infused at a known rate $F_{^3H}$ simultaneously with the unlabeled glucose $G$ that comes from the $R_{a_{exo}}$ infusion. We now utilize the radioactive tracer Steele Equation 1.26 where $sa = G[^3H]/G$

$$R_{a_Q} = \frac{F_{^3H}}{sa} - V\frac{G}{sa}\frac{d(sa)}{dt} \tag{1.28}$$

We can substitute Equation 1.27 into 1.28 to obtain an expression for EGP

$$EGP = \frac{F_{^3H}}{sa} - V\frac{G}{sa}\frac{d(sa)}{dt} - R_{a_{exo}}. \tag{1.29}$$

$V$ can be assumed to be the population average, however its high variability can potentially lead to significant errors. Even more profound errors occur because the single compartment assumption in the derivation of the Steele equation breaks down. This could be corrected by including a "pool-fraction" $p$ [49, 51], which represents a 'fraction' of the glucose space.

$pV$ would be considered the volume of the plasma compartment, however the correct value of $p$ is also known to vary greatly from patient to patient. For this reason it is more sensible to "clamp" $sa$, by carefully infusing $F_{^3H}$ and $R_{a_{exo}}$ to obtain a nearly constant $sa$. When $sa$ is clamped in this way $d(sa)/dt \approx 0$. In this way we circumvent the need to know $V$, and utilize the ideal clamp version of equation 1.29

$$EGP = \frac{F_{^3H}}{sa} - R_{a_{exo}} \tag{1.30}$$

This clamp formula can also be used without any infusion $R_{a_{exo}}$. This would allow for the quantification of EGP under steady state and fasting conditions.

The main limitation of this single tracer methodology is that $Ra_{meal}$ for an orally ingested meal cannot be quantified because a single tracer cannot distinguish between endogenous and exogenous glucose. If a researcher desires to measure both, at a minimum two tracers must be included. This technique is known as the Dual Tracer Methodology.

### Dual Tracer Methodology

In the dual tracer methodology one tracer is embedded in the meal and the other is infused intravenously. The second tracer is used to trace the first tracer and the first tracer is used to trace the total glucose in the meal.

The two tracers typically used are $G[^{13}C]$ and $G[^3H]$ [46]. The $G[^{13}C]$ is embedded in the meal prior to ingestion at a known $ttr_{meal}$ ($\approx 0.04 - 0.05$). The $G[^3H]$ tracer is infused intravenously at a specified rate $F_{^3H}$.

It is a two step process to calculate $Ra_{meal}$ in the dual tracer method. First, we determine the rate of appearance of the $G[^{13}C]$ glucose via the use of the radioactive Steele Equation 1.26

$$R_{a_{^{13}C}} = \frac{F_{^3H}}{sa_{meal_{2T}}} - V\frac{G[^{13}C]}{sa_{meal_{2T}}}\frac{d(sa_{meal_{2T}})}{dt} \tag{1.31}$$

where $sa_{meal_{2T}}$ in this case is defined as

$$sa_{meal_{2T}} = \frac{G[^3H]}{G[^{13}C]} \tag{1.32}$$

where $meal$ is for meal rate of appearance and $2T$ is for dual-tracer method. Note, the $G[^3H]$ tracer can be infused at a rate similar to the anticipated rate of appearance of $G[^{13}C]$, $R_{a_{^{13}C}}$, to minimize changes in $sa_{meal_{2T}}$ [49] and thus minimize the error that comes from the second term in 1.31.

Second, we divide the resulting $R_{a_{^{13}C}}$ by the meal enrichment $e_{meal}$ and use Equation 1.24 (assuming purity is 1) to obtain $Ra_{meal}$

$$Ra_{meal} = \frac{R_{a_{^{13}C}}}{e_{meal}} = R_{a_{^{13}C}}(\frac{1}{ttr_{meal}} + 1). \tag{1.33}$$

This step essentially takes into account that only a small portion of the meal contains the $G[^{13}C]$ tracer. If the meal was 100% $G[^{13}C]$ then the second step would not be necessary.

Now, to calculate EGP we need to determine the glucose that solely comes from endogenous sources. To do this, we break the overall rate of appearance of glucose, $Ra_{tot}$, into its constitutive parts

$$Ra_{tot} = Ra_{meal} + EGP + \cancel{F_{^3H}}^{\approx 0} \tag{1.34}$$

$F_{^3H}$ is eliminated because it is very small relative to the other terms. We may rearrange this equation and solve for EGP

$$EGP = Ra_{tot} - Ra_{meal}. \tag{1.35}$$

With this relation we can solve for EGP if we know $Ra_{tot}$ and $Ra_{meal}$. We already know $Ra_{meal}$ from equation 1.33, so to find $Ra_{tot}$ we create a new tracer variable [46]

$$sa_{tot_{2T}} = \frac{G[^3H]}{G} \tag{1.36}$$

where $tot$ is for total rate of appearance and $2T$ is for dual-tracer method.

In the identical way as before with $Ra_{meal}$, we now utilize the radioactive Steele Equation 1.26 but with $sa_{tot_{2T}}$ to determine $Ra_{tot}$

$$Ra_{tot} = \frac{F_{^3H}}{sa_{tot_{2T}}} - V\frac{G}{sa_{tot_{2T}}}\frac{d(sa_{tot_{2T}})}{dt}. \tag{1.37}$$

With this relationship we can solve for EGP using 1.35.

Because the same tracer $G[^3H]$ is used to create the two tracer variables ($sa_{meal_{2T}}$ and $sa_{tot_{2T}}$), they cannot be controlled independently. Thus it is impossible to hold both variables near constant resulting in significant errors. This is the primary weakness of the dual-tracer technique. By introducing one more tracer it becomes possible, by modulating infusion rates of each tracer, to achieve simultaneously nearly constant $sa$ for both tracers.

### Triple Tracer Methodology

The most advanced and accurate method for measurement of postprandial glucose metabolism is the triple tracer method. The triple tracer method is similar to the dual tracer method described previously. In fact, $Ra_{meal}$ is calculated identically as in the dual tracer method (Equation 1.31 to 1.33). The key difference from the dual to the triple tracer method is that a third tracer is included to aid in the accurate assessment of EGP.

The third tracer is typically a glucose molecule labeled with deuterium, $^2H$ [46]. It is referred to as $G[^2H]$ and is a stable isotope so its mass must be accounted for.

To utilize the third tracer, we begin with equation 1.11 and break up $G_q$ into the three tracers $G[^{13}C]$, $G[^3H]$, and $G[^2H]$. Also, we break up $G_Q$ into the natural glucose from the meal $G_{nat_{meal}}$ and the natural glucose from endogenous sources $G_{nat_{EGP}}$

$$G = G_{nat_{meal}} + G_{nat_{EGP}} + G[^{13}C] + \cancel{G[^3H]}^{\approx 0} + G[^2H] \tag{1.38}$$

$G[^3H]$ is negligible because it is a radioactive tracer and is delivered in very small quantities. $G[^{13}C]$, $G[^2H]$ are measurable by mass spectrometry. $G_{nat_{meal}}$ can be obtained from the simple expression

$$G_{nat_{meal}} = \frac{G[^{13}C]}{ttr_{meal}}. \tag{1.39}$$

$G_{nat_{EGP}}$ can now be solved for

$$G_{nat_{EGP}} = G - \frac{G[^{13}C]}{ttr_{meal}} - G[^{13}C] - G[^2H]. \tag{1.40}$$

We define a new tracer variable $z_{EGP_{3T}}$ that utilizes this new endogenous glucose concentration $G_{nat_{EGP}}$ ($3T$ is for three tracers)

$$z_{EGP_{3T}} = \frac{G[^2H]}{G_{nat_{EGP}}} \tag{1.41}$$

Once again utilizing the Steele Equation 1.16 we get

$$EGP = \frac{F_{^2H}}{z_{EGP_{3T}}} - V\frac{G_{nat_{EGP}}}{z_{EGP_{3T}}}\frac{d(z_{EGP_{3T}})}{dt}. \tag{1.42}$$

So why is this an improvement over the dual tracer methodology? Because we can control the concentration of $G[^2H]$ glucose through its infusion rate $F_{^2H}$ and therefore minimize the changes in $z_{EGP_{3T}}$. This reduces errors in our calculation of EGP by making the second (and more uncertain term) in Equation 1.42 smaller.

### 1.4.6 Typical Measurement Results Using Tracer Methodology

Example triple-tracer measurements of $Ra_{meal}$ and $EGP$ are shown in Figure 1.13. Two studies, a resting study (blue) and an exercising study (orange), are plotted in each frame. $Ra_{meal}$ is calculated from Equation 1.33 and $EGP$ is calculated from Equation 1.42. The grey areas show the exercise periods, which only correspond to the exercise study.

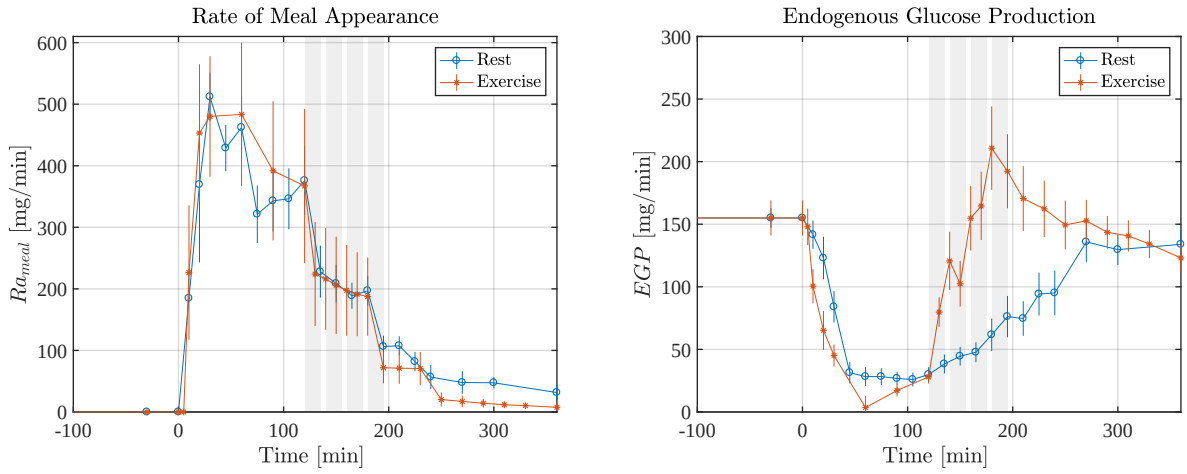


Figure 1.13: Typical measured rate of meal appearance ($Ra_{meal}$) and endogenous glucose production ($EGP$) for an average healthy (non-diabetic) resting subject and an average healthy exercising subject. Meal ingestion for each group occurs at $t = 0$. The exercising group has four 15 minute exercise bouts from t=120-195 shown by shaded regions. $Ra_{meal}$ during fasting is 0 [mg/min]. Upon ingestion of the meal $Ra_{meal}$ rapidly increases to a maximum near 500 [mg/min], and then slowly declines over the next 6 hours to nearly 0. $EGP$ starts at 155 [mg/min] and after meal ingestion it is suppressed to nearly 0 in both cases. In the resting case $EGP$ slowly rises back to basal levels over the following few hours, however, in the exercising case it rapidly increases to 200 [mg/min] during the exercise period. Vertical lines are SEM.

## 1.5 Previous Mathematical Models of Insulin-Glucose Dynamics

The types of models used to represent insulin-glucose dynamics range from minimal to intricate. We have reviewed three of the most popular and well-studied models.

### 1.5.1 Oral Minimal Model of Glucose Kinetics

The oral minimal model (OMM) [55, 56] is a model of insulin-glucose dynamics that can be used to assess a subject's insulin sensitivity ($SI$) from a glucose tolerance test. It has also been used as a basic model of glucose metabolism for predictive purposes [1, 57]. It is a nonlinear lumped parameter model of whole body glucose metabolism and is made up of two equations. Equation 1.43 is a single compartment model that governs insulin action ($X$), as variable that describes the ability of insulin to promote glucose uptake and suppress glucose production by the liver. Equation 1.44 is a single compartment model that governs glucose dynamics in plasma. The model equations are

$$\frac{dX}{dt} = -p_2 X + p_3(I - I_b) \tag{1.43}$$

$$\frac{dG}{dt} = -S_G(G - G_b) - XG + \frac{Ra_{meal}}{V^G} \tag{1.44}$$

The variables are $X$ and glucose concentration in plasma ($G$). The inputs are the measured insulin concentration in plasma ($I$) and the rate of meal appearance ($Ra_{meal}$). The constants are basal glucose concentration ($G_b$) in plasma, basal insulin concentration in plasma ($I_b$), glucose effectiveness ($S_G$), i.e. the ability of glucose itself to promote glucose uptake and suppress its own production per volume of distribution (typically set to a population averaged value of $S_G = 0.014$ [1/min] [56]), and $V^G$ is the volume of distribution of glucose in the body (set to a population average value of $V^G = 1.7$ [dL/kg] [56]). The parameters $p_2$ and $p_3$ are also treated as constants, however they are unknown and to-be-determined. The ratio of $p_3$ to $p_2$ times $V^G$, define whole-body SI

$$SI = \frac{p_3}{p_2} V^G. \tag{1.45}$$

The units of $SI$ are [dL/kg/min per $\mu$U/mL]. The parameter can be defined as the insulin action on lowering glucose concentration per unit insulin concentration.

### Addition of Exercise into the OMM

Even though there are very strict assumptions that limit the validity of the OMM, a few attempts have been made to include exercise effects [1, 58]. Both attempts utilized a similar approach, with additional terms added to the OMM to account for the increase in peripheral glucose uptake and the increase in hepatic glucose production. These additional terms included several parameters, which were identified using nonlinear least-squares.

### Model Review

The intended use of the OMM is to assess a subject's $SI$ for diagnostic purposes. The model is too simplified to be used for predictive purposes, except in the most restricted cases. This is because of the many model assumptions: insulin and glucose start from and return to basal levels, the parameters of the model are constant throughout the study, glucose is a one compartment model, and that insulin action in the liver and glucose are grouped together. Also, because the model structure is so limited (by design), it cannot easily be amended to add the effects of exercise.

To the credit of its creators, the model has been extremely useful for its intended purpose - to diagnose diabetes. Many types of glucose tolerance tests can be analyzed through identifying SI via least-squares curve fitting.

In an effort to further simply estimation of SI, the author has solved the OMM analytically. The analytical method has been validated vs. the numerical least-squares method and is presented in Appendix B of this dissertation.

The exercise additions to the OMM by Roy and Breton [1, 58] are problematic for various reasons. First, many assumptions in the OMM are violated when exercise commences. The authors do not account for the observations that glucose effectiveness and insulin-sensitivity change during exercise. Next, liver uptake and peripheral uptake are lumped together, so the main effect of enhanced peripheral uptake cannot be accounted for individually. Several parameters were added to the model with the exercise addition, and these parameters were identified through nonlinear least-squares, rather than directly from physiology. This makes the value of the parameters questionable and they may not accurately describe the mechanism for which they are intended.

### 1.5.2 Meal Glucose Insulin Model of Type 1 Diabetes

Cobelli and Dalla Man et al. have produced one of the most comprehensive and best-validated models of insulin-glucose dynamics, known as the Meal Glucose-Insulin Model (GIM). The model was initially described for healthy and type 2 diabetic subjects in [59]. Shortly thereafter, a T1D module was added [60]. A few years later a physical activity module was added [61]. The GIM is the foundation of the UVa/Padova Type 1 Diabetes simulator, approved by the FDA for preclinical trials in 2009 [62].

The basis of the GIM consists of a two compartment model of glucose, and a two compartment model of insulin. Note that notation was adopted from the original article [59], and thus the nomenclature section of this dissertation should not be referenced to describe this particular model. A block diagram describing the GIM is shown in Figure 1.14.

The glucose subsystem consists of a two compartment model (see Figure 1.15)

$$\frac{dG_p}{dt} = EGP(t) + Ra(t) + U_{ii}(t) - E(t) - k_1 G_p + k_2 G_t \tag{1.46}$$

$$\frac{dG_t}{dt} = -U_{id}(t) + k_1 G_p - k_2 G_t \tag{1.47}$$

$$G = \frac{G_p}{V^G}. \tag{1.48}$$

where $G_p$ is the mass of glucose in the plasma and rapidly equilibrating tissues, $G_t$ is the mass of glucose in the slowly equilibrating tissues, $G$ is the plasma glucose concentration, $EGP$ is the endogenous glucose production, $Ra$ is the rate of glucose appearance in plasma, $E$ is renal extraction, and $U_{ii}$ and $U_{id}$ are the insulin-independent and insulin-dependent glucose utilizations, respectively.

The insulin model consists of two base compartments (see Figure 1.15), plus one remote compartment representing insulin action in the interstitial fluid (not depicted). The insulin

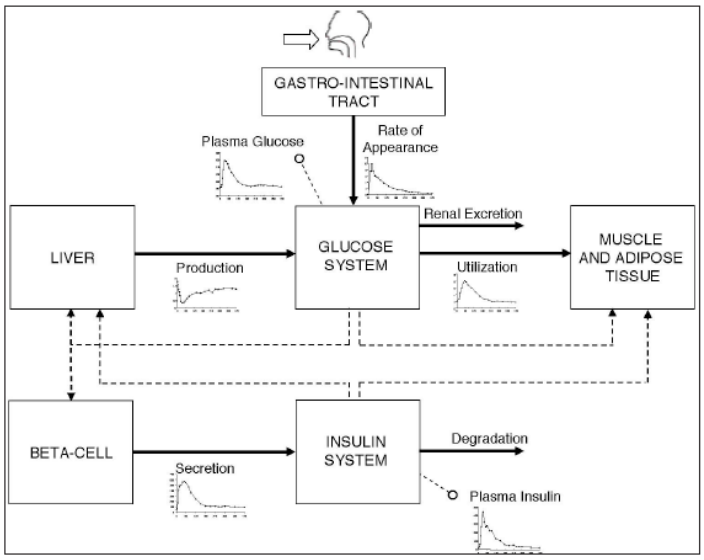


**Figure 1**. Scheme of the glucose–insulin control system. Continuous lines denote fluxes of material and dashed lines control signals. In addition to plasma glucose and insulin concentration measurements, glucose fluxes (i.e., meal rate of appearance, production, utilization, and renal extraction) and insulin fluxes (i.e., secretion and degradation) are also shown (see text).

Figure 1.14: Meal Glucose Insulin Model (GIM) proposed in [59] and [60]. The block diagram shows several subsystems. In a subject with type 1 diabetes, the beta-cell subsystem is irrelevant, and is instead replaced with the subcutaneous insulin infusion subsystem described in [60]. The GIM model is one of the most comprehensive and well-validated insulin-glucose models available. Image taken from [60], used without permission.

concentration in the liver, periphery, and interstitial fluid is described by

$$\frac{dI_l}{dt} = -(m_1 + m_3(t)) \cdot I_l + m_2 I_p + S(t) \tag{1.49}$$

$$\frac{dI_p}{dt} = -(m_2 + m_4) \cdot I_p + m_1 I_l \tag{1.50}$$

$$I = \frac{I_p}{V^I} \tag{1.51}$$

$$\frac{dX}{dt} = -p_{2U} X + p_{2U} \cdot (I - I_b). \tag{1.52}$$

$I_l$ and $I_p$ are the insulin masses in plasma and in liver. $I$ is the plasma insulin concentration and $I_b$ is basal. $X$ is the 'insulin-action' or concentration, given as [pmol/L], on glucose utilization in the periphery. Insulin-dependent glucose uptake ($U_{id}$) is dependent on the glucose concentration $G_t$ and $X$ and is assumed to be saturable in a Michaelis-Menten manner. Parameters $V_m$ and $K_m$ are dependent on $X$

$$U_{id} = \frac{V_m(X) \cdot G_t}{K_m(X) + G_t}. \tag{1.53}$$

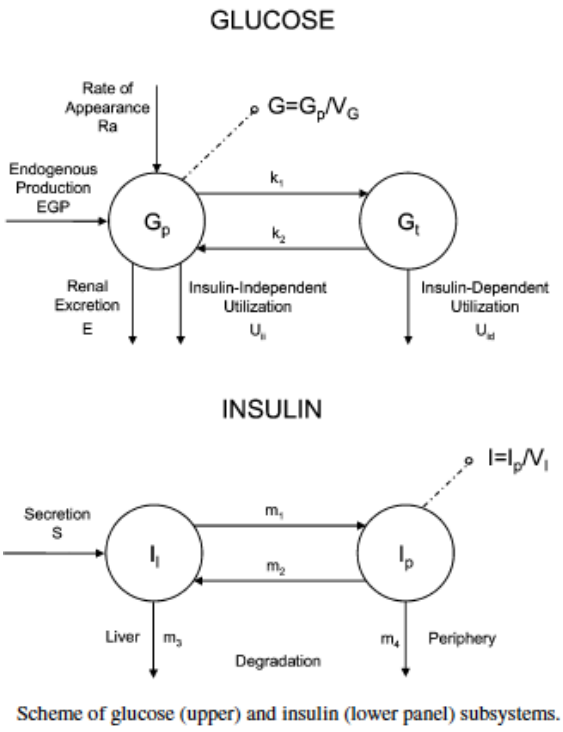


Figure 1.15: The GIM model is centered around two subsystems, the glucose subsystem and the insulin subsystem. The two glucose compartments represent the rapidly equilibrating tissues ($G_p$) and the slowly equilibrating tissues ($G_t$). These can be thought to represent glucose in the circulatory system and glucose in the insulin-dependent peripheral tissues such as muscle and adipose tissue. The two insulin compartments represent insulin in the liver and insulin in the circulatory system. There is also a third insulin compartment $X$ (not depicted), that represents insulin action on peripheral glucose uptake. Image taken from [59], used without permission.

In Equation 1.49, $S(t)$ is insulin secretion from beta-cells. For the purposes of this dissertation, we are focusing on type 1 diabetes, and thus we are not interested in the insulin secretion module of the GIM. Instead we are interested in the insulin infusion model that was proposed in a later publication [60] as an addition to the GIM.

The insulin infusion model consists of two ODEs that track the mass of monomeric ($I_{sc2}$) and the mass of nonmonomeric ($I_{sc1}$) insulin

$$\frac{dI_{sc1}}{dt} = -(k_d + k_{a1}) \cdot I_{sc1} + IIR(t) \tag{1.54}$$

$$\frac{dI_{sc2}}{dt} = k_d I_{sc1} - k_{a2} I_{sc2}. \tag{1.55}$$

$k_d$ is the rate of dissociation. $k_{a1}$ and $k_{a2}$ are the rate constants of nonmonomeric and monomeric insulin absorption into the circulatory system.

### Addition of Exercise into Meal Glucose-Insulin Model of Type 1 Diabetes

An addition to the GIM to include the effects of physical activity was introduced by Dalla Man and Breton [1, 61]. They chose to include the effects of exercise directly into their expression for *insulin-dependent* glucose uptake, shown here as Equation 1.53. Of the three candidate models for exercise-enhanced insulin-dependent glucose uptake, the one they chose is defined as

$$U_{id} = G_t \frac{V_{m0} \cdot (1 + \beta Y) + V_{mx} \cdot (1 + \alpha Z \cdot W) \cdot (X + I_b) - V_{mx} I_b}{K_m \cdot \big((1 - \gamma Z \cdot W \cdot (X - I_b)\big) + G_t}. \tag{1.56}$$

This model adjusts the Michaelis-Menten constants $V_m$ and $K_m$ by relating them to variables $X$, $Y$, $Z$, and $W$. $X$ is the familiar insulin action (Equation 1.52), $Y$ models the short term *acute* effects of exercise on glucose uptake, and $Z$ and $W$ model the prolonged changes to insulin sensitivity, lasting for several hours after exercise ends. The effect of each of these variables is plotted in Figure 1.16. For full definition of the variables, see [1, 61].

This approach to exercise-modeling introduces several free-parameters, namely $\alpha$, $\beta$, and $\gamma$. These parameters were most likely identified using nonlinear least-squares (details for some parameters are lacking in the original publication).

### Model Review

GIM development was enhanced with access to a large dataset of state of the art metabolic tracer data. This allowed for the identification of many detailed modules, such as a models for liver endogenous glucose production, beta-cell insulin-secretion, gastrointestinal-tract glucose absorption, and renal glucose excretion.

There are several elements of this model that, although important, are beyond the scope of this dissertation. This includes the model for glucose absorption through the gastrointestinal tract which provides an estimate for the output $Ra_{meal}$, and the model for endogenous glucose production, which gives an output of $EGP$. Fortunately in this dissertation we have access to direct measurements for the output of these complex processes, $Ra_{meal}$ and $EGP$. Additionally, the GIM includes a model of insulin secretion $S(t)$. In this dissertation we are dealing with either C-peptide negative T1D subjects (no pancreatic insulin secretion) or healthy subjects in which we have known plasma insulin concentrations from measurement. Thus we have not examined the secretion model. There are also other phenomena considered of secondary importance that were included in the GIM, such as renal excretion. Here, we have not discussed these secondary effects.

The approach to exercise modeling introduced as part the the GIM includes several free-parameters, namely $\alpha$, $\beta$, and $\gamma$. These parameters were most likely identified using nonlinear least-squares. Although numerical parameter identification is generally used in PKPD modeling, it has its pitfalls - specifically its inability to identify robustly parameters for complex models, especially in highly nonlinear models such as the GIM. Still, the results from the GIM exercise addition are reasonable and seem to predict reasonably glucose levels during exercise.

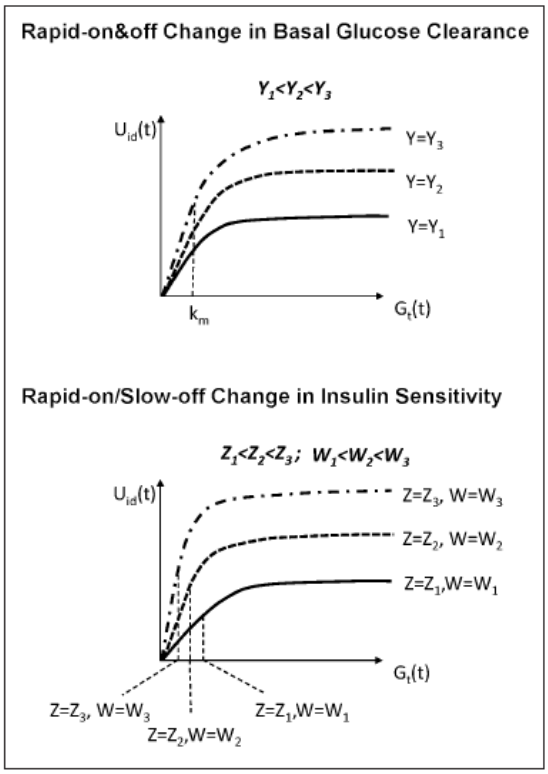


**Figure 5.** Effect of *Y*, *Z*, and *W* on the relationship between tissue glucose [$G_t(t)$] and glucose utilization ($U_{id}$): a rise in *Y* produces an increase in the steady-state value of $U_{id}$, whereas a rise in *Z* and/or *W* produces an increase on both $U_{id}$ steady-state values and its speed of rising.

Figure 1.16: Exercise model included Meal Glucose-Insulin Model of Type 1 Diabetes. Curves show the effects of the various exercise variables $Y$ $Z$ and $W$ on insulin-dependent uptake ($U_{id}$). For full definition of the variables, see [1, 61]. Figure taken from [61], used without permission.

However, the inclusion of the exercise effects in the model maybe not be physiological. These effects are added directly to the *insulin-dependent* glucose uptake function $U_{id}$ even though exercise has been shown to induce glucose uptake largely independent of changes in insulin concentration [35, 39]. Thus actual uptake may not behave in the same saturable manner as that proposed in the GIM. Also, to the author's knowledge, there is no inclusion of the effects of exercise on increasing $EGP$ during exercise. This is a significant weakness of the exercise module in the GIM.

One more criticism of the GIM is the sheer size and complexity of the model. This prevents the non-expert from understanding the important aspects of the model and makes interpretation of the underlying physiology difficult. For example, rate-parameters such as $k_{a2}$ do not relay information about the underlying physical process. It is not clear from explanations given in [61] that $k_{a2}$ is dependent on tissue perfusion and local vascularization (i.e. surface area) which are known to change during exercise. Without physical interpre-

tation it is not clear how, and which, parameters values may change during exercise unless one already has significant prior knowledge of insulin-glucose dynamics. One of the main objectives of this dissertation is to provide a model that makes the physiological mechanisms of insulin-glucose dynamics clear.

Regardless of the critiques, the GIM represents the largest effort in glucose modeling to-date and is one of the most accurate models available. Thanks to continued efforts and over a century of experience between Drs. Cobelli, Dalla Man, Kovatchev, Breton and many others, the GIM has been approved by the FDA as a substitute in lieu of pre-clinical trials [63]. This tool is now being used across the world to test control algorithms for the artificial pancreas. This is a first-of-its-kind achievement, and paves the way for the development of more *in silico* tools that can be used to expedite the development of new medical technologies.

### 1.5.3 Sorensen Model of Insulin-Glucose Kinetics

One of the most comprehensive models of insulin-glucose dynamics was developed by Sorensen in 1984 [64]. The glucose model consists of 8 compartments, the brain vascular space, the brain interstitial space, the lungs and heart, the gut, the liver, the kidney, the peripheral vascular space, and finally the peripheral interstitial space. The governing equations for each of these compartments is shown in Equation 1.57-1.64. An accompanying schematic is shown in Figure 1.17. With 8 compartments, the model has more granularity than most models of glucose metabolism. The GIM has two glucose compartments and the OMM has only one.

The 8 glucose model equations are

$$V_{BV}^{G}\frac{dG_{BV}}{dt} = Q_{B}^{G}\cdot(G_H - G_{BV}) - \frac{V_{BI}}{\tau_B}\cdot(G_{BV} - G_{BI}) \tag{1.57}$$

$$V_{BI}\frac{dG_{BI}}{dt} = \frac{V_{BI}}{\tau_B}\cdot(G_{BV} - G_{BI}) - \mathrm{r}_{BGU} \tag{1.58}$$

$$V_{H}^{G}\frac{dG_{H}}{dt} = Q_{B}^{G}G_{BV} + Q_{L}^{G}G_{L} + Q_{K}^{G}G_{K} + Q_{P}^{G}G_{PV} - Q_{H}^{G}G_{H} - \mathrm{r}_{RBCU} \tag{1.59}$$

$$V_{G}^{G}\frac{dG_{G}}{dt} = Q_{G}^{G}\cdot(G_H - G_{G}) - \mathrm{r}_{GGU} \tag{1.60}$$

$$V_{L}^{G}\frac{dG_{L}}{dt} = Q_{A}^{G}G_{H} + Q_{G}^{G}G_{G} - Q_{L}^{G}G_{L} + \mathrm{r}_{HGP} - \mathrm{r}_{HGU} \tag{1.61}$$

$$V_{K}^{G}\frac{dG_{K}}{dt} = Q_{K}^{G}\cdot(G_H - G_{K}) - \mathrm{r}_{KGE} \tag{1.62}$$

$$V_{PV}^{G}\frac{dG_{PV}}{dt} = Q_{p}^{G}\cdot(G_H - G_{PV}) - \frac{V_{PI}}{\tau_P^G}\cdot(G_{PV} - G_{PI}) \tag{1.63}$$

$$V_{PI}\frac{dG_{PI}}{dt} = \frac{V_{PI}}{\tau_P^G}\cdot(G_{PV} - G_{PI}) - \mathrm{r}_{PGU}. \tag{1.64}$$

Sorensen's model assumes the circulatory system is a closed system, with volumetric blood flow $Q$ through different tissue compartments. The mass flow rate of glucose into

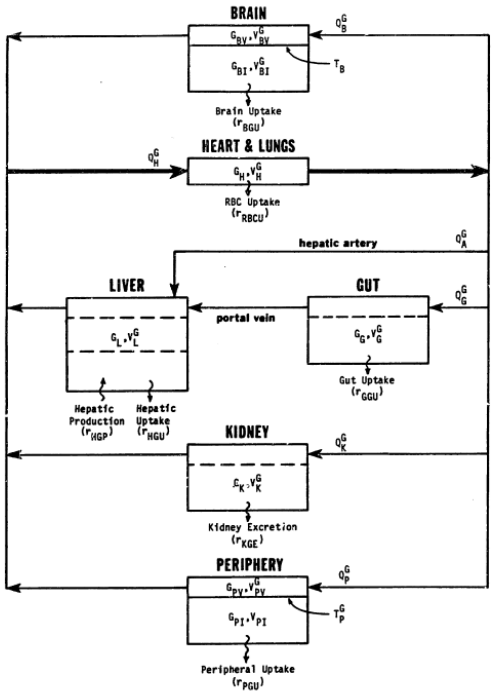


Figure 1.17: Schematic of 8 compartment glucose model of Sorensen [64].

and out of each compartment is accounted for by multiplying the compartment specific $Q$ by the concentration at the inlet and the concentration at the outlet, assumed to be the concentration of the compartment. Glucose metabolism rate r is modeled as a separate rate constant in each compartment.

Sorensen also developed a comprehensive insulin model, made up of 7 compartments. The compartments are the brain, the heart and lungs, the gut, the liver, the kidney, and the periphery. The ODEs governing each compartment are

$$V_B^I \frac{dI_B}{dt} = Q_B^I \cdot (I_H - I_B) \tag{1.65}$$

$$V_H^I \frac{dI_H}{dt} = Q_B^I I_B + Q_L^I I_L + Q_K^I I_K + Q_P^I I_{PV} - Q_H^I I_H \tag{1.66}$$

$$V_G^I \frac{dI_G}{dt} = Q_G^I \cdot (I_H - I_G) \tag{1.67}$$

$$V_L^I \frac{dI_L}{dt} = Q_A^I I_H + Q_G^I I_G - Q_L^I I_L + \mathrm{r}_{PIR} - \mathrm{r}_{LIC} \tag{1.68}$$

$$V_K^I \frac{dI_K}{dt} = Q_K^I \cdot (I_H - I_K) - \mathrm{r}_{KIC} \tag{1.69}$$

$$V_{PV}^I \frac{dI_{PV}}{dt} = Q_p^I \cdot (I_H - I_{PV}) - \frac{V_{PI}}{\tau_P^I} \cdot (I_{PV} - I_{PI}) \tag{1.70}$$

$$V_{PI} \frac{dI_{PI}}{dt} = \frac{V_{PI}}{\tau_P^I} \cdot (I_{PV} - I_{PI}) - \mathrm{r}_{PIC} \tag{1.71}$$

This model has almost an identical structure to the glucose model but there are some key differences. The blood flow rate of the glucose model $Q^G$ is replaced by the plasma flow rate $Q^I$ because insulin does not enter RBCs and the effective flow rate is equivalent to the plasma flow rate. Insulin clearance is only assumed to occur in the liver, kidney, and the periphery.

### Addition of Exercise into the Sorensen Model

Lenart and Parker [65] have added an addition to the Sorensen model to account for exercise. This addition includes a model of glucose uptake in skeletal muscle during exercise and a model for the enhancement of $EGP$ during exercise.

Two main exercise additions were made in [65]. The first was the increase in peripheral glucose uptake (PGU), which was modeled by introducing a third multiplier to the metabolic sink in the peripheral compartment

$$PGU = M^I \cdot M^G \cdot M^E \cdot 35. \tag{1.72}$$

$M^I$, $M^G$, and $M^E$ are dimensionless multipliers representing the effect of insulin, glucose, and exercise respectively on peripheral glucose uptake. Basal peripheral glucose uptake is 35 [mg/min]. $M^I$ and $M^G$ were taken from the previous Sorensen model, and the new addition is the quantity $M^E$ defined as

$$M^E = 1 + \frac{PGU_A \cdot PAMM \cdot 28}{35}. \tag{1.73}$$

$PGU_A$ is the active muscle peripheral glucose uptake rate [mg/min/kg$_{muscle}$] and PAMM is the percent of active muscle mass.

The second exercise addition was to alter the hepatic glucose production ($HGP$ a.k.a. $EGP$) to account for exercise. This was done by introducing another multiplier

$$HGU = M^G \cdot M^I \cdot M^\Gamma \cdot M^E \cdot 155. \tag{1.74}$$

$M^G$, $M^I$, and $M^\Gamma$ are dimensionless multipliers representing the effects of glucose, insulin, and glucagon respectively on $HGP$. The additional exercise multiplier is defined as

$$M^E = 1 + \frac{HGP_A \cdot PAMM}{155}. \tag{1.75}$$

$HGP_A$ is the augmented rate of glucose production [mg/min] in response to exercise and PAMM is the percent active muscle mass.

There was one final, yet secondary, exercise addition, that accounted for the observed increased insulin uptake during exercise. Lenart first assumes that liver and kidney insulin uptake is linearly dependent on the concentration by fixing the product of extraction fraction and flow rate. This essentially models insulin clearance as linearly dependent on insulin concentration. Second, the expression for peripheral insulin uptake was altered to account for the observation by [66] that peripheral insulin uptake increases during exercise.

### Model Review

Sorensen's model is one of the most comprehensive models in the literature. However, the model size makes it intractable to non-experts, and hampers its ability to be used in model predictive control algorithms.

The structure of the model is very regular and easy to follow. The model uses very basic concepts to predict glucose transport, assuming an extraction fraction, a flowrate, and a diffusion time for each tissue. The downside is that many aspects are the model are fixed, and thus it is not clear how to adapt the model to conditions that are different than what is was designed for.

The exercise additions made by Lenart and Parker [65] were straightforward, but may have pitfalls because they assume that $PGU$ and $HGU$ are nonlinear in glucose, insulin, glucagon, and exercise. This nonlinearity can lead to significant overestimates at PGU when all the multiplier terms have significant magnitude. Also, the $HGP$ expression (Equation 1.74) may not be modeled correctly because it was simply added as a multiplier and did not accounting for glucagon.

## 1.6 Dissertation Objective: Develop an Insulin-Glucose Dynamical Model that Includes the Acute Effects of Exercise

Automatic control of blood glucose has long been a goal for management of type 1 diabetes. However, because of the many dangers of safely dosing insulin, a fully autonomous artificial pancreas is still not possible. As discussed in this chapter, exercise is one of the main hurdles to a fully autonomous system. This is because of significant exercise-induced changes to insulin-glucose dynamics that exasperate the already significant difficulty of accounting for the long time-lag of subcutaneously injected insulin. One method for automated control in the artificial pancreas is model predictive control [29, 67–69]. Model predictive control, because it makes dosing decisions based not just on the current state, but predicted states, is likely the best suited control technique for handling exercise. However, control actions based on model predictions are only as good as the predictions themselves. For this reason, it is important to have a high-fidelity and robust model. For the case of exercising with T1D, optimal control can be achieved if the model is able to make reliable predictions of glucose levels during exercise.

**The objective** of this dissertation is to develop an insulin-glucose dynamics model that includes the acute (i.e. immediate) effects of exercise. This model can eventually be used as a critical component of an artificial pancreas control system. We will develop this model with the following principles in mind:

- *Physiology-based.* We wish to keep the model grounded in concrete physical mechanisms, rather than using ambiguous parameters that are derived from curve fitting.
- *Independently measured parameters.* To prevent overfitting of the model, we wish to utilize parameters that were measured or derived from independent studies.
- *Parsimony.* The model will only be made as complex as necessary. We wish to capture the important physical mechanisms associated with insulin-glucose dynamics and exercise, but we do not want the model to have so many states and complexities that it would be difficult for a well-trained engineer to understand. Additionally, model complexity makes model predictive control more difficult. We will use phenomenological models when necessary to avoid the complexities of biochemistry.

To achieve a *physiology-based* model some processes will be handled though direct modeling of diffusive mass-transfer. Other processes will be modeled using traditional pharmacokinetic compartmental models. Bridging these two approaches amounts to a *multiscale* model.

When developing the model, we will include what we believe are the important mechanisms that govern insulin-glucose dynamics during exercise:

- Capillary recruitment

- Endogenous glucose production ($EGP$)
- Skeletal muscle glucose uptake

By including these mechanisms into a complete model we hope to gain insight into their relative contributions to glucose uptake during exercise. We anticipate that an understanding of these mechanisms will give insight into many phenomena such as insulin-resistance associated with poor capillary recruitment, the effect of insulin-on-board on EGP, as well as many others.

With these principles and goals in mind, we will derive a insulin-kinetics model in Chapter 2 and a glucose-dynamics model in Chapter 3. In Chapter 4 we will couple the two models for application to a T1D subject and compare model predictions to clinical data. Then finally, the model will be demonstrated with 10 test cases in Chapter 5.

# Chapter 2

# Modeling the Acute Effects of Exercise on Insulin-Kinetics

## Chapter Overview

Insulin is a hormone that promotes glucose uptake in various tissues, and it is critically important in maintaining glucose homeostasis in humans. This chapter focuses on developing a model of insulin pharmacokinetics during exercise (Figure 2.1). Pharmacodynamics aspects

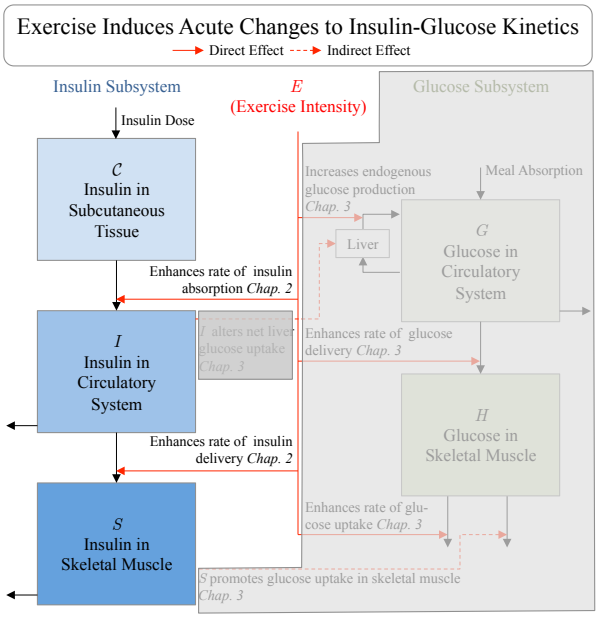


Figure 2.1: The focus of this chapter will be on the insulin model (unshaded region). The rate that insulin moves between regions depends on the exercise intensity $E$ (red arrows). The glucose model in the shaded region will be presented in Chapter 3.

of insulin on glucose uptake will be presented in Chapter 3.

Section 2.1 includes background information about the importance of insulin-kinetics and some background. In Section 2.2, the insulin-kinetics model is derived. For brevity, some details of the derivation are relegated to Appendix A. Section 2.3 will present model verification and results, and a discussion will follow in Section 2.4.

## 2.1 Introduction

Persons with type 1 diabetes (T1D) must inject insulin to survive. The preferred method of delivery is an injection into the subcutaneous tissue (SC). After injection, insulin is slowly absorbed into the bloodstream, and then eventually delivered to insulin sensitive tissues, where its availability facilitates glucose metabolism [44, 70].

Though the SC injection method is safe and mostly painless, the rates of insulin absorption and insulin delivery are highly variable from one injection to the next and from person to person. The problem with this variability is that if insulin becomes available too quickly, hypoglycemia can occur, causing dizziness and/or fainting. On the other hand if the insulin becomes available too slowly, then hyperglycemia can occur, causing adverse long-term health effects. This difficulty prevents us from predicting and accounting for the long time-delay from insulin injection to availability in tissue, and it is one of the main reasons robust and safe automated insulin dosing algorithms have not yet been developed.

Predicting insulin availability becomes even more difficult during exercise because not only do glucose metabolism rates change due to increased glucose demand, but insulin absorption rates from subcutaneous tissue (SC) ($k_a^I$) and delivery rates to skeletal muscle (SM) ($k_d^I$) have also been shown to increase [41–43, 71–74]. It has been postulated that the observed changes are caused by an increase in blood flow rate [75–77] and some studies have also shown that injection site location has a significant effect [42, 72, 77]. Increased delivery rate has also been associated with an increase in microvascular blood volume (MBV) [43, 73, 74].

These studies have been illuminating and have shown experimental correlation between blood flow, MBV, and $k_a^I$ and $k_d^I$, however many lack a rigorous treatment of the underlying transport phenomena. In the same vein, most models of insulin absorption in the literature are data-driven where experimental data is used to identify simple kinetic parameters [78]. These approaches are expedient and indeed useful from an engineering standpoint, however they unfortunately circumvent inclusion of the underlying transport phenomena and physiology of the problem. Indeed, when a more mechanistic model is available, it may be possible to improve designs of algorithms for control of treatments. To bridge the gap between observations and physiology, a rigorous treatment of the underlying transport phenomenon is needed. The focus of this study is to derive a physiology-based pharmacokinetic (PBPK) model to elucidate the relationship between $k_a^I$, $k_d^I$, and exercise intensity $E$. We draw on concepts from the research area of microcirculation and nutrient delivery [79]. Drug and nutrient delivery are typically characterized by two parameters: the capillary tissue perfusion

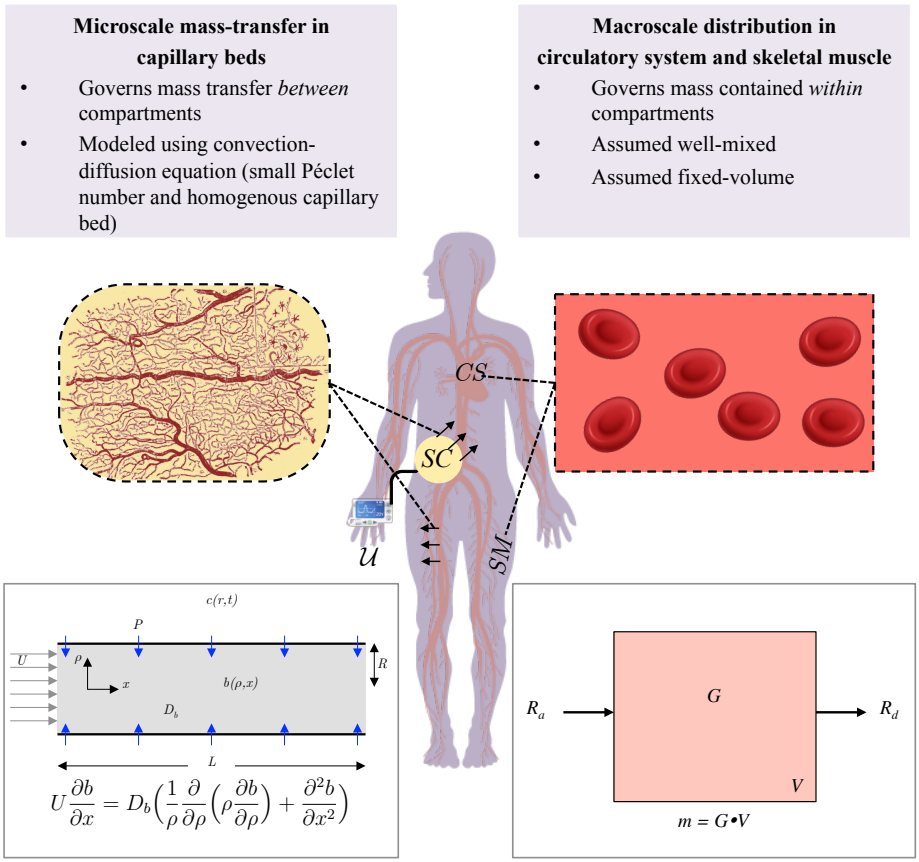


Figure 2.2: A multiscale approach is used to model insulin-kinetics.

rate ($Q$) and capillary permeability surface area ($PS$). These parameters characterize mass-transfer *between* different regions in the body and will be modeled at the *microscale*, where diffusion is handled directly through solution of the convection-diffusion equation. Insulin distribution *within* different regions in the body will be modeled at the *macroscale* using a compartmental approach. This multiscale approach is illustrated in Figure 2.2.

This chapter is laid out as follows: first, the theory and mathematics that underlie the insulin kinetics model will be explained. Because the model is derived from fluid mechanics that utilize partial differential equations (PDE) to describe the fields of interest, we will use scaling arguments to convert the PDE models into simpler ordinary differential equation (ODE) models. The parameters of the model are taken from the literature and their validity will be discussed. The accuracy of the derived model will be demonstrated on T1D human data taken from a group of resting subjects and a separate group of exercising subjects. The predicted plasma insulin concentrations will be compared to average measurements from these two cohorts. The physical interpretation of the model, the prediction accuracy, and

the implications on glucose metabolism and closed loop control will be discussed.

## 2.2 Methods

### 2.2.1 Model Development

#### System Overview

Insulin-kinetics is modeled in five steps: insulin pump infusion into the interstitial fluid of the subcutaneous (SC) tissue, diffusion into SC absorbing capillaries and convection into the circulatory system (CS), mixing and distribution in the CS, convection into skeletal muscle (SM) delivering capillaries and diffusion into the interstitial fluid (ISF), and finally clearance by the liver/kidneys in the CS and clearance by insulin degradation in the the SM. The abstract model is shown schematically in Figure 2.3(left) and in physiological detail in Figure 2.3(right). Absorbing and delivering capillaries are part of the SC and SM domain, respectively.

The human silhouette of Figure 2.3 shows that each domain exists at a different volume scale. The SC domain is only a few milliliters and is defined as only the SC tissue in contact with infused insulin. The CS domain is a few liters, and it is defined as being all the blood that is confined to the larger vessels and organs. The SM domain is tens of liters and it is defined as being all the skeletal muscle tissues and it also includes other SC tissues that are not a part of the SC domain because they are not in close proximity to the infusion site. It is worth mentioning that both capillaries and ISF are contained in the SC and SM domains, and that blood in the capillaries makes up only a small fraction ($< 1\%$ [80, p. 220]) of the volume of these domains. Hence the capillary volume is not included as part of the volume of distribution.

#### Note on Nomenclature

The model consists of multiple domains, each with their own domain specific parameters. In order to be specific with nomenclature, subscripts and superscripts will be used to denote the domain (SC, CS, or SM) and the substance that the parameter belongs to, respectively. In some cases, a parameter will be normalized by either a mass or volume, and will be denoted by a second subscript, $_N$. As an example

$$V^I_{SM_N} \tag{2.1}$$

is the normalized volume of distribution of insulin ($I$)in the skeletal muscle (SM) domain. In some equations a peculiar volume parameter shows up with a superscript $^{tiss}$. This indicates a volume of tissue, rather than a volume of distribution.

#### Interstitial Fluid of the Subcutaneous Domain

The SC domain consists of ISF and capillaries. In this section we will consider the dynamics of the insulin in the ISF. A Following section will consider the dynamics of the capillaries.

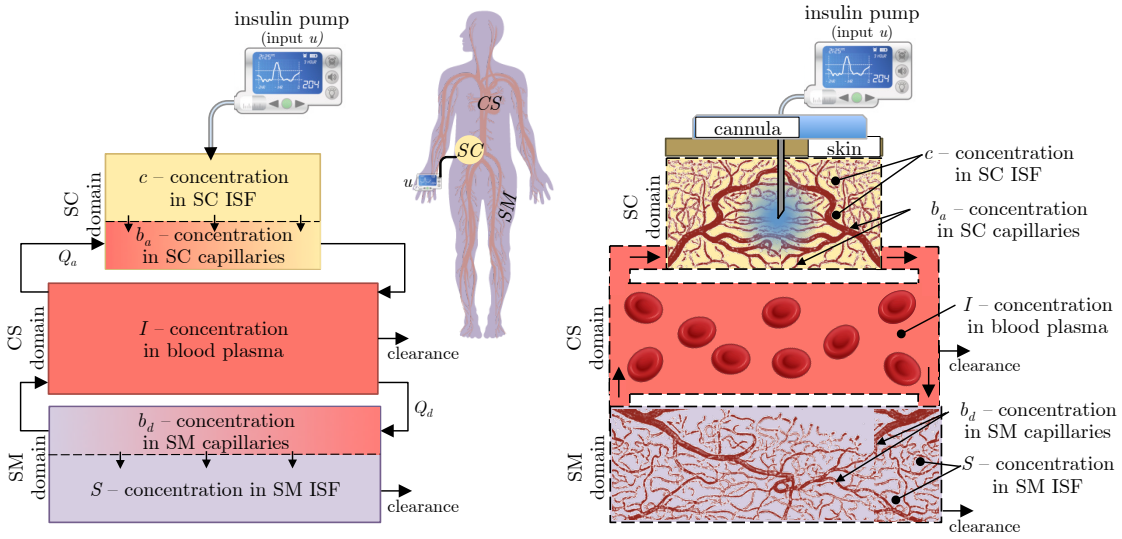


Figure 2.3: (left) Abstract schematic of the proposed insulin model. (right) Physiological representation of model. The model consists of three distinct domains: the subcutaneous (SC) domain, the circulatory system (CS) domain, and the skeletal muscle (SM) domain. The human silhouette illustrates that each domain exists at a different volume scale: the SC domain consists of only tissue in the vicinity of the infusion site, and is order of milliliters, the CS domain is order of a few liters, the SM domain is order of tens of liters. The SM domain contains both the SM tissue and the SC tissue that is not in the vicinity of the infusion site. Capillaries and ISF are both contained in the SC and SM domains, and each have their own separate dynamics. $c$ is the concentration in the SC ISF, which we integrate over to obtain $\mathcal{C}$. Insulin is infused into the SC tissue where the total mass is $\mathcal{C}$, then it diffuses into the *absorbing* capillaries where its concentration is $b_a$, then is convected into the CS where its concentration is $I$, then is convected into the SM *delivering* capillaries were its concentration is $b_d$, and finally diffuses into the SM ISF where its concentration is $S$. Arrows show insulin clearance directly from the CS by the liver and kidneys. Clearance also occurs in the SM tissue by insulin degradation. Blood flows at a tissue perfusion rate of $Q_a^I$ and $Q_d^I$ through the SC tissue and SM tissue, respectively.

Insulin is infused directly into the ISF of the SC tissue. The SC ISF consists of only the ISF in the vicinity of the infusion and not the ISF of the rest of the body. We assume a continuous and homogeneous SC domain and the concentration of insulin $c(r,t)$ in the ISF is governed by the spherical diffusion equation, with one source and one sink. The source $u$ represents the insulin pump infusion rate per unit volume. The sink $\dot{m}_a$ represents the absorption mass flow rate per unit volume. $D_{ISF}$ is the diffusion coefficient of insulin in the

ISF and $c_o(r)$ is the initial concentration profile of insulin.

$$\frac{\partial c}{\partial t} = D_{ISF}\frac{1}{r^2}\frac{\partial}{\partial r}\Big(r^2\frac{\partial c}{\partial r}\Big) - \dot{m}_a + u \tag{2.2}$$

subject to

$$c = c_o(r) \text{ at } t = 0 \text{ for all } r \tag{2.3}$$

$$\frac{\partial c}{\partial r} = 0 \text{ at } r = 0 \tag{2.4}$$

$$\frac{\partial c}{\partial r} = 0 \text{ as } r \to \infty. \tag{2.5}$$

The two boundary conditions 2.4 and 2.5 are symmetric and zero flux conditions, respectively, at the center and the outer boundary of the SC domain. To simplify the model, we convert the PDE into an ODE by applying the assumption of an infinite and homogeneous SC domain. We integrate Equation 2.2 over an arbitrarily large volume of SC tissue, $V_{SC}^{tiss}$, to get

$$\frac{\partial}{\partial t}\int_{V_{SC}^{tiss}} c\ dV = D_{ISF}\int_{V_{SC}^{tiss}} \nabla^2 c\ dV - \int_{V_{SC}^{tiss}} \dot{m}_a\ dV + \int_{V_{SC}^{tiss}} u\ dV \tag{2.6}$$

Note that the precise value of $V_{SC}^{tiss}$ is inconsequential as we integrate over an arbitrary but sufficiently SC large volume to capture all the insulin wetted tissue. The integral of the diffusive term ($\nabla^2 c$) is zero by application of the divergence theorem and BC 2.5 (shown in Appendix A.1). We define three new variables: $\mathcal{C}$ [Units(U)] is the total dose residing in the SC domain or the insulin-on-board(IOB), $\mathcal{U}$ is the insulin infusion rate [U/min] (from the pump), and $\dot{\mathcal{C}}_a$ is the mass flow rate of insulin absorbed from the ISF [U/min] into the capillaries.

$$\mathcal{C} = \int_{V_{SC}^{tiss}} c\ dV \tag{2.7}$$

$$\mathcal{U}(t) = \int_{V_{SC}^{tiss}} u\ dV \tag{2.8}$$

$$\dot{\mathcal{C}}_a = \int_{V_{SC}^{tiss}} \dot{m}_a\ dV. \tag{2.9}$$

Because we have integrated in space, we now have a single ODE that governs the ISF in the SC domain

$$\frac{\partial \mathcal{C}}{\partial t} = -\dot{\mathcal{C}}_a + \mathcal{U}(t) \tag{2.10}$$

subject to

$$\mathcal{C} = \mathcal{C}_o \text{ at } t = 0 \tag{2.11}$$

where $\mathcal{C}_o$ is the volume integral of $c_o(r)$ which is equal to the total insulin initially present in the SC tissue, or the initial IOB. The form of $\dot{\mathcal{C}}_a$ will be defined in a coming section.

### Circulatory System Domain

The CS domain is the intermediate domain between the SC domain, where insulin is absorbed, and the SM domain, where the insulin is delivered. $\mathcal{I}$ denotes the total mass of insulin in the CS domain, and insulin is confined to the blood plasma at concentration $I$. To model the insulin in the CS, we assume that mixing occurs rapidly and is therefore uniformly distributed. This allows us to use a traditional single compartment model. To derive this model, we start with a simple mass balance for insulin

$$\frac{d\mathcal{I}}{dt} = \dot{\mathcal{I}}_{in} - \dot{\mathcal{I}}_{out} - \dot{\mathcal{I}}_{cl}. \tag{2.12}$$

where, $\dot{\mathcal{I}}_{in}$ is the insulin mass flow into the CS domain via convection, $\dot{\mathcal{I}}_{out}$ is the insulin mass flow out of the CS domain via convection, and $\dot{\mathcal{I}}_{cl}$ is the plasma insulin clearance rate. The control volume around the CS in Figure 2.3 shows two entrances and two exits, we specify these for the absorbing (subscript $_a$) and the delivering (subscript $_d$) capillaries as

$$\dot{\mathcal{I}}_{in} = \dot{\mathcal{I}}_{in_d} + \dot{\mathcal{I}}_{in_a} \tag{2.13}$$

$$\dot{\mathcal{I}}_{out} = \dot{\mathcal{I}}_{out_d} + \dot{\mathcal{I}}_{out_a} \tag{2.14}$$

We express Equation 2.12 as a concentration $I$ using the well-mixed assumption, $\mathcal{I} = V_{CS}^I \cdot I$, where $V_{CS}^I$ is the volume of distribution of insulin in the CS domain. For clearance we assume a linear model for the plasma insulin clearance rate, $\mathcal{I}_{cl} = \mathrm{r}_{CS}^I \cdot I$ [81], where $\mathrm{r}_{CS}^I$ [mL/min] is the rate constant for the clearance of insulin from the CS domain. We substitute these relationships into 2.12 along with Equations 2.13 and 2.14 to obtain

$$\frac{dI}{dt} = \frac{\dot{\mathcal{I}}_{in_d} + \dot{\mathcal{I}}_{in_a} - \dot{\mathcal{I}}_{out_d} - \dot{\mathcal{I}}_{out_a}}{V_{CS}^I} - \mathrm{r}_{CS_N}^I \cdot I. \tag{2.15}$$

$\mathrm{r}_{CS_N}^I = \mathrm{r}_{CS}^I / V_{CS}^I$ [1/min] is the volume normalized rate constant for the clearance of insulin from the CS domain.

### Absorbing and Delivering Capillaries

Insulin is absorbed from the SC domain into the capillaries by permeating the capillary wall through endothelial pores and junctions [37]. It is delivered to the SM tissue in the same manner. We assume that the absorption and delivery processes are driven by pure diffusion (i.e. flux is driven only by concentration gradients). This assumption allows us to model the physics of absorption and delivery identically. The only difference between the two are parameter values and the sign of the flux. Generally, $b$ will denote the concentration of insulin in a capillary. More specific, $b_a$ will denote the concentration in an absorbing SC capillary and $b_d$ will denote the concentration in a delivering SM capillary. We find the

solution for the general concentration $b$, and then apply it to both domains to find $b_a$ and $b_d$ by simply applying domain specific parameters.

First, we assume that our single capillary model has uniform properties along its length. We will also assume that the capillary bed is homogeneous, i.e. each capillary in the domain has identical properties, and is uniformly perfused at tissue perfusion rate $Q$. In the real case, properties and $Q$ are heterogeneous, and thus our assumption will prevent us from capturing some non-linear effects. However, because capillaries have a low permeability to insulin the effects of heterogeneity will be small [38].

The concentration $b$ in a capillary is governed by the cylindrically symmetric convection-diffusion equation with axial flow only. A schematic of this flow is shown in Figure 2.4 (left) and the corresponding BVP for $b$ is defined in Equations 2.16 to 2.19. In the BVP, $D_b$ is the diffusion coefficient of insulin in blood plasma, $U$ is the plasma flow velocity in the axial direction $x$, $R$ is the radius of the vessel in the radial direction $\rho$, $L$ is the length of the vessel, and $P$ is the permeability of the vessel wall

$$U\frac{\partial b}{\partial x} = D_b\Big(\frac{1}{\rho}\frac{\partial}{\partial \rho}\Big(\rho\frac{\partial b}{\partial \rho}\Big) + \frac{\partial^2 b}{\partial x^2}\Big) \tag{2.16}$$

subject to

$$b = I \text{ at } x = 0 \text{ for } \rho = [0, R] \tag{2.17}$$

$$\frac{\partial b}{\partial \rho} = 0 \text{ at } \rho = 0 \tag{2.18}$$

$$q = P(c - b) \text{ at } \rho = R. \tag{2.19}$$

We assume a linear concentration gradient across the capillary wall and we use permeability $P$ to relate flux at the wall to the concentration on each side of the wall. $c$ is the concentration in the ISF that surrounds the capillary and $I$ is the concentration at the inlet, which we assume is equal to the concentration in the CS.

The BVP and corresponding schematic shows that $b$ is directly dependent on $\rho$ and $x$. In addition to this local spatial dependence in the capillary domain, $b$ is also dependent on time, $t$, and on its global location in the ISF domain, $r$, through the boundary conditions Equation 2.17 and Equation 2.19. Thus, in general $b(\rho, x, I(t), c(r, t))$. Fortunately, because we have a separation of time and length scales between the SC ISF, the SC capillaries, and the CS, we can treat $I(t)$ and $c(r, t)$ as fixed when solving $b$. This also allows us to approximate $\partial b/\partial t \approx 0$ (no accumulation in capillaries). We further simplify by arguing that because we have a moderate Péclet number (Pe) [82] and a large aspect ratio (AR), we can convert the PDE 2.16 in $\rho$ and $x$ to an ODE that only depends on $x$. Details of the simplifications can be found in Appendix A.2, But, the main results are that: (1) we have a low Péclet number and thus the concentration boundary layer is large and the radial concentration gradient is small and (2) blood rapidly traverses a capillary, and thus we can hold $I$ and $c$ constant when solving for $b$. Mathematically this allows us to make the approximation $b(\rho, x, I(t), c(r, t)) \approx b(x)$.

The ODE that results from the simplifications is

$$\frac{db}{dx} = \Big(\frac{P2\pi RL}{U\pi R^2}\Big)\frac{1}{L}(c-b). \tag{2.20}$$

$$b = I \text{ at } x = 0 \tag{2.21}$$

In examining this coefficient, we notice that $P2\pi RL$ is the permeability surface area ($PS$) and $U\pi R^2$ is the volume flow rate ($Q$) of a cylindrical capillary. The solution to the ODE is (Details in Appendix A.3)

$$b(x,r,t) = c(r,t) - (c(r,t) - I(t))e^{-\frac{PS}{Q}\frac{x}{L}} \tag{2.22}$$

$b$ describes the concentration along the length of a cylindrical capillary as a function of axial position $x$, SC location $r$, and $t$. Remember that $r$ and $t$ were arbitrarily fixed when solving for $b$ locally, but $b$ is a field variable that depends on time and the location in the SC domain through BCs. Thus by allowing BCs to vary with $r$ and $t$, the solution is valid for both the absorption and delivery processes.

The absorption solution is therefore determined, subject to domain specific parameters and variables for $PS$ and $Q$. $PS_a^I$, $Q_a^I$, and $c$ are used for the absorption solution and $PS_d^I$, $Q_d^I$, and $S$ are used for the delivery solution (replace $c$ with $S$). Note that the solution is only dependent on the ratio of parameters $PS$ and $Q$. The ratio of these two parameters tells us whether the absorption/delivery rate is limited by convection (flow limited) or by diffusion (surface area limited). As will be seen, because of the low permeability of capillaries to insulin, this problem is surface area limited.

### Interstitial Fluid of the Skeletal Muscle Domain

We chose to include a model of insulin delivery to SM because it is well known that insulin action occurs in a compartment remote from plasma insulin which has been identified as the ISF [70]. To model the ISF of the SM domain, we start with a simple mass balance on a single compartment model

$$\frac{d\mathcal{S}}{dt} = \dot{\mathcal{S}}_d - \dot{\mathcal{S}}_{cl}. \tag{2.23}$$

Here $\mathcal{S}$ is the total amount of insulin present in the SM ISF, $\dot{\mathcal{S}}_d$ is the insulin delivery mass flow rate by capillaries, $\dot{\mathcal{S}}_{cl}$ is the insulin mass flow rate due to clearance.

We wish to express Equation 2.23 in terms of $S$, the insulin concentration in the SM ISF. To do this we need to assume that the compartment is well mixed so that $\mathcal{S} = V_{SM}^I \cdot S$, where $V_{SM}^I$ is the volume of distribution of insulin in the SM. To test this assumption, we can compare the timescale of delivery to the timescale of spreading through the ISF. The timescale of delivery is the diameter of a capillary, $2R$, divided by the permeability of a vessel to insulin, $P^I$. The timescale of spreading is the diffusion distance squared, which in our case is the intercapillary distance ($ICD$) squared, divided by the diffusivity in the ISF,

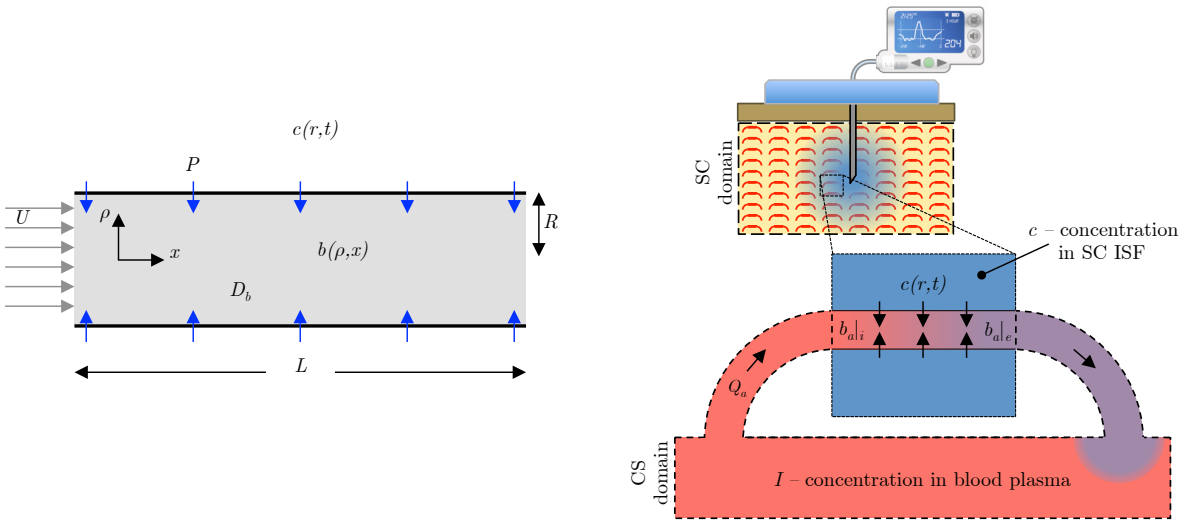


Figure 2.4: (left) Schematic of flow in a capillary. Blood enters from the left at uniform velocity $U$ and concentration initial concentration $b|_i$. $D_b$ is the diffusion coefficient in blood plasma. $L$, $R$, and $P$ are the capillary length, radius, and permeability, respectively. The outer vessel walls is assumed to have a uniform drug concentration $c(r,t)$, evaluated at a fixed $r$ and $t$. (right) Zoomed out view of a single capillary in the subcutaneous (SC) domain, hence $b_a$ instead of the general $b$. The light blue in the background represents the region of drug wetted SC tissue with homogeneous capillaries (red pipes) uniformly distributed. Each capillary can be thought to act as a local mass-exchanger with inlet concentration $b_a|_i$ and exit concentration $b_a|_e$. By integrating over the entire volume of drug-wetted SC tissue, $V_{SC}^{tiss}$ we obtain the total drug absorbed from the SC tissue per unit time, $\dot{\mathcal{C}}_a$.

$D_{ISF}$. Using $R = 3 \cdot 10^{-4}$ cm, $P^I = 10^{-6}$ cm/s, $ICD = 10R$, and $D_{ISF} = 10^{-6}$ cm$^2$/s, the timescale of delivery is $10^3$ s and the timescale of spreading through the SM ISF is 10 s. Because spreading occurs much more quickly than delivery, we can assume the SM ISF compartment to be well-mixed. As with the CS domain, we also assume linear clearance $\dot{\mathcal{S}}_{cl} = \mathrm{r}^I_{SM} \cdot S$. Substituting into Equation 2.23 we get

$$\frac{dS}{dt} = \frac{\dot{\mathcal{S}}_d}{V^I_{SM}} - \mathrm{r}^I_{SM_N} \cdot S. \tag{2.24}$$

### Coupling the Domains

Now that we have an expression for each domain, our next goal is to couple the domains. We do this by relating the fluxes across the domain boundaries.

In quasi-steady state, a control volume around the SC domain (shown by dotted line in Figure 2.3 (right)) reveals that the insulin absorbed from SC tissue is simply equal to the

insulin mass flow rate out of the domain, minus the mass flow rate into the domain

$$\dot{\mathcal{C}}_a = \dot{\mathcal{I}}_{in_a} - \dot{\mathcal{I}}_{out_a}. \tag{2.25}$$

If we apply the same logic to the SM domain and accounting for the change in sign, we have the relation

$$\dot{\mathcal{S}}_d = -(\dot{\mathcal{I}}_{in_d} - \dot{\mathcal{I}}_{out_d}). \tag{2.26}$$

Because the mass flow rate of insulin crossing the boundary between the capillary domain and the plasma domain is the volume flow rate times the concentration, we can express the convective fluxes into about out of the CS domain (see Figure 2.4(right)) as functions of the insulin concentration and volume flow rate

$$\dot{\mathcal{I}}_{in_a} = \int_{V_{SC}^{tiss}} Q_a^I b_a|_e \; dV = \int_{V_{SC}^{tiss}} Q_a^I \big(c - (c-I)e^{\frac{-PS_a^I}{Q_a^I}}\big) \; dV \tag{2.27}$$

$$\dot{\mathcal{I}}_{out_a} = \int_{V_{SC}^{tiss}} Q_a^I b_a|_i \; dV = \int_{V_{SC}^{tiss}} Q_a^I I \; dV \tag{2.28}$$

$$\dot{\mathcal{I}}_{in_d} = \int_{V_{SM}^{tiss}} Q_d^I b_d|_e \; dV = \int_{V_{SM}^{tiss}} Q_d^I \big(S - (S-I)e^{\frac{-PS_d^I}{Q_d^I}}\big) \; dV \tag{2.29}$$

$$\dot{\mathcal{I}}_{out_d} = \int_{V_{SM}^{tiss}} Q_d^I b_d|_i \; dV = \int_{V_{SM}^{tiss}} Q_d^I I \; dV \tag{2.30}$$

Where we have evaluated $b$ in Equation 2.22 at $x = 0$ or $x = L$ for inlet $_i$ and exit $_e$, respectively. Parameters are made specific to either the absorption or delivery capillaries.

We now substitute Equations 2.27 and 2.28 into 2.25

$$\dot{\mathcal{C}}_a = \int_{V_{SC}^{tiss}} Q_a^I \big(c - (c-I)e^{\frac{-PS_a^I}{Q_a^I}} - I\big) \; dV \tag{2.31}$$

$$\dot{\mathcal{C}}_a = Q_a^I (1 - e^{\frac{-PS_a^I}{Q_a^I}}) \int_{V_{SC}^{tiss}} c - I \; dV \tag{2.32}$$

$$\dot{\mathcal{C}}_a = Q_a^I (1 - e^{\frac{-PS_a^I}{Q_a^I}}) \mathcal{C}. \tag{2.33}$$

We have assumed uniform tissue properties $Q_a^I$ and $PS_a^I$. The final equality is a result of assuming that $c \gg I$. This is a valid assumption considering that initially $c$ is highly concentrated ($10^8$ $[\mu U/mL]$ out of the vial), which is much greater than $I$ ($10^2$ $[\mu U/mL]$) because insulin is highly diluted in the CS domain.

Similarly, we substitute Equations 2.29 and 2.30 into 2.26

$$\dot{\mathcal{S}}_d = -\int_{V_{SM}^{tiss}} Q_d^I \big(S - (S-I)e^{\frac{-PS_d^I}{Q_d^I}} - I\big) \; dV \tag{2.34}$$

$$\dot{\mathcal{S}}_d = Q_d^I V_{SM}^{tiss} (1 - e^{\frac{-PS_d^I}{Q_d^I}})(I - S). \tag{2.35}$$

$S$ and $I$ are pulled out of the integral because they not spatially dependent. The parameter $Q_d^I V_{SM}^{tiss}$ results because $Q_d^I$ is volume flow of blood per unit volume of tissue and we need the total flow rate through the SM to quantify total mass flux. This is not the case in Equation 2.33 because $\mathcal{C}$ has units of mass, rather than concentration.

Equations 2.25, 2.26, 2.33, and 2.35 are substituted into Equations 2.10, 2.15, and 2.24 to obtain the final form of the insulin model, shown in the model summary section.

The main dynamics of the SC and SM capillary beds are contained within the general rate parameter

$$k = Q(1 - e^{-\frac{PS}{Q}}). \tag{2.36}$$

We define the rate constants of absorption and delivery as

$$k_a^I = Q_a^I(1 - e^{\frac{-PS_a^I}{Q_a^I}}) \tag{2.37}$$

$$k_d^I = Q_d^I(1 - e^{\frac{-PS_d^I}{Q_d^I}}). \tag{2.38}$$

Both depend on the tissue perfusion rate $Q$ and the permeability surface area $PS$ in their respective tissues. $k_d^I$ is plotted in Figure 2.9 as function of exercise intensity $E$.

We have independently derived $k$ for the purposes of modeling insulin absorption. A similar solution was previously derived for the purposes of studying the microcirculation and nutrient delivery by Renkin [79] and further discussed in [38]. To our knowledge this is the first time this parameter has been used for the purposes of modeling insulin absorption.

### 2.2.2 Inputs and Parameters

Some model parameters are taken directly from the literature, and others need to be derived from physiologically based assumptions. All the parameters are summarized in Table 2.1.

#### Exercise Intensity, *E*

For the parameters that are dependent on exercise, we define a new input, $E$, to quantify exercise intensity. We define $E$, as a ratio of $\mathrm{V0}_{2_{max}}$

$$E = \frac{\mathrm{V0}_2}{\mathrm{V0}_{2_{max}}}. \tag{2.39}$$

$E = 0$ is at rest and $E = 1$ is at maximal exercise. $E$ is a continuous input to the insulin absorption model. Specifically, $Q$ and $PS$ will depend directly on $E$, and the magnitudes $Q$ and $PS$ will directly determine the insulin absorption and delivery rates $k$.

### Tissue Perfusion Rate, $Q$

The tissue perfusion rates, $Q$, in the SC tissue and SM tissues have been quantified in many studies, at rest and during exercise [83, 84]. Our goal is to incorporate how $Q$ changes with exercise level. Saltin [84] measured leg blood flow (LBF) at different levels of cardiac output (CO) and found a linear relation. If we assume that LBF is equivalent to $Q$ and that CO is proportional to $\mathrm{V0}_{2_{max}}$, then we can use the data of Saltin to define a linear relationship between $Q_d^I$ and $E$

$$Q_d^I(E) = (1-h)\cdot(Q_{d_{rest}} + \lambda_d E) \text{ [mL}_b\text{/mL}_{tiss}\text{/min]} \tag{2.40}$$

Where $Q_{d_{rest}}$=0.038 [mL$_b$/mL$_{tiss}$/min] is the resting value of blood flow from [83] and the slope of $\lambda_d$=1.1 [mL$_b$/mL$_{tiss}$/min per $E$] comes from Saltin's relationship between LBF and CO [84]. The factor $h$ represents the hematocrit (assumed 40%) and accounts for the fact that insulin does not enter red blood cells and so the effective flow rate for insulin is only 60% that of whole blood. Note that for convenience we have to converted from customary units of $Q$ [mL$_b$/100g$_{tiss}$/min] to [mL$_b$/mL$_{tiss}$/min] using an average tissue density of 1 [g/mL$_{tiss}$], which falls between the average tissue density for SC (0.91 g/mL$_{tiss}$) tissue and SM tissue (1.09 g/mL$_{tiss}$) [85].

We can use a similar approach to define a linear relationship between $Q_a^I$ and $E$. We assume a linear relationship between $Q_a^I$ and $E$ and then fit a line to data from literature on resting and exercising adipose tissue blood flow (ATBF). Resting ATBF is $Q_{a_{rest}} = 0.028$ [mL$_b$/mL$_{tiss}$/min] [83]) and ATBF at moderate intensity exercise ($E \approx 0.5$) is taken to be on average 0.063 [mL$_b$/mL$_{tiss}$/min] [71, 86–88]). We fit a line to these two data points an obtain slope $\lambda_a = 0.0705$ [mL$_b$/mL$_{tiss}$/min per $E$] to obtain

$$Q_a^I(E) = (1-h)\cdot(Q_{a_{rest}} + \lambda_a E) \text{ [mL}_b\text{/mL}_{tiss}\text{/min]} \tag{2.41}$$

$Q_d^I$ and $Q_a^I$ are plotted in Figure 2.5. At rest the blood flow in the two different types of tissues are nearly the same, but as expected SM is much more sensitive to exercise than SC tissue. $Q_d^I$ experiences a more than 20-fold increase at maximum exercise vs. a mere 2-fold increase in $Q_a^I$.

### Permeability Surface Area, $PS$

PS is a measure of how permeable a capillary bed is to a certain solute. Many theorize that $PS$ increases during exercise because capillary recruitment increases the overall surface area in exercising muscle by fully perfusing capillaries that are underutilized at rest [89–91]. Renkin was one of the first to show this in a 1966 paper [91] where he demonstrated a near doubling of $PS$ during muscle contractions, shown in Figure 2.6.

In light of this study, capillary recruitment has been identified as a potentially important mechanism for the enhancement of nutrient exchange and delivery during exercise. Many others have sought to quantify capillary recruitment. One of the most popular proxies for

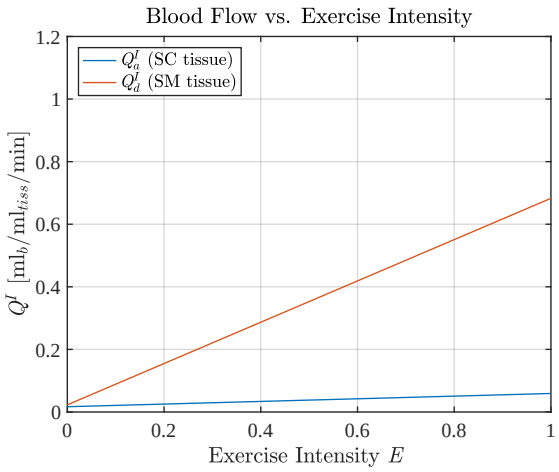


Figure 2.5: The blood flow relationship to be used in the proposed insulin absorption and delivery model. Tissue perfusion rate $Q^I$ is assumed to be linearly dependent on exercise intensity $E$. $Q_d^I$, the flow rate in skeletal muscle (SM), is much more sensitive to exercise than the flow rate in subcutaneous (SC) tissue $Q_a^I$, indicated by a 20-fold increase, compared to a mere 2-fold increase. Note that we have assumed 40% hematocrit and so $Q^I = 0.6Q$.

recruitment is the quantification of microvascular blood volume (MBV) by contrast enhanced

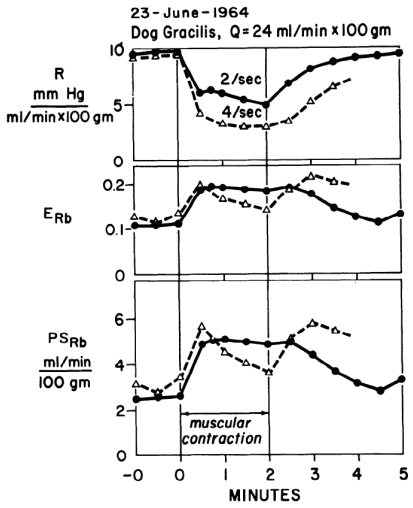


Figure 2.6: Results of Renkin [91] showing how $PS$ increases due to muscle contractions caused by electrical stimulation. In the bottom frame $PS$ nearly doubles during muscle contractions. Renkin attributed this to the recruitment of capillaries "We conclude that the increase in PS[...]produced during metabolic vasodilatation [is] brought about by an increase in the capillary surface area effectively in contact with flowing blood[...]it appears most likely that this change is brought about by the opening of precapillary sphincters which are closed under resting conditions."

ultrasound [92–94]. We will utilize this proxy to quantify recruitment, which is described by the recruitment factor $R$.

We model $PS$ as a saturable process that is dependent on $E$. The saturability assumption stems from the concept of a finite reservoir of previously unrecruited capillaries that are recruited during exercise. The following functions describe how $PS$ depends on $E$ and $R$

$$PS_a^I(E) = PS_{a_{rest}}^I \cdot (1 + R_a tanh(\gamma E)) \tag{2.42}$$

$$PS_d^I(E) = PS_{d_{rest}}^I \cdot (1 + R_d tanh(\gamma E)) \tag{2.43}$$

Here $PS_{a_{rest}}^I$ and $PS_{d_{rest}}^I$ are $PS$ values at rest in the SC and SM domains, respectively. $\gamma$ is a free parameter that serves to modulate how quickly the function reaches its plateau value. $R_a$ and $R_d$ are the recruitment factors. We need to find values for 5 parameters: $PS_{a_{rest}}^I$,$R_a$,$PS_{d_{rest}}^I$,$R_d$, and $\gamma$.

First, we quantify the difference between the resting permeabilities of each tissue, $PS_{a_{rest}}^I$ and $PS_{d_{rest}}^I$. This is difference is difficult to ascertain as data on capillary density in SC tissue compared to capillary density in SM tissue is sparse. Only a few studies have quantified MBV in both SC tissue and SM tissue [95–97]. These studies have shown MBV of SM tissue is the same order of SC tissue, but data on capillary recruitment in SC is sparse. Because of the dearth of data, we assume the simplest case, that resting capillary density in SC tissue is the same as that of SM tissue, $PS_{d_{rest}}^I = PS_{a_{rest}}^I$.

Next, we wish to quantify the recruitment factor $R_d$ in each tissue. We define the second term in Equation 2.43 as a new function $f_d$ that describes recruitment

$$f_d = R_d tanh(\gamma E). \tag{2.44}$$

$f_d$ can be thought of as the proportional increase in the number of perfused capillaries in the delivering (SM) tissue. For example $f_d = 0$ is no increase, $f_d = 0.5$ is a 50% increase, and $f_d = 2$ is a 200% increase. We quantify $f_d$ by using MBV as a proxy. Results of several MBV studies are shown in Figure 2.7, where MBV was quantified at different levels of exercise. By dividing the MBV value at exercise by the MBV value at rest (basal), we obtain values of $f_d$ at various exercise levels.

The ratios show considerable variation and are plotted as dots in Figure 2.8. The corresponding curve is Equation 2.44 with best-fit parameters $R_d$ and $\gamma$. Because quality of fit is relatively insensitive to $\gamma$, we assign $\gamma = 10$, which indicates rapid recruitment even during light ($E = 0.25$) exercise. The plateau value that best describes the data was $R_d = 1.46$, indicating that maximal recruitment is approx 146%, a value consistent with various studies on microvascular recruitment, which place maximal recruitment in the range of 100 to 300 % [91, 98]. With values for $PS_{d_{rest}}^I$, $\gamma$, and $R_d$ we have fully characterized our recruitment function Equation 2.43.

Our last step is to estimate the recruitment factor of SC tissue $R_a$. Unfortunately, data on capillary recruitment in SC tissue during exercise is extremely limited. Because of this, we use data from two studies on capillary recruitment during rest following a meal. Each of these studies show MBV increases approximately 50% following a meal [96, 97], verifying

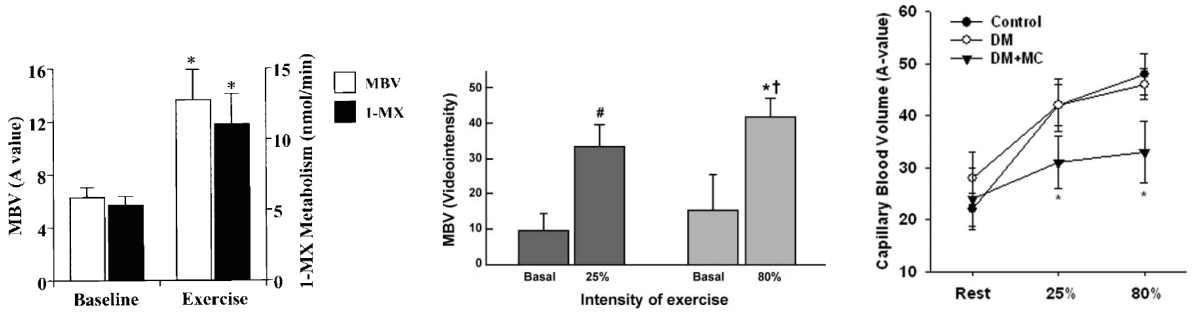


Figure 2.7: Figures from three studies showing the effects of exercise on capillary recruitment, as quantified by changes in microvascular blood volume (MBV). All studies indicate that MBV more than doubles during exercise, with only limited differences between light and heavy exercise. The ratios of MBV during exercise to MBV at rest are plotted in Figure 2.8 and used to fit parameters $\gamma$ and $R_d$. (left) [92] Recruitment is 115% after exercise as assessed by MBV and independently by the rate of 1-methylxanthine (MX) metabolism (another proxy for recruitment) in rat hindlimb adductor muscles. (center) [99] MBV is shown to increase roughly 240% during light and 163% during heavy forearm exercise in humans. (right) [94] MBV in the human forearm is shown to increase 91% during light and 118% during heavy forearm exercise. Figures are used without permission.

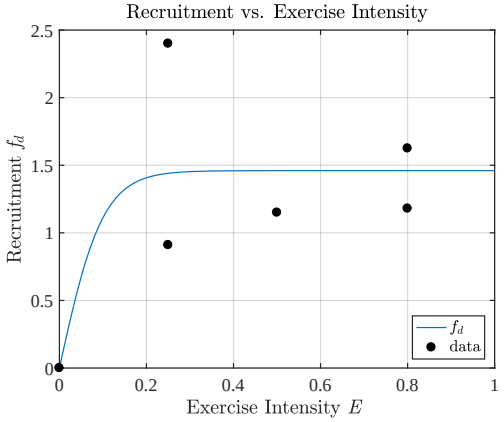


Figure 2.8: The relationship between capillary recruitment and exercise intensity is assumed to be a saturable process. The black dots are derived from the experimental results of various studies on capillary recruitment[92, 93, 100], which are summarized in Figure 2.7. Recruitment $f_d$ is defined to be zero at rest ($E = 0$) and is fit to data to find $R_d$ and $\gamma$ in Equation 2.44. $f_d$ rapidly increases to a plateau value of $R_d = 1.46$, indicating a 146% increase in capillary density during exercise.

that SC capillaries do have the ability to recruit. However, we expect that SC recruitment is significantly lower in SC tissue than in SM tissue for two reasons: (1) SC tissue is not as nutrient hungry as SM during exercise and (2) SC tissue blood flow only increases 2-3-fold during exercise, as compared to the 20-fold increase in SM tissue. Taken together, if the evolutionary necessity of capillary recruitment is to provide tissue with nutrients during exercise, then it would seem a needless adaptation for SC tissue to also possess the same recruitment ability at SM tissue. The observation that SC blood flow is only about 10% of

SM blood flow during exercise would indicate that nutrient delivery to SC is not as critical as in SM. Following this logic, we allow SC capillaries to recruit only 40% during exercise, significantly lower than the 150% in SM. We set $R_a = 0.4$

Lastly, we need at least one measured value for $PS$ to complete our system. Recently $PS$ has been directly measured in humans [101, 102] during hyperinsulinemia. This measure corresponds to the value of $PS^I_{a_{rest}}$ and is 0.005 [$\text{mL}_b/\text{mL}_{tiss}/\text{min}$].

Substituting our parameter values, we can fully identify our $PS$ recruitment model. Equations 2.42 and 2.43 become

$$PS^I_a(E) = 0.005(1 + 0.4\ tanh(10E))\ [\text{mL}_b/\text{mL}_{tiss}/\text{min}] \tag{2.45}$$

$$PS^I_d(E) = 0.005(1 + 1.46\ tanh(10E))\ [\text{mL}_b/\text{mL}_{tiss}/\text{min}] \tag{2.46}$$

$PS^I$ is plotted vs $E$ in Figure 2.9(left). As $E$ increases, $PS^I$ rapidly rise to their plateau values. By $E = 0.25$ capillaries are fully recruited.

With expressions for $Q^I$ and $PS^I$ it is illustrative to examine how the absorption and delivery rates $k^I_a$ and $k^I_d$ will depend on $E$. By substituting $Q^I_a$ and $PS^I_a$ (Equations 2.41 and 2.45) into $k^I_a$ (Equation 2.37) and substituting in $Q^I_d$ and $PS^I_d$ (Equations 2.40 and 2.46) into $k^I_d$ (Equation 2.38), we obtain the curves seen in Figure 2.9. $k^I_d$ increases much more rapidly than $k^I_a$ because recruitment is proportionally greater. Also, $k^I_d$ reaches its plateau value more rapidly due to a more rapid increase in $Q^I$.

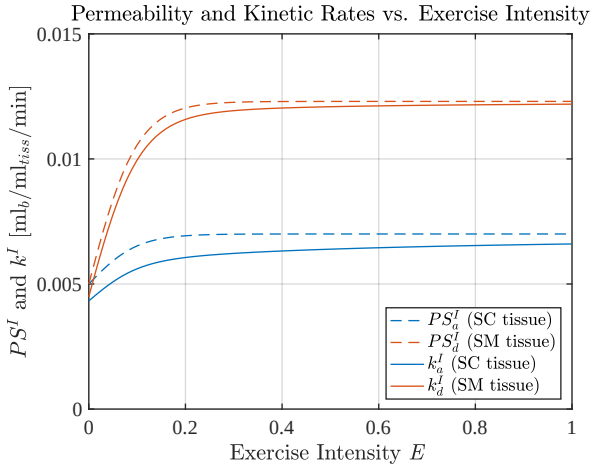


Figure 2.9: Insulin permeability surface area ($PS^I$, Equations 2.45 and 2.46) and kinetic rate ($k^I$, Equations 2.37 and 2.38) are plotted vs. exercise intensity $E$. Exercise-induced capillary recruitment rapidly increases $PS^I$ reaching a plateau value at at only $E = 0.25$. The plateau exists because there is a finite reservoir of capillaries in the tissue and once they are all fully perfused then surface area can no longer increase. $PS^I_d$ plateaus at a higher value because the delivering skeletal muscle (SM) capillaries have a higher recruitment factor than the absorbing subcutaneous (SC) capillaries. The absorption rate $k^I_a$ and delivery rate $k^I_d$ rates both increase very similarly to $PS$ because insulin kinetics are surface area limited, not flow limited. $k^I_a$ does not plateau as quickly as $k^I_d$ because $Q^I_a$ is significantly lower than $Q^I_d$ during exercise, and thus $k^I_a$ remains partly flow limited.

### Volume of Distribution, $V^I$ and Tissue Volume, $V^{tiss}$

Insulin distributes in a different fluid in each of the three domains: the ISF in the SC, the blood plasma in the CS, and the ISF in the SM.

For the SC domain, we are fortunate that we do not need to know the volume of distribution. This is because we have a known input and diffusive transport on a uniform domain simplifies to an ODE (see derivation of Equation 2.10).

For the CS and SM domain, the metabolic clearance rate depends on the concentration, and thus it must be solved for. Hence, we convert the total mass in the system to a concentration by dividing by the volume of distribution.

Insulin is a water soluble hydrophilic molecule. Thus the volume of distribution of insulin is nearly equal to the volume of water in each domain, which corresponds to the volume of blood plasma and ISF. There may be a small redistribution of fluids during exercise that may decrease the volume of plasma by 10-15% [103], but this change is small and as such we will treat the volume of distribution as constant and independent of exercise.

The volume of distribution we use for the CS domain is equal to the volume of the blood plasma, which normalized by the weight of an average man is $V^I_{CS_N} = 0.5$ [dL/kg$_{BW}$] [44, 104]. The volume of distribution that we use in the SM domain is roughly equal to the volume of the ISF, which normalized by BW is $V^I_{SM_N} = 1.2$ [dL/kg$_{BW}$] [44, 64, 104].

$V^{tiss}$ is fundamentally different from the volume of distribution, it is the volume of tissue in the compartment. This parameter only shows up in the SM compartment (Equation 2.52) because we must know the total volume flow rate ($Q^I_d \cdot V^{tiss}_{SM}$) in order to calculate the mass flux. The volume of tissue in the SM compartment is $V^{tiss}_{SM} = 0.54$ [L/kg$_{BW}$] [83], i.e. 54% of body weight at an assumed 1 [kg/L] density. Approximately half of $V^{tiss}_{SM}$ is SM tissue, with the other half SC tissue (we remind the reader that SC tissue far from the infusion site is part of SM domain).

### Metabolic Clearance Rate, $\mathrm{r}^I$

In the proposed insulin model, metabolic clearance of insulin occurs in both the CS domain and the SM domain. This poses a small problem because measurements of insulin clearance almost exclusively assume that insulin is only cleared from the CS, and does not track clearance from the SM domain. For this reason, we must make certain model assumptions in order to estimate the respective clearance contributions from each domain.

The total clearance rate of insulin, $\mathrm{r}^I_{tot}$, is measured by infusing insulin directly into the CS domain via an IV catheter, waiting for steady-state, then measuring the plasma insulin concentration. By assuming that clearance is linearly dependent on plasma insulin concentration, $\mathrm{r}^I_{tot}$ can be determined. Several have measured $\mathrm{r}^I_{tot}$: Feo [105] measured 13 [mL/min/kg$_{bw}$], Thorsteinsson measured 23 [mL/min/kg$_{bw}$] in one study [106] and 16 [mL/min/kg$_{bw}$] in another [107]. Taking the average of these studies, we choose $\mathrm{r}^I_{tot} = 17 \cdot$BW [mL/min], where the numerical value is multiplied by body weight (BW) for consistency with previous definitions.

Our model has two domains from which clearance occurs, thus we will estimate each domain's contribution to insulin clearance. $\mathrm{r}^I_{tot}$ must be equal to the sum of the clearance in each compartment. By assuming that clearance is linearly related to concentration in each compartment we have

$$\mathrm{r}^I_{tot} I = \mathrm{r}^I_{CS} I + \mathrm{r}^I_{SM} S \tag{2.47}$$

where $\mathrm{r}^I_{CS}$ and $\mathrm{r}^I_{SM}$ are the clearance rates in the CS and SM compartments, and multiply by the local concentrations. Rearranging, we have

$$\mathrm{r}^I_{CS} = \mathrm{r}^I_{tot} - \mathrm{r}^I_{SM} \frac{S}{I}. \tag{2.48}$$

Next, we utilize Equation 2.24 and 2.35, to solve for $\mathrm{r}^I_{SM}$. By assuming at rest ($E = 0$) and steady state, then rearranging, Equation 2.24 becomes

$$\mathrm{r}^I_{SM} = V^{tiss}_{SM} k^I_d(0)\big(\frac{I}{S} - 1\big). \tag{2.49}$$

We have also assumed that $\mathrm{r}^I$ does not change with exercise. Some have shown that $\mathrm{r}^I$ marginally increases during and following exercise [108, 109], however because of limited data we will assume $\mathrm{r}^I$ is independent of exercise.

The last relationship that we need is the ratio $S/I$ at steady-state. At basal levels of insulin, concentration measurements for $S$ are difficult to obtain, due to difficulty of in obtaining reliable microdialysis needle measurements at low insulin concentrations. However, several studies have compared $S$ to $I$ at physiological hyperinsulinemia [44, 70, 101, 110–112]. These studies have consistently shown approximately a 2:1 ratio for $I : S$. Hence, we set $S/I = 1/2$.

Substitution of $S/I$ into Equations 2.48 and 2.49, we obtain $\mathrm{r}^I_{SM} = 200$ [mL/min] and $\mathrm{r}^I_{CS}$= 1370 [mL/min]. This corresponds to a volume-normalized clearance rate $\mathrm{r}^I_{SM_N} = 0.02$ [1/min] $\mathrm{r}^I_{CS_N}$= 0.32 [1/min], meaning that 2% of the SM insulin content is cleared per minute, and 32% of the CS insulin content is cleared per minute. This is the same order, but lower than the 0.04 [1/min] measured in dogs by Bergman [44].

### 2.2.3 Model Summary

Equations 2.25, 2.26, 2.33, and 2.35 are substituted into Equations 2.10, 2.15, and 2.24 to obtain the final form of the insulin model. The final model equations are

$$\frac{d\mathcal{C}}{dt} = -k_a^I \mathcal{C} + \mathcal{U}(t) \tag{2.50}$$

$$\frac{dI}{dt} = \frac{k_a^I \mathcal{C}}{V_{CS}^I} - \frac{V_{SM}^{tiss} k_d^I \cdot (I - S)}{V_{CS}^I} - \mathrm{r}_{CS_N}^I \cdot I \tag{2.51}$$

$$\frac{dS}{dt} = \frac{V_{SM}^{tiss} k_d^I \cdot (I - S)}{V_{SM}^I} - \mathrm{r}_{SM_N}^I \cdot S \tag{2.52}$$

subject to

$$\mathcal{C} = \mathcal{C}_o \text{ at } t = t_o \tag{2.53}$$

$$I = I_o \text{ at } t = t_o \tag{2.54}$$

$$S = S_o \text{ at } t = t_o \tag{2.55}$$

with functions defined as

$$k_a^I = Q_a^I (1 - e^{\frac{-PS_a^I}{Q_a^I}}) \tag{2.56}$$

$$k_d^I = Q_d^I (1 - e^{\frac{-PS_d^I}{Q_d^I}}). \tag{2.57}$$

$$Q_a^I(E) = (1 - h) \cdot (Q_{a_{rest}} + \lambda_a E) \tag{2.58}$$

$$Q_d^I(E) = (1 - h) \cdot (Q_{d_{rest}} + \lambda_d E) \tag{2.59}$$

$$PS_a^I(E) = PS_{a_{rest}}^I \cdot (1 + R_a tanh(\gamma E)) \tag{2.60}$$

$$PS_d^I(E) = PS_{d_{rest}}^I \cdot (1 + R_d tanh(\gamma E)). \tag{2.61}$$

The initial conditions, $\mathcal{C}_o$, $I_o$, and $S_o$, are found by evaluating our system at resting ($E$=0) and steady-state. This yields the relationships

$$0 = -k_a^I(0)\mathcal{C}_o + \mathcal{U}(t_o) \tag{2.62}$$

$$0 = \frac{k_a^I(0)\mathcal{C}_o}{V_{CS}^I} - \frac{V_{SM}^{tiss} k_d^I(0)(I_o - S_o)}{V_{CS}^I} - \mathrm{r}_{CS_N}^I \cdot I_o \tag{2.63}$$

$$0 = \frac{V_{SM}^{tiss} k_d^I(0)(I_o - S_o)}{V_{SM}^I} - \mathrm{r}_{SM_N}^I \cdot S_o \tag{2.64}$$

These are linear equations, and can be algebraically solved for $\mathcal{C}_o$, $I_o$, and $S_o$.

The model represents the movement through three distinct domains; the SC, the CS, and the SM. This system of three ODEs represents a significant simplification from the system of PDEs that we started with. The main assumptions that have allowed us to arrive at the simplified system are as follows: (1) uniform capillary properties $PS$ and $Q$, (2) $c$ is much greater than $I$, (3) insulin clearance from the CS and SM is a linear process, and the metabolic rates are constants (4) the volume of distribution in each compartment is constant. Other less direct assumptions are that we have a moderate Péclet number and large capillary AR, and the length of a capillary is small compared to the region of drug wetted SC tissue.

Some potentially important unmodeled phenomena include: no degradation of insulin in the SC tissue, no hexameric to dimeric/monomeric dissociation prior to absorption, heterogeneity of tissue, insulin absorption through the lymph vessels, and changes in clearance rate $r^I$ and volume of distribution $V^I$ during exercise.

### 2.2.4 Human Subjects Data

The data used in this study comes from two separate research studies on T1D human subjects and is the secondary use of existing data. The main differences between the two cohorts is that one examined T1D patients under resting conditions (T1DR), and the other examined T1D patients under exercising conditions (T1DE). The protocols are illustrated in Figure 2.10. Data from T1DR was previously published in [6] where diurnal variations in insulin sensitivity were examined, however that study did not focus on modeling insulin absorption and delivery. The T1DE data is previously unpublished. All data has been provided by the Mayo Clinic through their own internal human subjects research (HSR) data protection protocols. For brevity, only the relevant protocol information will be discussed here. Detailed protocol information on T1DR can be found in [6]. The meal and exercise protocol information on T1DE can be found in a similar study on healthy patients [113]. Important dosing and demographic information is summarized in Table 2.2.

#### Cohort of subjects with Type 1 Diabetes at Rest (T1DR)

T1DR consisted of 19 subjects. All meals were provided by the clinical research unit (CRU) metabolic kitchen promptly at 0700 h. Subjects received weighed meals, with each comprising 33 % of the total estimated calorie intake based on Harris Benedict calorie requirements, including a low level of physical activity, with $\sim$ 50 g of carbohydrate in each meal. The meal consisted of Jell-O with dextrose, eggs (scrambled or omelet), and ham slices. At meal time, an insulin dose that corresponded to the patient's normal insulin-carb ratio was infused through an insulin pump. A few subjects preferred steak slices to ham. The macronutrient contents of the meals were identical. No snacks or calorie-containing drinks were permitted between meals unless otherwise required to treat hypoglycemia (point-of-care glucose $\leq$ 60 mg/dL) as per institutional guidelines. Unfinished food was weighed and excluded from calculated caloric intake. Each labeled meal was preceded by at least 3 h and followed by 6 h of inactivity when the subjects were resting in bed to enable periodic blood draws. All subjects were on an insulin pump. Thirteen subjects were taking insulin aspart, whereas the remaining six were taking insulin lispro. Insulin pump data was downloaded and used to quantify the insulin infusion rate $\mathcal{U}(t)$.

Insulin levels were measured by a two-site immunoenzymatic assay performed on the DxI automated immunoassay system (Beckman Coulter, Inc., Chaska, MN), The DxI method also reliably detects both insulin aspart and insulin lispro analogs (13) that have been tested in the Mayo clinical laboratory and cross-checked in the Mayo CTSA immunochemical laboratory.

Of the 19 patients in the T1DR group, 2 patients were removed due to missing data.

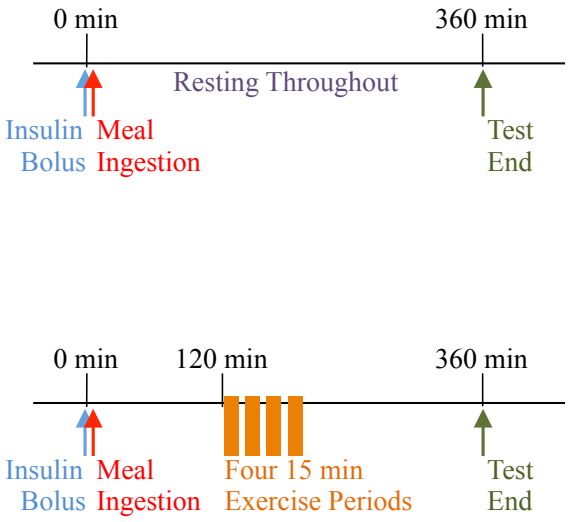


Figure 2.10: Timeline for the mixed-meal tolerance test (MMTT) T1D resting protocol (T1DR, top) and the T1D exercising protocol (T1DR, bottom). At time 0 the subjects in T1DR ingested a 50 [g] CHO mixed-meal and the subjects in T1DE ingested 75 [g]. The insulin bolus was infused through an insulin pump at time 0, with bolus size calculated according to the subject's normal insulin-to-carb ratio. The T1DR group rested throughout the entire study period. The T1DE group exercised at 50% $V0_{2_{max}}$ for four 15 minute exercise periods, starting at minute 120.

Table 2.1: Parameters used in insulin-kinetics model

| Parameter | Description | Unit | Value | Source |
|---|---|---|---|---|
| $V^I_{CS_N}$ | Normalized volume of distribution of insulin in circulatory system | $\mathrm{dL/kg}_{BW}$ * | 0.5 | [44, 104] |
| $V^I_{SM_N}$ | Normalized volume of distribution of insulin in skeletal muscle | $\mathrm{dL/kg}_{BW}$ * | 1.2 | [44, 64, 104] |
| $V^{tiss}_{SM_N}$ | Normalized volume of tissue in skeletal muscle domain | $\mathrm{mL/kg}_{BW}$ * | 540 | [83] |
| $\mathrm{r}^I_{CS_N}$ | Normalized clearance rate of insulin in circulatory system | 1/min | 0.32 | [105–107]† |
| $\mathrm{r}^I_{SM_N}$ | Normalized clearance rate of insulin in skeletal muscle | 1/min | 0.02 | [105–107]† |
| $Q_{a_{rest}}$ | Tissue perfusion rate absorbing (SC) tissue at rest | $\mathrm{mL}_b/\mathrm{mL}_{tiss}/\mathrm{min}$ | 0.028 | [83] |
| $Q_{d_{rest}}$ | Tissue perfusion rate in delivering (SM) tissue at rest | $\mathrm{mL}_b/\mathrm{mL}_{tiss}/\mathrm{min}$ | 0.038 | [83] |
| $h$ | Hematocrit percentage in blood | 1 | 0.4 | [104] |
| $\lambda_a$ | Slope relating $Q$ in absorbing (SC) tissue to exercise | $\mathrm{mL}_b/\mathrm{mL}_{tiss}/\mathrm{min}$ | 0.071 | [71, 86–88] |
| $\lambda_d$ | Slope relating $Q$ in delivering (SM) tissue to exercise | $\mathrm{mL}_b/\mathrm{mL}_{tiss}/\mathrm{min}$ | 1.1 | [84] |
| $PS^I_{a_{rest}}$ | Permeability surface area to insulin in absorbing (SC) capillaries | $\mathrm{mL}_b/\mathrm{mL}_{tiss}/\mathrm{min}$ | 0.005 | § |
| $PS^I_{d_{rest}}$ | Permeability surface area to insulin in delivering (SM) capillaries | $\mathrm{mL}_b/\mathrm{mL}_{tiss}/\mathrm{min}$ | 0.005 | [101, 102] |
| $R_a$ | Capillary recruitment factor in absorbing (SC) tissue | 1 | 0.40 | [96, 97] ‡ |
| $R_d$ | Capillary recruitment factor in delivering (SM) tissue | 1 | 1.46 | [92–94] ‡ |
| $\gamma$ | Saturation coefficient for $PS^I$ | 1 | 10 | [92–94] ‡ |

* Multiplied by BW prior to being used in model. See demographics for BW.
† Derived from total clearance rate.
§ Assumed to be the same as $PS^I_{d_{rest}}$.
‡ Derived by curve fitting to MBV literature data in SC and SM tissue.

**Cohort of subjects with Type 1 Diabetes with Exercise (T1DE)**

T1DE consisted of 12 patients. Subjects did not engage in vigorous physical activities for 72 h before screen and study visits. In the screening visit participants performed a graded exercise test on a treadmill to determine $V0_{2_{max}}$ according to guidelines (American College of Sports Medicine Guidelines for Exercise Testing and Prescription, 7th Edition) and ensure stable cardiac status. Expired gases were collected and analyzed using indirect calorimetry. $V0_{2_{max}}$ was determined when at least two of the following three criteria were met: 1) participant too tired to continue exercise, 2) respiratory exchange ratio exceeded 1.0; or 3) a plateau was reached in oxygen consumption with increasing workload. The purpose of this test was to use individual $V0_{2_{max}}$ data to determine workload during the moderate-intensity $V0_{2_{max}}$ protocol during the study day.

For the study visit all subjects spent 40 h in the CRU. On day 1 subjects were admitted to the CRU at 1600. Thereafter a Modular Signal Recorder accelerometer (MSR Electronics, Seuzach, Switzerland) was placed and maintained for the rest of the study period (data not used in the current work). They were then provided a standard 10 kcal/kg meal (55 % carbohydrate, 15% protein, and 30% fat) consumed between 1700 and 1730. No additional food was provided until the next morning. A heart rate monitor was also attached to capture heart rate during the study (data not used in the current work). On day 2 at 0600 h, an intravenous cannula was inserted retrogradely into a hand vein for periodic blood draws. The hand was placed in a heated (55C) Plexiglas box to enable drawing of arterialized-venous blood for glucose and hormone analyses. At 0700 a mixed-meal study was performed.

A mixed meal containing 75 grams of glucose was ingested at time 0. At meal time, an insulin dose that corresponded to the patient's normal insulin-carb ratio was infused through an insulin pump. At 120 min following the first bite, subjects stepped on a treadmill to exercise at moderate-intensity activity (50 % $V0_{2_{max}}$): i.e., four bouts of walking at 3-4 miles/h for 15 min with rest periods of 5 min between each walking bout: total duration 75 min. The workload during physical activity was continuously monitored by heart rate responses and measurements of $V0_{2_{max}}$ during exercise to maintain target 50% $V0_{2_{max}}$ exercise intensity. Accelerometer recordings were collected throughout the study period to monitor and quantitate activity levels (data not used in the current work). Following the last blood draw the hand vein cannula was removed. Lunch at 1300 and dinner at 1900 were provided, each meal contributing 33% of daily estimated caloric intake. The patient was discharged the next morning at 0800.

Originally there were 14 patients in the T1DE group, 2 patients were deemed outliers and removed because they exhibited extremely rapid absorption rates compared to the rest of the group.

### 2.2.5 Simulation, Input, and Data Considerations

Equations 2.50 - 2.61 are solved using MATLAB ode15, a built in explicit ODE solver. The initial conditions were found by solving the steady-state resting Equations 2.62 - 2.64.

Table 2.2: Demographics of T1D subjects

| Variable | Resting Protocol (n=17) | Exercising Protocol (n=12) |
|---|---|---|
| Age (Years) | 39.7 ± 14.3* | 43.5 ± 12.9 * |
| Sex (M/F) | 9M, 8F | 8M, 6F |
| Weight (Kg) | 74.4 ± 5.3* | 85.9 ± 21.9 * |
| HbA1C(%) | 7.11 ± 0.6* | 7.5 ± 0.6 * |
| Average Bolus Size (U) | 4.1 | 6.7 |
| $V0_{2_{max}}$ | Not measured | 23.8 ± 5.4 * |

* ± Standard deviation

$t_o = -420$ min was the initial time of the simulation which corresponded to about 12 midnight when the subjects were sleeping and had approximately steady-state and basal insulin levels.

The averaged insulin pump infusion rate $\mathcal{U}(t)$ and measured plasma insulin concentration $I_{data}$ were used for comparison and validation of model predictions. The initial input $\mathcal{U}(t_o)$ was set to the average infusion rate at $t_o$. For the T1DE cohort $E = 0.5$ during exercise periods (120-135, 140-155, 160-175, 180-195 min) and $E = 0$ elsewhere. A small time delay with a time-constant of 1 min was given to the $E$ signal to account for HR lag time after exercise begins and ends. For the T1DR cohort $E = 0$ throughout.

## 2.3 Results

### 2.3.1 Model Comparison with Resting Patient Cohort (T1DR)

Using the average measured input $\mathcal{U}(t)$ from the resting cohort (T1DR), the insulin kinetics model was simulated for an average resting patient to produce predictions of $I$ and $S$. Figure 2.11(left) plots the predictions along with the measured insulin concentration $I_{data}$. Overall predictions agree reasonably well with measurements. The predicted insulin reaches a peak of 28 [$\mu$U/mL], a slight underestimation of the measured peak plasma insulin concentration 32 [$\mu$U/mL]. Also, the peak insulin occurs only 20 minutes after injection, compared to 45 minutes for the measured data. These discrepancies occur because of underestimated parameter values and because the model does not include insulin dissociation in SC tissue. This will be further explained in the discussion section.

The concentration in the SM domain, $S$, slowly rises due to the slow diffusion of insulin into the SM tissue. It eventually reaches a maximum of 13 [$\mu$U/mL], up from the baseline concentration of 6 [$\mu$U/mL]. $S$ was not measured in the current study and hence we cannot verify the predictions for $S$, however they are in reasonable agreement with lymph insulin data taken by Bergman after an intravenous insulin infusion [55].

### 2.3.2 Model Comparison with Exercising Patient Cohort (T1DE)

Next, using the average measured input $\mathcal{U}(t)$ and $E(t)$ from the exercising cohort (T1DE), the insulin kinetics model was simulated for an average exercising patient to produce predictions of $I$ and $S$. Figure 2.11(right) shows the comparison of simulation to measured data.

Overall, $I$ in the exercise simulation closely follows $I_{data}$. In the resting period prior to exercise $I$ reaches a peak of 30 [$\mu$U/mL], a slight underestimate of the measured peak of 33 [$\mu$U/mL]. Again, the predicted peak occurs much earlier than the measured peak because the model does not include insulin dissociation in SC tissue.

Once exercise begins, $I$ rapidly increases by 30% from 25 [$\mu$U/mL] to 32 [$\mu$U/mL]. This occurs as a result of the 50% increase in the insulin absorption rate $k_a^I$ brought on by capillary recruitment in the SC tissue. $I_{data}$ shows a similar 30% increase from 22 to 29 [$\mu$U/mL].

A sawtooth pattern in the predictions emerges as a result of 15 minutes on, 5 minutes off, exercise bouts. This is verified by $I_{data}$ which exhibits a slight drop during the 5 minute resting periods. This drop occurs because of de-recruitment of capillaries and/or changes in $V_{CS}^I$ (changes in $V_{CS}^I$ are not included in the model). After exercise ends, the predictions settle to a nearly perfect agreement with the data up until the cessation of the study at minute 360.

$S$ slowly rises after the injection due to the slow diffusion of insulin into the SM tissue. Then $S$ reaches a local maximum near minute 60 at a concentration of 13 [$\mu$U/mL]. It maintains this level until exercise commences at minute 120. At this point, the rate of insulin delivery $k_d^I$ increases by 150% due to capillary recruitment and as a result, $S$ begins a rapid rise, peaking at a concentration of 21 [$\mu$U/mL], a 60% increase. This increased

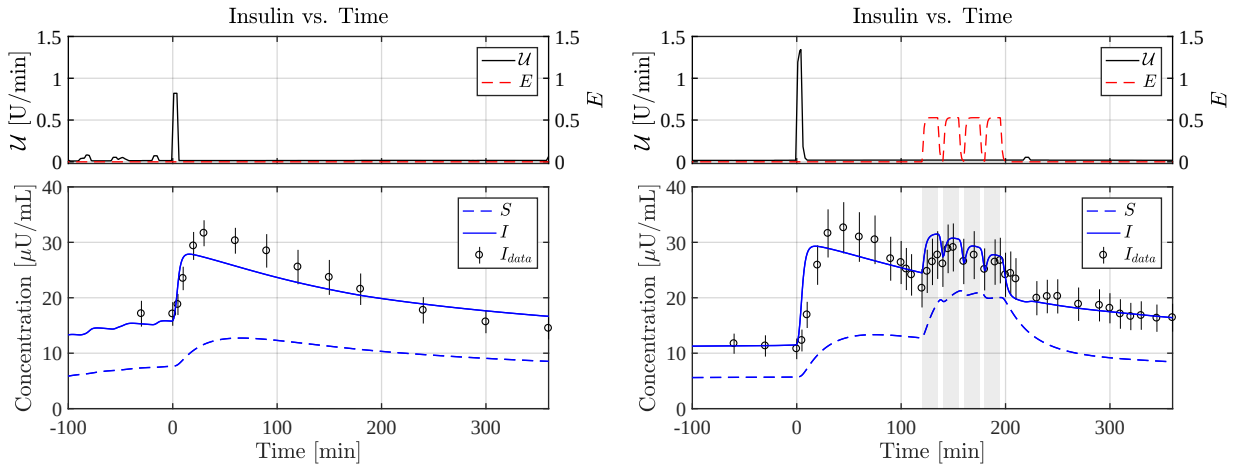


Figure 2.11: Simulated insulin concentration for an average resting (left) and exercising patient (right). Inputs $\mathcal{U}(t)$ and $E$ are shown in the top frames. Measured insulin concentration data is shown as a dot with standard deviation ($I_{data}$). Predictions of insulin concentrations in the plasma $I$ (solid lines) and skeletal muscle interstitial fluid $S$ (dotted lines) are shown in the bottom frames. 15 minute exercise bouts with 5 minute breaks are shown as shaded regions. Both cases closely follow the data, with a slight underestimation of peak plasma insulin concentration. Upon the commencement of exercise at minute 120 the $I_{data}$ rises from 22 to 29, and maintains until exercise ends at minute 195. Similarly during exercise $I$ rises 30% from 25 [$\mu$U/mL] to 32 [$\mu$U/mL]. This increase is a result of the enhanced absorption rate $k_a^I$ associated with capillary recruitment. A significant increase in $S$ is also predicted, increasing 60% from 13 [$\mu$U/mL] to 21 [$\mu$U/mL] over the entire exercise period. This is due to the enhanced delivery rate $k_d^I$ associated with capillary recruitment in the SM. This predicted increase in $S$ has significant implications on glucose metabolism, potentially leading to hypoglycemia during exercise.

concentration is maintained until after the exercise period ends, at which point $S$ rapidly decreases to near baseline.

### 2.3.3 Predicted Insulin-Kinetics

In order to illuminate the effects that capillary recruitment has on insulin delivery to SM tissue, we have quantified two kinetic measures. The first is the extraction fraction of insulin ($ef^I$) [%] which measures the percentage arteriovenous change in insulin concentration after blood passes through SM tissue. The second is the insulin delivery mass flow rate ($\dot{\mathcal{S}}_d$) [$\mu$U/min] from the CS to SM tissue.

The extraction fraction of insulin ($ef^I$) is defined as

$$ef^I = \frac{I_{arterial} - I_{venous}}{I_{arterial}} \cdot 100. \tag{2.65}$$

$ef^I$ is a measure of how effectively insulin in the CS is delivered to the SM tissue. A high $ef^I$ means that a large amount of insulin is removed from the CS on each pass through the SM tissue. $ef^I$ of can be directly measured using arteriovenous catheterization, however in

our study $ef^I$ is not measured. Instead, we will use the developed model to express $ef^I$ as a derived quantity. $ef^I$ can be written in terms of $I$ and $S$ by approximating that $I_{arterial} = I$ and $I_{venous} = b_d|_e$. Using Equation 2.22 we can estimate $b_d|_e$ and plug the solution into Equation 2.65 to get

$$ef^I = \frac{(1 - e^{\frac{-PS_d^I}{Q_d^I}})(I - S)}{I} \cdot 100. \tag{2.66}$$

The insulin delivery mass flow rate ($\dot{\mathcal{S}}_d$) also is not measured directly. However, it can be estimated from the model. We do this by multiplying the total flow rate to the SM tissue $V_{SM}^{tiss} Q_d^I$ by the predicted arteriovenous difference (numerator of Equation 2.66). Our derived estimate is identical to Equation 2.35 and is repeated

$$\dot{\mathcal{S}}_d = Q_d^I V_{SM}^{tiss} \cdot (1 - e^{\frac{-PS_d^I}{Q_d^I}})(I - S). \tag{2.67}$$

$ef^I$ and $\dot{\mathcal{S}}_d$ are plotted vs. time in Figure 2.12 for both the resting (T1DR, blue line) and the exercising (T1DE, orange line) groups. The exercise periods are shown in the shaded regions, but do not apply to the resting group.

Baseline $ef^I$ is about 10 %, which is slightly lower than the 15%-20% measured in [70, 114]. Upon meal ingestion in both groups $ef^I$ increases temporarily because of an increase

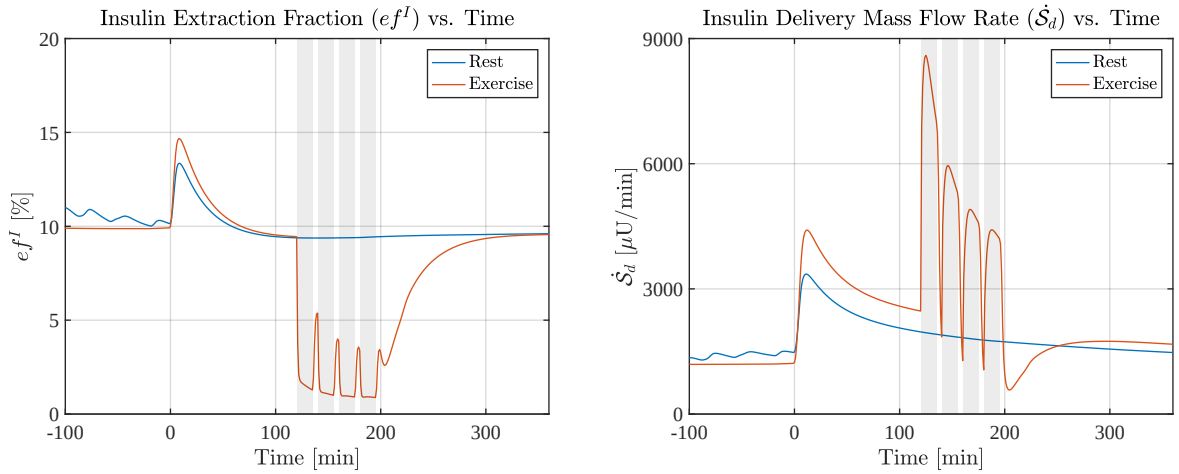


Figure 2.12: (left) Calculated insulin extraction fraction $ef^I$ from the resting (T1DR, blue line) and exercising (T1DE, orange line) simulations. (right) Corresponding insulin delivery mass flow rate $\dot{\mathcal{S}}_d$. Resting $ef^I$ is 10%. Upon meal ingestion $ef^I$ temporarily increases to nearly 15% because of an increase in $I$. During the exercise periods (shaded regions) of the T1DE group, the $ef^I$ drops as low as 1.5%. This is a result of the 10-fold increase in $Q_d^I$, which cuts the transit time by a factor of 10, thus decreasing the arteriovenous (A-V) difference. But the A-V difference does quite drop by a factor of 10 because because capillary recruitment increases $PS_d^I$ by 150%. Hence, even with the significant drop in $ef^I$ during exercise, the magnitude of $\dot{\mathcal{S}}_d$ still increases 2-3 fold during exercise. This huge increase in $\dot{\mathcal{S}}_d$ is responsible for the 60% increase in $S$ shown in Figure 2.11(right).

in $I$. The observed higher $ef^I$ and $\dot{\mathcal{S}}_d$ in the period up until minute 120 is because of the 50 % larger insulin dose in the T1DE group than the T1DR group.

In the both groups $ef^I$ returns to baseline within 2 hours of the insulin injection. Upon the commencement of exercise at minute 120 in the T1DE group there is a precipitous drop in $ef^I$. This is because of a 10-fold increase in the tissue perfusion rate $Q_d^I$, which cuts the transit time by a factor of 10, reducing the arteriovenous difference. However, the drop in $ef^I$ during exercise does not completely characterize insulin delivery because delivery is proportional to the product of arteriovenous difference and $Q$. $ef^I$ drops by a factor of 5, but $Q_d^I$ increases by a factor of 10, and hence the insulin delivery rate $\dot{\mathcal{S}}_d$ increases 2-3 fold, as shown in Figure 2.12(right). This tremendous increase in insulin delivery, from 3000 [$\mu$U/min] to nearly 9000 [$\mu$U/min] is responsible for the increase in $S$ shown in Figure 2.11.

There is also a noticeable drop in $\dot{\mathcal{S}}_d$ after exercise ends. This can be attributed to $S$ being nearly the same concentration as $I$ around minute 200, seen in Figure 2.11(right).

### 2.3.4 Test Case: Dependence of Insulin Kinetics on Timing of Exercise

This test case will predict $S$ for several different timings of exercise with respect to a 6 [U] bolus given at time 0. The hypothesis is that the sooner a T1D exercises after the bolus the more significant the insulin delivery to SM and the more significant the peripheral glucose uptake ($GU$).

The proposed model predicts exercise-induced changes in insulin kinetics. However, to understand how these changes are relevant to insulin dosing they must be interpreted in the context of $GU$. To do this, we make a rough estimate of *insulin-dependent GU* in the periphery during exercise. There are certainly other mechanism of $GU$ during exercise, such as *insulin-independent GU* [35] and insulin/exercise synergistic effects on $GU$ [40], but quantifying these are beyond the scope of this test case. These effects will be included in Chapter 3.

Castillo and Bergman [44, 70] showed that when glucose is clamped at basal levels, the rate of glucose uptake ($RGU$) [mg/min] in the periphery is roughly proportional to insulin concentration in the periphery

$$RGU = \mathrm{r}_{SM}^{GI} S \tag{2.68}$$

Where $\mathrm{r}_{SM}^{GI}$ is the rate constant relating the $RGU$ to $S$. $\mathrm{r}_{SM}^{GI}$ can also be thought of as the insulin sensitivity ($SI$) at basal glucose concentration. $\mathrm{r}_{SM}^{GI}$ was estimated to be 5 to 10 [mg/min per $\mu$U/mL] at basal glucose concentration [70].

To quantify $GU$ in a given time period, we integrate Equation 2.68 over time frame $t_1$ to $t_2$ (note that $RGU = d(GU)/dt$)

$$GU = \mathrm{r}_{SM}^{GI} \int_{t_1}^{t_2} S \; dt \tag{2.69}$$

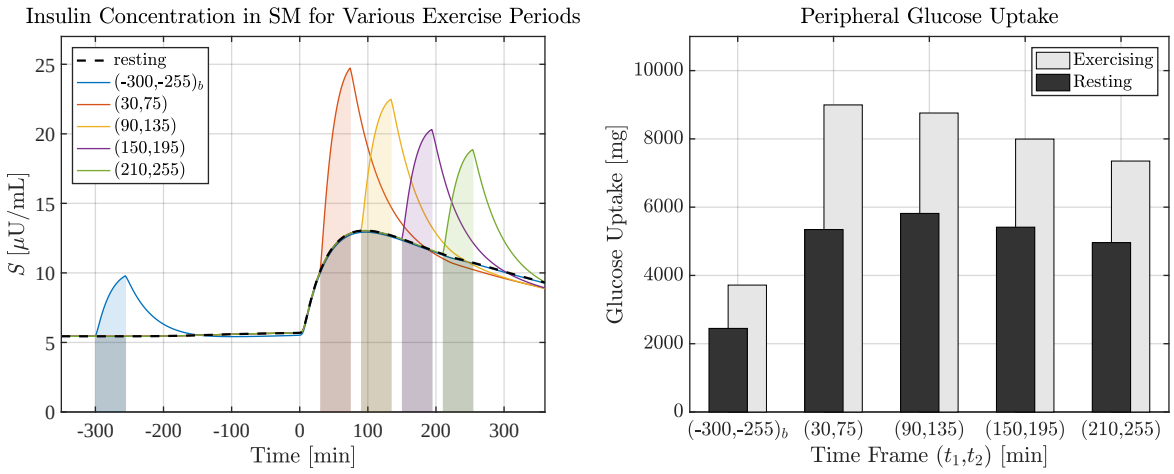


Figure 2.13: The timing of exercise with respect to the bolus has a significant impact on peak insulin $S$ and glucose uptake ($GU$). (left) Five test cases with moderate ($E = 0.5$) 45 minute exercise periods were simulated (solid lines). For comparison a resting case was simulated (black dotted line). The exercise case from t=(-300, -255)$_b$ shows an increase in $S$ from 5.5 to 10 [$\mu$U/mL] and corresponds to exercise under basal insulin conditions. For the exercise case from t=(30, 75) $S$ increases from 10 to 25 [$\mu$U/mL], indicating that when exercise occurs shortly after the bolus, the effects on $S$ are profound. As more time is put between the bolus and the exercise bout, the effect on $S$ is diminished. (right) Peripheral $GU$ was estimated with Equation 2.69 from the shaded AUC regions shown on the left. For the exercising case from (-300, -255)$_b$, $GU$ is 3.7 [g], a 1.2 [g] increase over the resting case. In comparison, for the exercising case from (30, 75) $GU$ is 9 [g], an increase of 3.6 [g] over the resting case. The sooner the exercise bout occurs after the bolus, the more significant the increase in predicted peripheral $GU$. These estimates of $GU$ do not account for synergistic effects of insulin and exercise [40], which may make exercise effects on $GU$ even more profound.

where we have set $GU$ to be 0 initially, and have assumed constant $r_{SM}^{GI}$ and basal glucose concentration throughout.

To calculate $GU$, we simulate $S$ from -400 to 360 min, while specifying a period of exercise. The five test periods of exercise are 45 minutes at moderate intensity ($E = 0.5$), and go from minute -300 to -255, 30 to 75, 90 to 135, 150 to 195, and 210 to 255. Results of these five simulations are shown in Figure 2.13(left) (solid lines). For comparison a rest case was also simulated (black dotted line). Using Equation 2.69 the resulting predictions of $S$ were used to calculate $GU$ over the 45 minute exercise periods. $GU$ is proportional to the AUC for each test case in Figure 2.13(left). The exercising cases AUC are shown as colors, and the corresponding resting AUC is shown as a grey region below. The comparison of $GU$ is plotted in Figure 2.13(right).

Figure 2.13(left) shows the timing of the exercise bout has a significant effect on peak $S$. When exercise occurs prior to the bolus, $S$ only increases from 5.5 to 10 [$\mu$U/mL], about an 80 % increase. In comparison, for the case where exercise occurs 30 minutes after the bolus, $S$ increase from 10 to 25 [$\mu$U/mL], a 150% increase. As more time is put between the bolus and the exercise bout, peak $S$ tapers down.

Figure 2.13(right) compares the $GU$ for each of these cases. The enhancement of $GU$

because of increased insulin delivery rate shows a strong dependence on exercise timing. Exercise 30 minutes after insulin infusion shows an increase in $GU$ from 5.4 [g] for the period at rest, to 9 [g] for the same period with exercise, a 70% increase of $GU$. In comparison, for the basal case starting at minute -300, $GU$ increased from 2.5 [g] to 3.7 [g], only a 50% increase.

## 2.4 Discussion

Enhanced absorption and delivery rates during exercise may have significant implications on the rate of glucose uptake and can potentially cause hypoglycemia. This is one reason why exercise is considered a major hurdle to closed loop control in T1D. An improved model of insulin kinetics during exercise can potentially improve safety by improving insulin availability predictions in model predictive control algorithms.

The objective of this work is to develop a physiology-based model of insulin-kinetics to understand why insulin has been observed to absorb from SC tissue and deliver to SM tissue more rapidly during exercise [41–43, 71, 72, 110]. We hypothesize that this enhanced rate of absorption/delivery is due to capillary recruitment, which increases surface area available for insulin transport.

*Model Development.* Most previous models of insulin absorption and delivery were data driven, with parameters identified from data, and did not provide rigorous treatment of the underlying physical transport phenomena. Starting with first principles, we developed a model of insulin absorption that included the effects of capillary recruitment on solute delivery, as first described by Renkin in 1966 [91]. We included this transport model (Equation 2.36) into a broader insulin-kinetics model. In this model we allowed the surface area and tissue perfusion rate to increase simulating capillary recruitment. The simple model predicts that insulin absorption/delivery rates are surface area dependent, not flow dependent, contrary to that reported by multiple authors [71, 77, 115]. Additionally, all parameters are based on physiological measurements taken from literature, and are not obtained from curve fitting. This helped us prevent overfitting, and gives confidence that the physical phenomena we are modeling are indeed the controlling ones.

*Model Comparison with data.* To test the model we compared plasma insulin predictions $I$ to plasma insulin measurements $I_{data}$ in Figure 2.11. For the resting group T1DR, the model agrees well with the data, but slightly underestimates the peak concentration. This is likely due to an underestimation of the $V_{CS}^I$ and $PS_a^I$. Population averaged values (Table 2.1) were used, rather than a curve fit value. If a slightly smaller $V_{CS}^I$ and slightly higher $PS_a^I$ were used, the predictions would closely match the data. The peak concentration is also skewed earlier than measurements because the insulin hexameric dissociation is not modeled here.

For the exercising group T1DE, the peak is also underestimated and skewed earlier. When exercise occurs a at minute 120, $I$ and $I_{data}$ rapidly increase 30%. This is a result of the 45% increase in $k_a^I$ (See Figure 2.9). A sawtooth pattern follows, and $I$ and $I_{data}$ both drop during the 5 minute resting periods. The model predicts these slight dips because of de-recruitment. An alternative explanation is that $V_{CS}^I$ increases temporarily due to the volume-contraction effect, which is estimated to be 10% [103]. This volume-contraction effect may also partly explain the 30% increase in $I_{data}$, however, it is doubtful that the 10% volume contraction could cause the full increase.

*Insulin absorption from subcutaneous depot.* Insulin transport is primarily a surface area dependent phenomenon. We have assumed that the capillary surface area in SC tissue

increases by 40% during exercise. This, along with a modest increase in $Q^I$, predicts that $k_a^I$ increases by 45% during exercise, with little dependence on exercise intensity $E$. Previous studies of the exercise-induced increase in $k_a^I$ have ranged 49 to 100% for insulin injected into the thigh [41, 42, 71, 72], and from 0-20% for insulin injected into the abdomen [42, 72]. If one assumes that thigh SC injections are near more vascularized SM tissue, as compared the abdominal SC injections, then these literature findings agree with our theory that SM has a greater ability to recruit ($R_d$=150%) than SC ($R_a$=40%). In our study insulin was infused into the abdomen with an insulin pump and we see a clear 30% increase in $I_{data}$ during exercise. We strongly believe this increase results from an increase in $k_a^I$. So why do we predict a 45% increase in $k_a^I$, while the literature only shows a 20% increase? Most of these measurements were taken in the 1980s using regular human insulin - not the rapid acting insulins that are typically used today. Modern insulins dissociate much faster and the rate-limiting step of absorption is likely penetration of the endothelial walls. In older insulins the rate limiting step was more skewed toward hexameric dissociation, and thus older insulins may have been less sensitive to changes in surface area brought on by capillary recruitment. To address this theory, new studies should be designed to estimate the effects of exercise on the absorption of rapid acting insulin through injection into the abdominal region.

It is also worth mentioning that the present hypothesis may explain the enhanced absorption of new delivery devices. The jet injector [116] and the localized heating pad [117] have each been shown to absorb significantly faster than with a typical syringe injection. If capillary recruitment occurs because of tissue trauma from the jet or heating from the pad then the enhanced absorption rate could be explained by the present hypothesis.

*Insulin delivery to skeletal muscle.* Insulin delivery to skeletal muscle has been shown to be the rate-limiting factor to glucose uptake because insulin concentration $S$ is directly proportional to glucose uptake [44, 55, 70]. The model predicts that the the insulin delivery rate $k_d^I$ increases 150% during exercise and as a result $S$ is predicted to increase 60% in the T1DE group (Figure 2.11). $S$ was not measured in our study so we cannot verify these model predictions. However, others have measured an increase of 10-25%, albeit under different conditions [43, 110]. Assuming that the 60% prediction is accurate we would expect, at minimum, a 60% increase in peripheral $GU$ over the case where there is no increase in $S$.

To understand why $S$ is predicted to increase dramatically, we calculate standardized measures of insulin delivery, the insulin extraction fraction $ef^I$ (Equation 2.66) and the insulin delivery mass flow rate $\dot{\mathcal{S}}_d$ (a.k.a. insulin uptake, Equation 2.67). Baseline $ef^I$ is estimated to be 10% (Figure 2.12), which is slightly lower than the 15-20% measured by Bergman [70] and Eggleston [114]. We believe this is due to underestimation of $PS^I$. Upon exercise $ef^I$ drops considerably because the perfusion rate increases 10-fold, reducing the transit time and the arteriovenous difference. No data exists for $ef^I$, during exercise and thus this drop cannot be verified.

$ef^I$ does not give a good indication of the delivery dynamics, because it alone cannot provide estimates of $\dot{\mathcal{S}}_d$, which directly determines the concentration $S$. The baseline $\dot{\mathcal{S}}_d$ is 1190 [$\mu$U/mL] or 18 [fmol/min/100mL$_{tiss}$] when normalizing by $V_{SM}^{tiss}$ and converting to

mol. This is remarkably close to the 15 [fmol/min/100mL$_{tiss}$] measured by Eggleston [114], and gives some confidence that the model accurately predicts insulin delivery, at least in baseline resting conditions. During exercise $\dot{\mathcal{S}}_d$ significantly increases. In the initial phase there is a large spike in $\dot{\mathcal{S}}_d$ from 3000 to 9000 [$\mu$U/mL], which causes the sharp increase in $S$ seen in Figure 2.11 at minute 120-135. Because of the rapidly changing dynamics we cannot compare directly with measurements from the literature, as they are typically taken at steady state. Instead, we look at the delivery rates during the fourth exercise bout, which are closer to steady state. During the fourth exercise bout the delivery rate is 4000 [$\mu$U/mL], corresponding to a 2-fold increase over baseline. Estimates from measurements show an increase from 0%-200% [66, 73]. Our predictions match the top end of measurements from literature, however, this large spread exemplifies that insulin delivery during exercise remains an open question.

*Glucose Uptake Implications.* Our test case examined how the timing of exercise affects glucose uptake. Exercise has the greatest effect on $S$ when the performed shortly after a bolus. This is because the absorption mass flow rate $\dot{\mathcal{C}}_a$ is equal to $\mathcal{C}$ (a.k.a. IOB) times $k_a^I$ (Equation 2.9).

We estimated $GU$ with a simple expression (Equation 2.69). The test case predictably showed that $GU$ is most affected by exercise for the test case when exercise begins only 30 minutes after the bolus. In this case $GU$ increased 70% over a resting baseline case, which shows why hypoglycemia commonly occurs in T1D when exercise follows a meal. If synergistic effects of exercise/insulin on $GU$ were included, this difference would be even more profound. There is also the fact that increasing $I$ suppresses endogenous glucose production, which would further exacerbate the problem of hypoglycemia during exercise.

*Modeling Gaps.* When deriving the insulin-kinetics model we have tried to balance model parsimony with accuracy. Perhaps the most significant model assumption was the decision not to include the hexamer to dimer/monomer dissociation step. We did this because we wanted to keep the model based in physics as much as possible. If we included the dissociation step we would either have to use an abstract model with parameters found through curve fitting or we would have to model the non-linear process of protein dissociation, which would have added significant complexity to the model. Lymphatic insulin absorption was also not included because it is believed to be of secondary importance [118].

One important but complex phenomenon that was not included is capillary bed heterogeneity. Renkin [38], showed that heterogeneity may explain why the capillary transport model he derived (and we derived independently as Equation 2.36) is inaccurate for many solutes. This inaccuracy may partly explain why our predicted $ef^I$ drops so low during exercise. Capillary recruitment may not just increase surface area, but also redistribute flow to longer capillaries enhancing transport [38]. To include heterogeneity would involve defining a distribution of capillary lengths for inclusion in the compartmental description. This may bring the model closer to 'truth' but the introduction of uncertainty through unknown distribution parameters may negate any gains made by including heterogeneity.

Lastly, some have also suggested that insulin transport may be a saturable process [114], which may change our results significantly. However, given our lack of understand of this

mechanism, there is not a clear path to include this in a model of insulin-kinetics.

*Parameter Selection and Uncertainty.* To keep our model rooted in physiology we avoided the use of curve fitting to estimate parameters. This allowed us to avoid overfitting, providing more confidence that the physical mechanisms in our model are being reliably captured. With this approach there is significant parameter uncertainty that needs to be addressed before the model can be validated.

The permeability surface area of insulin $PS^I$ is difficult to measure and highly uncertain. This is because $PS^I$ cannot be directly measured with current techniques, and thus its value is based on assuming a homogeneous capillary bed model and measured related quantities (see Appendix A.5). In other words, $PS$ is a model-dependent parameter. Because of this difficultly, postprandial and exercise $PS^I$ values are lacking. It is for this reason we need to create a recruitment model based on MBV to show how $PS^I$ changes during exercise.

Another parameter that is problematic is $\mathrm{r}^I$. Typically $\mathrm{r}^I$ is typically measured at steady-state, during rest, and assuming that clearance occurs from a single compartment. This is known to be incorrect, as insulin has been shown to be cleared directly from the SM [44]. To deal with this, we derived a value for $\mathrm{r}^I_{SM}$ by setting total clearance equal to the clearance in both compartments (Equation 2.47). Also, little is known about how $\mathrm{r}^I$ changes during exercise. Reduction of blood flow to the liver (the primary site of insulin clearance) to account for increased flow to SM may fundamentally alter $\mathrm{r}^I$. There is also the possibility that $\mathrm{r}^I_{SM}$ is enhanced during exercise because of muscle contraction and $GU$. To obtain a higher fidelity model, $\mathrm{r}^I$ must be estimated during exercise to a higher degree of certainty.

Last, MBV has been used sparingly to characterize capillary recruitment in SC tissue [95–97]. In fact, we found no studies that examined changes in SC MBV during exercise and we had no choice but to use SC MBV measurements obtained postprandially, where recruitment is 50%. More studies need to be done to understand recruitment in SC tissue during exercise.

*Model Insights.* For the first time, to the author's knowledge, we have incorporated the effects of exercise-induced capillary recruitment on insulin-kinetics. By using independent measurements of $PS^I$, we have obtained reasonably accurate predictions of insulin concentration in plasma.

The model also provides an interesting insight about natural limits on absorption. If we assume that absorption is driven by pure diffusion then $PS^I_a$ may represent a hard upper-limit on $k^I_a$. This is because even if hexameric dissociation occurs instantaneously upon injection, $PS^I_a$ would still provide resistance to transport. This model therefore may represent the upper limit of $k^I_a$. We predict that the peak $I$ occurs 20 minutes after injection, which is 30 minutes earlier than $I_{data}$. There thus may be little room for the design of faster absorbing insulin. Additionally, because insulin transport to SM is the rate limiting step of $GU$, modeling the hexameric dissociation step may be unnecessary, as it may not change $S$ much.

Last, this model shows how lack of capillary recruitment is a possible cause of insulin resistance. In type II diabetes it has been shown that capillary recruitment is less prominent [94]. Without recruitment the model shows that insulin is not delivered to SM as quickly.

*Future Directions.* The model gives reasonable predictions for an average patient. However we have yet to take inter-patient and intra-patient variability into account. Insight about the variability of insulin absorption can be gained from characterizing the variability of tissue vascularization in patient populations. The incorporation of the variability of capillary beds into the model could make a significant improvement to accuracy in different patients.

Also, the SM domain grouped all peripheral tissues into a single compartment. In fact the SC tissue far from the infusion site, the resting SM, and the exercising SM should all be their own compartments, as they have different flow rates and would recruit separately. The model can potentially be improved by making this split.

In the future, we would also need to validate the model on various levels of exercise intensity $E$. In this study we only evaluated our model for $E$=0.5. Also, a module should be added for predicting $E$ based on real-time activity sensor inputs such as heart-rate monitors and accelerometers.

Finally and most importantly, the insulin-kinetics model needs to be incorporated into a model of glucose-metabolism. This will make the relationship between exercise, insulin-kinetics, and glucose-metabolism much more evident. This work will begin in Chapter 3, where a model of glucose-metabolism during exercise is derived.

## 2.5 Conclusion

We have derived an insulin-kinetics model that includes the effects of exercise on insulin absorption from the subcutaneous tissue and insulin delivery to skeletal muscle. Using parameters based in physiology found in the literature, the model gives reasonable predictions of plasma insulin concentrations during rest and exercise periods. During exercise the absorption rate is predicted to increase by 45% and the delivery rate by 150% compared to rest. These kinetic changes significantly alter the insulin concentration in skeletal muscle which induces significant glucose uptake. The model provides insight into the physiology that governs insulin-kinetics. In the future the model can be incorporated into a broader model of glucose-metabolism, which can provide higher fidelity predictions during exercise that are useful in model predictive control algorithms for the artificial pancreas.

# Chapter 3

# Modeling the Acute Effects of Exercise on Glucose-Dynamics

## Chapter Overview

Acute exercise directly affects glucose-dynamics in three ways: it increases endogenous glucose production to keep up with glucose demand, it enhances the rate of glucose delivery

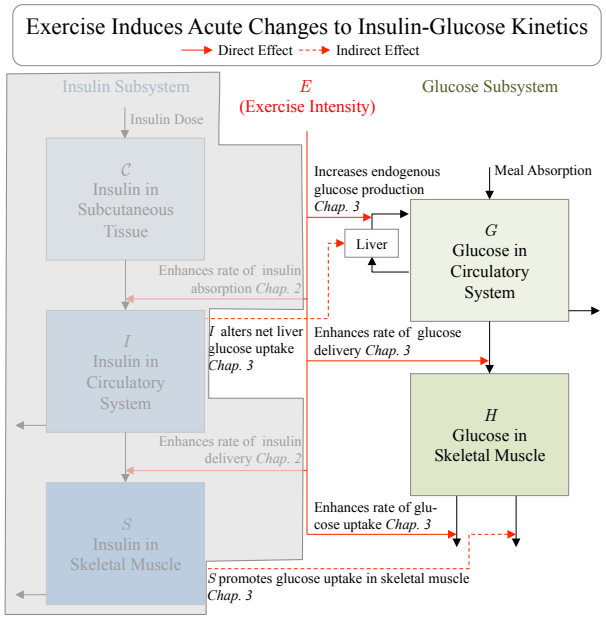


Figure 3.1: The focus of this chapter will be on the glucose subsystem model (unshaded region). There are three direct effects (red arrows) of exercise $E$ on glucose-dynamics. There are also 2 indirect effects of $E$ (dotted red arrows, from insulin) on glucose-dynamics. The insulin model in the shaded region was presented in Chapter 2.

from the blood to the skeletal muscle via capillary recruitment, and it directly induces glucose uptake in the skeletal muscle due to increased muscle demand for energy. There are also two indirect effects of exercise on glucose metabolism. These occur because insulin-kinetics are altered, which then alter glucose-dynamics. These five primary processes are shown in a block diagram in Figure 3.1. This chapter focuses on developing a model of glucose-dynamics during exercise.

In Section 3.1 some background and introductory information will be provided. In Section 3.2, the glucose-dynamics model is derived. For brevity, some details of the derivation are relegated to Appendix A. Section 3.3 will present model verification and results, and a discussion will follow in Section 3.4.

## 3.1 Introduction

Only four grams of glucose exist in the adult human circulatory system at any moment in time [36]. During exercise, this amount of glucose can be burned up in less than 10 minutes. Fortunately, the human body possesses an outstanding glucose-control system to keep glucose levels very near normal basal levels of 90 [mg/dL], even during rigorous exercise. This control system utilizes several hormones, mainly insulin and glucagon, to maintain glucose homeostasis. Unfortunately, in type 1 diabetes (T1D) this control system is faulty because insulin can no longer be secreted by the pancreas. Because of the lack of endogenously produced insulin, it must be replaced through injection, typically into the subcutaneous (SC) tissue. However, the appropriate insulin dose is highly variable and depends on food type/load of carbohydrates in the meal, current glucose levels, stress levels [5], physical activity [8] and a host of other factors [7]. An artificial pancreas (AP) that can autonomously and safely adjust the insulin dose would greatly improve the lives of those with T1D.

There are significant hurdles to the design of the AP. Many of these hurdles stem from the time-lag between SC injected insulin and the eventual action of insulin to lower glucose levels [44]. Onset of action is 15-30 minutes after injection and continues for 3-5 hours. This time-lag means that an effective and robust artificial pancreas must preemptively calculate the appropriate dose of insulin. This is especially difficult when exercise is involved because exercise significantly alters insulin-glucose dynamics [2] and therefore the appropriate insulin dose. If exercise is carried out when insulin-on-board (IOB) levels are high because of a recent insulin dose then dangerous hypoglycemia may occur [2, 24], which can cause dizziness, confusion, fainting, and in the most extreme cases, death.

Because of the potentially catastrophic ramifications of exercise in T1D patients, artificial pancreas controllers must explicitly account for the effects of exercise. This has been achieved mainly by shutting off insulin delivery during exercise [67]. However, by shutting down insulin delivery there is the other significant danger of diabetic ketoacidosis (DKA). For this reason, it is attractive to use a model predictive control (MPC) system in the AP to account for

exercise in a more systematic and robust manner [29, 69]. MPC requires a 'model' so that future predictions can be used to make a dosing decision at the current time.

Several pharmacokinetic-pharmacodynamic models of insulin-glucose dynamics exist in the literature, and range from minimal and simple to complex and broad. Some of the most popular models are the oral minimal model (OMM) developed by Bergman and Cobelli [55, 56], the glucose-insulin meal (GIM) model developed by Dalla Man and Cobelli [59, 60], and the Sorensen model [64]. Though originally derived to model insulin-glucose dynamics during rest, these three models have been amended in various ways to account for exercise [1, 58, 61, 65].

Each models has its own benefits and drawbacks. The OMM, as its name suggests, has the advantage that it contains the 'minimal' amount of variables and parameters needed to represent a subject's insulin-glucose dynamics. However, because of the limited model structure, it can only be applied in very limited situations and significant modifications would need to be made to fully amend the model for exercise conditions. The GIM is a more comprehensive insulin-glucose model and is perhaps the best validated model available in the literature. An exercise module has been added to the GIM [61], and it provides reasonable predictions. However, various important effects, such as capillary recruitment and exercise effects on endogenous glucose production were not directly included. The Sorensen model [64] is perhaps the most comprehensive model available, with a total of 15 compartments used to represent glucose-insulin dynamics. Roy and Lenart [65] amended the Sorensen model to include the effects of exercise. However, this exercise model has been validated in a post-hoc manner, only being used to describe the data that was used to obtain the exercise model parameters, and thus it may be subject to overfitting. Also, because of the model complexity, some of the exercise effects may not have been properly included. To the authors knowledge, the exercise addition to the Sorensen model has not been validated on any modern datasets.

Regardless of any criticism, each of the mentioned models have made significant contributions to our understanding of insulin-glucose dynamics. Still, none were developed specifically to handle exercise.

**Objective:** In this work, the objective is to develop a model of insulin-glucose dynamics specifically for exercise. The desire for modeling exercise effects will inform the model structure, and the focus will be on modeling phenomenon that are known to change *acutely* with exercise.

*Acute* effects are defined as the short term immediate changes to insulin-glucose dynamics during exercise. We are not focused on the *prolonged* effects of exercise. We estimate that there are five primary acute effects of exercise on insulin-glucose dynamics, as shown in Figure 3.1. This chapter focuses on modeling the three main acute effects of exercise on glucose-dynamics. The other two acute effects of exercise are limited to insulin-kinetics and are derived in Chapter 2. There are also two indirect effects of exercise on glucose-dynamics (shown by dotted lines in Figure 3.1). These will be also be included in the model, but discussion will be limited.

The three direct acute effects are (1) the change in the rate of glucose delivery ($k_d^G$) to

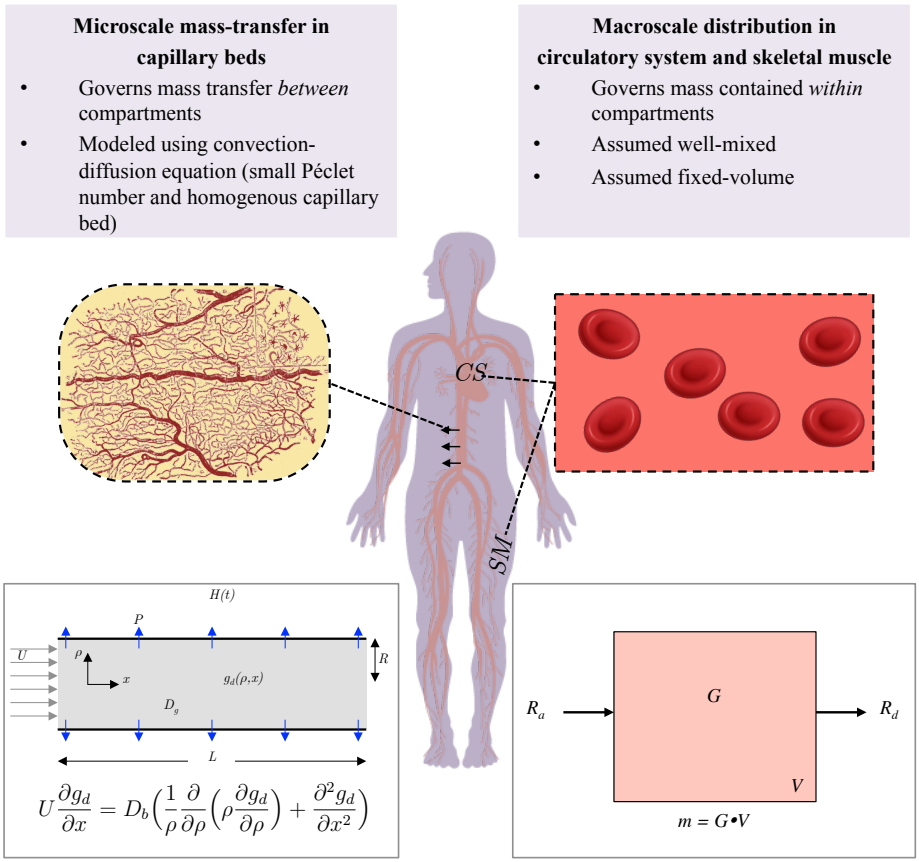


Figure 3.2: A multiscale approach is used to model glucose-dynamics.

peripheral tissues resulting from increases in the tissue perfusion rate and capillary recruitment, (2) the increase in the rate of endogenous glucose production ($EGP$) resulting from glucagaon release during exercise, and (3) the increase in the rate of glucose uptake ($RGU$) in peripheral tissues resulting from muscle contractions.

To include these effects we utilize a multiscale modeling approach. We include capillary recruitment by modeling *microscale* mass transfer through capillaries using the convection-diffusion equation. Distribution of glucose through the body is handled by *macroscale* models of the various whole-body glucose pools, represented by compartments. Exercise effects on $EGP$ and $RGU$ will be modeled phenomenologically and will act on the compartments directly. Figure 3.2 illustrates the multiscale modeling approach. The details of the model derivation are shown in Section 3.2.

## 3.2 Methods

### 3.2.1 Model Development

Glucose is distributed in several regions of the body: the circulatory system (CS), the peripheral interstitial fluid (ISF), the brain, the liver, the kidneys, the heart, the gut, and several other organs. In order to model the glucose balance in the blood, each of these regions needs to be accounted for. Sorensen [64] created a complete and exhaustive model of the glucose system, with each important compartment modeled. However, Sorensen modeled glucose at rest, and did not account for physiological changes brought on by exercise. These physiological changes are significant, altering not just how quickly glucose is delivered to each compartment, but how quickly glucose is metabolized. The purpose of this work is to evaluate the effects of exercise on glucose-dynamics and metabolism. This is done by creating a pharmacokinetic/dynamics (PKPD) model that focuses on the major quantified effects of exercise:

1. the change in the rate of glucose delivery ($k_d^G$) to peripheral tissues resulting from increases in the tissue perfusion rate and capillary recruitment
2. the increase in the rate of endogenous glucose production ($EGP$) resulting from glucagaon release during exercise
3. the increase in the rate of glucose uptake ($RGU$) in peripheral tissues resulting from muscle contractions

Because we are only focused on these three main effects, we do not need the same level of granularity and detail as the Sorensen model. The presently developed glucose model will consist of only two domains, the CS domain and the peripheral domain made up of subcutaneous and skeletal muscle tissue (SM) domain. A simple schematic of the model is shown in Figure 3.3. We will account for metabolism in other organs as simple sources or sinks, or alternatively, by incorporating previously developed models.

The change in $k_d^G$ will be modeled using concepts from microcirculation research that relate delivery rates to tissue perfusion rates ($Q_d$) and permeability surface area ($PS_d^G$). The increase in $EGP$ will be accounted for by incorporating direct measurements obtained using tracer methods, and also via an independently derived model of $EGP$. The increase in $RGU$ will be accounted for by utilizing data from literature that relates exercise intensity ($E$) to to $RGU$.

#### Note on Nomenclature

The model consists of multiple domains, each with their own domain specific parameters. In order to be concise with nomenclature, subscripts and superscripts will be used to denote the domain and the substance that the parameter belongs to, respectively. $V$ denotes either a volume of distribution of a volume of tissue. A superscript $V^{tiss}$ indicates a volume of

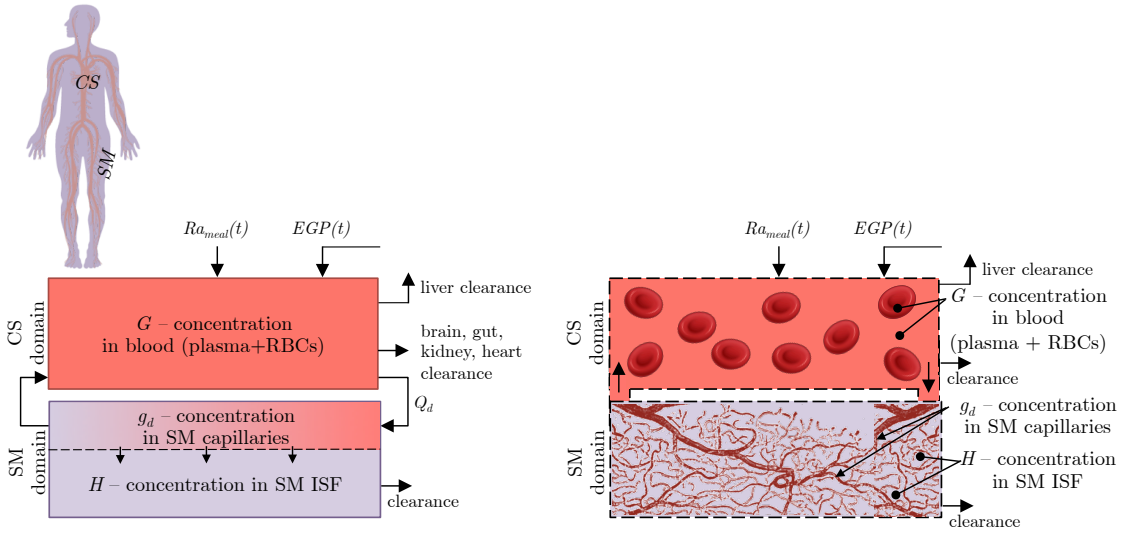


Figure 3.3: (left) Abstract schematic of the proposed glucose model. (right) Physiological representation of model. The model consists of two distinct domains: the circulatory system (CS) domain, and the skeletal muscle (SM) domain (the SM domain also includes subcutaneous tissue). The human silhouette illustrates which region each domain represents in the human body. Capillaries and ISF are both contained in the SM domain, and each are modeled separately. The life of glucose proceeds as follows: glucose is either absorbed from the GI tract ($Ra_{meal}$) or is released from the liver ($EGP$) and enters the CS. Glucose in the CS, at concentration $G$, is then either delivered to the brain, gut, kidney, or heart and metabolized, or taken up by the liver. Alternatively, glucose in the CS is delivered to SM by capillaries, which have blood flow rate $Q_d$ and glucose concentration $g_d$. Glucose in the SM domain, at concentration $H$, is taken up (cleared) by cells.

tissue, any other superscript denotes a volume of distribution (i.e. $V^G$). In some cases, a parameter will be normalized by either a mass or volume, and will be denoted by a second subscript, $_N$. As an example

$$V^G_{SM_N} \tag{3.1}$$

is the volume of distribution of glucose ($G$) in the skeletal muscle (SM) domain. The parameter is also normalized ($N$) by the total domain volume. A subscript $_b$ represents the basal value of a variable, i.e. $G_b$ is the basal glucose concentration.

### Circulatory System Domain, CS

The circulatory system (CS) domain includes all blood vessels and the heart, minus the capillaries in the skeletal muscle (SM) domain, which are $< 5\%$ of the total blood volume [104]. A schematic of the CS domain is shown in Figure 3.3.

The rate of change of the mass of glucose in the CS domain $\mathcal{G}$ is described by

$$\frac{d\mathcal{G}}{dt} = \dot{\mathcal{G}}_{in} - \dot{\mathcal{G}}_{out} - \dot{\mathcal{G}}_{cl} \tag{3.2}$$

where $\dot{\mathcal{G}}_{in}$, and $\dot{\mathcal{G}}_{out}$ are the mass flow rates of glucose into and out of the CS domain. $\dot{\mathcal{G}}_{cl}$ is the clearance mass flow rate from the CS domain. $\dot{\mathcal{G}}_{in}$ includes glucose originating from three sources: (1) ingested glucose absorbed through the gastrointestinal tract (GI) (rate of meal appearance, $Ra_{meal}$), (2) glucose absorbed from endogenous sources such as the liver and kidneys (endogenous glucose production, $EGP$), and (3) glucose entering the domain by convection from the SM domain (returning glucose from the delivering capillaries, $\dot{\mathcal{G}}_{in_d}$). $\dot{\mathcal{G}}_{in}$ can be written as

$$\dot{\mathcal{G}}_{in} = Ra_{meal}(t) + EGP(t) + \dot{\mathcal{G}}_{in_d}. \tag{3.3}$$

On the other hand $\dot{\mathcal{G}}_{out}$ includes only glucose departing the CS domain for the SM domain, which is denoted $\dot{\mathcal{G}}_{in_d}$

$$\dot{\mathcal{G}}_{out} = \dot{\mathcal{G}}_{out_d} \tag{3.4}$$

$\dot{\mathcal{G}}_{cl}$ includes clearance from the brain, heart, kidneys, gut, and liver. All glucose metabolic clearance rates $\mathrm{r}^G$ with the exception of the liver, are assumed constant. These approximates for each organ come from [45]. The brain, heart, kidneys, and gut will be referred to as 'fixed' rate tissues, and the rate of glucose uptake of these tissues $RGU_{CS_{fix}}$ is equal to the sum of the metabolic clearance rates

$$RGU_{CS_{fix}} = \mathrm{r}^G_{brain} + \mathrm{r}^G_{heart} + \mathrm{r}^G_{kidney} + \mathrm{r}^G_{gut}. \tag{3.5}$$

Developing a new model of liver glucose uptake is beyond the scope of the current work. However, considering that the liver has been estimated to absorb 50-60 % of total ingested glucose [119, 120], a model must be included. We adapt the liver glucose uptake model developed by Sorensen [64, p. 117]. Unlike the 'fixed' organs, the rate of glucose uptake in the liver $RGU_{CS_{liv}}$ is strongly dependent on both glucose and insulin concentrations. Lacking information on the effects of exercise on liver glucose uptake, we will assume that $RGU_{CS_{liv}}$ is independent of $E$. $RGU_{CS_{liv}}$ will be assumed to depend on $G$ and $S$, the insulin concentration in a compartment remote from the CS. Details of $RGU_{CS_{liv}}$ will be discussed in Section 3.2.2. The clearance rate $\dot{\mathcal{G}}_{cl}$ is equal to the total rate of glucose uptake from the CS domain $RGU_{CS_{TOT}}$, which is the sum of the fixed tissues and liver

$$\dot{\mathcal{G}}_{cl} = RGU_{CS_{TOT}} = RGU_{CS_{liv}}(G,S) + RGU_{CS_{fix}}. \tag{3.6}$$

The last step in developing our governing equation for the CS domain is to assume that glucose is well mixed (i.e. uniformly distributed) at concentration $G$ with a fixed volume of distribution $V^G_{CS}$. Applying the well-mixed assumption $\mathcal{G} = V^G_{CS} \cdot G$ and substituting Equations 3.3 - 3.6 into 3.2 we get

$$\frac{dG}{dt} = \frac{\dot{\mathcal{G}}_{in_d} - \dot{\mathcal{G}}_{out_d}}{V^G_{CS}} - \frac{RGU_{CS_{liv}}(G,S) + RGU_{CS_{fix}}}{V^G_{CS}} + \frac{Ra_{meal}(t) + EGP(t)}{V^G_{CS}}. \tag{3.7}$$

This equation models the plasma concentration of glucose in the CS domain. The specifics of the terms $\dot{\mathcal{G}}_{in_d}$ and $\dot{\mathcal{G}}_{out_d}$ will be defined in Section 3.2.1. The last two terms are time-dependent because they are measured fluxes, discussed in Section 3.2.2. However, $EGP(t)$ can be replaced by a model of $EGP(G,S,E)$, which is developed in Section 3.2.1.

**Skeletal Muscle Domain**

The skeletal muscle (SM) domain consists of all the peripheral tissues of the body (SM and SC tissue), which include the delivering capillaries (capillaries that perfuse the peripheral tissues) and the interstitial fluid (ISF). $\mathcal{H}$ is the total mass of glucose in the SM domain. Mass conservation on this domain yields

$$\frac{d\mathcal{H}}{dt} = \dot{\mathcal{H}}_{in} - \dot{\mathcal{H}}_{out} - \dot{\mathcal{H}}_{cl}. \tag{3.8}$$

$\dot{\mathcal{H}}_{in}$ is the mass flow rate of glucose entering the SM, $\dot{\mathcal{H}}_{out}$ is the mass flow rate of glucose exiting the domain, and $\dot{\mathcal{H}}_{cl}$ is the clearance mass flow rate of glucose from the SM. As in the CS domain, we will assume that glucose in the SM is well-mixed, and thus $\mathcal{H} = V_{SM}^{G} \cdot H$, where $H$ is the concentration of glucose in the ISF of the SM domain.

Glucose is continuously delivered to the SM tissue from the CS domain. The difference between the inlet mass flow rate $\dot{\mathcal{H}}_{in}$ and the outlet mass flow rate $\dot{\mathcal{H}}_{out}$ is equal to the rate of glucose delivery to the SM tissue

$$\dot{\mathcal{H}}_{d} = \dot{\mathcal{H}}_{in} - \dot{\mathcal{H}}_{out}. \tag{3.9}$$

$\dot{\mathcal{H}}_{cl}$ requires more rigorous treatment. Metabolic clearance of glucose (cellular uptake) can occur from either insulin-dependent or exercise-induced (a.k.a. insulin-independent) mechanisms [36].

Each of these mechanisms is postulated to be dependent on recruitment of the GLUT4 transporter to the cell membrane [36, 121–123]. GLUT4 is the transporter responsible for facilitating diffusion of glucose across the cell membrane. The higher the concentration of GLUT4 on the cell membrane, the faster the rate of uptake. Both insulin and exercise have been shown to increase the concentration of GLUT4 on the cell membrane. Some have postulated a 'two-pool' GLUT4 theory, which claims that separate pools of GLUT4 transports are reserved for insulin-induced recruitment and exercise-induced recruitment [123]. This theory would seem to support the idea of additive mechanisms, however there is still debate on whether insulin and exercise induced uptake is additive. A few prominent researchers have claimed that the effects are truly additive [121]. Others have claimed that there is a synergistic effect of insulin and exercise, where the combination of both leads to higher rates $RGU_{SM_{TOT}}$ than one would expect from the sum of each mechanism separately [40]. However, data on the synergistic interaction of insulin and exercise is limited and not well-understood. We will model the effects as simply additive, neglecting synergistic effects. The insulin-induced rate of glucose uptake is denoted as $RGU_{SM_{ins}}$ and the exercise-induced as $RGU_{SM_{exr}}$. The clearance rate, or total rate of glucose uptake $RGU_{SM_{TOT}}$, in the skeletal muscle domain is assumed to be the sum of both mechanisms of glucose uptake

$$\dot{\mathcal{H}}_{cl} = RGU_{SM_{TOT}} = RGU_{SM_{ins}} + RGU_{SM_{exr}}. \tag{3.10}$$

The specific expressions for each mechanism of uptake is derived in the next section. The final result is

$$RGU_{SM_{TOT}} = \frac{H}{H_b}(\mathrm{r}^G_{SM_{ins}} S + \mathrm{r}^G_{SM_{exr}} E) + \mathrm{r}^G_{SM_0}. \tag{3.11}$$

$\mathrm{r}^G_{SM_{ins}}$ and $\mathrm{r}^G_{SM_{exr}}$ are called the insulin sensitivity and exercise sensitivity of glucose uptake in skeletal muscle, respectively. With this expression, we have implicitly assumed that $RGU_{SM_{ins}}$ and $RGU_{SM_{exr}}$ are non-saturable and purely additive processes. Non-saturability has been assumed because $RGU$ doesn't significantly deviate from linear until very high glucose concentration $> 250$ [mg/dL] [124]. However, in T1D, non-saturability may be a poor assumption, as discussed in Chapter 4. In the next section the mathematical expressions representing each of these mechanisms are derived.

### Insulin-Dependent Glucose Uptake, $RGU_{SM_{ins}}$

The rate of glucose uptake induced by insulin, $RGU_{SM_{ins}}$, is dependent on both glucose concentration and insulin concentration. To illustrate this process, consider a permeable cell membrane in SM insulin-sensitive tissue. A schematic is shown in Figure 3.4. In this case, we want to derive an expression for $RGU_{SM_{ins}}$, so we set $E = 0$.

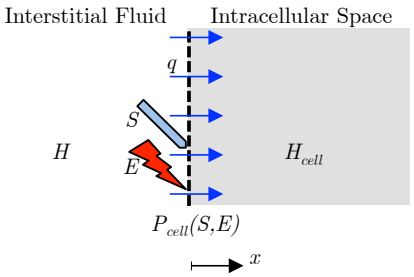


Figure 3.4: Schematic of insulin-sensitive cell with a cell membrane that is permeable to glucose. $q$ is the flux across the cell membrane. $x$ is the positive direction toward the center of the cell. $H$ and $H_{cell}$ are the glucose concentrations inside and outside the cell. $P_{cell}$ is the permeability of the cell membrane to glucose. $S$ is the insulin concentration outside the cell and $E$ is the exercise intensity (shown as muscle contraction); both are shown as modulators of $P_{cell}$. $P_{cell}$ is assumed to depend on $S$ and $E$ in an additive fashion.

According to Fick's law the concentration difference drives flux $q$

$$q = -D_{cell}\frac{d\mathrm{h}}{dx}. \tag{3.12}$$

Where $D_{cell}$ is the diffusivity of glucose through the cell membrane, h is the local glucose concentration, and $x$ the coordinate toward the center of the cell. Note we are considering a very small portion of the cell membrane, which can be approximated with Cartesian coordinates.

By assuming a constant gradient across the cell membrane we rewrite as

$$q = P_{cell}(H - H_{cell}). \tag{3.13}$$

Where $P_{cell}$ is the permeability of the cell membrane to glucose, $H$ is the glucose concentration outside the cell (same as concentration in the ISF), and $H_{cell}$ is the glucose concentration inside the cell. Further assuming that $H_{cell} \ll H$, and then multiplying Equation 3.13 by the total surface area of all insulin-sensitive cells in the SM domain we get

$$qA = RGU_{SM_{ins}} = P_{cell}AH. \tag{3.14}$$

The permeability of the cell to glucose, $P_{cell}$, is known to depend on the insulin concentration $S$. This stems from the observation that the primary glucose transporter GLUT4 is recruited to the cell membrane roughly proportionally to $S$ [122], barring saturation. We thus assume $P_{cell} = kS$. Substituting and combining $k$ with $A$ into a single constant, $\alpha$, we obtain

$$RGU_{SM_{ins}} = \alpha SH. \tag{3.15}$$

This expression has the same functional dependence as that proposed by Bergman [125] in the well-studied oral glucose minimal model [55, 56, 126, 127]. This form has also been validated at clamped basal insulin with varying glucose by [128], and clamped basal glucose and varying insulin by Castillo [70]. In the later study, $RGU$ was found to be proportional to $S$ at fixed basal glucose $H_b$. Following this observation, we evaluate Equation 3.15 at $H_b$

$$RGU_{SM_{ins}}|_{H_b} = \alpha H_b S. \tag{3.16}$$

We define proportionality factor between $RGU_{SM_{ins}}|_{H_b}$ and $S$ to be $\mathrm{r}^G_{SM_{ins}}$=$\alpha H_b$. The constant of $\mathrm{r}^G_{SM_{ins}}$ can be thought of as the insulin sensitivity. However, to generalize the expression for all glucose concentrations, we desire to find the proportionality factor $\alpha$. We simply solve for $\alpha = \mathrm{r}^G_{SM_{ins}}/H_b$ and substitute to obtain

$$RGU_{SM_{ins}} = \mathrm{r}^G_{SM_{ins}}\frac{H}{H_b}S + \mathrm{r}^G_{SM_0}. \tag{3.17}$$

This is the final expression for $RGU_{SM_{ins}}$. We have added an additional term $\mathrm{r}^G_{SM_0}$ to account for the observation that even at zero insulin, there is still finite glucose uptake in the $SM$ tissue.

### Exercise-Induced Glucose Uptake, $RGU_{SM_{exr}}$

Exercise significantly increases glucose uptake by skeletal muscle (SM) independent of changes in insulin or glucose concentrations. This has been repeatedly shown by measuring leg glucose uptake during exercise, while clamping glucose and insulin concentrations at basal concentrations [35, 39, 40, 129, 130]. To include this effect in our model we will derive an expression for exercise-induced rate of glucose uptake, $RGU_{SM_{exr}}$.

We start by again considering glucose uptake into a cell in the SM domain, shown schematically in 3.4. In this case, we focus on the effect that exercise intensity $E$ has on $P_{cell}$. We start with a similar expression to Equation 3.14, modified for exercise

$$RGU_{SM_{exr}} = P_{cell} A H. \tag{3.18}$$

Richter has shown that $RGU_{SM_{exr}}$ is roughly proportional to intensity[90, p. 926]. This behavior is consistent with $P_{cell}$ being proportional to $E$; $P_{cell} = kE$. Defining $\beta = kA$, we obtain

$$RGU_{SM_{exr}} = \beta E H. \tag{3.19}$$

Evaluating this expression at $H_b$, we obtain

$$RGU_{SM_{exr}}|_{H_b} = \beta H_b E. \tag{3.20}$$

We define the proportionality factor between $RGU_{SM_{exr}}|_{H_b}$ and $E$ as $\mathrm{r}^G_{SM_{exr}} = \beta H_b$. The constant $\mathrm{r}^G_{SM_{exr}}$ can be thought of as the exercise sensitivity. To estimate $\mathrm{r}^G_{SM_{exr}}$ we use data from several studies (shown in Section 3.2.2) that have measured leg RGU at basal glucose [35, 39, 40, 129, 130]. We solve for $\beta = \mathrm{r}^G_{SM_{exr}}/H_b$ and substitute into Equation 3.19 to obtain our final expression

$$RGU_{SM_{exr}} = \mathrm{r}^G_{SM_{exr}} \frac{H}{H_b} E. \tag{3.21}$$

The form of this expression is confirmed by the results from studies with varying $E$ and fixed $H$ [35, 39, 40, 129, 130] and fixed $E$ and varying $H$ [90, p. 922].

One final assumption is that the activity is primarily leg exercise, i.e. walking or bicycling. This is because $\mathrm{r}^G_{SM_{exr}}$ is derived based on measurements of glucose uptake across the leg during these activities. This should be a good assumption if the subject is walking or bicycling but for exercise that focuses on the upper body a different value of $\mathrm{r}^G_{SM_{exr}}$ may need to be derived.

*Final Expression Governing $H$.* The final expression for $H$ can be found by substituting Equations 3.9 and 3.11 (note: $\dot{\mathcal{H}}_{cl} = RGU_{SM_{TOT}}$) into 3.8, and assuming a well-mixed compartment ($\mathcal{H} = V^G_{SM} \cdot H$)

$$\frac{dH}{dt} = \frac{\dot{\mathcal{H}}_d}{V^G_{SM}} - \frac{1}{V^G_{SM}} \Big( \frac{H}{H_b} (\mathrm{r}^G_{SM_{ins}} S + \mathrm{r}^G_{SM_{exr}} E) + \mathrm{r}^G_{SM_0} \Big). \tag{3.22}$$

The first term is the rate of glucose delivery from the CS domain into the SM compartment, and the second term represents insulin-dependent and exercise-induced glucose uptake. The constant term $\mathrm{r}^G_{SM_0}$ is the rate of glucose uptake at zero insulin.

### Model of Endogenous Glucose Production

One of the limitations of using $EGP$ input data is that the data is only valid under the conditions for which it was measured. In our case the data was taken for a mixed meal tolerance test with exercise beginning at minute 120. To allow for an estimate of $EGP$ under other conditions, we have created a model of $EGP$ based on data from literature, and validated on the triple-tracer measurements from our exercising patient cohort. We assume a form for our model

$$EGP = EGP_b \cdot \frac{G_b}{G}\frac{S_b}{S}(1+L) \tag{3.23}$$

where $EGP_b$ is the basal value of $EGP$, set to be equal and opposite to $RGU_{TOT}$ under basal conditions. $EGP$ is chosen to be inversely proportional to $G$ and $S$ based on observations of near complete $EGP$ suppression following a meal [54, 113]. $L$ is the exercise-action on $EGP$, and is governed by an ODE that takes exercise intensity $E$ as its input

$$\frac{dL}{dt} = \frac{1}{\tau_{EGP}}(-L + \eta E). \tag{3.24}$$

The parameter $\tau_{EGP}$ is the time-constant that represents the time-lag of increased exercise-action on $EGP$. The parameter $\eta$ is the maximum exercise-action on $EGP$. For example, an $\eta$=2 [unitless] allows EGP to increase by a maximum of 200% as a result of exercise. $L$ can be thought of as a surrogate for glucagon release that occurs during exercise. $L$ is delayed because changes in $EGP$ due to exercise are known to lag the onset of exercise [35, 39, 113]. Details of parameter selection for the $EGP$ model are given in Section 3.2.2. $EGP(t)$ indicates when measured $EGP$ is used as an input into the model. $EGP(G, S, E)$ indicates when the modeled $EGP$ is used.

### Delivering Capillaries

Glucose is delivered to the SM domain via convection from the CS domain into the 'delivering' capillaries, which belong to the SM domain. Once in these delivering capillaries, glucose then diffuses into the ISF by permeating the capillary wall through endothelial pores and junctions [37]. We assume that the delivery processes is driven by pure diffusion; flux across the endothelial walls is driven only by concentration gradients, not pressure differences, microfiltration effects, or facilitated diffusion. This assumption allows us to model the physics of delivery using Fick's Law.

The concentration in a delivering capillary is governed by the cylindrically symmetric convection-diffusion equation with axial flow only and pure diffusion at the walls

$$U\frac{\partial g_d}{\partial x} = D_g\Big(\frac{1}{\rho}\frac{\partial}{\partial \rho}\Big(\rho\frac{\partial g_d}{\partial \rho}\Big) + \frac{\partial^2 g_d}{\partial x^2}\Big) \tag{3.25}$$

$$q = P_g(H - g_d) \text{ at } \rho = R. \tag{3.26}$$

$g_d$ is the concentration in a delivering SM capillary, $D_g$ is the diffusion coefficient of glucose in plasma, $P_g$ the permeability of the capillary wall to glucose, and $U$ is the velocity of blood through capillaries. We utilize the same solution that was derived for insulin delivery in Chapter 2 (Appendices A.2 and A.3), but will use different parameter values to make the solution specific to glucose

$$g_d(x,t) = H(t) - (H(t) - G(t))e^{-\frac{PS_d^G}{Q_d}\frac{x}{L}} \tag{3.27}$$

$g_d$ changes with time $t$ and axial distance, $x$. $PS_d^G$ is the permeability surface area of a delivering capillary to glucose, $Q_d$ is the tissue perfusion rate in the delivering capillaries (RBCs and plasma), and $L$ is the length of a capillary. To obtain Equation 3.27, we have made several assumptions: (1) we have a low Péclet number and thus the mass-transfer boundary layer is large and the radial concentration gradient is small, this allows us model the concentration $g_d$ as constant in the cross section. (2) blood rapidly traverses the capillary and thus boundary conditions can be held fixed when solving for $g_d$ (3) the capillary has uniform properties along its length, and (4) the capillary bed is homogeneous, meaning each capillary in the domain has identical properties and is uniformly perfused.

In the real case the capillary bed is heterogeneous, and thus our homogeneous assumption may prevent us from capturing some non-linear effects. These may indeed be important for modeling glucose delivery [38], however absent detailed information about the heterogeneity of a typical capillary bed, and with the desire to model parsimony, we assume homogeneous capillary beds.

### Coupling the Domains

Now that we have an expression for each domain, our next goal is to couple the domains. We do this by relating the fluxes across the domain boundaries.

In quasi-steady state, a control volume around the SM domain (shown by the dotted line in Figure 3.5) reveals that $\dot{\mathcal{H}}_d$, the total glucose delivered to the SM tissue, is equal to the difference between the mass flow rate back into the CS domain from the delivering capillaries, $\dot{\mathcal{G}}_{in_d}$, and out of the CS domain to the delivering capillaries $\dot{\mathcal{G}}_{out_d}$.

$$\dot{\mathcal{H}}_d = -(\dot{\mathcal{G}}_{in_d} - \dot{\mathcal{G}}_{out_d}). \tag{3.28}$$

Simply stated, if the glucose flux leaving the CS is greater than the glucose flux reentering the CS, then a finite amount of glucose was *delivered* to the SM.

Now, the mass flow rate of glucose crossing the boundary of a domain is equal to the local concentration $g_d$, times the volume flow rate $Q_d$. We can thus express the convective terms $\dot{\mathcal{G}}_{in_d}$ and $\dot{\mathcal{G}}_{out_d}$ as

$$\dot{\mathcal{G}}_{in_d} = \int_{V_{SM}^{tiss}} Q_d g_d|_e \, dV = Q_d V_{SM}^{tiss}\left(H - (H-G)e^{\frac{-PS_d^G}{Q_d}}\right) \tag{3.29}$$

$$\dot{\mathcal{G}}_{out_d} = \int_{V_{SM}^{tiss}} Q_d g_d|_i \, dV = Q_d V_{SM}^{tiss} G \tag{3.30}$$

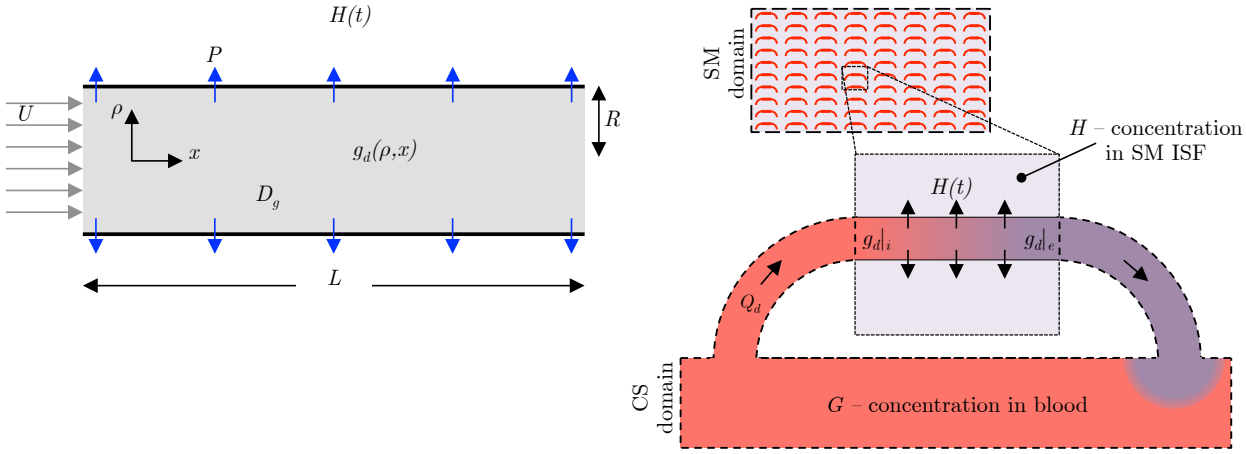


Figure 3.5: (left) Schematic of flow in a capillary. Blood enters from the left at uniform velocity $U$ and initial concentration $g_d|_i$. $D_g$ is the diffusion coefficient of glucose in blood plasma. $L$, $R$, and $P$ are the capillary length, radius, and permeability, respectively. The outside of the vessel wall is assumed to be wetted with a uniform drug concentration $H(t)$. (right) Mass transfer from a single capillary from a bed of homogeneous capillaries in the skeletal muscle (SM) domain. Each capillary can be thought to act as a local mass-exchanger with inlet concentration $g_d|_i$ and exit concentration $g_d|_e$. By integrating over the entire volume of SM tissue $V_{SM}^{tiss}$ and therefore all capillaries in the SM, we obtain the total drug delivered to the SM tissue from the CS per unit time, $\dot{\mathcal{H}}_d$.

$g_d|_i$ and $g_d|_e$ are the glucose concentrations at the inlet about outlet of the delivering capillaries in the $SM$ domain. Their specific values were found by evaluating Equation 3.27 at $x = 0$ and $x = L$. Substituting Equations 3.29 and 3.30 into 3.28, we obtain

$$\dot{\mathcal{H}}_d = V_{SM}^{tiss} Q_d (1 - e^{\frac{-PS_d^G}{Q_d}})(G - H). \tag{3.31}$$

3.31 and 3.28 can be substituted into the field equations 3.7 and 3.22 to obtain the final form of the glucose model.

The coefficient in Equation 3.31 is the rate constant that governs glucose flux between the two domains

$$k_d^G = Q_d (1 - e^{\frac{-PS_d^G}{Q_d}}). \tag{3.32}$$

$k_d^G$ depends on the tissue perfusion rate $Q_d$ and the permeability surface area $PS_d^G$. Depending on the value of these parameters, the problem is either surface area limited or flow limited. For typical glucose parameters, the problem is a mix between flow limited and surface area limited. Changes in perfusion rate and surface area during exercise both serve to increase the delivery rate.

A similar solution was previously derived for the purposes of studying the microcirculation and nutrient delivery by Renkin [79] and further discussed in [38]. We have independently derived $k_d^G$ for the purposes of modeling glucose delivery during exercise.

**Insulin Concentration,** $S$

The glucose model takes insulin concentration in the SM domain, $S$, as an input. However, the data only has measurements of the insulin concentration in plasma, $I$. Thus, we add one more equation to the model to capture the time-lag from $I$ and $S$. We model insulin-kinetics identically to how we modeled glucose in the $SM$ domain; Utilizing a one compartment model, which takes our measured $I$ as an input.

$$\frac{dS}{dt} = \frac{V_{SM}^{tiss} k_d^I (I(t) - S)}{V_{SM}^I} - \mathrm{r}_{SM_N}^I \cdot S \tag{3.33}$$

$$k_d^I = Q_d^I (1 - e^{\frac{-PS_d^I}{Q_d^I}}) \tag{3.34}$$

$$PS_d^I(E) = PS_{d_{rest}}^I (1 + R_d tanh(\gamma E)) \tag{3.35}$$

$k_d^I$ is the insulin delivery rate and depends on exercise through the tissue perfusion rate of plasma (assumed 40% hematocrit), $Q_d^I$, and the the capillary permeability surface area to insulin $PS_d^I$. $\mathrm{r}_{SM_N}$ is the normalized metabolic clearance rate of insulin in the $SM$ domain.

This equation was derived in Chapter 2, and the details will not be discussed here. The parameters of the insulin model will be discussed in the next section.

### 3.2.2 Inputs and Parameters

The glucose model consists of glucose sources ($Ra_{meal}$ and $EGP$), glucose metabolic clearance rates ($\mathrm{r}^G$), and glucose delivery rates ($k^G$). The glucose inputs were measured in humans using metabolic tracers. The metabolic clearance rates are modeled based on glucose uptake measurements found in literature. Delivery rates are taken from microcirculation measurements found in literature.

r and $k$ are affected by exercise intensity $E$ due to increased demand, increased perfusion rate, and capillary recruitment. In some cases, these parameters have been measured at different levels of $E$. In others, no measurements exist, and the parameters need to be derived.

The inputs and the selection of parameters is described below. All the model parameters are summarized in Table 3.1.

### Exercise Intensity, $E$

For the parameters that are dependent on exercise, we define input $E$, which quantifies exercise intensity. We define $E$, as a ratio of $\mathrm{V0}_{2_{max}}$

$$E = \frac{\mathrm{V0}_2}{\mathrm{V0}_{2_{max}}}. \tag{3.36}$$

$E = 0$ is at rest and $E = 1$ is at maximal exercise. $E$ is a continuous input to the model. Specifically, $Q_d$ and $PS_d^G$ will depend directly on $E$, and in turn the magnitudes of $Q_d$ and $PS_d^G$ will directly determine the delivery rate $k_d^G$.

### Glucose Inputs ($Ra_{meal}$ and $EGP$ )

The two glucose inputs to the model are the rate of meal appearance $Ra_{meal}$, which is the rate that an ingested meal reaches the CS, and the rate of endogenous glucose production $EGP$, which is the rate that glucose is produced (and released in the CS) by endogenous sources in the body (mainly the liver). The difference between the glucose inputs and the total rate of glucose uptake ($RGU$) is responsible for the balance of glucose in the bloodstream, and directly determines $G$. A typical measured $Ra_{meal}$ and $EGP$ for a 75 [g] carbohydrate (CHO) meal in a healthy (non-diabetic) resting subject and exercising subject is shown in Figure 3.6. Each of these inputs are expressed in [mg/min], and are included in the glucose model in Equation 3.7.

Notice that $EGP$ rapidly increases during exercise. This is the body's natural response to the increased glucose uptake associated with exercise. Without this robust increase in $EGP$, hypoglycemia may occur.

The accurate measurement of postprandial glucose fluxes is difficult. We have utilized the most reliable method, the triple-tracer method, to measure $Ra_{meal}$ and $EGP$. This method utilizes three independent tracers to clamp tracer to tracer ratios. Details of this methodology can be found in the introductory Chapter 1.4 and in the original paper in which the method was described [46].

Slight pre-processing of $EGP$ and $Ra_{meal}$ was done. To ensure that under no perturbation, steady-state is achieved, $EGP$ was scaled to be equal to basal $RGU_{TOT}$, which on average is 155 [mg/min] [45, p. 219]. Also, measurements of $Ra_{meal}$ tend to be an overestimate of actual $Ra_{meal}$. To correct for this, $Ra_{meal}$ was scaled so that its area under the curve is equal to 0.9 $d$, where $d$ is the total dose (i.e. a 75 [g] meal), and 0.9 is the ratio of the ingested meal that is absorbed into the bloodstream [131].

### EGP Model Parameters

An alternative to using the direct triple-tracer measurements of $EGP$, as shown in the previous section is to use the $EGP$ model described by Equations 3.23 and 3.24.

The EGP model contains two parameters, $\tau_{EGP}$ and $\eta$. $\tau_{EGP}$ represents the time-lag of increased exercise-action on $EGP$. The parameter $\eta$ is the maximum exercise-action on

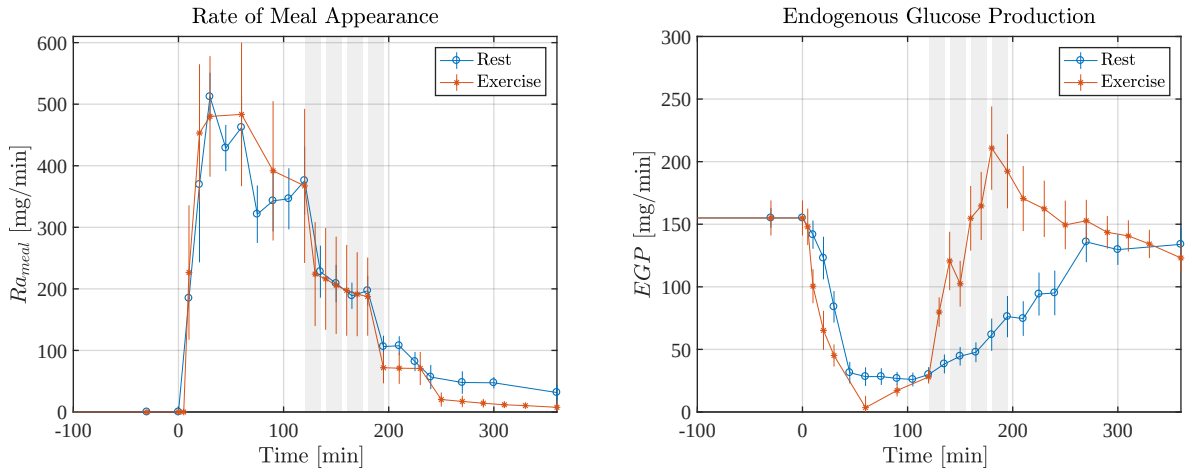


Figure 3.6: Typical measured rate of meal appearance ($Ra_{meal}$) and endogenous glucose production ($EGP$) for an average healthy (non-diabetic) resting subject and an average healthy exercising subject. Meal ingestion for each group occurs at $t = 0$. The exercising group has four 15 minute exercise bouts from t=120-195 shown by shaded regions. $Ra_{meal}$ during fasting is 0 [mg/min]. Upon ingestion of the meal $Ra_{meal}$ rapidly increases to a maximum near 500 [mg/min], and then slowly declines over the next 6 hours to nearly 0. There is not a significant difference in $Ra_{meal}$ between the resting and exercising subject. On the other hand, there is a profound difference in $EGP$ during exercise. $EGP$ is initially 155 [mg/min] and is rapidly suppressed upon meal ingestion. In the resting group it slowly rises back to basal levels as glucose levels and insulin levels return back to basal. In contrast, during exercise $EGP$ rapidly increases, reaching a maximum of 210 [mg/min] (35 % above basal). This rapid increase in $EGP$ is an important effect to include in a model of glucose metabolism during exercise. Vertical lines are SEM.

$EGP$. For example, an $\eta$=2 [unitless] allows EGP to increase by a maximum of 200% as a result of exercise.

These parameters are estimated from data taken from two studies by Ahlborg [35, 39], where exercise was done at 60% $V0_{2_{max}}$ in [35] and 30% $V0_{2_{max}}$ in [39]. The model fit is shown in Figure 3.7, along with the data from [35, 39]. The estimated parameters are $\tau_{EGP}$=20 [min] and $\eta$=4 [unitless].

### Rate of Glucose Uptake from the Circulatory System, $RGU_{CS}$

The total rate of glucose uptake from the circulatory system is equal to the sum of glucose uptake in the liver, brain, heart, kidney, and gut. As specified in Equations 3.6, and repeated here

$$RGU_{CS_{TOT}} = RGU_{CS_{liv}}(G, S) + RGU_{CS_{fix}} \tag{3.37}$$

As previously defined in Equation 3.5, we lump the the brain, heart, kidney, and gut into $RGU_{CS_{fix}}$, as they are considered constant rates in our model. Uptake by these tissues has not been shown to be significantly dependent on exercise [132], nor glucose or insulin concentration. The values that we have chosen for the $RGU$ of each of these organs was

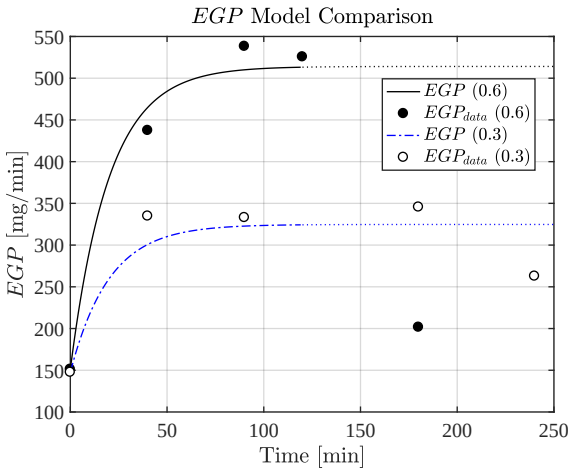


Figure 3.7: The EGP model is plotted (solid and dashed lines) vs. exercise intensity $E$. The model is defined in Equations 3.23 and 3.24 and parameters are identified by fitting to data from [35, 39], where $EGP$ was measured at 30% (open circles) and 60% (closed circles) $V0_{2_{max}}$. Notice that after prolonged exercise (>120 [min]) the $EGP_{data}$ drops off drastically, while the model stays constant. This is due to depletion of glycogen stores. The derived EGP model is not valid beyond 2-3 hours because it assumes sufficient glycogen storage for conversion to glucose. The extended segment (dotted line) indicates where the model is no longer valid.

taken from [45, p. 219]; $r^G_{brain} = 71$ [mg/min], $r^G_{heart} = 4$ [mg/min], $r^G_{kidney} = 4$ [mg/min], and $r^G_{gut}16.6$ [mg/min]. Thus $RGU_{CS_{fix}}$ is

$$RGU_{CS_{fix}} = 95.6 \text{ [mg/min]} \tag{3.38}$$

For the liver, we have adapted a model of liver glucose uptake developed by Sorensen [64]. This model augments the basal rate of liver glucose uptake $r^G_{liv}$ according to current glucose and insulin concentrations. $RGU_{CS_{liv}}$ is

$$RGU_{CS_{liv}} = r^G_{liv} M(G) M(S) \tag{3.39}$$

$M(G)$ and $M(S)$ are multiplicative factors that specify how $RGU_{CS_{liv}}$ depends on glucose and insulin concentrations $G$ and $S$. $M(G)$ and $M(S)$ are both modeled as saturable functions of $G$ and $S$. In the original Sorensen model, $M(G)$ and $M(S)$ depended on the glucose and insulin concentration in the liver. In our model, we have not included the liver as a separate compartment, and thus we instead assume that $M(G)$ is dependent on the glucose concentration in the blood, and that $M(S)$ is dependent on the insulin concentration in the SM tissue. This should be a reasonable modification, as the time-lag between our remote compartment should be similar to the time-lag in Sorensen's liver compartment.

The final liver model is

$$RGU_{CS_{liv}} = r^G_{liv}\big(5.66 + 5.66 \cdot tanh(2.44(\frac{G}{G_b} - 1.48))\big) M \tag{3.40}$$

$$\frac{dM}{dt} = \frac{1}{\tau_{liv}} 2.0 \cdot tanh(0.55 \frac{S}{S_b}). \tag{3.41}$$

$M$ is modeled with a time-lag $\tau_{liv} = 25$ [min] to account for the observation that the liver does not immediately respond to increases in $S$. All of the numbers were derived by Sorensen and based on data from experiments on liver glucose uptake.

$\mathrm{r}^G_{liv}$ was set to 15 [min/min], a slight downward adjustment from the typical 20 [mg/min]. This ensured that $RGU_{liver}$ is approximately equal to 50% of total glucose ingested, which is consistent with studies by [120]. At basal glucose and insulin concentrations, $RGU_{CS_{TOT}} =$ 110.6 [mg/min]. The remainder of the 155 [mg/min] of glucose uptake occurs in the $SM$ domain.

### Rate of Glucose Uptake from the Skeletal Muscle, $RGU_{SM}$

The expression for skeletal muscle rate of glucose uptake ($RGU_{SM}$) was derived in Section 3.2.1 (Equation 3.11)

$$RGU_{SM_{TOT}} = \frac{H}{H_b}(\mathrm{r}^G_{SM_{ins}} S + \mathrm{r}^G_{SM_{exr}} E) + \mathrm{r}^G_{SM_0}. \tag{3.42}$$

This expression contains three parameters; $\mathrm{r}^G_{SM_{ins}}$, $\mathrm{r}^G_{SM_{exr}}$, and $\mathrm{r}^G_{SM_0}$. These represent, respectively, the metabolic clearance rate due to insulin (i.e. insulin sensitivity), the metabolic clearance rate due to exercise (i.e. exercise sensitivity), and the metabolic clearance rate at zero insulin and zero exercise. Castillo and Bergman [70] estimated $\mathrm{r}^G_{SM_{ins}}$ by measuring $RGU_{SM_{TOT}}$ during rest at various SM insulin concentrations $S$, while holding glucose at basal concentrations. Their estimate ranged between $2 - 20$ [mg/min per $\mu$U/mL]. From this range we choose a reasonable insulin sensitivity of $\mathrm{r}^G_{SM_{ins}} = 5$ [mg/min per $\mu$U/mL].

To find the value of $\mathrm{r}^G_{SM_0}$ we evaluate Equation 3.42 during rest under basal conditions. $RGU_{SM_{TOT}}(E = 0, H = H_b, S = S_b)$ is equal to the basal metabolic clearance rate in peripheral tissue, $\mathrm{r}^G_{peri} = 44.6$ [mg/min] [45, p. 219]; the difference between basal $EGP$ (155 [mg/min]) and basal $RGU_{CS_{TOT}}$ (110.6 [mg/min]). Substituting, we obtain

$$\mathrm{r}^G_{SM_0} = \mathrm{r}^G_{peri} - \mathrm{r}^G_{SM_{ins}} S_b. \tag{3.43}$$

In our model, we are not interested in the value of $\mathrm{r}^G_{SM_0}$, as it is just a result of assuming that $RGU$ is linear in $S$. We thus eliminate $\mathrm{r}^G_{SM_0}$ by substituting Equation 3.43 back into Equation 3.42. After some rearranging, we get

$$RGU_{SM_{TOT}} = \mathrm{r}^G_{SM_{ins}}\big(\frac{H}{H_b} S - S_b\big) + \mathrm{r}^G_{SM_{exr}} \frac{H}{H_b} E + \mathrm{r}^G_{peri}. \tag{3.44}$$

This expression can then be evaluated with an estimate for $S_b$. Generally $S_b$ is approximately 50% of the plasma basal insulin concentration $I_b$ [44, 70, 101, 110–112]. In our model, $I_b$ is a measured input and thus $S_b$ can be estimated from Equation 3.33.

For the exercise sensitivity parameter $\mathrm{r}^G_{SM_{exr}}$, we utilize data from several studies on leg glucose uptake during exercise [35, 39, 40, 129, 130]. Each of these studies was carried out at

basal glucose and insulin concentrations. First, we evaluate Equation 3.44 at $H = H_b$ and $S = S_b$, leaving $E$ as a variable

$$RGU_{SM_{TOT}}|_{H_b,S_b} = \mathrm{r}^G_{SM_{exr}} E + \mathrm{r}^G_{peri}. \tag{3.45}$$

We estimate $\mathrm{r}^G_{SM_{exr}}$ by fitting the linear function (Equation 3.45) to $RGU$ data aggregated from several studies that have measured leg glucose uptake (LGU) at various levels of exercise [35, 39, 40, 129, 130]. We assume that LGU is equivalent to $RGU_{SM_{TOT}}$. This is reasonable because for walking and bicycling, the primary site of glucose uptake is the legs.

The data from the previous exercise studies is plotted in Figure 3.8. Equation 3.45 is fit to the data (neglecting the point at $E$=0.9) and is plotted in blue. The resulting slope is $\mathrm{r}^G_{SM_{exr}} = 860$ [mg/min] per unit $E$. This means that at 50% $E$, $RGU_{SM_{TOT}}$ would rise by 430 [mg/min].

The linear regression fits well in the range of moderate-exercise intensities ($E$=0.3-0.6), but because we have neglected the $E$=0.9 data point, the line underestimates uptake in the high-intensity range. This was done because only one datapoint was available at high-intensity exercise, and if included the best-fit line is significantly skewed upward, preventing accurate estimates of $RGU$ in the more reliable moderate-intensity exercise range. Additionally, the human data we have gathered is taken during moderate-intensity exercise, and thus for comparison purposes it is more important to predict $RGU$ at moderate-intensity than high-intensity exercise.

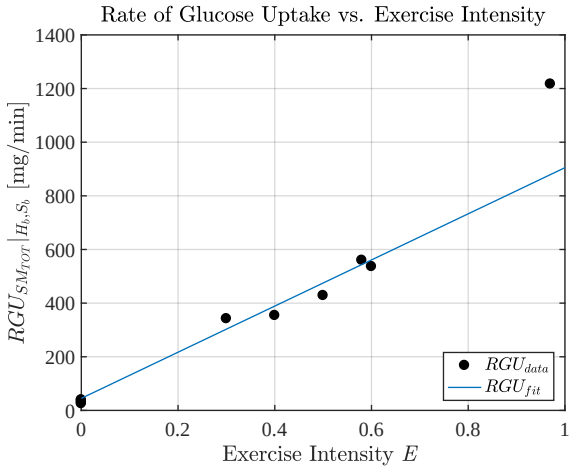


Figure 3.8: Relationship between total rate of glucose uptake in the skeletal muscle $RGU_{SM_{TOT}}$ and exercise intensity $E$, at basal glucose $H_b$ and basal insulin $S_b$. Equation 3.45 is shown (blue line), and the slope $\mathrm{r}^G_{SM_{exr}} = 860$ is fit to all aggregated data [35, 39, 40, 129, 130], excluding the $E = 0.9$ data point. As an example, at 50% $E$, if all else is held constant, $RGU_{SM_{TOT}}$ would rise by 430 [mg/min], 10-fold over resting $RGU$.

### Tissue Perfusion Rate, $Q$

The tissue perfusion rate, $Q_d$, in SM tissue has been quantified in many studies at rest and during exercise [83, 84]. Saltin [84] measured leg blood flow (LBF) at different levels of cardiac output (CO) and found a linear relation. If we assume that LBF is equivalent to $Q_d$ and that is CO is proportional to $\mathrm{V0}_{2_{max}}$, then we can use the data of Saltin to define a linear relationship between $Q_d$ and $E$

$$Q_d(E) = Q_{d_{rest}} + \lambda_d E \ [\mathrm{ml}_b/\mathrm{ml}_{tiss}/\mathrm{min}] \tag{3.46}$$

Where the resting value of SM blood flow $Q_{d_{rest}} = 0.038$ $[\mathrm{ml}_b/\mathrm{ml}_{tiss}/\mathrm{min}]$, comes from [83] and the slope $\lambda_d = 1.1$ $[\mathrm{ml}_b/\mathrm{ml}_{tiss}/\mathrm{min}$ per $E]$ comes from Saltin's relationship between LBF and CO [84]. Note that for convenience we have to converted from customary units of $Q_d$ $[\mathrm{ml}_b/100\mathrm{g}_{tiss}/\mathrm{min}]$ to $[\mathrm{ml}_b/\mathrm{ml}_{tiss}/\mathrm{min}]$ using an average tissue density of 1 $\mathrm{g/ml}_{tiss}$, which falls between the average tissue density for SC (0.91 $\mathrm{g/ml}_{tiss}$) tissue and SM tissue (1.09 $\mathrm{g/ml}_{tiss}$) [85]. $Q_d$ is plotted in Figure 3.9. $Q_d$ experiences a more than 20-fold increase at maximum $E$.

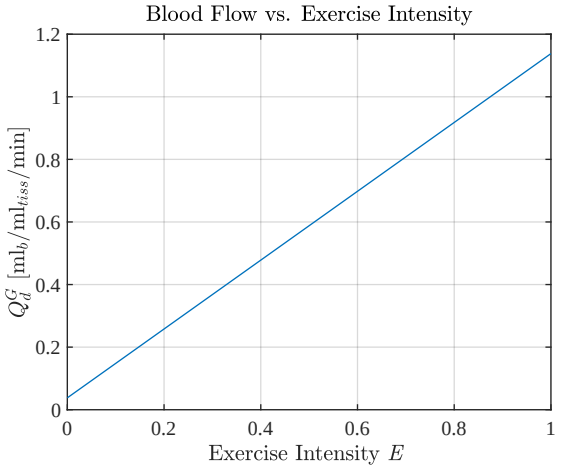


Figure 3.9: The blood flow relationship to be used in the proposed glucose model. Tissue perfusion rate in the skeletal muscle ($Q_d$) is assumed to be linearly dependent on exercise intensity($E$) and increases 20-fold at high-intensity exercise. Relationship taken from [84].

### Permeability Surface Area, $PS_d^G$

Permeability surface area ($PS$) is a measure of how permeable a capillary bed is to a certain solute. Many theorize that $PS$ increases during exercise because capillary recruitment increases the overall surface area in exercising muscle by fully perfusing capillaries that are underutilized at rest [89–91]. Renkin was one of the first to show this in a 1966 paper [91]

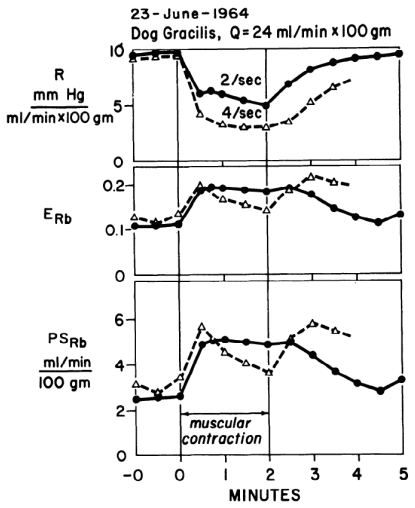


Figure 3.10: Results of Renkin [91] showing how $PS$ increases due to muscle contractions caused by electrical stimulation. In the bottom frame $PS$ nearly doubles during muscle contractions. Renkin attributed this to the recruitment of capillaries "We conclude that the increase in $PS$ ... ...produced during metabolic vasodilatation [is] brought about by an increase in the capillary surface area effectively in contact with flowing blood... ...it appears most likely that this change is brought about by the opening of precapillary sphincters which are closed under resting conditions."

where he demonstrated a near doubling of $PS$ during muscle contractions, shown in Figure 3.10.

In light of this study, capillary recruitment has been identified as a potentially important mechanism for the enhancement of nutrient exchange and delivery during exercise. Many others have sought to quantify capillary recruitment by other means. One of the most popular proxies for recruitment is the quantification of microvascular blood volume (MBV) by contrast enhanced ultrasound [92–94]. We will utilize this proxy to quantify recruitment, which is described by the recruitment factor, $R_d$.

We model $PS_d^G$ as a saturable process that is dependent on $E$. The saturability assumption stems from the concept of a finite reservoir of previously unrecruited capillaries that are recruited during exercise. The following function describes how $PS_d^G$ depends on $E$ and $R_d$

$$PS_d^G(E) = PS_{d_{rest}}^G(1 + R_d tanh(\gamma E)) \tag{3.47}$$

$PS_d^G$ refers to the permeability specific to glucose in the delivering capillaries of the SM domain. $PS_{d_{rest}}^G$ is the $PS_d^G$ value at rest. $\gamma$ is an unimportant free parameter that serves to modulate how quickly the function reaches its plateau value. $R_d$ is the recruitment factor, which indicates the maximum proportional increase in $PS_d^G$. We need to find values for three parameters: $PS_{d_{rest}}^G$,$R_d$, and $\gamma$.

Starting with $R_d$ we define the second term in Equation 3.47 as a new function $f_d$ that

describes recruitment

$$f_d = R_d tanh(\gamma E). \tag{3.48}$$

$f_d$ can be thought of as the proportional increase in the number of perfused capillaries in the SM tissue; $f_d = 0$ is no increase, $f_d = 0.5$ is a 50% increase, and $f_d = 2$ is a 200% increase. We quantify $f_d$ by using MBV as a proxy. Results of several MBV studies are shown in Figure 3.11, where MBV was quantified at different levels of exercise. By dividing the MBV value at exercise by the MBV value at rest (basal), we obtain values of $f_d$ at various exercise levels. These ratios are plotted as dots in Figure 3.12. The corresponding curve is Equation 3.48 with best-fit parameters $R_d$ and $\gamma$. Because goodness of fit is relatively insensitive to $\gamma$, we assign $\gamma = 10$, which indicates rapid recruitment even during light ($E = 0.25$) exercise. The plateau value that best describes the data is $R_d = 1.46$, indicating that maximal recruitment is approx 146%, a value consistent with various studies on microvascular recruitment, which place maximal recruitment in the range of 100 to 300 % [91, 98].

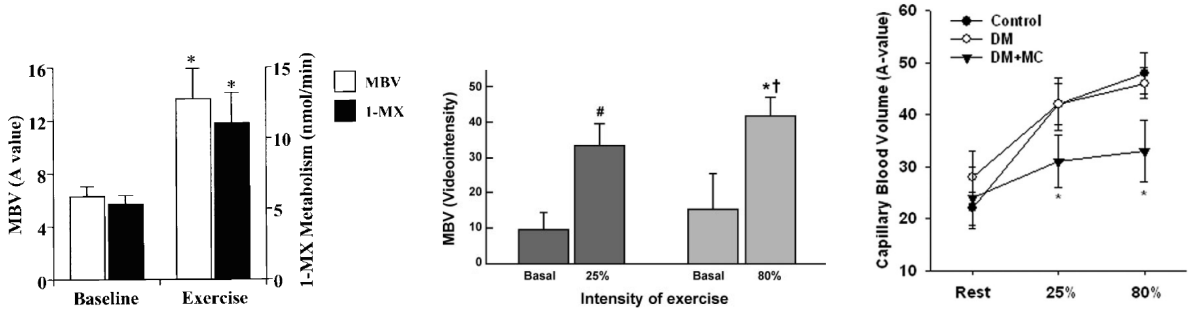


Figure 3.11: Three studies showing the effects of exercise on capillary recruitment, as quantified by changes in microvascular blood volume (MBV). All studies show that capillary density more than doubles during exercise, with only limited differences between light and heavy exercise. The ratios of MBV during exercise to MBV at rest are plotted in Figure 3.12 and used to fit parameters $\gamma$ and $R_d$. (left) [92] Recruitment is 115% after exercise as assessed by MBV and independently by the rate of 1-methylxanthine (MX) metabolism (another proxy for recruitment) in rat hindlimb adductor muscles. (center) [99] MBV is shown to increase roughly 240% during light and 163% during heavy forearm exercise. (right) [94] MBV in the human forearm is shown to increase 91% during light and 118% during heavy forearm exercise. Figures are used without permission.

The only other parameter that needs to be estimated to fully define Equation 3.47 is $PS^G_{d_{rest}}$. For this, we take direct measurements of from the literature[80, p. 33] [101, 102], which put $PS^G_{d_{rest}}$ in the range of 0.6-2.0 [ml$_b$/100g$_{tiss}$/min]. The wide range is due to the observation that capillary permeability changes during fasting, postprandial, or hyperinsulinemic conditions. Lacking complete data to describe $PS^G_{d_{rest}}$, we use a reasonable value of $PS^G_{a_{rest}} = 1.0$ [ml$_b$/100g$_{tiss}$/min] or 0.01 [ml$_b$/ml$_{tiss}$/min]. This value also predicts a reasonable resting glucose extraction fraction of 3-4%, which is consistent with measurements in literature.

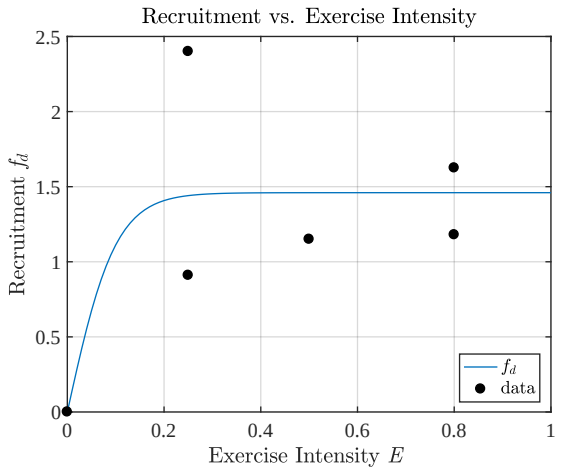


Figure 3.12: The relationship between capillary recruitment and exercise intensity is assumed to be a saturable process. The black dots are derived from the experimental results of various studies on capillary recruitment [92, 93, 100], which are summarized in Figure 3.11. Recruitment $f_d$ is defined to be zero at rest ($E = 0$) and is fit to data to find $R_d$ and $\gamma$ in Equation 3.48. $f_d$ rapidly increases to a plateau value of $R_d = 1.46$, indicating a 146% increase in capillary density during exercise.

With estimates for each of our parameters: $R_d$, $\gamma$, and $PS^G_{a_{rest}}$ we have fully identified our $PS^G_d$ model. $PS^G_d$ is plotted vs $E$ in Figure 3.13. As $E$ increases, $PS^G_d$ rapidly rises to its plateau values. By $E = 0.25$, capillary recruitment is essentially complete.

With expressions for $Q_d$ and $PS^G_d$ it is illustrative to examine how the glucose delivery rate $k^G_d$ depends on $E$. By substituting Equations 3.46 and 3.47 into Equation 3.32, we obtain the $k^G_d$ curve in Figure 3.13. $k^G_d$ follows a path very similar to $PS^G_d$. This is because $Q_d$ is high during exercise, and thus is not the limiting factor in glucose delivery. Rather, the limiting factor in glucose delivery is surface-area, and so $PS^G_d$ almost directly determines $k^G_d$.

### Volume of Distribution, $V^G$ and Tissue Volume, $V^{tiss}$

Glucose is a small molecule that readily dissolves in water. Hence, the volume of distribution of glucose is approximately the volume of water in each compartment.

Glucose in the CS is contained in both the plasma and the red blood cells (RBC). Equilibration between the two is rapid [64, p. 43] and thus glucose in the CS can be modeled as a single compartment. This volume relates the entire content of glucose the CS to the plasma concentration, and is called the volume of distribution $V^G_{CS}$. Specifically, it is a measure of the fluid volume that would be required to contain the total amount of glucose present in the CS, $\mathcal{G}_{CS_{TOT}}$, at the same concentration as that measured in the plasma, $G$.

$$\mathcal{G}_{CS_{TOT}} = \mathcal{G}_{CS_p} + \mathcal{G}_{CS_{RBC}} = G \cdot V^G_{CS}. \tag{3.49}$$

Where $\mathcal{G}_{CS_p}$ and $\mathcal{G}_{CS_{RBC}}$ is the amount of glucose contained in the plasma and red blood cell components of blood, respectively. Assuming a hematocrit of 40%, and that the concentra-

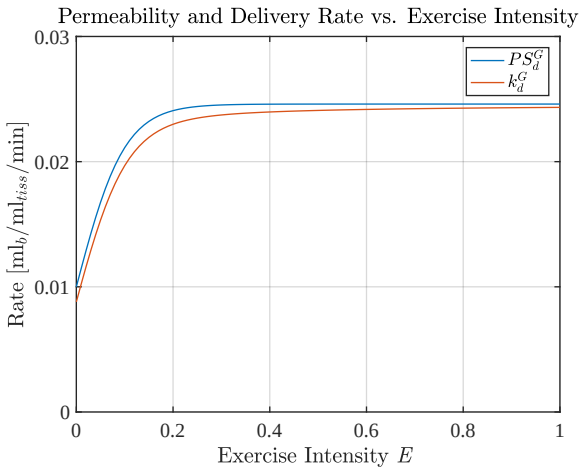


Figure 3.13: Permeability surface area (Equation 3.47) rapidly increases with exercise, reaching a plateau value at at only $E = 0.25$. The plateau exists because there is a finite reservoir of capillaries in the tissue and once they are all fully perfused then surface area can no longer increase. The delivery rate $k_d^G$ (Equation 3.32) increases similarly to $PS_d^G$. This is expected because during exercise, at high perfusion rates $Q_d$, glucose delivery is surface area (diffusion) limited rather than flow limited, and so is mainly dependent on $PS_d^G$.

tion of glucose in the RBCs is 76% of plasma [64, p. 43] we can quantify the mass in plasma and RBCs as

$$G \cdot V_{CS}^G = (0.6 \cdot G + 0.4 \cdot 0.76 \cdot G)V^B \tag{3.50}$$

where $V^B$ is the total blood volume. Solving for $V_{CS}$ we obtain

$$V_{CS} = (0.904)V^B. \tag{3.51}$$

We normalize by body weight to obtain

$$V_{CS_N} = (0.904)V_N^B. \tag{3.52}$$

If we estimate $V_N^B = 0.77$ [dL/kg], then $V_{CS_N}^G = 0.7$ [dL/kg]. With this volume of distribution, our predictions can be directly compared to measurements of plasma glucose.

In the SM domain, glucose only distributes in the ISF. Thus, the volume of distribution in the SM domain, $V_{SM_N}^G$, is taken as the volume of ISF, which was estimated to be $V_{SM_N}^G = 0.96$ [dL/kg] [64, p. 43]. In the model, $V_{SM}^G$ and $V_{CS}^G$ are used. They are obtained by multiplying the normalized volume distribution by the subject's body weight (BW).

The combined volume of distribution $V_{SM_N}^G + V_{CS_N}^G \approx 1.7$ [dL/kg], which is consistent with one-compartment estimates from the literature ranging from 1.5-2 [dL/kg] [133]. This gives some confidence in our estimates of the volume of distribution.

$V^{tiss}$ is fundamentally different from the volume of distribution, it is the volume of tissue in the domain. This parameter shows up because we must know the total volume flow rate

$(Q_d \cdot V_{SM}^{tiss})$ in order to calculate the mass flux. The volume of tissue in the SM domain is estimated to be $V_{SM_N}^{tiss} = 0.54$ [L/kg] [83], i.e. 54% of body weight at an assumed 1 kg/L density. Approximately half of $V_{SM}^{tiss}$ is SM tissue, with the other half SC tissue. As previously mentioned, despite naming the second compartment the SM domain, it also includes SC tissue.

**Insulin Model Parameters**

The insulin model was derived in Chapter 2 and details of how the parameters were obtained are omitted here. The volume of distribution of insulin that we use in the SM domain is roughly equal to the volume of the ISF, which normalized by BW is $V_{SM_N}^I = 1.2$ [dL/kg] [44, 64, 104]. The normalized metabolic clearance rate of insulin from the SM is $\mathrm{r}_{SM_N}^I = 0.02$ [1/min]. The capillary permeability surface area to insulin is $PS_d^I$ =0.005 [$\mathrm{ml}_b/\mathrm{ml}_{tiss}$/min].

### 3.2.3 Model Summary

The field equations are

$$\frac{dG}{dt} = -\frac{V_{SM}^{tiss} k_d^G(E) \cdot (G - H)}{V_{CS}^G} - \frac{RGU_{CS_{liv}}(G, M(S)) + RGU_{CS_{fix}}}{V_{CS}^G} + \frac{Ra_{meal}(t) + EGP(t)}{V_{CS}^G} \tag{3.53}$$

$$\frac{dH}{dt} = \frac{V_{SM}^{tiss} k_d^G(E) \cdot (G - H)}{V_{SM}^G} - \frac{RGU_{SM_{ins}}(H, S) + RGU_{SM_{exr}}(H, E)}{V_{SM}^G}. \tag{3.54}$$

$$\frac{dS}{dt} = \frac{V_{SM}^{tiss} k_d^I(E) \cdot (I(t) - S)}{V_{SM}^I} - \mathrm{r}_{SM_N}^I \cdot S \tag{3.55}$$

$$\frac{dM}{dt} = \frac{1}{\tau_{liv}} 2.0 \cdot tanh(0.55 \frac{S}{S_b}) \tag{3.56}$$

subject to

$$G = G_o \text{ at } t = t_o \tag{3.57}$$

$$H = H_o \text{ at } t = t_o \tag{3.58}$$

$$S = S_o \text{ at } t = t_o \tag{3.59}$$

$$M = M_o \text{ at } t = t_o. \tag{3.60}$$

The complete glucose metabolism model is a system of four non-linear ordinary differential equations with non-constant coefficients. $G$ is the plasma concentration of glucose in the CS domain. $H$ is the ISF concentration of glucose in the SM domain. $S$ is the ISF concentration of insulin in the SM domain, with measured plasma insulin concentration $I$ as an input. $M$ is the glucose uptake multiplier that affects $RGU_{CS_{liv}}$ from Sorensen [64].

Rates of glucose uptake ($RGU$) are defined as

$$RGU_{CS_{fix}} = \mathrm{r}^G_{brain} + \mathrm{r}^G_{heart} + \mathrm{r}^G_{kidney} + \mathrm{r}^G_{gut}. \tag{3.61}$$

$$RGU_{CS_{liv}} = \mathrm{r}^G_{liv}\big(5.66 + 5.66 \cdot tanh(2.44(\frac{G}{G_b} - 1.48))\big)M \tag{3.62}$$

$$RGU_{SM_{ins}} = \mathrm{r}^G_{SM_{ins}}\big(\frac{H}{H_b}S - S_b\big) + \mathrm{r}^G_{peri} \tag{3.63}$$

$$RGU_{SM_{exr}} = \mathrm{r}^G_{SM_{exr}}\frac{H}{H_b}E. \tag{3.64}$$

The kinetic rates $k$, which depend on exercise intensity $E$, are defined as.

$$k^G_d(E) = Q_d(1 - e^{\frac{-PS^G_d}{Q_d}}) \tag{3.65}$$

$$k^I_d(E) = Q^I_d(1 - e^{\frac{-PS^I_d}{Q^I_d}}) \tag{3.66}$$

$$Q_d(E) = Q_{d_{rest}} + \lambda_d E \tag{3.67}$$

$$Q^I_d(E) = (1 - h) \cdot Q_d \tag{3.68}$$

$$PS^G_d(E) = PS^G_{d_{rest}}(1 + R_d tanh(\gamma E)) \tag{3.69}$$

$$PS^I_d(E) = PS^I_{d_{rest}}(1 + R_d tanh(\gamma E)). \tag{3.70}$$

$Q_d$ is the total blood perfusion rate and $Q^I_d$ is only the plasma blood perfusion rate. The difference is the $h = 40\%$ hematocrit.

Additionally, we have the $EGP$ model

$$EGP = EGP_b \cdot \frac{G_b}{G}\frac{S_b}{S}(1 + L) \tag{3.71}$$

$$\frac{dL}{dt} = \frac{1}{\tau_{EGP}}(-L + \eta E) \tag{3.72}$$

$$L = 0 \text{ at } t = t_o. \tag{3.73}$$

The $EGP$ model can be used in place of the measurements for $EGP(t)$. In this chapter, we will only use the measured input $EGP(t)$. In subsequent chapters we will use the model for $EGP$.

The parameters of the entire model are defined in Table 3.1.

### 3.2.4 Initial Conditions

The initial conditions are chosen by to be equal to basal measurements for $G$ and $I$. For $H$ and $S$, which are not measured, Equations 3.54 and 3.55 are evaluated at basal resting

Table 3.1: Parameters used in glucose-dynamics model for healthy subjects

| Parameter | Description | Unit | Value | Source |
|---|---|---|---|---|
| $r^G_{brain}$ | Metabolic clearance rate of glucose in the brain | mg/min | 71 | [45, p. 219] |
| $r^G_{heart}$ | Metabolic clearance rate of glucose in the heart | mg/min | 3.7 | [45, p. 219] |
| $r^G_{kidney}$ | Metabolic clearance rate of glucose in the kidneys | mg/min | 3.7 | [45, p. 219] |
| $r^G_{gut}$ | Metabolic clearance rate of glucose in the gut | mg/min | 16.6 ‡ | [45, p. 219] |
| $r^G_{peri}$ | Basal metabolic clearance rate of glucose in the peripheral tissue | mg/min | 45.2 | [45, p. 219] |
| $r^G_{liv}$ | Basal metabolic clearance rate of glucose in the liver | mg/min | 14.8 ‡ | [45, p. 219] |
| $r^G_{SM_{ins}}$ | Insulin sensitivity of glucose clearance in skeletal muscle | mg/min per $\mu$U/mL | 5 | [70] |
| $r^G_{SM_{exr}}$ | Exercise sensitivity of glucose clearance in skeletal muscle | mg/min per $E$ | 860 | [35, 39, 40, 129, 130]§ |
| $V^G_{CS_N}$ | Normalized volume of distribution of glucose in circulatory system | mL/kg * | 0.7 | [64] |
| $V^G_{SM_N}$ | Normalized volume of distribution of glucose in skeletal muscle | mL/kg * | 0.96 | [64] |
| $V^{tiss}_{SM_N}$ | Normalized volume of tissue in skeletal muscle | mL/kg * | 540 | [83] |
| $\tau_{liv}$ | Time lag of insulin action of liver glucose uptake | min | 25 | [64] |
| $Q_{d_{rest}}$ | Tissue perfusion rate in skeletal muscle tissue at rest | $mL_b/mL_{tiss}$/min | 0.038 | [83] |
| $PS^G_{d_{rest}}$ | Capillary permeability surface area to glucose during rest | $mL_b/mL_{tiss}$/min | 0.01 | [80, 101, 102] |
| $R_d$ | Capillary recruitment factor in delivering (SM) tissue | 1 | 1.46 | [92–94] § |
| $\gamma$ | Capillary recruitment saturation rate | 1 | 10 | [92–94] § |
| $\lambda_d$ | Sensitivity of tissue perfusion rate to exercise | $mL_b/mL_{tiss}$/min per $E$ | 1.1 | [84] |
| $\tau_{EGP}$ | Time lag of exercise action on endogenous glucose production | min | 20 | [35, 39]§ |
| $\eta$ | Maximum exercise action on endogenous glucose production | 1 | 4 | [35, 39]§ |
| $V^I_{SM_N}$ | Normalized volume of distribution of insulin in skeletal muscle | mL/kg * | 1.2 | [44, 64] |
| $r^I_{SM_N}$ | Normalized metabolic clearance rate of insulin in skeletal muscle | 1/min | 0.02 | [105–107]§ |
| $PS^I_{d_{rest}}$ | Capillary permeability surface area to insulin during rest | $mL_b/mL_{tiss}$/min | 0.005 | [101, 102] |
| $h$ | Hematocrit percentage in blood | 1 | 0.4 | [104] |

* Multiplied by BW prior to being used in model. See demographics for BW.
† Derived from total clearance rate.
‡ Adjusted to ensure that total liver uptake is approx 50% of ingested glucose [119, 120].
§ Parameter is derived from data taken from specified sources.

conditions ($G = G_b$,$H = H_b$,$S = S_b$, $E = 0$)

$$G(t_o) = G_{b_{data}} \tag{3.74}$$

$$H(t_o) = G_{b_{data}} - \frac{\mathrm{r}^G_{peri}}{V^{tiss}_{SM} k^G_d|_{E=0}} \tag{3.75}$$

$$S(t_o) = \frac{V^{tiss}_{SM} k^I_d I_{b_{data}}}{\mathrm{r}^I_{SM} + V^{tiss}_{SM} k^I_d} \tag{3.76}$$

$$M(t_o) = 1 \tag{3.77}$$

$M$ is initially 1 because this gives basal $RGU_{CS_{liv}} = \mathrm{r}^G_{liv}$.

### 3.2.5 Human Subjects Data

The data used in this study comes from two separate research studies on healthy (non-diabetic) human subjects and is the secondary use of existing data. A summary of the demographic information is shown in Table 3.2. Detailed protocol and demographic information can be found in [54, 113]. Note, these two studies were not paired; different subjects were used for each group. We will refer to the resting group as 'rest' or 'resting' and the exercising group as 'exercise' or 'exercising'.

In each study the time of meal ingestion was the same (0700), the meal content was the same (55 % carbohydrate, 15% protein, and 30% fat), the number of subjects was the same (n=12) and the triple-tracer protocol was the same [46]. The only significant difference in the studies is that one group exercised in the period from $t$ =120 to 195 [min] following meal ingestion. Figure 3.14 shows the timeline for each protocol.

#### Brief Protocol Information

The following protocol information applies to the 'resting' and 'exercising' subjects, except where specified.

The 'exercising' subjects did not engage in vigorous physical activities for 72 h before screen and study visits. In the screening visit participants performed a graded exercise test on a treadmill to determine $\mathrm{V0}_{2_{max}}$ according to guidelines (American College of Sports Medicine Guidelines for Exercise Testing and Prescription, 7th Edition) and ensure stable cardiac status. Expired gases were collected and analyzed using indirect calorimetry. $\mathrm{V0}_{2_{max}}$ was determined when at least two of the following three criteria were met: 1) participant too tired to continue exercise, 2) respiratory exchange ratio exceeded 1.0; or 3) a plateau was reached in oxygen consumption with increasing workload. The purpose of this test was to use individual $\mathrm{V0}_{2_{max}}$ data to determine workload during the moderate-intensity $\mathrm{V0}_{2_{max}}$ protocol during the study day.

For the study visit all subjects spent 40 h in the CRU. On day 1 subjects were admitted to the CRU at 1600. They were then provided a standard 10 kcal/kg meal (55 % carbohydrate,

15% protein, and 30% fat) consumed between 1700 and 1730. No additional food was provided until the next morning. On day 2 at 0600 h, an intravenous cannula was inserted retrogradely into a hand vein for periodic blood draws. The hand was placed in a heated (55C) Plexiglas box to enable drawing of arterialized- venous blood for glucose and hormone analyses. At 0700 a mixed-meal study was performed.

A mixed meal containing 75 grams of glucose was ingested at time 0. At 120 min following the first bite, the 'exercising' subjects stepped on a treadmill to exercise at moderate-intensity activity (50 % $V0_{2_{max}}$): i.e., four bouts of walking at 3-4 miles/h for 15 min with rest periods of 5 min between each walking bout: total duration 75 min. The workload during physical activity was continuously monitored by heart rate responses and measurements of $V0_{2_{max}}$ during exercise to maintain target 50% $V0_{2_{max}}$ exercise intensity. Following the last blood draw the hand vein cannula was removed. Lunch at 1300 and dinner at 1900 were provided, each meal contributing 33% of daily estimated caloric intake. The patient was discharged the next morning at 0800.

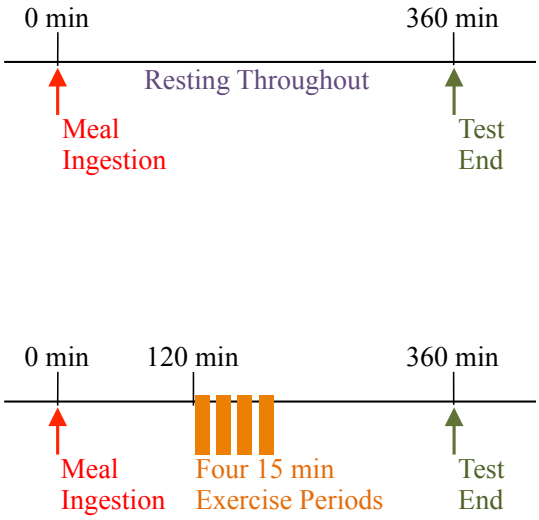


Figure 3.14: Timeline for the mixed-meal tolerance test (MMTT) resting protocol and exercising protocol. Each test was done using only healthy (non-diabetic) subjects. At time 0 the subjects in the resting group ingested a 50 [g] CHO mixed-meal and the subjects in exercising group ingested 75 [g]. The resting group rested throughout the entire study period. The exercise group exercised at 50% $V0_{2_{max}}$ for four 15 minute exercise periods, starting at minute 120.

Table 3.2: Demographics of healthy (non-diabetic) subjects

| Variable | Resting Protocol† (n=12) | Exercising Protocol† (n=12) |
|---|---|---|
| Age (Years) | 36.0 ± 11.3 | 37.1 ± 13.2 |
| Sex (M/F) | 9M, 3F | 5M, 7F |
| Weight (kg) | 72.4 ± 15.8 | 70.9 ± 16.6 |
| HbA1C(%) | 5.1 ± 0.4 | 5.1 ± 0.3 |
| $V0_{2_{max}}$ | -* | 32.3 ± 7.3 |

± is standard deviation
* Not measured
† Data originally published in [54](rest) and [113](exercise).

### 3.2.6 Simulation, Input, and Data Considerations

Each simulation was started using the initial conditions derived in Equations 3.74-3.77. To obtain an average patient, all data was averaged for the 12 patients in each cohort. The error bars indicate the SEM. MATLAB was used to simulate the system. A timestep of 0.1 [min] was used.

As previously mentioned, $EGP$ and $Ra_{meal}$ were preprocessed. The basal value of $EGP$ was set to be 155 [mg/min] by linearly scaling the raw $EGP$ data. The AUC of $Ra_{meal}$ set to be $0.9 \cdot d$ [131, 133], where $d$ is the meal dose. To meet this requirement the raw $Ra_{meal}$ was scaled linearly. $EGP$ model predictions were not used to produce the results here, Chapter 4 will utilize the $EGP$ model.

## 3.3 Results

Model simulation results are shown in Figures 3.15 - 3.20. First, insulin and glucose concentration predictions are plotted. Then, extraction fraction and rate of glucose delivery to SM tissue are plotted, which provide insight into the model's ability to predict glucose-kinetics between the compartments. Last, glucose input and uptake are plotted, which shows the importance of different $RGU$ mechanisms at different times in the postprandial period.

Figure 3.15 shows the postprandial insulin response to a meal ingested at $t = 0$ for a resting patient and an exercising patient. The measured plasma insulin input $I_{data}$ and the predicted SM ISF insulin concentration $S$ based on Equation 3.55 are plotted. The grey bars indicate the four 15 minute exercise periods.

The peak plasma insulin concentration $I_{data}$ is nearly the same between groups, reaching about 55 [$\mu$U/mL]. Similarly, the peak predicted $S$ is about 20 [$\mu$U/mL], occurring at 100 [min] in each group. At $t$ =120 [min], the moment before exercise, $I_{data}$ is 33 [$\mu$U/mL] in the exercising group. At the same timepoint in the resting group $I_{data}$ is 29 [$\mu$U/mL].

The trajectories for each group begin to diverge after exercise occurs. This is plainly seen by the rapid decrease in $I_{data}$ during exercise. A much slower decay is seen in the resting group. In the exercising group $I_{data}$ falls to 10 [$\mu$U/mL] by $t = 145$ [min]. The

resting group doesn't reach 10 [$\mu$U/mL] until $t$ = 180 [min], a full 35 minutes later. The predicted $S$ also decays as an accelerated rate, falling to 5 [$\mu$U/mL] by $t$ = 200 [min]. The resting group doesn't reach 5 [$\mu$U/mL] until almost an hour later. The observation that insulin concentrations quickly drop during exercise is consistent with previous observations that insulin production by the pancreas is suppressed during exercise [134].

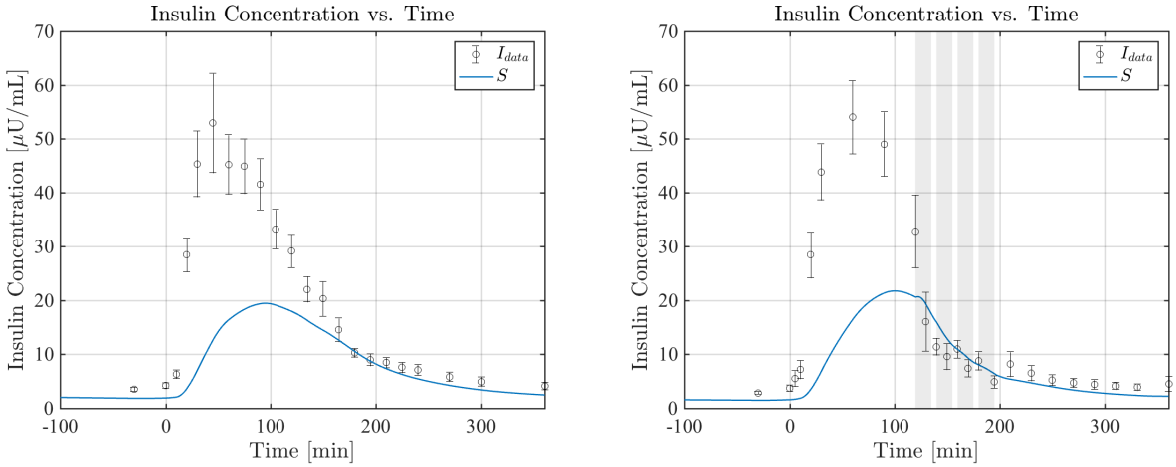


Figure 3.15: Postprandial (meal at $t$ =0 [min]) measured plasma insulin concentration $I_{data}$ (dots) and predicted (blue line) skeletal muscle insulin concentration $S$ vs. time for a resting subject (left) and exercising subject (right). The grey bars indicate the four 15 minute exercise periods. Notice that plasma insulin concentration rapidly declines during the exercise period, reaching near basal levels by $t$ =200 [min]. On the other hand, for the resting group, the insulin concentration falls at a slower rate. The observation that insulin concentrations quickly drop during exercise is consistent with previous observations that insulin production by the pancreas is suppressed during exercise [134]. This reaction helps prevent hypoglycemia by reducing the insulin concentration in insulin-sensitive tissues.

The postprandial glucose response is shown in Figure 3.16. There is strong agreement between the model predictions $G$ and measurements $G_{data}$. Peak $G$ is about 170 [mg/dL] and is nearly identical for both the exercise and rest groups. In fact, prior to exercise (shown as shaded regions), the glucose response for both groups is nearly identical. The predicted $G$ at $t$ = 120 (the moment before exercise) is 130 [mg/dL], a slight overestimate of measured $G_{data}$, which is about 115 [mg/dL] in each group. This overestimation is likely due to measurement error of $Ra_{meal}$, which exhibits a slight uptick around this time (see Figure 3.6).

Only after exercise do the glucose responses of each group begin to diverge. In the resting group, glucose decays slowly, and reaches basal levels at around $t$ =160 [min]. In comparison, the exercising group drops below basal by $t$ =130 [min], only 10 minutes after exercise begins. This significant drop is accurately captured by the model. After entering hypoglycemic territory ($G \approx 70$ [mg/dL]), $G$ no longer drops, and maintains at about 75 [mg/dL]. $G$ is maintained because of the significant increase in $EGP$ (see Figure 3.6). The jagged glucose response during exercise is a result of the direct dependence of $RGU_{SM_{exr}}$ on $E$, which jumps from $E$=0 to 0.5 almost instantaneously. After exercise ceases, $G$ returns

to basal levels. The $G$ predictions slightly diverge from $G_{data}$ after $t = 250$ [min]. This is most likely due to steady-state error in $EGP$ measurements, which did not return back the set basal rate of 155 [mg/min].

The SM ISF glucose concentration $H$ starts at approximately 90% of $G$. After meal ingestion $G$ rapidly rises, with $H$ rising at a much slower rate due to slow diffusion of glucose from the CS to the SM. During exercise $H$ drops to an extremely low level of about 40 [mg/dL]. This significant drop occurs because the glucose delivery mass flow rate $\mathcal{H}_d$ cannot keep up with the demand of exercising muscle. Details of glucose-dynamics will shed more light on this prediction.

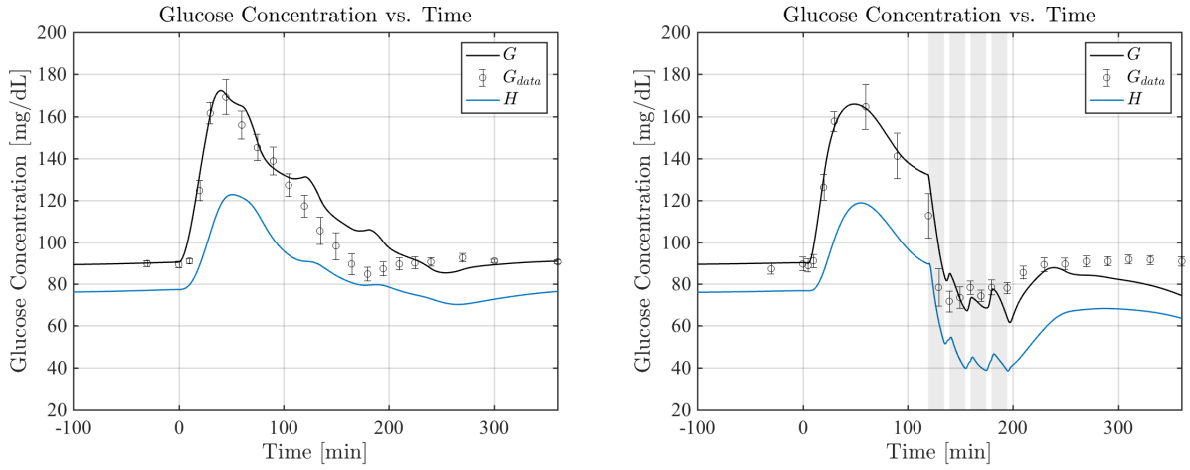


Figure 3.16: Postprandial (meal at $t$ =0 [min]) glucose concentrations vs. time for a resting subject (left) and exercising subject (right). $G_{data}$ (dots) and $G$ (black line) are the measured and predicted plasma glucose concentrations. $H$ (blue line) is the predicted SM glucose concentration. The grey bars indicate the four 15 minute exercise periods. There is strong agreement between the model plasma predictions $G$ and measurements $G_{data}$. Measurements for $H$ are not available for comparison. In both groups, prior to exercise $G$ and $H$ take nearly identical trajectories. After exercise $G_{data}$ drops into hypoglycemic territory in less than 10 minutes. For the resting group, hypoglycemia does not occur, and glucose does not reach basal levels until $t$ =160 [min]. For the resting group, the lowest predicted $G$ and $H$ were approximately 85 [mg/dL] and 70 [mg/dL]. In comparison, the exercising group had a nadir of 70 [mg/dL], and 40 [mg/dL]. This indicates that $H$ is more sensitive to exercise than $G$, likely for two reasons: (1) glucose uptake occurs directly in the SM tissue and thus immediately decreases $H$, and (2) the counteracting increase in $EGP$ occurs in the CS compartment immediately increasing $G$.

Next, we evaluate the predicted glucose-kinetics, that is how glucose moves from the CS to the SM. The extraction fraction ($ef$) and the rate of glucose delivery ($\mathcal{H}_d$) are plotted vs time in Figures 3.17 and 3.18.

The extraction fraction ($ef$) is defined as

$$ef = \frac{G_{arterial} - G_{venous}}{G_{arterial}} \cdot 100. \tag{3.78}$$

$ef$ is a measure of how effectively a substance in the CS is delivered to the tissue (in this case the SM). The $ef$ of glucose can be directly measured using arteriovenous catheterization. A

high $ef$ means that a large amount of glucose is removed from the CS on each pass through the tissue.

In our study $ef$ is not measured directly. Instead, we will use the developed model to express $ef$ as a derived quantity. $ef$ can be written in terms of $G$ and $H$ by approximating that $G_{arterial} = G$ and $G_{venous} = g_d|_e$. Using Equation 3.27 we can estimate $g_d|_e$ and plug the solution into Equation 3.78 to get

$$ef = \frac{(1 - e^{\frac{-PS_d^G}{Q_d}})(G - H)}{G} \cdot 100. \tag{3.79}$$

We can estimate $ef$ by simply substituting in our predictions for $G$ and $H$. The resulting $ef$ is plotted vs. time in Figure 3.17.

The glucose delivery rate $\mathcal{H}_d$ is also not measured directly. However, it can also be estimated from the model. We do this by multiplying the total flow rate to the SM tissue $V_{SM}^{tiss} Q_d$ by the predicted arteriovenous difference. Our derived estimate of $\mathcal{H}_d$ is

$$\mathcal{H}_d = V_{SM}^{tiss} Q_d (1 - e^{\frac{-PS_d^G}{Q_d}})(G - H). \tag{3.80}$$

$\mathcal{H}_d$ is plotted in Figure 3.18.

Clearly, $ef$ and $\mathcal{H}_d$ are related quantities; a larger $ef$ typically leads to a larger $\mathcal{H}_d$. However, if $Q_d$ significantly increases, this will lead to a lower extraction fraction due to less time for exchange, but likely a higher $\mathcal{H}_d$. For this reason, $ef$ can sometimes be a misleading measure of glucose-kinetics. $\mathcal{H}_d$ provides a more direct quantification of glucose-kinetics.

Prior to the commencement of exercise, both groups exhibit very similar values of $ef$. Initially $ef$ is 3.5 %, consistent with direct measurements found in literature [45, p. 219]. Upon meal ingestion at $t = 0$ [min], $ef$ increases to just above 8% due to the substantial increase in $G - H$. After the initial steep rise, $ef$ decreases and then paradoxically increases again, maxing out at about 7 %. This paradoxical rise is due to the slow decay of $Ra_{meal}$, which buoys $G$ in the period between $t = 80$ to 120 [min]. In this same period $H$ continues to drop, resulting in an increased $G - H$ and thus an increased $ef$.

After the commencement of exercise, the dynamics of $ef$ between the two groups sharply diverge. In the resting group, $ef$ wobbles but slowly decays back to 4%. In the exercising group, $ef$ significantly drops during the exercise period to less than 2%. This significant drop is is explained by a decrease in the exchange time. This is because of a drastically increased flow rate, increasing 10-fold during exercise periods. After exercise ends, the $ef$ drastically increases again to nearly 9%. This peak is because $Q_d$ drops to basal rates and $G - H$ is still large. Over the next hour glucose in the SM is replenished and $G - H$ returns to normal levels, providing an extraction fraction of 3.5% by $t = 360$ [min].

The corresponding glucose delivery rate $\mathcal{H}_d$ is plotted in Figure 3.18. Prior to exercise, $\mathcal{H}_d$ shows a very similar pattern to $ef$ in both groups. Initially, $\mathcal{H}_d$ is 45 [mg/min], the basal glucose uptake rate in SM. After meal ingestion $\mathcal{H}_d$ rises to about 200 [mg/min] in both groups.

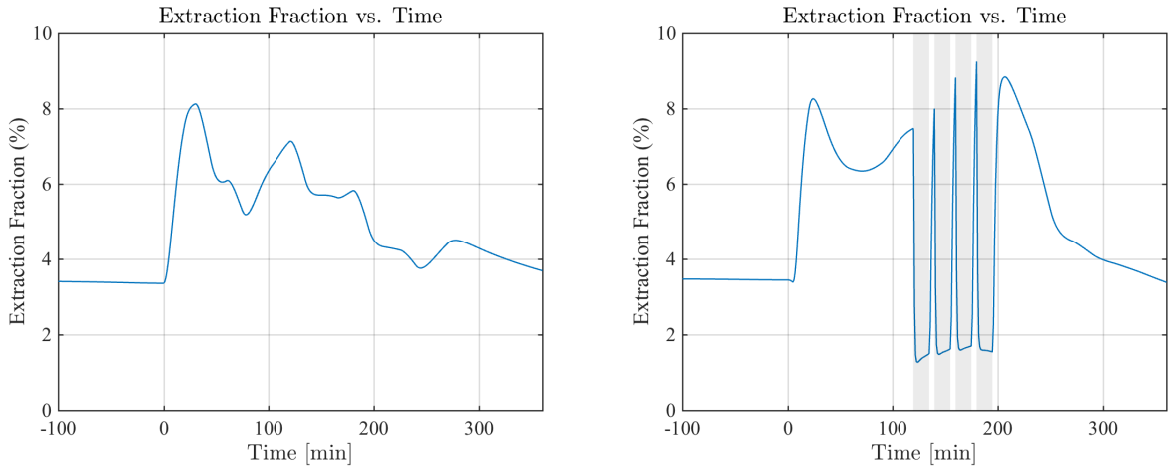


Figure 3.17: Extraction fraction ($ef$) is predicted to increase following a meal and drop significantly during exercise. The figure shows predicted extraction fraction vs. time for a resting subject (left) and an exercising subject (right). The grey bars indicate the four 15 minute exercise periods. In both groups the extraction fraction at basal is approximately 3.5 %, consistent with measurement [45, p. 219]. Upon meal ingestion, the extraction fraction increases to nearly 8 % due to the the increased $G - H$ gradient. In the exercising group, the extraction fraction drops considerably during exercise due to the sharply increased blood flow ($Q_d$ increases nearly 10-fold during exercise). This is because the exchange time is decreased 10-fold This predicted drop in the extraction fraction is in contradiction to measurements [40] and may represent a weakness of the model to accurately predict glucose exchange between the CS and SM compartments.

In the moment before exercise commences ($t = 120$ [min]) $\mathcal{H}_d$ is about 150 [mg/min] in both groups. After exercise begins, $\mathcal{H}_d$ approximately doubles, maxing out at 350 [mg/min]. By the second bout of exercise (second spike), $\mathcal{H}_d$ has slightly decreased to about 275 [mg/min]. This slight decrease occurs because uptake is assumed proportional to $H$, which considerably drops during exercise. As soon as exercise ceases $\mathcal{H}_d$ drops because $Q_d$ drops. Over the next 50 minutes, $\mathcal{H}_d$ further decreases because glucose demand in the $SM$ muscle decreases and $G - H$ returns to basal levels.

In Figure 3.19, the relationship between $\mathcal{H}_d$ and extraction fraction $ef$ is plotted over the period $t = 0$ to 360 [min] with $t$ as a parameter. During rest (blue line), when flow $Q_d$ and permeability surface area $PS_d^G$ are assumed fixed, an increase in $ef$ and $\mathcal{H}_d$ is caused by an increase in $G - H$. The exercising group (orange line) follows the same path, until exercise commences, causing an upward movement to the left. During exercise, both $Q_d$ and $PS_d^G$ increase to facilitate glucose delivery $\mathcal{H}_d$. However, the significant increase in $\mathcal{H}_d$ does not keep up with demand, and causes $H$ to drop, so $G - H$ increases until $\mathcal{H}_d$ is equal to demand. During this period, $ef$ decreases significantly because an increase in $Q_d$ decreases the capillary exchange time.

Figure 3.20 shows the relative magnitude of different glucose input and uptake mechanisms vs. time. Measured inputs $Ra_{meal}$ and $EGP$ are plotted as positive dotted lines. Predicted uptake $RGU_{CS_{TOT}}$ and $RGU_{SM_{TOT}}$ are plotted as negative solid lines.

Prior to exercise, the corresponding input and uptake mechanism for each group follow

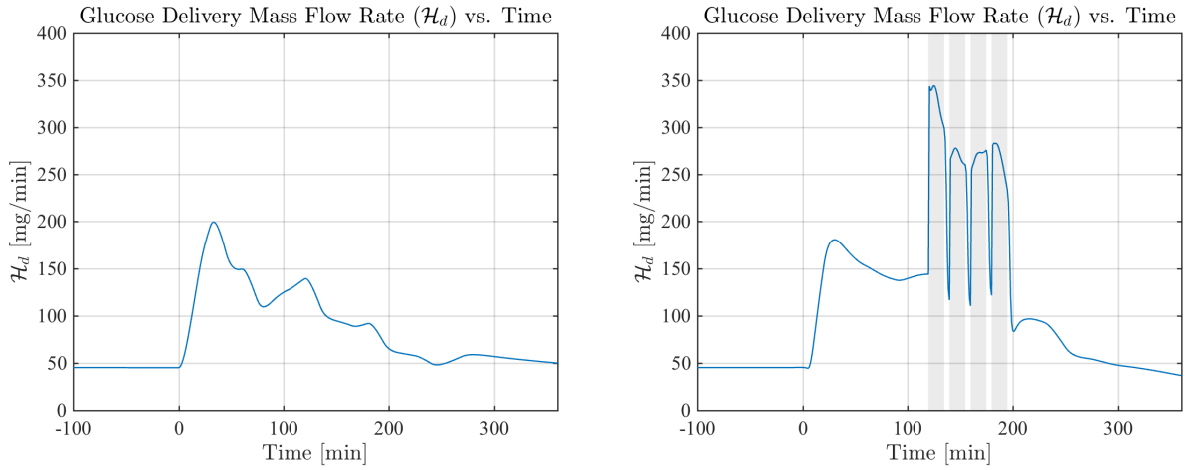


Figure 3.18: Glucose delivery rate ($\mathcal{H}_d$) significantly increases during exercise. The figure plots predicted $\mathcal{H}_d$ vs. time for a resting subject (left) and an exercising subject (right). The grey bars indicate the four 15 minute exercise periods. Initially $\mathcal{H}_d = 45$ [mg/min], equal to the basal SM uptake rate. In both groups upon meal ingestion, $\mathcal{H}_d$ rapidly increases to nearly 200 [mg/min]. In the resting group, $\mathcal{H}_d$ slowly drops back to basal levels because the $G$-$H$ gradient decreases after the initial rapid rise. In the exercising group $\mathcal{H}_d$ sharply increases, peaking at 350 [mg/min]. This significant increase is attributed to increases in: capillary surface area (tissue recruitment), tissue perfusion rate (higher blood flow), and an enhanced $G - H$ gradient caused by a significant increase in glucose demand in exercising muscle. The plateau value of $\mathcal{H}_d$ during exercise occurs when the delivery rate equals glucose demand.

similar trajectories. $Ra_{meal}$ rapidly rises from 0 [mg/min] to nearly 500 [mg/min] after meal consumption at $t = 0$ [min] and then slowly decreases back to 0. $EGP$ is initially equal to 155 [mg/min], which at steady state is equal and opposite to the $RGU_{TOT}$ ($RGU_{CS_{TOT}} + RGU_{SM_{TOT}}$). Upon ingestion of the meal, $EGP$ is rapidly suppressed and reaches a nadir of nearly 0 [mg/min] after about an hour. Simultaneously $RGU_{CS_{TOT}}$ increases significantly due to $RGU_{CS_{liv}}$ (not shown). $RGU_{SM_{TOT}}$ also increases in response to the meal, although it is lagged in comparison to $RGU_{CS_{TOT}}$. This is because $RGU_{SM_{TOT}}$ is proportional to $S$ which is significantly delayed because of the slow diffusion of insulin into the SM.

In the time period after exercise commences, $Ra_{meal}$ is essentially unchanged between the two groups. However, $EGP$, initially suppressed, is significantly enhanced in the exercising group, increasing from nearly 0 to 210 [mg/min] in an hour. This enhancement is not seen in the resting group. This rise of $EGP$ in the exercising group compensates for the significant exercised-induced increase in $RGU_{SM_{TOT}}$, shown as negative spikes. These spikes in $RGU_{SM_{TOT}}$ have a peak magnitude of 600 [mg/min] and eventually decrease to about 300 [mg/min]. In both groups, $RGU_{CS_{TOT}}$ is initially the primary contributor to total uptake. The resting group continues this trend. However in the exercising group $RGU_{CS_{TOT}}$, which is dependent on $G$, rapidly decreases to basal levels due to the drop of $G$ that results from exercise.

In Table 3.3 we have quantified the relative importance of each glucose input and uptake mechanism. This was done by integrating each function over the period from from $t = 0$ to

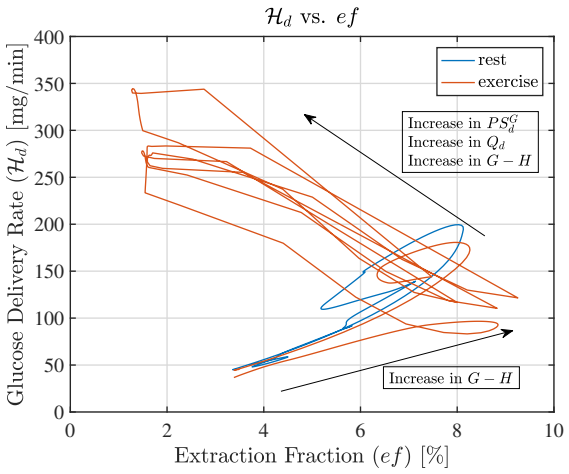


Figure 3.19: The relationship between glucose delivery mass flow rate $\mathcal{H}_d$ and extraction fraction $ef$ over the period $t = 0$ to 360 [min], $t$ is a parameter. During rest (blue line), when flow $Q_d$ and permeability surface area $PS_d^G$ are assumed fixed, an increase in the $ef$ causes a monotonic increase in $\mathcal{H}_d$. In the exercising group (orange line), both $Q_d$ and $PS_d^G$ increase due to increased blood perfusion and capillary recruitment. Because of the significant increase in $Q_d$ the exchange time is less, causing a decrease in $ef$ (movement to the top left). The prediction that $ef$ decreases during exercise is not consistent with previous observations [40].

360 [min] to find the AUC.

$Ra_{TOT}$ in the exercising group is 9 [g] more than in the resting group. This is entirely due to the increased $EGP$ that resulted from exercise (29.7 vs. 39.5 [g]). There was no difference in meal size, so $Ra_{meal}$ is nearly identical in the two groups.

Proportionally, more uptake occurred in the CS ($RGU_{CS_{TOT}}$) in the resting group than in the exercising group (66.7 vs 55.8 %). This is related to the prediction that glucose uptake by the liver $RGU_{SM_{liv}}$ is significantly higher in the resting group than the exercising group, 31.4 and 26.4 [g], respectively. Essentially, during rest, uptake preferentially occurs directly from the CS by the liver [119], and during exercise uptake preferentially occurs in the periphery.

Over the entire exercise period 17.6 [g] of glucose uptake occurred in the SM due to exercise. The AUC of $RGU_{SM_{ins}}$ is noticeably insensitive to exercise with a difference of only a few grams.

Finally, we quantified splanchnic ($RGU_{spl}$) and extrasplanchnic ($RGU_{espl}$) glucose uptake; $RGU_{spl} = RGU_{CS_{liv}} + \mathrm{r}_{gut}^G$ and $RGU_{espl} = RGU_{TOT} - RGU_{spl}$. The model predicts that splanchnic glucose uptake is less important than extrasplanchnic glucose uptake when exercise is involved, 38 % in the resting group and 29.8 % in the exercising group.

### 3.3.1 EGP Prediction Validation

Although the previous simulation utilized direct triple-tracer measurements of $EGP$, we wanted to demonstrate the ability of our $EGP$ model to predict the measured $EGP$. Figure

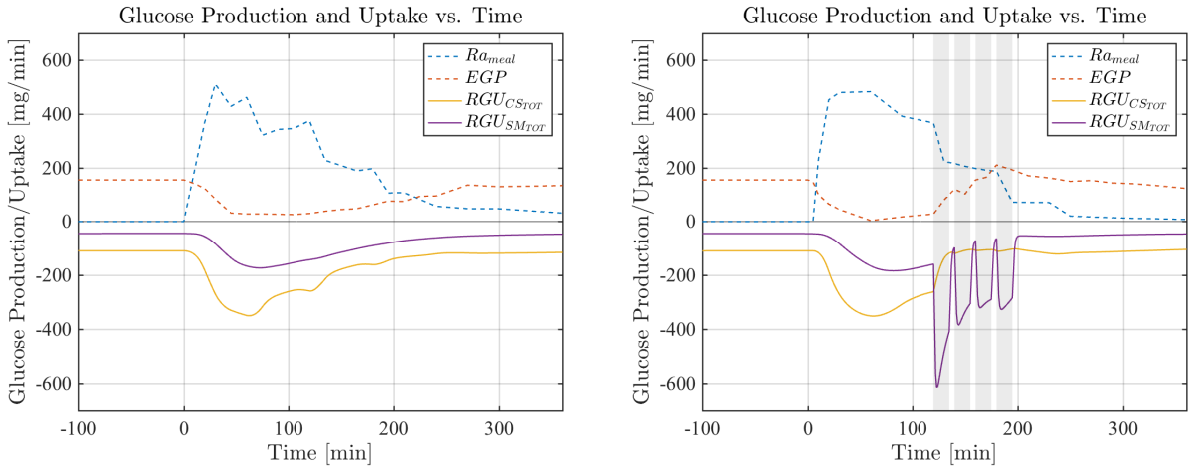


Figure 3.20: Glucose production and uptake vs. time for a resting subject (left) and an exercising subject (right). Measured glucose inputs are shown as positive dotted lines. Glucose uptake is shown as negative solid lines. The grey bars indicate the four 15 minute exercise periods. Prior to exercise the corresponding input and uptake mechanisms for each group are similar. After exercise commences at $t = 120$, the trajectories of each group begin to deviate. Although exercise does not seem to significantly affect $Ra_{meal}$, $EGP$ is significantly affected. Both are nearly 0 at $t = 120$ [min], but exercise increases EGP to 210 [mg/min] in about an hour. This increase in $EGP$ counteracts the significant exercise-induced increase in the rate of glucose uptake in skeletal muscle ($RGU_{SM_{TOT}}$), preventing hypoglycemia.

3.21 shows predicted $EGP$ vs. measured $EGP$. Remember that the EGP model was identified on *independent* data taken from [35, 39], and there was no curve fitting done to obtain the predictions shown in Figure 3.21.

The $EGP$ predictions match very well with the data, with a slight overestimation of the suppression effect - the predictions are slightly lower than the measurements indicate. In the exercising case, the magnitude of the $EGP$ response is almost the same as the data, however there is a slight time-lag of about 25 minutes.

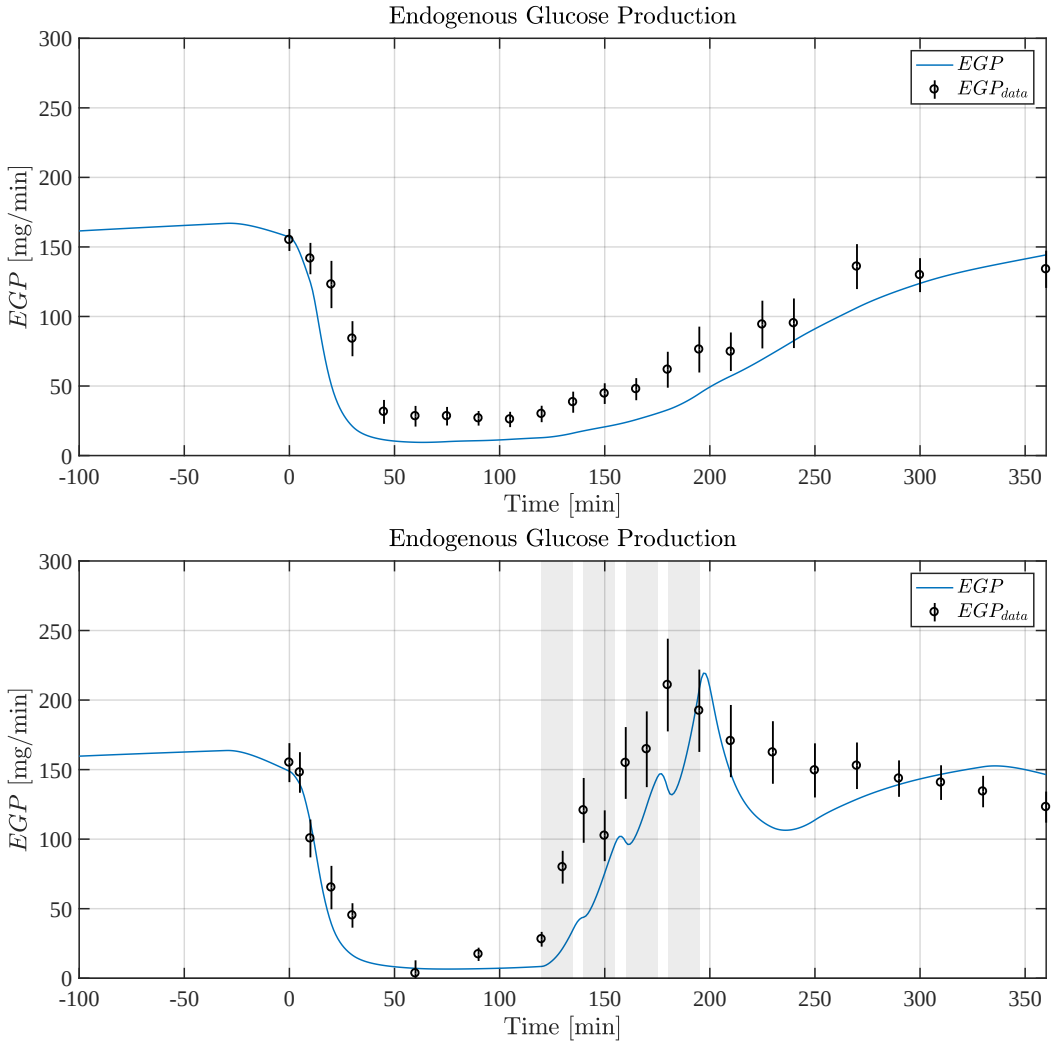


Figure 3.21: *EGP* response to a mixed meal tolerance test. (top) EGP during exercise. (bottom) EGP with exercise periods from minute 120 to minute 195. Grey region represents exercise period. Notice the strong agreement between the model *EGP* (which was identified from independent data) and $EGP_{data}$.

## 3.4 Discussion

We have developed a model of postprandial glucose metabolism with exercise and have demonstrated the model on human data from two groups, one resting in the period following meal ingestion, and one exercising for 75 minutes in the period following meal ingestion. The three main effects that exercise has on glucose metabolism are included in the model: (1) changes to *EGP*, (2) changes in the SM rate of glucose uptake and (3) changes in glucose-kinetics.

*EGP* is known to be an important factor in maintaining glucose at sufficient concentrations during exercise, increasing 2-fold over basal levels during prolonged exercise [35]. We

Table 3.3: Individual glucose uptake contributions

| | AUC* [g] | | % Total* | |
|---|---|---|---|---|
| Group | rest | exer | rest | exer |
| Measured Inputs ⋆ | | | | |
| $Ra_{TOT}$ | 98.4 | 107.0 | 100 | 100 |
| $Ra_{meal}$ | 68.7 | 67.5 | 69.8 | 63.1 |
| $EGP$ | 29.7 | 39.5 | 30.2 | 36.9 |
| Predicted Uptake ⋆ | | | | |
| $RGU_{TOT}$ | 98.4 | 108.7 | 100 | 100 |
| $RGU_{CS_{TOT}}$ | 65.6 | 60.6 | 66.7 | 55.8 |
| $RGU_{CS_{liv}}$ | 31.4 | 26.4 | 31.9 | 24.3 |
| $RGU_{CS_{fix}}$ | 34.2 | 34.2 | 34.8 | 31.5 |
| $RGU_{SM_{TOT}}$ | 32.8 | 48.1 | 33.3 | 44.2 |
| $RGU_{SM_{ins}}$ | 32.8 | 30.5 | 33.3 | 28 |
| $RGU_{SM_{exr}}$ | 0 | 17.6 | 0 | 16.2 |
| $RGU_{spl}$ † | 37.3 | 32.4 | 38.0 | 29.8 |
| $RGU_{espl}$ ‡ | 61.0 | 76.3 | 62.0 | 70.2 |

* All measures are taken from $t = 0$ to 360 [min]
⋆ Indentations are subsets
† Splanchnic uptake: $RGU_{spl} = RGU_{CS_{liv}} + r^G_{gut}$
‡ Extrasplanchnic uptake: $RGU_{espl} = RGU_{TOT} - RGU_{spl}$

have accounted for this significant infusion of glucose by directly including measurements of $EGP$ taken during exercise (Figure 3.6). These $EGP$ measurements, in addition to direct measurements of $Ra_{meal}$ allow us to directly account for all of the glucose input into the system, without the need for modeling these terms. The inclusion of these measurements into our model of glucose metabolism represent a significant advantage over previous attempts to develop models of glucose metabolism during exercise [58, 64, 65]. As an additional contribution, a model of $EGP$ was developed, but the work in this chapter did not include the $EGP$ model.

Changes in SM glucose uptake during exercise were included in the model by developing a phenomenological model that relates the rate of glucose uptake to exercise intensity $E$ (Equation 3.64). This model was identified by aggregating data from various studies that measure directly the peripheral glucose uptake during exercise (See Figure 3.8) via arteriovenous catheterization. The inclusion of this uptake model allows us to evaluate how enhanced glucose uptake during exercise impacts $G$.

Changes in glucose-kinetics were included by developing a microscale model of mass-transfer in capillaries. This predicted glucose delivery rate $k^G_d$ (Equation 3.65 and Figure 3.13) in the delivering capillary bed and depends on the tissue perfusion rate $Q_d$ and the capillary bed permeability surface area to glucose $PS^G_d$.

*Model Validation.* Overall, model predictions of $G$ agree well with average patient data taken from experiments on a group of 12 resting patients and a separate group of 12 exercising

patients (Figure 3.16).

In the resting group, the peak predicted $G$ is almost identical to the peak measured $G_{data}$. During the decay period, $G$ falls back to basal levels at a rate slightly slower than measured. This can potentially be be attributed to measurement error in $Ra_{meal}$, which has spurious oscillations in this same time frame (Figure 3.6). This may be due to non-steady state specific activity (SA) associated with the triple-tracer methodology [135]. For the exercising group, peak $G$ is nearly identical to $G_{data}$. Shortly after exercise commences, $G$ precipitously drops to 70 [mg/dL] in less than 10 minutes. This drop is almost perfectly aligned with $G_{data}$ and indicates that the model gives reasonable predictions of glucose metabolism during exercise. As a result of an increase in $EGP$, $G$ reaches a new steady state, maintaining around 70 [mg/dL]. After the cessation of exercise, $G$ once again returns close to basal levels. Soon after exercise ends $EGP$ drops below basal production and the predicted $G$ drops, then stays below $G_{data}$. This disagreement between prediction and data may be because measured $EGP$ is underestimated in the time frame following exercise.

Though on the surface the predictions seem to match the data, the agreement needs further validation. This is because as with all models that include significant uncertainty, some adjustments were made to facilitate comparison.

First, original parameters for the liver glucose uptake model adapted from Sorensen [64] predicted liver uptake that was too high. To correct for this $r_{liv}^{G}$ was slightly decreased, down to 15 [mg/min] from the accepted value of 20 [mg/min]. This effectively reduced the predicted liver glucose uptake so that total splanchnic uptake was in agreement with the 55%-60% of meal ingestion measured by Felig [119] and Defronzo [119].

Second, it is possible that moderate measurement error exists for $EGP$ and $Ra_{meal}$. Directly measuring glucose fluxes is a painstaking and laborious process [135], and although significant care is taken to ensure the measurements are as accurate as possible, the methodology is still error prone, especially during rapid changes in glucose concentration. For this reason, we have adjusted measurements for $EGP$ by forcing the basal value of $EGP$ to be 155 [mg/min], a value equal and opposite to basal $RGU_{TOT}$. $Ra_{meal}$ was also adjusted so that its AUC is equal to 90% of the total glucose ingested, consistent with the early findings of Radziuk [131].

The derived $EGP$ model (Equation 3.71 and 3.72) was partially validated in Figure 3.21. The predictions slightly overestimate the suppression effect of $G$ and $S$ and there is a minor lag in the effect of exercise on $EGP$, but overall the model shows good agreement vs. data. This model was not incorporated into the results in this Chapter, but it will be utilized in subsequent chapters.

Finally, it must be mentioned that all comparisons were made for an average patient and hence no effort was made to include any interpatient variability. It is expected that interpatient variability is significant, and that exercise may affect one individual to a different magnitude than another, especially in the cases of insulin-resistance.

*Model Insights.* The model provides several insights into the physiology of glucose-kinetics, and metabolism.

First, $EGP$ provides needed glucose during exercise. Figure 3.20 shows that following the meal, $EGP$ is suppressed in both groups. In the resting group, $EGP$ slowly rises back to basal levels over several hours. In the exercising group, $EGP$ sharply increases after exercise commences, reaching a maximum of 210 [mg/min]. In this same time period, $Ra_{meal}$ is about 200 [mg/min]. Summing the two, there is a total of 410 [mg/min] of glucose input during exercise, which is equal and opposite to $RGU_{TOT}$. $EGP$ provides over 50% of the glucose required to prevent hypoglycemia. Previous studies have shown that in a fasting state ($Ra_{meal}$=0 [mg/min]) $EGP$ rises as high as 400-500 [mg/min] [35] to prevent hypoglycemia. This is consistent with our results that show that a total of 410 [mg/min] is required to prevent hypoglycemia during exercise. In diabetic patients, a robust $EGP$ response during exercise may not occur because of prolonged hyperinsulinemia. This may help explain why persons with T1D often experience hypoglycemia during exercise.

Another insight about $EGP$ that can be gathered from the model predictions is how it effectively acts as a 'safety net' that prevents hypoglycemia in the CS while allowing hypoglycemia in the SM. Figure 3.16 shows that during exercise $G$ drops to 70 [mg/dL] (a low but safe level of glucose) and $H$ drops all the way to 40 [mg/dL]. This occurs because $EGP$ enters directly into the CS, while exercise-induced uptake occurs locally in the SM. The fact that we have two compartments with relatively slow glucose exchange rates provides a moderating influence on $G$, allowing the CS to maintain $G$ at a high enough concentration to provide glucose to the most demanding and critical organ, the brain.

We also gain some insight about glucose-kinetics (i.e. the transfer of glucose between compartments). We evaluate the predicted glucose-kinetics by analyzing the exercise-induced changes in $k_d^G$, $\mathcal{H}_d$, and $ef$. Glucose delivery rate $k_d^G$ increases 2-fold during exercise (Figure 3.13), however this predicted increase does not keep up with demand during exercise. As a result, $H$ decreases to about 40 [mg/dL] (Figure 3.16) before the $G-H$ gradient is sufficient to increase $\mathcal{H}_d$ enough to keep up with a demand of nearly 300 [mg/min] (Figure 3.18). During the same time, $ef$ drops to only 2% (Figure 3.17), despite the 2-fold increase in $k_d^G$ from capillary recruitment. This is because the 10-fold increase in $Q_d$ reduces the time available for glucose exchange in capillary beds, reducing $ef$.

Figure 3.19 shows how $\mathcal{H}_d$ and $ef$ are related during rest and exercise. At rest, $ef$ and $\mathcal{H}_d$ increase together, because they both only depend on $G-H$. During exercise, the dynamics change because increases in $PS_d^G$ and $Q_d$ increase the glucose delivery rate $k_d^G$. Naturally, this causes an increase in $\mathcal{H}_d$ however $ef$ falls because the capillary exchange time is significantly reduced.

Exercise is predicted to have significant effects on the relative contributions of each mechanism to total glucose input and metabolism. We've examined this by calculating the AUC of each mechanism over the entire postprandial period (Table 3.3). The model predicts the following: (1) Enhanced $EGP$ in the exercising group is a significant contribution to total glucose input (+10 [g] over the resting group). Considering that increased $EGP$ is the mechanism responsible for preventing hypoglycemia during exercise, this is not surprising. (2) A 75 minute exercise period significantly increases glucose uptake (+17 [g]). (3) Glucose uptake due to insulin in the SM tissue is noticeably insensitive to exercise (only a 2 [g] difference

from the resting group to the exercising group). This may be due to insulin-kinetics only being marginally affected by exercise in healthy patients with functioning $\beta$-cells, whose insulin production is scaled back during exercise (see Figure 3.15). However, it is worth noting that we are not modeling the synergistic effects of insulin and exercise on uptake, which some have found may be significant [40]. Thus our predictions of $RGU_{SM_{ins}}$ may be an underestimate. (4) Glucose uptake by the liver is lower in the exercising group (-5 [g]). This is the result of two effects. The primary effect is that $G$ rapidly falls during exercise, reducing $RGU_{CS_{liv}}$ which depends significantly on $G$. The secondary effect is that $I$ and $S$ fall during exercise, which decreases insulin-action on glucose uptake in the liver. (5) The last prediction is that splanchnic uptake as a proportion of total uptake is lower in the exercising group (- 8 %). This is consistent with the previous prediction of decreased liver uptake during exercise, as the liver is the primary site of splanchnic uptake.

The authors must stress that each of these predictions, while consistent with direct observations from literature, are speculative. A more accurate model structure and improved parameter values may change predictions and paint a different picture of postprandial glucose metabolism during exercise.

*Modeling and Experimental Shortcomings.* Results also indicate some significant modeling weaknesses that need to be addressed in order to validate the model and improve accuracy. Many of these modeling weaknesses are borne from a lack of experimental data that can be used to measure parameters and validate certain model expressions.

The significant drop of $H$ to 40 [mg/dL] may not be an accurate prediction. This can be explained by two potential modeling weaknesses. The first is that our derived model for solute exchange in capillary beds (Equation 3.65) does not accurately predict glucose transport because of both unmodeled transport phenomena such as microfiltration and potentially active transport, inaccurate assumptions such a capillary homogeneity. The second reason for inaccurate kinetic predictions is the uncertainty in the permeability surface area $PS_d^G$.

These inaccuracies in glucose transport are apparent because even though model predictions during fasting and resting agree with observation ($ef \approx$ 3-4 %), $ef$ during exercise is predicted to drop to 2%, which is inconsistent with direct measurements of $ef$ showing an *increase* to 8% across the leg during exercise [39, 40]. Various prominent researchers such as Renkin [38] have proposed that capillary bed heterogeneity could be the culprit in the inability of homogeneous capillary exchange models to accurately capture observed behaviors.

Measurements of capillary permeability to glucose vary significantly, from 0.6-2.0 [$\text{ml}_b/100\text{g}_{tiss}$/min], with some estimates as high as 5.0 [$\text{ml}_b/100\text{g}_{tiss}$/min]. The difficulty in consistently and accurately quantifying $PS_d^G$ stems from measurement techniques, that are model-dependent, and confounding factors, such as hyperglycemia, hyperinsulinemia, stress, and whether the patient is in a fasting or postprandial state. Any of these factors can significantly alter $PS_d^G$. This may explain why the $G - H$ gradient is larger than would be expected throughout the postprandial period. Future work should include the dependence of $PS_d^G$ on fasting/postprandial state, physiological hyperglycemia, and hyperinsulinemia.

Future work should seek to improve the capillary transport model (Equation 3.65) by

either adapting a fully phenomenological model for capillary exchange, or by attempting to improve the model by including more unmodeled phenomenon. Specifically, more microcirculation experiments need to be done to obtain a better estimate of $PS_d^G$. This may be achieved by performing arteriovenous catheterization studies during exercise of varying intensities, while simultaneously measuring glucose in the SM ISF and tissue perfusion rate.

Another aspect of the model that warrants further consideration is the lumping of all active SM, resting SM, and SC tissue into one compartment. In the current model the predictions for $H$ represent the average concentration in all three of these compartments. While this simplifies the model structure and reduces parameters, it also ignores some potentially important phenomena. First, active SM and resting SM have been shown to have different $ef$ during exercise [35]. This has been explained by a redistribution of blood flow to prioritize active muscle over resting muscle. Along the same lines, SC tissue during exercise exhibits different glucose-kinetics than that of SM muscle. Ideally, each of these tissue groups should be represented by an independent compartment. It is expected that if these compartments were added, the glucose concentration in active SM would be lower than in the resting SM and SC tissues because of local glucose uptake in active SM. Future work should address whether the addition of these three compartments would improve model predictions.

Also, the model for peripheral glucose uptake $RGU_{SM_{exr}}$ was developed for low and moderate intensity leg exercise. For other types of exercise, as well as high intensity exercise, the model may be inaccurate. We have also assumed that uptake $RGU_{SM_{exr}}$ is not a saturable process. At glucose concentrations greater than 300 [mg/dL] this assumption may be invalid [90, 124]. Also, $RGU_{SM_{exr}}$ did not include any synergistic effects of glucose and exercise, meaning that insulin-induced uptake and exercise-induced uptake are considered independent and additive processes. Last, the exercise uptake model did not include a significant time-lag, meaning that exercise-induced glucose uptake occurs immediately at the onset of exercise.

Another missing piece is that $RGU_{SM_{ins}}$ does not include uptake hysteresis (i.e. time dependent insulin resistance). Castillo and Bergman [70] did observe this phenomenon, but again limited data and the desire for model parsimony led us to not to include this effect.

The liver glucose uptake model $RGU_{CS_{liv}}$ was adapted from Sorensen [64] and does not include the effects of exercise. It is clear that glucose uptake in the liver is a significant contributor to total postprandial glucose uptake during rest [119, 120, 131], but less is understood about liver glucose uptake during exercise. The lack of a validated model of $RGU_{CS_{liv}}$ during exercise is a significant weakness of the present work.

The present model was only validated on healthy patients with fully functional $\beta$-cells. To accurately represent a type 1 diabetic patient the model needs to be expanded to include a model of insulin resistance, $EGP$ in a diabetic, and subcutaneous insulin infusion. The latter has already been developed in Chapter 2, which models insulin-kinetics during exercise. A full coupled model of insulin-glucose dynamics will be presented in Chapter 4.

Finally, the last shortcoming of the model is that there is significant parameter uncertainty, which is the case in any biological model. This shortcoming is directly related to experimental shortcomings, which cannot directly quantify certain parameters, especially for individual patients, because of measurement error. To capture the interpatient variability,

much more data needs to be taken under various exercising conditions.

*Model Applications.* Despite the limitations and uncertainty of the model, the predictions are reasonable during rest and exercise. An understanding of how glucose concentrations change during exercise can provide insight into optimal control tuning. Additionally, the inclusion of a model of glucose kinetics between the CS and SM provides insight into how interstitial fluid glucose concentrations change postprandially and during exercise. This understanding can be used to improve continuous glucose monitors, which sample glucose from the interstitial fluid.

One of the most difficult and crucial conditions to control in T1D patients is when exercise occurs in the postprandial state. This is because insulin-on-board is high, which causes $EGP$ to be suppressed and insulin-induced glucose uptake to be high. Because of this, the addition of exercise can quickly push a person into hypoglycemia. This model provides a means to understand the interplay between $EGP$, liver uptake, peripheral uptake, and exercise induced uptake, and how their combined effects can lead to dangerous hypoglycemia.

The most obvious application of this work is the use of the model in an model predictive control algorithm in the artificial pancreas. Because exercise remains a significant hurdle, a model that can accurately predict glucose concentrations during exercise will greatly improve control.

## 3.5 Conclusion

A multiscale model was developed to predict postprandial glucose-dynamics during exercise. For the first time we have included the effects of capillary recruitment on glucose-dynamics. We have also developed and validated a novel model of $EGP$ during exercise. Overall, the glucose-dynamics model agrees reasonably well with an average healthy (non-diabetic) resting and exercising subject. A main advantage of the model was the inclusion of direct measurements of glucose production, eliminating the need to model these complex phenomena. Instead, the focus was on modeling the various uptake terms and the glucose-kinetics between the circulatory system and the skeletal muscle. It was found that a homogeneous model of glucose delivery provided predictions of the extraction fraction that were too low, despite the inclusion of enhanced capillary surface area associated with tissue recruitment. The presented model provides a framework for developing a more accurate model of glucose dynamics. This model can eventually be used in model predictive control algorithms in the artificial pancreas.

# Chapter 4

# Coupling the Insulin-Glucose Models and Validation on a Type 1 Diabetic Subject

## Chapter Overview

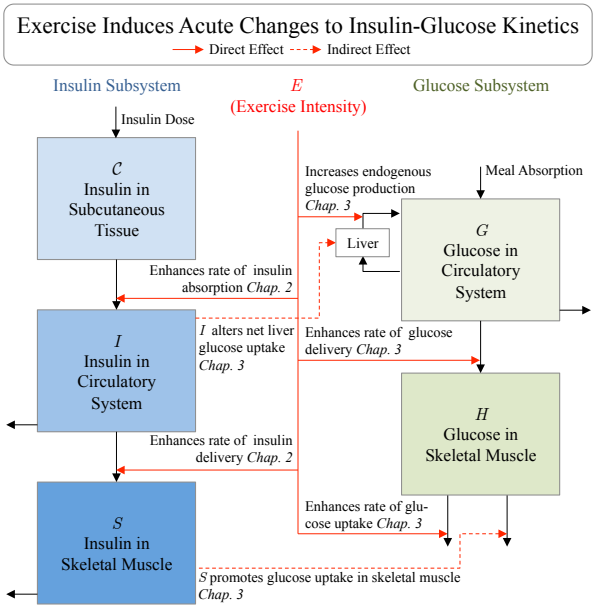


Figure 4.1: The focus of this chapter will be on coupling the insulin subsystem model to the glucose subsystem model, and then validating the model for a T1D subject by comparing model outputs with measurements. The solid red lines are the direct effects of exercise and the dotted-lines are the indirect effects that result from the coupling of the models.

The focus of this chapter will be on coupling the insulin-kinetics model to the glucose-dynamics model, and then validating the coupled model for a T1D subject by comparing model outputs with measurements. The insulin-kinetics model derived in Chapter 2 was derived for a subject with T1D. However, the glucose-dynamics model derived in Chapter 3 was for a healthy non-diabetic subject. In coupling the two models we must make appropriate parameter adjustments so that the glucose-dynamics model can be applied to a subject with T1D.

## 4.1 Model Coupling for Subject with Type 1 Diabetes

The final insulin model equations are taken from Chapter 2 (Equations 2.50-2.61). The final glucose model equations are taken from Chapter 3 (Equations 3.53-3.73). Coupling the two models is straightforward. In the original glucose model we assumed that $I(t)$ was given as a measured input. Now, we instead predict $I$ using the insulin model. The coupled system is summarized below.

$$\frac{d\mathcal{C}}{dt} = -k_a^I(E)\cdot\mathcal{C} + \mathcal{U}(t) \tag{4.1}$$

$$\frac{dI}{dt} = \frac{k_a^I(E)\cdot\mathcal{C}}{V_{CS}^I} - \frac{V_{SM}^{tiss}k_d^I(E)\cdot(I-S)}{V_{CS}^I} - \mathrm{r}_{CS_N}^I\cdot I \tag{4.2}$$

$$\frac{dS}{dt} = \frac{V_{SM}^{tiss}k_d^I(E)\cdot(I-S)}{V_{SM}^I} - \mathrm{r}_{SM_N}^I\cdot S \tag{4.3}$$

$$\frac{dG}{dt} = -\frac{V_{SM}^{tiss}k_d^G(E)\cdot(G-H)}{V_{CS}^G} - \frac{RGU_{CS_{liv}}(G,M(S)) + RGU_{CS_{fix}}}{V_{CS}^G} + \frac{Ra_{meal}(t) + EGP(G,S,L(E))}{V_{CS}^G} \tag{4.4}$$

$$\frac{dH}{dt} = \frac{V_{SM}^{tiss}k_d^G(E)\cdot(G-H)}{V_{SM}^G} - \frac{RGU_{SM_{ins}}(H,S) + RGU_{SM_{exr}}(H,E)}{V_{SM}^G} \tag{4.5}$$

$$\frac{dM}{dt} = \frac{1}{\tau_{liv}}2.0\cdot tanh(0.55\frac{S}{S_b}) \tag{4.6}$$

$$\frac{dL}{dt} = \frac{1}{\tau_{EGP}}\cdot(-L+\eta E) \tag{4.7}$$

$\mathcal{U}$ is given as [$\mu$U/min]. $\mathcal{C}$ has units of [$\mu$U]. Insulin concentrations $I$ and $S$ have units [$\mu$U/mL]. Glucose concentrations $G$ and $H$ have units [mg/dL]. Insulin-action on liver glucose uptake $M$ and exercise-action on endogenous glucose production $L$ are unitless.

Kinetic functions that govern the movement of between compartments are defined as

$$k_a^I(E) = Q_a^I(1 - e^{\frac{-PS_a^I}{Q_a^I}}) \tag{4.8}$$

$$k_d^I(E) = Q_d^I(1 - e^{\frac{-PS_d^I}{Q_d^I}}) \tag{4.9}$$

$$Q_a^I(E) = (1-h)\cdot(Q_{a_{rest}} + \lambda_a E) \tag{4.10}$$

$$Q_d^I(E) = (1-h)\cdot(Q_{d_{rest}} + \lambda_d E) \tag{4.11}$$

$$PS_a^I(E) = PS_{a_{rest}}^I \cdot (1 + R_a tanh(\gamma E)) \tag{4.12}$$

$$PS_d^I(E) = PS_{d_{rest}}^I \cdot (1 + R_d tanh(\gamma E)) \tag{4.13}$$

$$k_d^G(E) = Q_d(1 - e^{\frac{-PS_d^G}{Q_d}}) \tag{4.14}$$

$$Q_d(E) = Q_{d_{rest}} + \lambda_d E \tag{4.15}$$

$$PS_d^G(E) = PS_{d_{rest}}^G \cdot (1 + R_d tanh(\gamma E)). \tag{4.16}$$

The rates of glucose uptake ($RGU$) and endogenous glucose production ($EGP$) functions are defined as

$$RGU_{CS_{fix}} = \mathrm{r}_{brain}^G + \mathrm{r}_{heart}^G + \mathrm{r}_{kidney}^G + \mathrm{r}_{gut}^G \tag{4.17}$$

$$RGU_{CS_{liv}} = \mathrm{r}_{liv}^G\big(5.66 + 5.66 \cdot tanh(2.44(\frac{G}{G_b} - 1.48))\big)M \tag{4.18}$$

$$RGU_{SM_{ins}} = \mathrm{r}_{SM_{ins}}^G\big(\frac{H}{H_b}S - S_b\big) + \mathrm{r}_{peri}^G \tag{4.19}$$

$$RGU_{SM_{exr}} = \mathrm{r}_{SM_{exr}}^G \frac{H}{H_b}E \tag{4.20}$$

$$EGP = EGP_b \frac{G_b}{G}\frac{S_b}{S}(1 + L). \tag{4.21}$$

The initial conditions are calculated by solving the following set of linear equations, which are assumed at resting ($E = 0$), steady-state, and basal concentrations. $G_b$ and is a free

parameter that can be set to any set-point. $EGP_b$ is set to 155 [mg/min].

$$0 = -k_a^I(0)\mathcal{C}_o + \mathcal{U}(t_o) \tag{4.22}$$

$$0 = \frac{k_a^I(0)\mathcal{C}_o}{V_{CS}^I} - \frac{V_{SM}^{tiss}k_d^I(0)(I_o - S_o)}{V_{CS}^I} - \mathrm{r}_{CS_N}^I \cdot I_o \tag{4.23}$$

$$0 = \frac{V_{SM}^{tiss}k_d^I(0)(I_o - S_o)}{V_{SM}^I} - \mathrm{r}_{SM_N}^I \cdot S_o \tag{4.24}$$

$$0 = -G_o + G_b \tag{4.25}$$

$$0 = -H_o + G_o - \frac{\mathrm{r}_{peri}^G}{V_{SM}^{tiss}k_d^G} \tag{4.26}$$

$$0 = -M_o + 1 \tag{4.27}$$

$$0 = L_o. \tag{4.28}$$

### 4.1.1 Parameter Adjustments for Subject with Type 1 Diabetes

The values of the parameters of the model are shown in Table 4.1. All the glucose model parameters reported in Chapter 3 are specific to healthy patients. In order to use the model to simulate a T1D patient, certain parameters need to be adjusted. All parameters are kept the same except for $\mathrm{r}_{liv}^G$, $\mathrm{r}_{gut}^G$ and $\mathrm{r}_{SM_{ins}}^G$. These three parameters will be adjusted to account for the observed insulin resistance that was found in T1D subjects [136].

We will assume that in a T1D subject, the constant glucose metabolic rates $\mathrm{r}_{brain}^G$, $\mathrm{r}_{heart}^G$, $\mathrm{r}_{kidney}^G$, and $\mathrm{r}_{peri}^G$ are unchanged between a T1D and healthy subject. These rates, given as [mg/min], do not depend on glucose concentration nor insulin concentration because they are mainly determined by the underlying metabolic demands of the tissue. Similarly, $\mathrm{r}_{SM_{exr}}^G$ is be kept the same, as it is a derived parameter (see Chapter 3.2.1) that is assumed to be dependent on tissue demands during exercise.

The remaining three glucose metabolic rate parameters are $\mathrm{r}_{liv}^G$, $\mathrm{r}_{gut}^G$ and $\mathrm{r}_{SM_{ins}}^G$. Insulin resistance in T1D subjects has been documented by DeFronzo [136]. The clearance rate of glucose in T1D subjects was found to be 61% *less* than in healthy subjects. We will thus adjust parameters $\mathrm{r}_{liv}^G$ and $\mathrm{r}_{SM_{ins}}^G$ by multiplying them by 3/8. For our model we still would like to keep the total body $RGU$ at 155 [mg/min]. Hence $\mathrm{r}_{gut}^G$ was adjusted upward from 16.6 to 25.8 [mg/min] to account for the drop in $\mathrm{r}_{liv}^G$. In summary, the three parameters that change from a healthy ($^{[H]}$) to a T1D subject ($^{[D]}$) are

$$\mathrm{r}_{liv}^{G\ [D]} = 3/8 \cdot \mathrm{r}_{liv}^{G\ [H]}\ [\mathrm{mg/min}] \tag{4.29}$$

$$\mathrm{r}_{gut}^{G\ [D]} = \mathrm{r}_{gut}^{G\ [H]} + 9.2\ [\mathrm{mg/min}] \tag{4.30}$$

$$\mathrm{r}_{SM_{ins}}^{G\ [D]} = 3/8 \cdot \mathrm{r}_{SM_{ins}}^{G\ [H]}\ [\mathrm{mg/min\ per\ } \mu\mathrm{U/mL}]. \tag{4.31}$$

The volume parameters, $V_{CS_N}^G$, $V_{SM_N}^G$ ,$V_{SM_N}^{tiss}$, are physical parameters that only depend on the size of the subject being studied, and thus will not change. We will further assume

that the T1D patient is well controlled, and without vascular complications. Hence vascular parameters $Q$ and $PS$ will be kept the same.

The remaining parameters characterize the liver. $\tau_{liv}$ will be assumed the same, as we lack data on the time-delay of insulin-action $RGU_{CS_{liv}}$ in T1D subjects. Last, we assume that exercise effects on $EGP$ are unaltered in T1D subjects and so $\tau_{EGP}$ and $\eta$ will be kept the same.

## 4.2 Validation Tests on T1D Subject

We now perform validation testing to evaluate the accuracy of the coupled T1D insulin-glucose model. We will perform two validation tests, one on an average resting T1D subject (T1DE) and one on an average exercising T1D subject (T1DE). The T1D clinical data was gathered at the Mayo Clinic in Rochester MN. Detailed protocol information can be found in Chapter 2.2.4. The parameters used in the two tests are listed in Table 4.1. An illustration of the two protocols is shown in Figure 4.2.

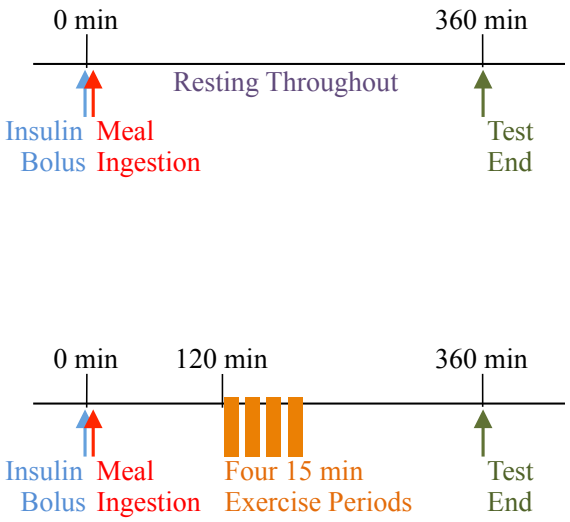


Figure 4.2: Timeline for the mixed-meal tolerance test (MMTT) T1D resting protocol (T1DR, top) and the T1D exercising protocol (T1DR, bottom). At time 0 the subjects in T1DR ingested a 50 [g] CHO mixed-meal and the subjects in T1DE ingested 75 [g]. The insulin bolus was infused through an insulin pump at time 0, with bolus size calculated according to the subject's normal insulin-to-carb ratio. The T1DR group rested throughout the entire study period. The T1DE group exercised at 50% $V0_{2_{max}}$ for four 15 minute exercise periods, starting at minute 120.

Table 4.1: Parameters for the insulin-kinetics model (top) and glucose-dynamics model (bottom).

| Parameter | Description | Units | Value | Source |
|---|---|---|---|---|
| $V^I_{CS_N}$ | Normalized volume of distribution of insulin in circulatory system | dL/kg$_{BW}$ | 0.5 * | [44, 104] |
| $V^I_{SM_N}$ | Normalized volume of distribution of insulin in skeletal muscle | dL/kg$_{BW}$ | 1.2 * | [44, 64, 104] |
| $V^{tiss}_{SM_N}$ | Normalized volume of tissue in skeletal muscle domain | mL/kg$_{BW}$ | 540 * | [83] |
| $\mathrm{r}^I_{CS_N}$ | Normalized clearance rate of insulin in circulatory system | 1/min | 0.32 | [105–107]† |
| $\mathrm{r}^I_{SM_N}$ | Normalized clearance rate of insulin in skeletal muscle | 1/min | 0.02 | [105–107]† |
| $Q_{a_{rest}}$ | Tissue perfusion rate absorbing (SC) tissue at rest | mL$_b$/mL$_{tiss}$/min | 0.028 | [83] |
| $Q_{d_{rest}}$ | Tissue perfusion rate in delivering (SM) tissue at rest | mL$_b$/mL$_{tiss}$/min | 0.038 | [83] |
| $h$ | Hematocrit percentage in blood | 1 | 0.4 | [104] |
| $\lambda_a$ | Slope relating $Q$ in absorbing (SC) tissue to exercise | mL$_b$/mL$_{tiss}$/min | 0.071 | [71, 86–88] |
| $\lambda_d$ | Slope relating $Q$ in delivering (SM) tissue to exercise | mL$_b$/mL$_{tiss}$/min | 1.1 | [84] |
| $PS^I_{a_{rest}}$ | Permeability surface area to insulin in absorbing (SC) capillaries | mL$_b$/mL$_{tiss}$/min | 0.005 | ‖ |
| $PS^I_{d_{rest}}$ | Permeability surface area to insulin in delivering (SM) capillaries | mL$_b$/mL$_{tiss}$/min | 0.005 | [101, 102] |
| $R_a$ | Capillary recruitment factor in absorbing (SC) tissue | 1 | 0.40 | [96, 97] ‡ |
| $R_d$ | Capillary recruitment factor in delivering (SM) tissue | 1 | 1.46 | [92–94] ‡ |
| $\gamma$ | Saturation coefficient for $PS$ | 1 | 10 | [92–94] ‡ |
| $\mathrm{r}^G_{brain}$ | Metabolic clearance rate of glucose in the brain | mg/min | 71 | [45, p. 219] |
| $\mathrm{r}^G_{heart}$ | Metabolic clearance rate of glucose in the heart | mg/min | 3.7 | [45, p. 219] |
| $\mathrm{r}^G_{kidney}$ | Metabolic clearance rate of glucose in the kidneys | mg/min | 3.7 | [45, p. 219] |
| $\mathrm{r}^G_{gut}$ | Metabolic clearance rate of glucose in the gut | mg/min | 25.8¶ | [45, p. 219][136] |
| $\mathrm{r}^G_{peri}$ | Basal metabolic clearance rate of glucose in the peripheral tissue | mg/min | 45.2 | [45, p. 219] |
| $\mathrm{r}^G_{liv}$ | Basal metabolic clearance rate of glucose in the liver | mg/min | 5.6¶ | [45, p. 219][136] |
| $\mathrm{r}^G_{SM_{ins}}$ | Insulin sensitivity of glucose clearance in skeletal muscle | mg/min per $\mu$U/mL | 1.9¶ | [70] |
| $\mathrm{r}^G_{SM_{exr}}$ | Exercise sensitivity of glucose clearance in skeletal muscle | mg/min per $E$ | 860 | [35, 39, 40, 129, 130]§ |
| $V^G_{CS_N}$ | Normalized volume of distribution of glucose in circulatory system | mL/kg | 0.7 * | [64] |
| $V^G_{SM_N}$ | Normalized volume of distribution of glucose in skeletal muscle | mL/kg | 0.96 * | [64] |
| $V^{tiss}_{SM_N}$ | Normalized volume of tissue in skeletal muscle | mL/kg | 540 * | [83] |
| $\tau_{liv}$ | Time lag of insulin action of liver glucose uptake | min | 25 | [64] |
| $PS^G_{d_{rest}}$ | Capillary permeability surface area to glucose during rest | mL$_b$/mL$_{tiss}$/min | 0.01 | [80, 101, 102] |
| $\tau_{EGP}$ | Time lag of exercise action on endogenous glucose production | min | 20 | [35, 39]§ |
| $\eta$ | Maximum exercise action on endogenous glucose production | 1 | 4 | [35, 39]§ |

* Multiplied by BW prior to being used in model. See demographics for BW
† Derived from total clearance rate as measured in specified sources
‡ Parameter is derived by fitting to microvascular blood volume data from specified sources
§ Parameter is derived by fitting to data from specified sources
‖ Assumed to be the same as $PS^I_{d_{rest}}$
¶ Parameter for type 1 diabetic subject. See Chapter 3 for healthy patient parameter.

### 4.2.1 Validation Test on a Resting T1D Subject

The T1DR protocol is illustrated in Figure 4.2. 17 T1D subjects underwent this protocol. Each subject was given a 50 [g] carbohydrate (CHO) meal at time = 0 [min] and took an insulin bolus through their insulin-pump according to their normal insulin-carb ratio (the dose averaged $\approx 4$ [U]). The subject then rested for the following 360 [min]. We simulate the model using the average measured inputs $\mathcal{U}(t)$, $Ra_{meal}(t)$, and $E(t) = 0$. The basal values of glucose was taken from experiment $G_b$=151 [mg/dL]. $EGP_b$ was set to 155 [mg/min].

The predicted outputs $I$, $G$, and $EGP$ are plotted in Figure 4.3, with the corresponding measurements $I_{data}$, $G_{data}$, and $EGP_{data}$.

The topmost frame in Figure 4.3 shows the insulin inputs $\mathcal{U}(t)$ and exercise intensity $E$. The frame below shows the $I$ predictions, which agree well with $I_{data}$, with a slight underestimation. This underestimation is likely because the permeability of the capillary bed to insulin, $PS_a^I$, was underestimated. Also, $I$ reaches its peak much earlier than $I_{data}$. This occurs because - as noted before - we did not model hexameric to dimeric/monomeric dissociation, which would have accounted for the time-lag of insulin absorption. We also notice that $I$ prior to the bolus is slightly lower than the data indicates. This likely occurs because the volume of distribution $V_{CS}^I$ is too large. For all our parameters we selected the population-average values, and thus the selected value of $V_{CS}^I$, may have been too low for the T1DR cohort. A slight adjustment of parameters $PS_a^I$ and $V_{CS}^I$ would have increased agreement between $I$ and $I_{data}$, however we wanted to avoid overfitting, and hence decided to keep population-averaged parameter values. Additionally, notice that prior to time 0 small insulin boluses are given, shown by small bumps in $\mathcal{U}$. These bumps slightly raised $I$ prior to the main bolus. Some subjects provided these small boluses prior to their main bolus in hopes of starting the test closer to euglycemia. This adversely affected the initial $G$ and $EGP$ predictions, as will be explained.

Glucose predictions are shown in the third frame of Figure 4.3. The red region represents hypoglycemia ($< 70$ [mg/dL]). Overall, agreement between $G$ and $G_{data}$ is reasonable and indicates that the model appropriately captures the main aspects of the post-postprandial glucose response. At the start of the test $G$ falls slightly because of the reduction in $EGP$ (see the bottom frame of Figure 4.3) that results from the increase in $I$ prior to time 0. This reduction in $EGP$ is a consequence of the model, and was not seen in the clinical data, which may indicate that our $EGP$ model is overly-sensitive to insulin. This causes $G$ to start off at a slightly lower concentration than $G_{data}$. Upon the meal ingestion, $G$ rapidly rises and it is in almost perfect agreement with $G_{data}$, but peaks at a slightly lower concentration, consistent with the lower concentration to start. $G$ then slowly returns back to basal levels around 150 [mg/dL] over the next few hours. Interestingly $G_{data}$ does not return to basal, and plateaus around 225 [mg/dL]. The plateau of $G_{data}$ may be because of time-dependent changes in the insulin sensitivity (SI) ($\mathrm{r}_{SM_{ins}}^G$) which were not modeled. These time-dependent changes in SI have been confirmed to exist by Castillo and Bergman [70]. If we were to include this effect by decreasing $\mathrm{r}_{SM_{ins}}^G$ as the meal progresses, the equilibrium value of $G$ would shift and plateau in a manner similar to $G_{data}$.

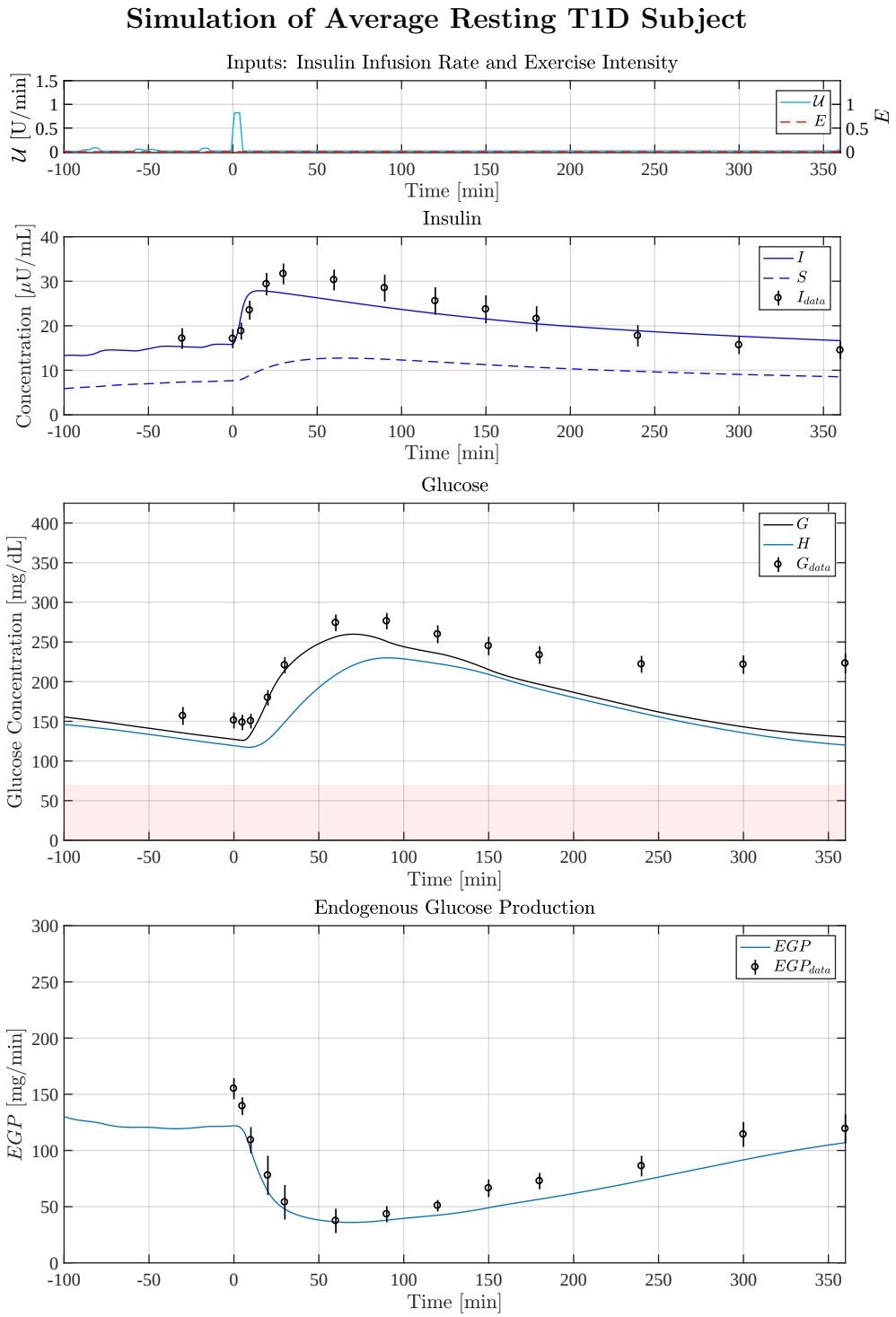


Figure 4.3: Results of validation test on a resting T1D subject. (top) Inputs insulin infusion rate $\mathcal{U}$ and exercise intensity $E$. (middle top) Insulin predictions. (middle bottom) Glucose predictions. (bottom) Endogenous glucose production predictions. Overall agreement is good, with only small discrepancies.

$EGP$ predictions are shown in the bottom frame of Figure 4.3. Overall, the agreement is strong. $EGP$ is suppressed at nearly the same rate as $EGP_{data}$, bottoms-out at the same value, and rises at nearly the same rate. However, there is some spurious behavior during the period prior to time 0. $EGP$ is predicted to drop from 155 [mg/min] to 120 [mg/min] (the early times where $EGP$=155 [mg/min] is not shown). We believe this occurs for one of two reasons. First, $EGP_{data}$ measurements were not captured prior to time 0, and they may have in fact been higher than EGP at time 0, which would have altered the $EGP_b$ value used in Equation 4.7. The other explanation is that our $EGP$ model may be too sensitive to small perturbations in insulin concentration. The $EGP$ model predicted a drop of 15% because $S$ increased from 4.5 to 7.5 [$\mu$U/mL]. In the real case the liver may only respond to significant changes in insulin concentration and small changes may not trigger suppression of glucose production. It may be possible to model $EGP$ so it does not respond to small perturbations in $S$, however it is not clear that the increased accuracy would offset the additional mathematical complexity.

To gain some insight into the dynamics that govern $G$, we examine the individual contributions of each mechanism of glucose production and uptake. Figure 4.4 plots the two mechanisms of glucose production, $Ra_{meal}$ and $EGP$, and the glucose uptake in each compartment $RGU_{CS_{TOT}}$ and $RGU_{SM_{TOT}}$. $RGU_{CS_{TOT}}$ is comprised of the constant glucose sinks of the brain, heart, gut, and kidney plus the glucose uptake by the liver $RGU_{CS_{liv}}$. $RGU_{SM_{TOT}}$ is comprised of both insulin-dependent and exercise-dependent glucose uptake in the muscle. $Ra_{meal}$ is plotted as a dotted line because it is a measured input. The remaining lines are solid because they are predictions.

After meal ingestion at time 0, $Ra_{meal}$ (blue dotted line) rapidly spikes. This causes the initial increase in $G$ seen in Figure 4.3. During this time, due to the rapid increase in insulin and glucose concentration, $EGP$ (red line) is rapidly suppressed. In the next hour $RGU_{CS_{TOT}}$ (yellow line) and $RGU_{SM_{TOT}}$ (purple line) slowly increase. The increase in $RGU_{CS_{TOT}}$ is due solely to liver uptake. At approximately minute 75, uptake exceeds production, and glucose levels begin to decline. From the plot it is clear that the liver is the main source of postprandial glucose uptake, skeletal muscle tissue is secondary.

### 4.2.2 Validation Test on Exercising T1D Subject

The protocol for the exercising group (T1DE) is illustrated in Figure 4.2. 12 T1D subjects underwent this protocol and each ingested a 75 [g] CHO meal at time 0. As in the resting group, subjects dosed insulin through their insulin-pump according to their normal insulin-carb ratio. The dose for T1DE averaged $\approx$ 6 [U], about 2 [U] more than TIDR. After meal ingestion the subjects rested for 120 [min]. At minute 120, the subjects underwent four 15 minute 50% $V0_{2_{max}}$ exercise bouts, with 5 minutes of rest between each bout. After exercise ended at minute 195, the patient was instructed to rest for the remainder of the test, until being released at minute 360.

We simulate the model using the average measured inputs taken on the 12 subjects $\mathcal{U}(t)$, $Ra_{meal}(t)$, and $E(t)$. The basal values of glucose was taken from experiment $G_b$=171

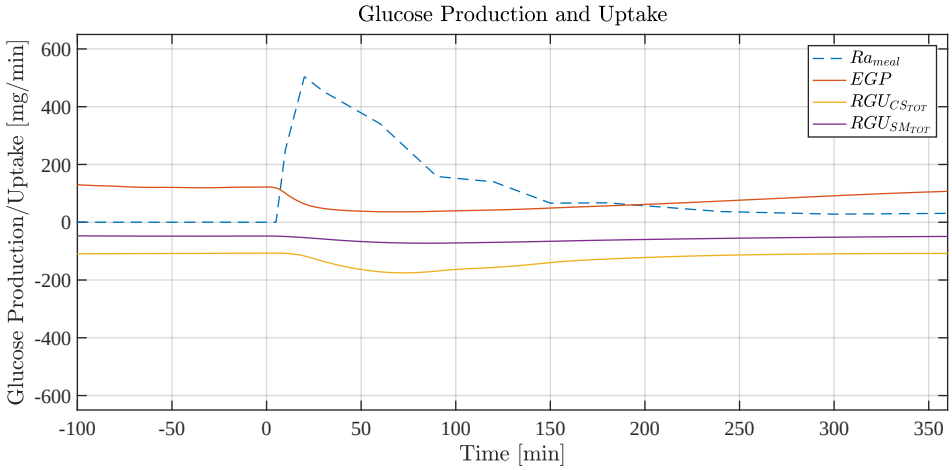


Figure 4.4: The calculated individual contributions of each mechanism of glucose production and uptake for the validation test on a resting T1D subject. Positive is production, negative is uptake. The dotted line for $Ra_{meal}$ indicates an input.

[mg/dL]. $EGP_b$ was set to 155 [mg/min]. The predicted outputs $I$, $G$, and $EGP$ are plotted in Figure 4.5, with the corresponding measurements $I_{data}$, $G_{data}$, and $EGP_{data}$. Note that the $EGP_{data}$ had significant error because of the difficultly of clamping the tracer-to-tracee ratios in T1D patients during exercise [113]. For this reason, we have post-processed the $EGP_{data}$ using linear scaling. This provided more realistic $EGP$ values, however it does not fix non-steady state errors, and hence the $EGP_{data}$ shown in Figure 4.5 should be regarded with some skepticism.

The topmost frame in Figure 4.5 shows the insulin inputs $\mathcal{U}(t)$ and exercise intensity $E$. The frame immediately below shows the predicted insulin concentrations $I$ with exercise periods indicated by grey regions. There is good agreement between $I$ and $I_{data}$. However, as in the resting case shown in Figure 4.3, $I$ is an underestimate of $I_{data}$ and peaks much earlier. This can be explained by the same reasoning as before: $PS_a^I$ is likely underestimated and we did not model hexameric dissociation. If these effects were included we anticipate better agreement.

At minute 120 exercise commences causing capillary recruitment (see Chapter 2.2.2). Due to the associated increase in capillary surface area the insulin absorption rate increases by 45%. This causes $I$ to increase by 30%, which is in almost perfect agreement with the 30% increase shown in $I_{data}$. This increase is maintained throughout the 15 minute exercise period, with slight dips during the 5 minute resting periods due to capillary de-recruitment. After exercise ends there is a rapid drop in both $I$ and $I_{data}$, which stay nearly identical until the end of the test.

The glucose predictions are shown in the third frame of Figure 4.5. The red region represents hypoglycemia ($< 70$ [mg/dL]). The subject eats a meal at time 0, and glucose rises to 350 [mg/dL]. Exercise commences at minute 120 and continues in four bouts until

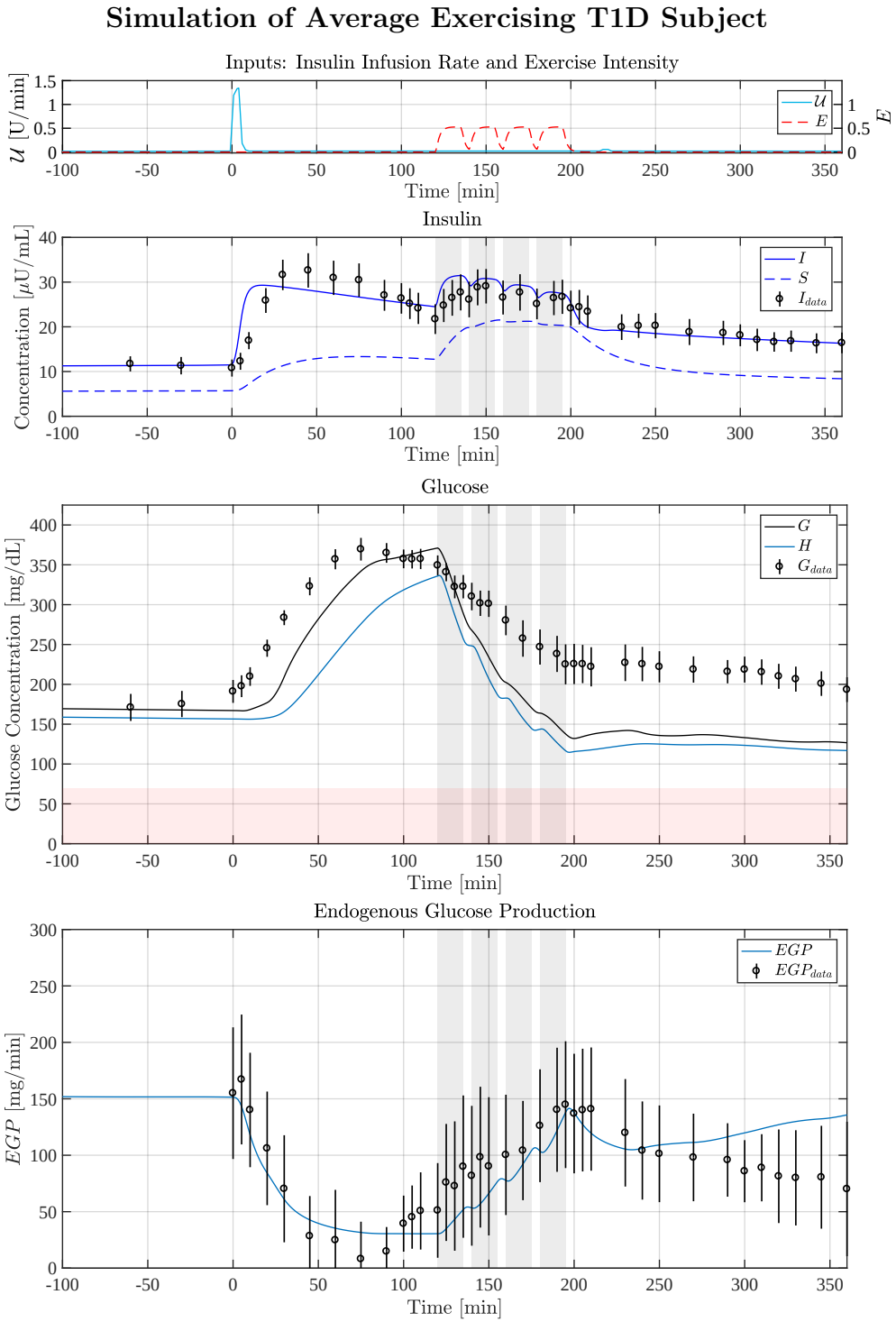


Figure 4.5: Results of validation test on an exercising T1D subject. (top) Inputs insulin infusion rate $\mathcal{U}$ and exercise intensity $E$. (middle top) Insulin predictions. (middle bottom) Glucose predictions. (bottom) Endogenous glucose production predictions. Exercise periods are indicated by grey regions. Note that EGP measurements had significant error, and were linearly scaled so that the basal level was 155 [mg/min].

minute 195. In this period there is a significant drop in glucose. After exercise glucose levels stabilize until the end of the study. Overall, agreement between model predictions of $G$ and $G_{data}$ is reasonable, however there are two significant discrepancies.

The first discrepancy is that the rise in $G$ after the meal ingestion has a nearly 30 minute lag compared to $G_{data}$. This lag can likely be explained by measurement error in $Ra_{meal}$. It is known that measurement of $Ra_{meal}$ using isotopic tracers is unreliable during the initial glucose rise following a meal [135] because the rapidly changing glucose levels make it nearly impossible to ensure a stable tracer-to-tracee ratio, leading to significant errors. If we examine the current $Ra_{meal}$ in Figure 4.6 (blue dotted line), we see that $Ra_{meal}$ has a lag in its initial rise, seen as a small notch around minute 20. If we compare to the $Ra_{meal}$ measured in other protocols, such as that shown in Figure 4.6 and in earlier chapters (Figure 3.6), it is clear that the current $Ra_{meal}$ exhibits a spurious lag. We thus expect that the reason for the 30 minute lag between $G$ and $G_{data}$ is because of error associated with $Ra_{meal}$.

The second discrepancy is that $G$ drops much more rapidly than $G_{data}$ during exercise. This discrepancy is likely due to model error. The overestimated drop occurs because the model overestimates the increase in skeletal muscle glucose uptake during exercise $RGU_{SM_{exr}}$. This likely occurs because we have not modeled glucose uptake as a saturable process, and instead assumed glucose uptake increases indefinitely as the glucose concentration increases (see Equation 3.64). In fact Rose and Richter found that glucose uptake saturates at a concentration of 300 [mg/dL] [123], which is precisely the range of glucose concentration that occurs in this dataset. Future work will explore improving the model for skeletal muscle glucose uptake so that the drop in $G$ during exercise can be estimated more accurately.

$EGP$ predictions are shown in the bottom frame of Figure 4.5. The predictions of $EGP$ closely follow $EGP_{data}$ throughout the entire period. However, we must note that predicted $EGP$ is dependent on $G$, which was shown to be predicted poorly during exercise. If a proper prediction of $G$ were achieved, it would have the effect of reducing $EGP$ during exercise which would cause disagreement of $EGP$ with $EGP_{data}$. Additionally, as previously mentioned the current $EGP_{data}$ has significant error (notice the enormous error bars), and hence these measurements should be taken with a grain of salt.

As in the resting case, for the exercising case we also examine the individual contributions of each mechanism of glucose production and uptake. Figure 4.6 plots the two mechanisms of glucose production, $Ra_{meal}$ and $EGP$, and the glucose uptake in each compartment $RGU_{CS_{TOT}}$ and $RGU_{SM_{TOT}}$. $RGU_{CS_{TOT}}$ is comprised of the constant glucose sinks of the brain, heart, gut, and kidney plus the glucose uptake by the liver $RGU_{CS_{liv}}$. $RGU_{SM_{TOT}}$ is comprised of both insulin-dependent and exercise-dependent glucose uptake in the muscle. $Ra_{meal}$ is plotted as a dotted line because it is a measured input. The remaining lines are solid because they are predictions.

After meal ingestion at time 0, $Ra_{meal}$ exhibits an uncharacteristic lag in its typically rapid rise. As mentioned, this is likely due to measurement error. $EGP$ (red line) is initially suppressed because of the meal, but rapidly rises starting at minute 120 due to the effects of exercise. It increases from 30 [mg/min] to 155 [mg/min] in about an hour. At the same time glucose uptake in the skeletal muscle ($RGU_{SM_{TOT}}$) has a tremendous spike, increasing

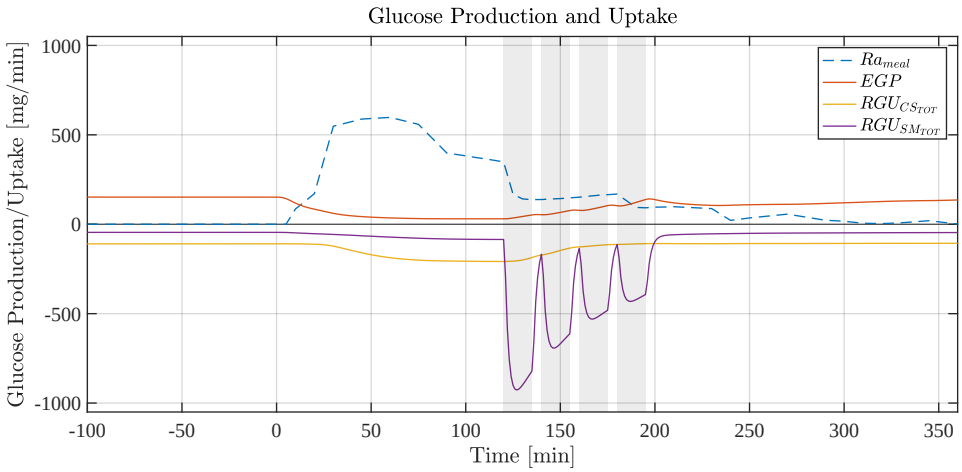


Figure 4.6: The calculated individual contributions of each mechanism of glucose production and uptake for the validation test on a exercising T1D subject. Positive is production, negative is uptake. The dotted line for $Ra_{meal}$ indicates an input. The predictions for skeletal muscle glucose uptake during exercise ($RGU_{SM_{TOT}}$) are likely significantly overestimated.

to nearly 1000 [mg/min]. As previously mentioned, this spike is likely an overestimate.

## 4.3 Validation Conclusions

The objectives of this chapter were: (1) to couple the insulin-kinetics model derived in Chapter 2 with the glucose-dynamics model derived in Chapter 3 and (2) to validate the model on data from a resting T1D cohort (T1DR) and a exercising T1D cohort (T1DE).

Figure 4.3 shows that for the T1DR cohort agreement between model predictions and data was strong. Though there was a slight underestimation of $I$, this can be easily remedied by slight adjustments of parameters. We currently use population-averaged parameters which may not coincide with the parameters of the average patient from our T1DR cohort. Predictions for $G$ also agreed well with data, although there was a significant difference between $G$ and $G_{data}$ in the later stages of the meal. This is likely because of the time-dependence of insulin sensitivity [70], which was not accounted for in our model. $EGP$ also agreed well with data, except for a slight discrepancy in the beginning, which was likely caused by the $EGP$ model being sensitive to small perturbations of insulin. In reality the liver may not be sensitive to small changes in insulin concentration, and thus the behavior of our $EGP$ model under small perturbations may not be physiological.

Figure 4.5 shows that for the T1DE cohort agreement between model predictions and data was strong for $I$, reasonable for $G$, and undetermined for $EGP$ because of poor data. The main discrepancy in our $G$ predictions was that $G$ dropped much more rapidly during exercise than the data would indicate. This can be attributed to the way that exercise-induced skeletal muscle glucose uptake ($RGU_{SM_{exr}}$) was modeled. In deriving our expression

for $RGU_{SM_{exr}}$ we assumed that it was a non-saturable process. In fact, glucose uptake is known to be saturable at high glucose concentrations [123]. Future work needs to focus on improving the model for $RGU_{SM_{exr}}$, perhaps by incorporating saturability.

Overall, the coupled insulin-glucose dynamics model performed well on both T1D cohorts, and can be considered validated for a resting T1D subject. However, more work needs to be done to improve the model before the it can be validated for exercise. Fortunately the model structure is well-understood and the parts of the model that have been determined to be insufficient can be made the focus on future work.

# Chapter 5

# Test Cases for Type 1 Diabetes Insulin-Glucose Exercise Model

## Chapter Overview

In this chapter we will examine the dynamics of the T1D insulin-glucose model by performing 10 real-world test cases. We will examine the effects of exercise timing, intensity, and capillary recruitment on insulin, glucose, and $EGP$ based on the coupled insulin-glucose dynamics model presented in Chapter 4.

The first five test cases will focus on examining the complete dynamics of the model. The two inputs, the insulin infusion rate $\mathcal{U}$ and the exercise intensity $E$ are plotted with accompanying $I$ (insulin in plasma), $S$ (insulin in skeletal muscle ISF), $G$ (glucose in plasma), and $H$ (glucose in skeletal muscle ISF). Also shown are plots of the different glucose production ($Ra_{meal}$ and $EGP$) and uptake mechanisms ($RGU_{CS_{TOT}}$ and $RGU_{SM_{TOT}}$).

The remaining five test cases examine how different exercise intensities affect the glucose response and the $EGP$ response. We plot the responses for exercise intensities ranging from resting $E$=0 to intense $E$=0.75 exercise. We remind the reader that $E$ is quantified as % $V0_{2_{max}}$. The insulin-kinetics do not significantly change at different levels of exercise, and hence they are not plotted in these cases. Also, in these cases the basal glucose level is set to 100 [mg/dL], unlike in the first five test cases where basal glucose was set to 150 [mg/dL].

In all plots, the grey shaded regions represent the exercise periods and the red shaded region represents hypoglycemia ($< 70$ [mg/dL]).

## 5.1 Test Case 1: Standard Meal with Bolus

This test case simulates the glucose response to a standard 75 [g] meal with a 6 [U] insulin bolus. No exercise is done. The basal rate was kept constant at 0.96 [U/hr].

Figure 5.1 shows the results of this simulation, which is used as a baseline for comparison with subsequent test cases. As we expect, $G$ rises after the meal is ingested at time 0. $Ra_{meal}$

in the bottom frame shows the rate of meal absorption that causes this rise. $G$ continues to rise until a peak of 300 [mg/dL], and then slowly drops back to basal levels. During this time $EGP$ is suppressed (see the red line in the bottom frame), and $RGU_{CS_{TOT}}$ rises due to an increase in liver glucose uptake.

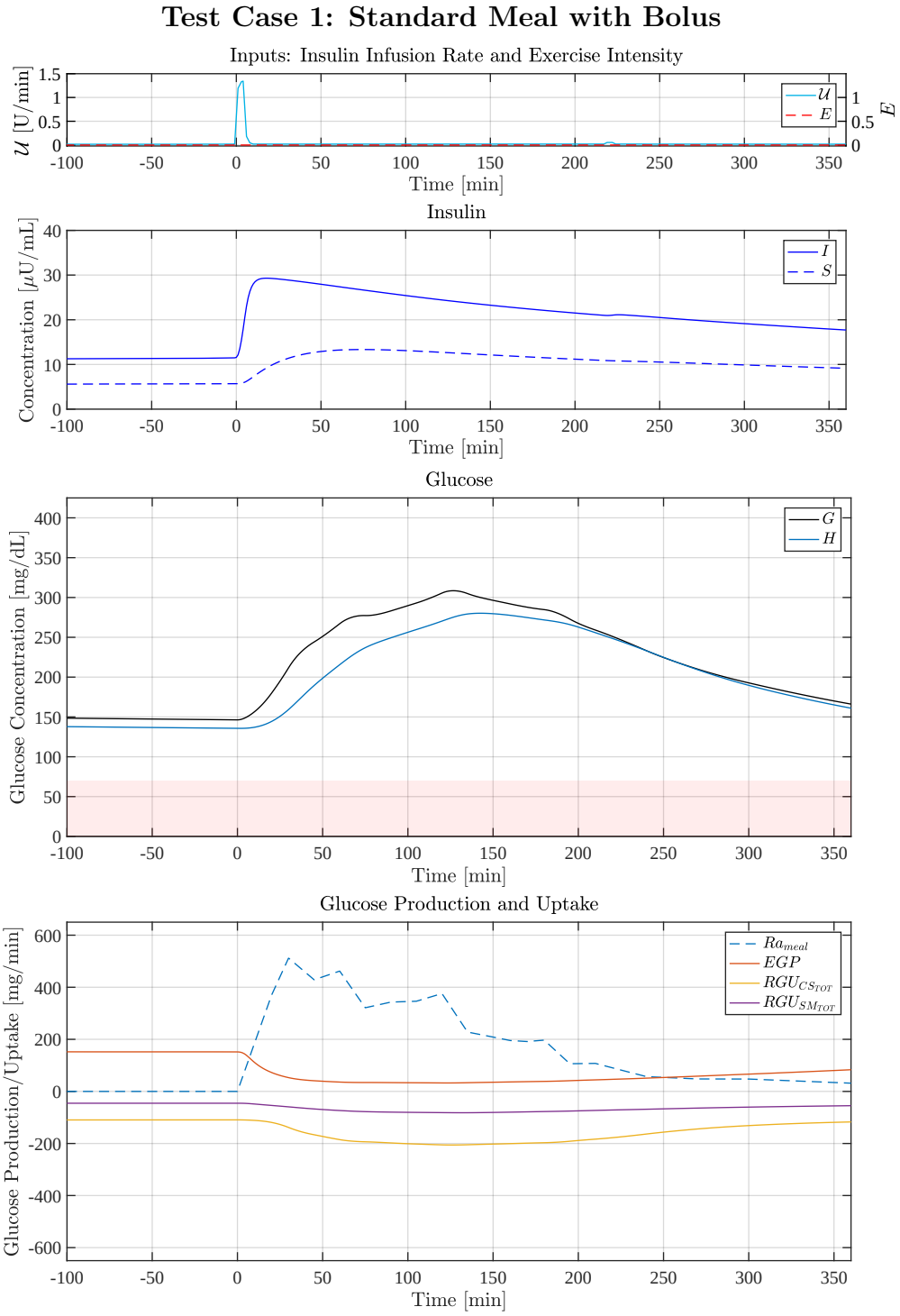


Figure 5.1: Baseline simulation for comparison with subsequent test cases. (top) Inputs insulin infusion rate $\mathcal{U}$ and exercise intensity $E$. (middle top) Insulin predictions. (middle bottom) Glucose predictions. (bottom) Glucose production is positive and uptake is negative.

## 5.2 Test Case 2: Standard Meal with Bolus and Light Exercise

This test case will simulate the glucose response to a standard 75 [g] meal with a 6 [U] insulin bolus. 60 minutes of 25% $V0_{2_{max}}$ exercise (light walking) starts 60 minutes after the meal is ingested. Basal rate was kept constant at 0.96 [U/hr].

We keep all simulation settings identical in this test case (Figure 5.2) as in test case 1 (Figure 5.1), except we have an 'early' exercise period. This early exercise period causes rapid glucose uptake in the skeletal muscle as can be seen by the purple line in the bottom frame of Figure 5.2. $G$ drops as a result of exercise, but only by about 60 [mg/dL]. The drop is only slight because glucose is entering the CS from the GI tract ($Ra_{meal}$). During exercise there is a significant increase in the insulin concentration due to capillary recruitment (middle top frame).

**Test Case 2: Standard Meal with Bolus and Light Exercise**

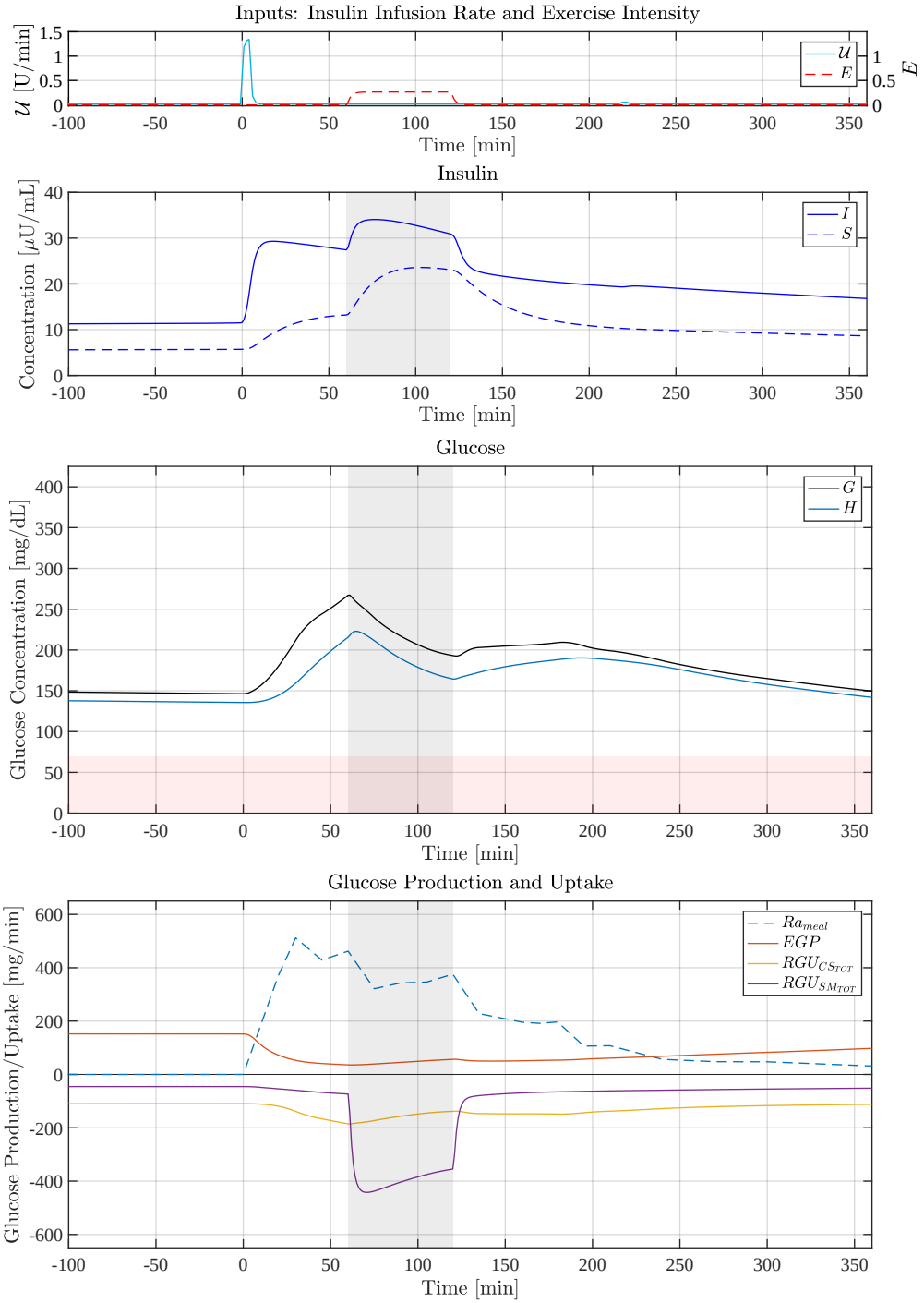


Figure 5.2: Early exercise causes rapid glucose uptake in the skeletal muscle, but the drop in $G$ is not significant because glucose is still rapidly being absorbed from the GI tract ($Ra_{meal}$). (top) Inputs insulin infusion rate $\mathcal{U}$ and exercise intensity $E$. (middle top) Insulin predictions. (middle bottom) Glucose predictions. (bottom) Glucose production is positive and uptake is negative.

## 5.3 Test Case 3: Standard Meal with Bolus and Heavy Exercise

This test case will simulate the glucose response to a standard 75 [g] meal with a 6 [U] insulin bolus. 60 minutes of 75% $V0_{2_{max}}$ exercise (running) starts 60 minutes after the meal is ingested. Basal rate was kept constant at 0.96 [U/hr].

Figure 5.3 shows the response to early heavy exercise and can be compared with early light exercise in the previous test case (Figure 5.2). Insulin levels are nearly identical between these two test cases because insulin-kinetics are 'saturable.' This means that there is only a finite reservoir of capillaries for recruitment and our model predicts that recruitment is rapid and is not strongly dependent on exercise intensity. Glucose levels on the other hand are not saturable, and glucose uptake in the SM is directly dependent on exercise, glucose concentration, and insulin concentration. This is why the 260 to 130 [mg/dL] drop in glucose during exercise in this case is much greater than in the previous test case that had light exercise (from 260 to 190 [mg/dL]).

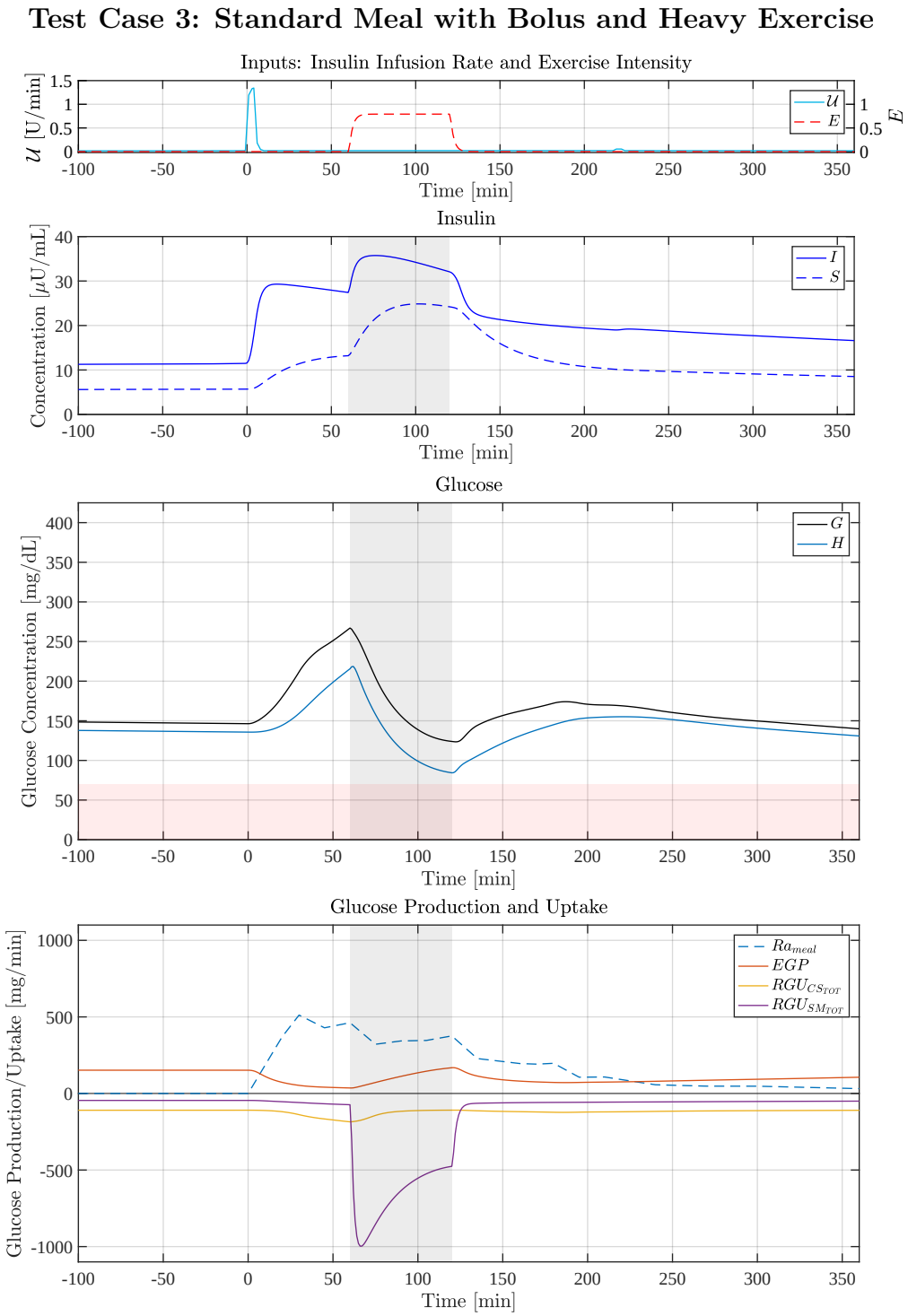


Figure 5.3: Glucose concentration significantly drops during exercise period. (top) Inputs insulin infusion rate $\mathcal{U}$ and exercise intensity $E$. (middle top) Insulin predictions. (middle bottom) Glucose predictions. (bottom) Glucose production is positive and uptake is negative.

## 5.4 Test Case 4: Standard Meal with Bolus and Late Heavy Exercise

This test case will simulate the glucose response to a standard 75 [g] meal with a 6 [U] insulin bolus. 60 minutes of 75% $V0_{2_{max}}$ exercise (running) starts 150 minutes after the meal is ingested. Basal rate was kept constant at 0.96 [U/hr].

Figure 5.4 shows the response to heavy late exercise. This test case can be compared to the previous test case where heavy early exercise was simulated (Figure 5.3). The only difference between the two test cases is the timing. $G$ drops to a much lower level in the late exercise case (from 300 to 85 [mg/dL]) than in the early exercise case (from 260 to 130 [mg/dL]). This enormous difference in the magnitude of the drop is explained by the observation that most glucose from the meal has already been absorbed by minute 150, and thus it cannot act as a buffer to hypoglycemia as in the previous case. Also, high insulin-on-board after a meal acts to keep insulin levels high, suppressing $EGP$ and further increasing the likelihood of hypoglycemia. This shows the importance of not just exercise intensity but exercise timing on $G$.

**Test Case 4: Standard Meal with Bolus and Heavy Late Exercise**

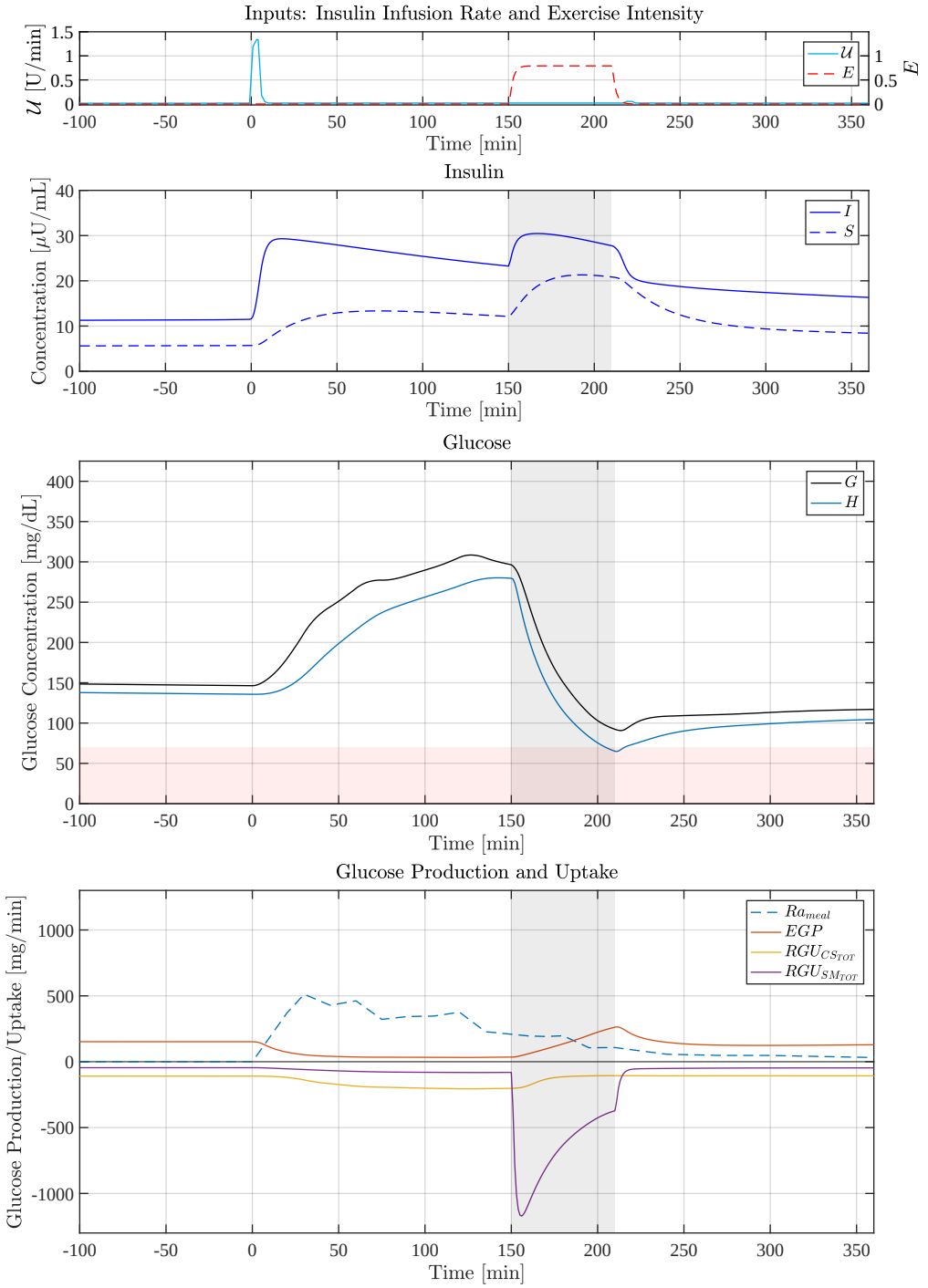


Figure 5.4: Timing, not just exercise intensity, has a significant impact on $G$. (top) Inputs insulin infusion rate $\mathcal{U}$ and exercise intensity $E$. (middle top) Insulin predictions. (middle bottom) Glucose predictions. (bottom) Glucose production is positive and uptake is negative.

## 5.5 Test Case 5: 60 Minutes of Moderate Exercise during Fast

This test case will simulate the glucose response to a 60 minute 50% $V0_{2_{max}}$ exercise bout (brisk walking) during fasting conditions. Basal rate was kept constant at 0.96 [U/hr].

Figure 5.5 shows the response. Notice that insulin concentrations $I$ and $S$ increase, even though there was no additional bolus of insulin given at time 0. This occurs because capillary recruitment increases the rate of absorption and delivery. Notice, however, that $I$ is slowly beginning to decrease back to the original basal levels by the end of the exercise period. If the exercise period were sufficiently long, then steady state would eventually be reached and $I$ and $S$ would settle back near their original levels. During this time, $G$ drops from 150 to 100 [mg/dL], but near the end of exercise approaches a minimum because the increase in $EGP$ eventually matches $RGU_{SM_{TOT}}$.

**Test Case 5: 60 Minutes of Moderate Exercise during Fast**

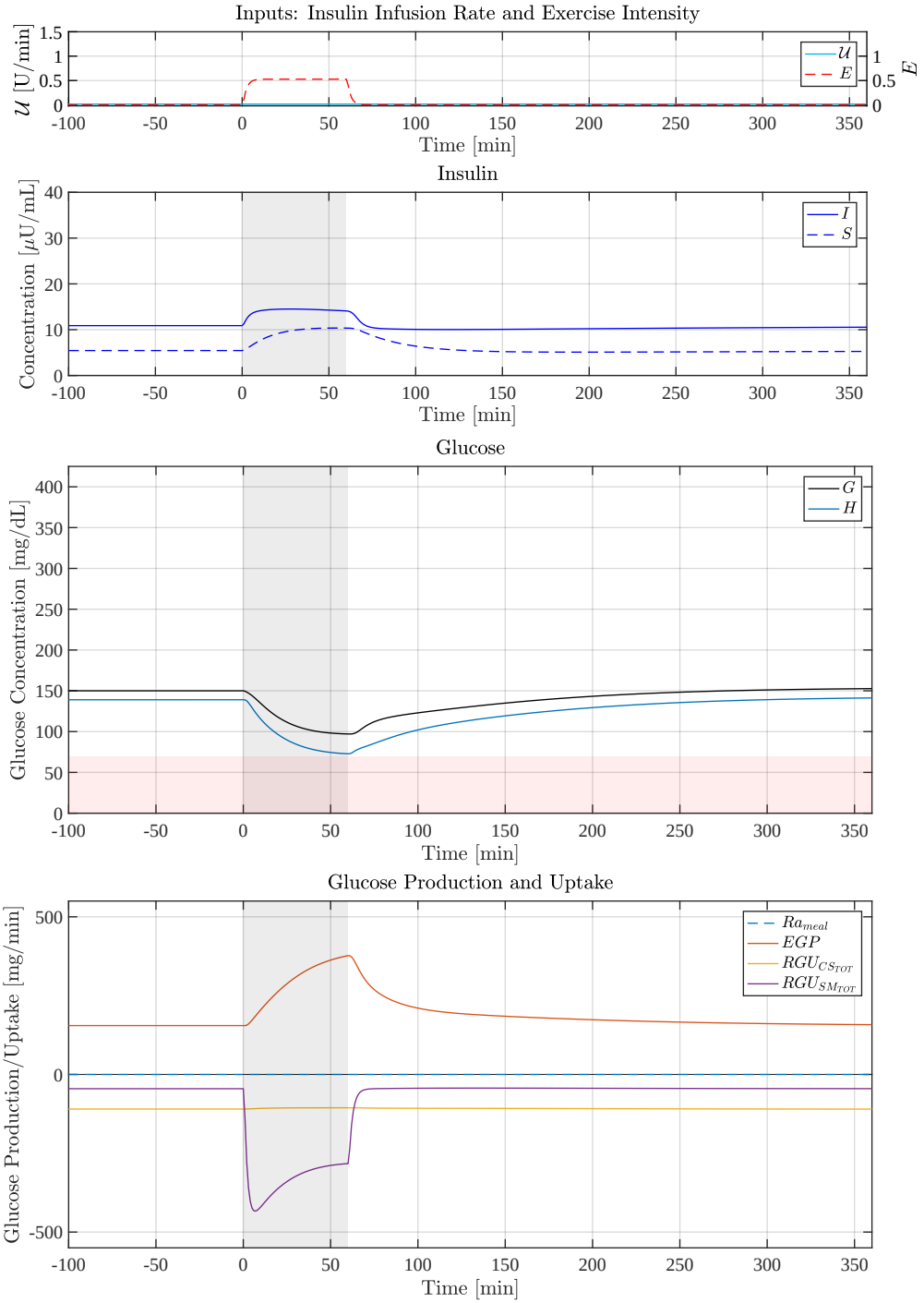


Figure 5.5: During a fast, $G$ drops during exercise until $EGP$ increases sufficiently to match skeletal muscle glucose uptake($RGU_{SM_{TOT}}$). (top) Inputs insulin infusion rate $\mathcal{U}$ and exercise intensity $E$. (middle top) Insulin predictions. (middle bottom) Glucose predictions. (bottom) Glucose production is positive and uptake is negative.

## 5.6 Test Case 6: 120 Minutes of Exercise at Various Intensities during Fast

This test case will simulate the glucose response to a 120 minute exercise bout at 0%, 25%, 50%, and 75% $V0_{2_{max}}$. Basal rate was kept constant at 0.96 [U/hr]. The basal glucose level is set to 100 [mg/dL], unlike in the previous test cases where basal glucose was set to 150 [mg/dL].

Figure 5.6 shows the glucose and $EGP$ response for different levels of exercise. The insulin-kinetics do not significantly change at different levels of exercise, and hence they are not plotted. The blue line is resting, red line is 25% $V0_{2_{max}}$, yellow line 50% $V0_{2_{max}}$, purple line is 75% $V0_{2_{max}}$.

The first thing we notice is that, as expected, $G$ most rapidly drops for the highest exercise intensity (purple line). However, the drop is arrested at about 65 [mg/dL] and starts to rise only 30 minutes after exercise begins. This rise occurs because $EGP$, seen in the bottom frame, rapidly increases. In comparing all the $G$ responses for the different exercise intensities we observe a curious result - that more intense exercise actually leads to less hypoglycemia than light exercise. This may seem counter-intuitive. It occurs because $EGP$ responds more rapidly and to a greater magnitude for more intense exercise. Anecdotal evidence supports this prediction. Persons with T1D often experience hyperglycemia during intense exercise periods because of the rapid release of glucagon, which we have modeled indirectly through our variable $L$. On the other hand, it is a common occurrence for those with T1D to experience hypoglycemia during a light walk, perhaps because their $EGP$ response is muted because it is only 'light' exercise which does not stimulate a strong $EGP$ response.

### Test Case 6: 120 Minutes of Exercise at Various Intensities during Fast

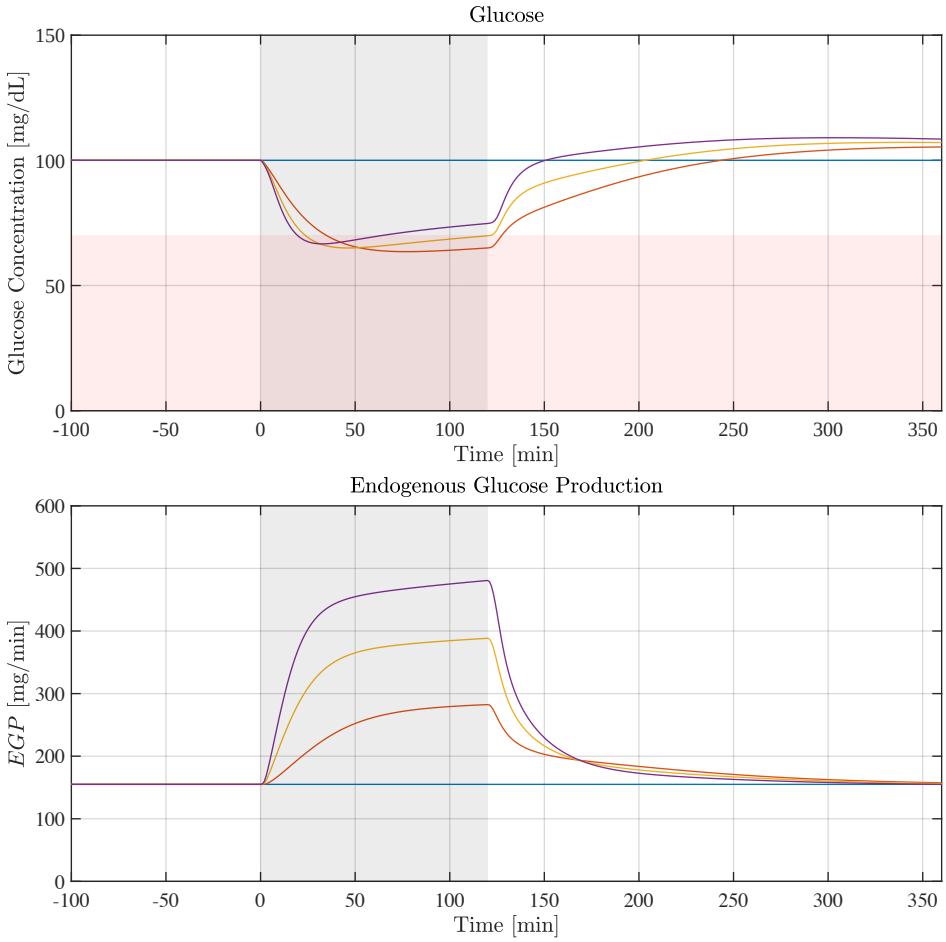


Figure 5.6: More intense exercise leads to less hypoglycemia than light exercise. (top) Plasma glucose concentration $G$ for various levels of exercise. (bottom) $EGP$ for various levels of exercise. Blue line is resting, red line is 25% $V0_{2_{max}}$, yellow line 50% $V0_{2_{max}}$, purple line is 75% $V0_{2_{max}}$.

## 5.7 Test Case 7: 120 Minutes of Interval Training Exercise at Various Intensities during Fast

This test case will simulate the glucose response to a total of 120 minutes of exercise at 0%, 25%, 50%, and 75% $V0_{2_{max}}$. There are 12 exercise bouts with a 10 minute duration and 5 minutes of rest. Basal rate was kept constant at 0.96 [U/hr].

Figure 5.7 shows the response to interval training exercise. We compare interval training exercise to continuous exercise (as in the previous test case Figure 5.6). In comparing the two test cases, there is very little difference in $G$. What is interesting is that a lower level of $EGP$ is needed to maintain essentially the same $G$. The $EGP$ response is much lower in magnitude, maxing out at 400 [mg/min] rather than 500 [mg/min] in the continuous exercise case. This is likely because the 5 minute breaks blunt the $EGP$ response, and also lowers the overall $RGU_{SM_{TOT}}$.

### Test Case 7: 120 Minutes of Interval Training Exercise at Various Intensities during Fast

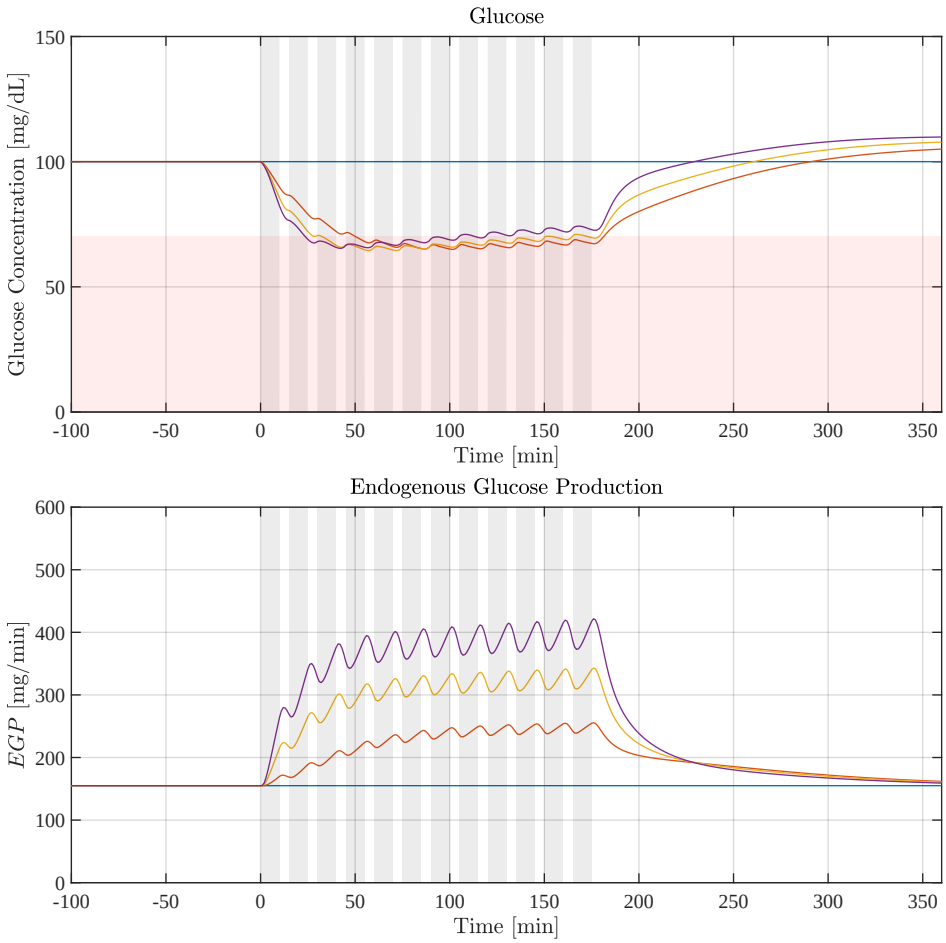


Figure 5.7: A lower level of $EGP$ is needed to maintain essentially the same $G$ as in the continuous exercise test case (See Figure 5.6). (top) Plasma glucose concentration $G$ for various levels of exercise. (bottom) $EGP$ for various levels of exercise. Blue line is resting, red line is 25% $V0_{2_{max}}$, yellow line 50% $V0_{2_{max}}$, purple line is 75% $V0_{2_{max}}$. There are 5 minutes of rest between each 10 minute exercise bout.

## 5.8 Test Case 8: 60 Minutes of Early Exercise After a Meal at Various Intensities

This test case will simulate the glucose response to 60 minutes of exercise at 0%, 25%, 50%, and 75% $V0_{2_{max}}$. Exercise begins 60 minutes after a meal is ingested. Basal rate was kept constant at 0.96 [U/hr].

This test case is the same as that shown in test case 3 (Figure 5.3), except we test various exercise intensities. The glucose response shows that, as expected, a higher exercise intensity leads to a greater drop in $G$. However, the sensitivity of glucose to higher levels of exercise decreases - the difference between the yellow (50% $V0_{2_{max}}$) and the purple line (75% $V0_{2_{max}}$) is only 25 [mg/dL]. This happens for two reasons. First, $EGP$ has a more significant counter-regulatory response at higher exercise intensities. Second, as glucose levels fall closer to basal levels, as they do in the intense exercise case, then skeletal muscle uptake is decreased because it is proportional to $G$ itself.

### Test Case 8: 60 Minutes of Early Exercise After a Meal at Various Intensities

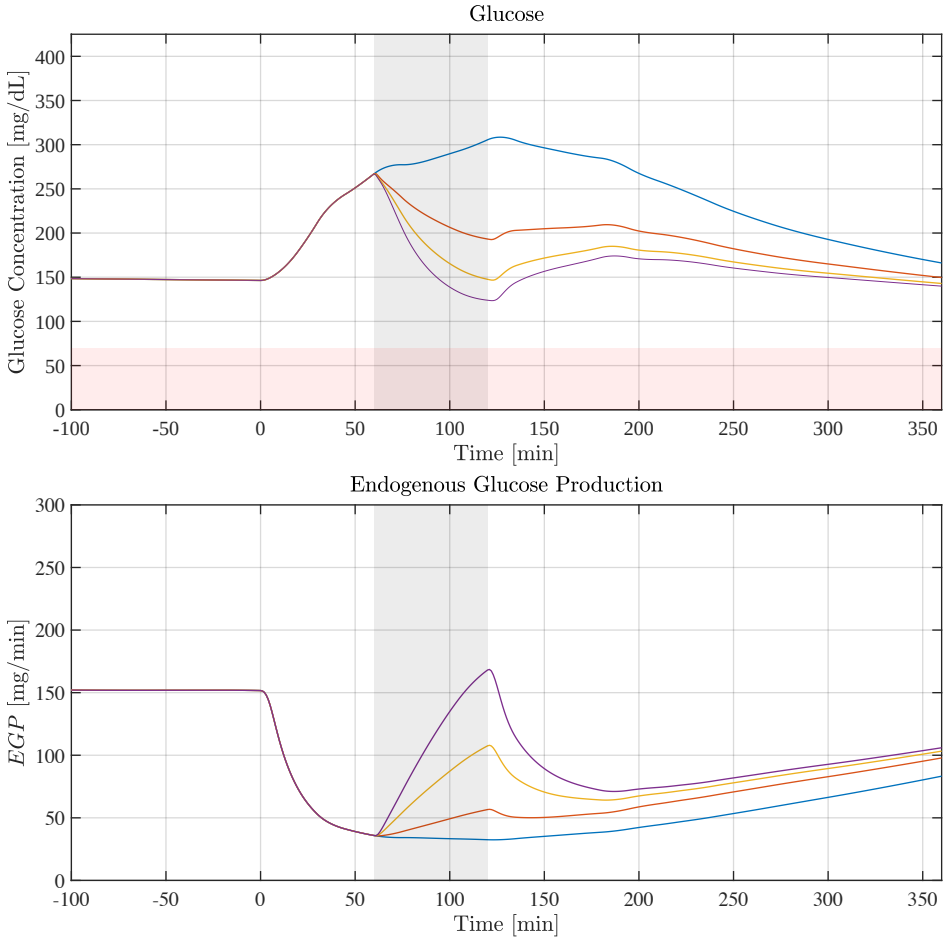


Figure 5.8: A higher exercise intensity leads to a greater drop in $G$. (top) Plasma glucose concentration $G$ for various levels of exercise. (bottom) $EGP$ for various levels of exercise. Blue line is resting, red line is 25% $V0_{2_{max}}$, yellow line 50% $V0_{2_{max}}$, purple line is 75% $V0_{2_{max}}$. Exercise begins 60 minutes after meal ingestion.

## 5.9 Test Case 9: 60 Minutes of Late Exercise After a Meal at Various Intensities

This test case will simulate the glucose response to 60 minutes of exercise at 0%, 25%, 50%, and 75% $V0_{2_{max}}$. Exercise begins 150 minutes after a meal is ingested. Basal rate was kept constant at 0.96 [U/hr].

This test case is the same as that shown in test case 4 (Figure 5.4), except we test various exercise intensities. We compare this test case to the test case 8 (Figure 5.8). As previously discussed, late exercise has a more significant effect on $G$ than does early exercise. This is because the ingested meal is nearly completely digested by minute 150, and $Ra_{meal}$ is no longer providing significant amounts of glucose. This increases the likelihood of hypoglycemia. Also, high insulin-on-board after a meal acts to keep insulin levels high, suppressing $EGP$ and further increasing the likelihood of hypoglycemia.

### Test Case 9: 60 Minutes of Late Exercise After a Meal at Various Intensities

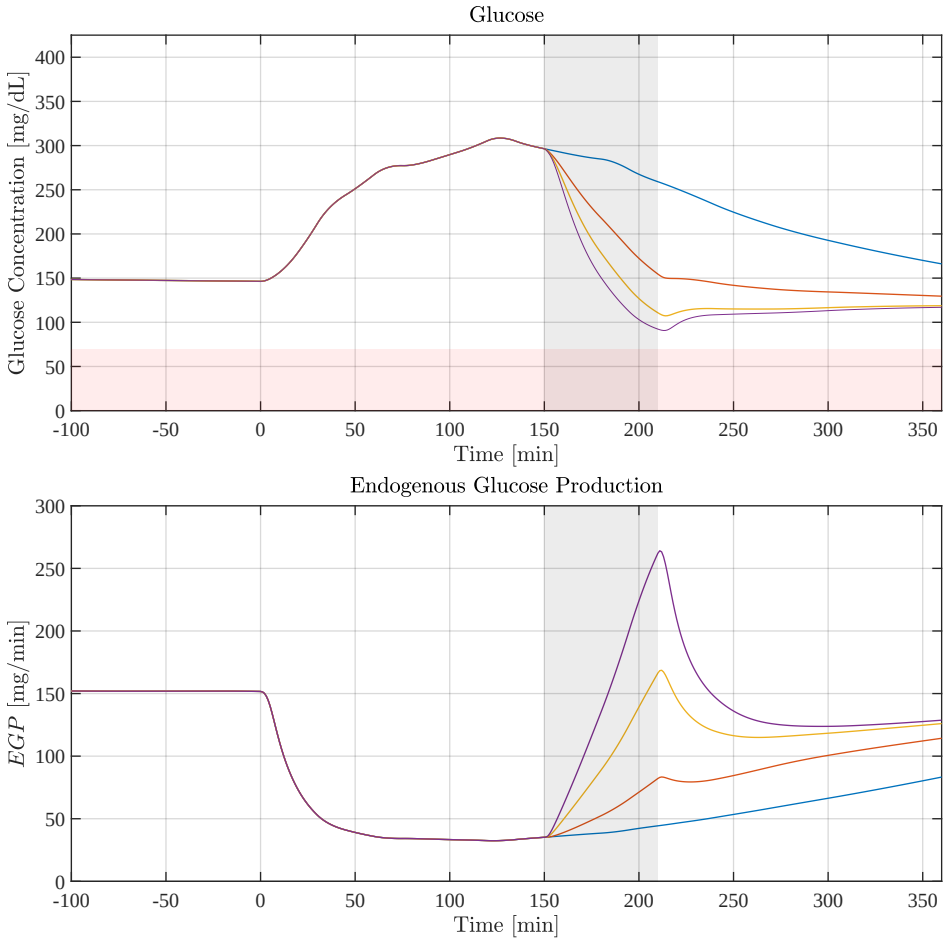


Figure 5.9: Late exercise has a more significant effect on $G$ than does early exercise. (top) Plasma glucose concentration $G$ for various levels of exercise. (bottom) $EGP$ for various levels of exercise. Blue line is resting, red line is 25% $V0_{2_{max}}$, yellow line 50% $V0_{2_{max}}$, purple line is 75% $V0_{2_{max}}$. Exercise begins 150 minutes after meal ingestion.

## 5.10 Test Case 10: 60 Minutes of Late Exercise After a Meal at Various Intensities without Capillary Recruitment

This test case will simulate the glucose response to 60 minutes of exercise at 0%, 25%, 50%, and 75% $V0_{2_{max}}$. Exercise begins 150 minutes after a meal is ingested. Capillary recruitment is turned off, so there is no increase in blood flow and no increase in capillary surface area associated with exercise. To do this we set the parameters $\lambda_a$, $\lambda_d$, $R_a$, and $R_d$ to 0. Basal rate was kept constant at 0.96 [U/hr].

The final test case is shown in Figure 5.10. This case allows us to explore the effect of capillary recruitment on $G$ and $EGP$. For reference we can compare to test case 9 (Figure 5.9), which is setup exactly the same, except includes the effects of capillary recruitment.

Capillary recruitment does not directly affect uptake or production mechanisms, it does however directly affect the transfer for insulin and glucose between compartments thereby altering concentrations $G$, $H$, $I$, and $S$, which have a direct effect on uptake and production.

By shutting off capillary recruitment we essentially limit the rate that glucose and insulin can move between compartments. This results in a lower $S$, and a lower $H$ during exercise. The lower $S$ directly affects liver glucose uptake and skeletal muscle glucose uptake (not depicted). A lower $S$ also affects $EGP$. The lower $H$ directly affects skeletal muscle glucose uptake as well, because uptake is linearly dependent on $H$. *These effects combine to blunt SM glucose uptake and increase $EGP$*, as can be seen by comparing this test case to test case 9 where recruitment is turned on (Figure 5.9). This leads to $G$ predictions that are significantly higher. Whether or not these predictions are more or less accurate remains to be determined, but the simple fact is that in the context of our model, capillary recruitment has a significant effect on glucose uptake and production, and may be critically important to accurately predicting $G$ during exercise.

## Test Case 10: 60 Minutes of Late Exercise After a Meal at Various Intensities without Capillary Recruitment

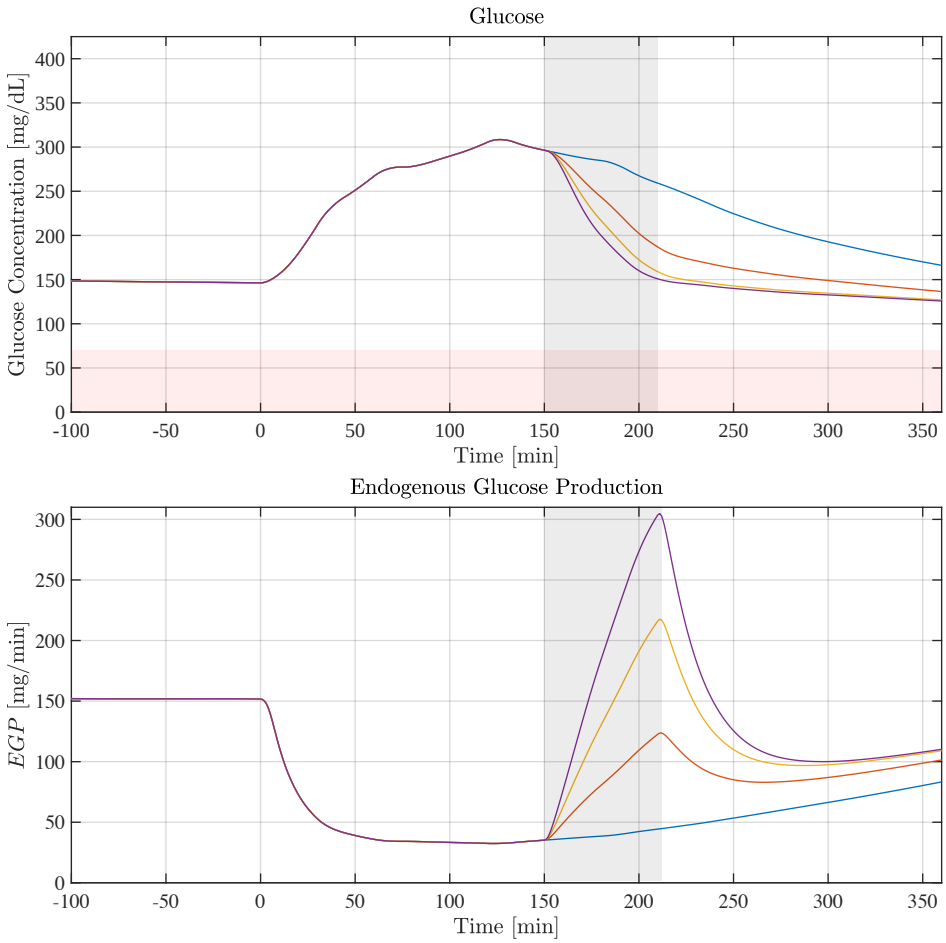


Figure 5.10: Capillary recruitment is turned off and thus blunts SM glucose uptake and increases $EGP$, which increases the predicted $G$. This can be seen by comparing this test case to test case 9 where recruitment is turned on (Figure 5.9). (top) Plasma glucose concentration $G$ for various levels of exercise. (bottom) $EGP$ for various levels of exercise. Blue line is resting, red line is 25% $V0_{2_{max}}$, yellow line 50% $V0_{2_{max}}$, purple line is 75% $V0_{2_{max}}$. Exercise begins 150 minutes after meal ingestion. Capillary recruitment is turned off, so there is no increase in blood flow and no increase in capillary surface area associated with exercise.

## 5.11 Insights and Conclusions from Test Cases

The 10 test cases provided significant insights into insulin-glucose dynamics during exercise. We summarize the insights in a list:

- *The timing of exercise with respect to a meal matters.* Earlier exercise tends to lead to less hypoglycemia than late exercise. This can be attributed less glucose absorption from the GI tract at minute 150 than minute 60, which prevents $Ra_{meal}$ from acting as a buffer to hypoglycemia.

- *Intense exercise leads to less hypoglycemia than light exercise.* This occurs because $EGP$ responds more rapidly and to a greater magnitude for more intense exercise.

- A lower level of $EGP$ is needed to maintain the same $G$ in the interval exercise case than in the continuous exercise test case. This is likely because the 5 minute breaks blunt the $EGP$ response, and also lower the overall $RGU_{SM_{TOT}}$.

- *Capillary recruitment has a significant effect on glucose uptake and production, and may be critically important to accurately predicting G during exercise. This also indicates that insulin-resistance may be partly explained by a lack of capillary recruitment.* By shutting off capillary recruitment we essentially limit the rate that glucose and insulin can move between compartments. In doing this we reduce the concentration of glucose and insulin in the SM compartment and because uptake is proportional to both, it is significantly reduced.

# Chapter 6

# Conclusion

Living with Type 1 Diabetes (T1D) is a challenge. Up to ten times per day those with T1D must ask themselves "How much insulin should I dose?" knowing that an incorrect dose may shorten their life. An artificial pancreas that can autonomously and safely dose insulin would greatly improve the lives of those with T1D. Despite great progress in the development of the artificial pancreas, there are still significant hurdles that must to be overcome before the system can be proven safe and effective in all living conditions. Exercise, because of the significant time-lag of injected insulin and the significant changes to insulin-glucose dynamics, is considered the most dangerous task for the artificial pancreas controller to handle. Some artificial pancreas systems utilize model predictive control algorithms to overcome the time-lag and difficulties of exercise. These controllers require a model that can accurately predict the exercise-induced changes to insulin-glucose dynamics, so that the T1D patient can be kept safe, even during spurious, rigorous, and/or long-duration exercise.

This dissertation focused on the development of a novel pharmacokinetics model of insulin-glucose dynamics that is specifically designed to include the effects of exercise. We modeled five primary glucoregulatory phenomena that are known to be sensitive to exercise. To validate the model, we compared predictions to data from four cohorts of human subjects studied during controlled clinical exercise trials. We also carried out several test cases to demonstrate the effects of exercise intensity and duration on blood glucose levels. The model provides significant insight into insulin dosing during exercise and can be used to improve model predictive control algorithms in the artificial pancreas.

## 6.1 Modeling Outcomes

The insulin-glucose dynamics model we have developed was specifically designed to include the five primary acute effects of exercise: the increase in endogenous glucose production, the increase in skeletal muscle glucose uptake, the increase in insulin absorption rate, the increase in insulin delivery rate, and the increase in glucose delivery rate.

When developing the model, our goal was to keep the model as physiologically-based as

possible, so that predictions could be understood in the context of real physical phenomena such as increased blood flow or increased surface area. In order to achieve this, we had to create a multiscale model that included both microscale phenomena and macroscale whole-body phenomena. Of course, the complexities of multiscale modeling needed to be balanced with model parsimony. For example, insulin and glucose transport in capillary beds was modeled at the microscale because this was deemed important for understanding how exercise alters insulin and glucose transport from the blood to skeletal muscle. However, other phenomena, such as glucose uptake in the liver, were modeled phenomenologically because it would not have been practical to model cellular level interactions.

There are inevitably more parameters in a multiscale model, and this makes overfitting more likely. To prevent this, all the parameters in our model were taken directly from the literature or extracted from experiments found in the literature. This is not to say we have eliminated the problem of overfitting, as there were some parameters that were not directly available in the literature and had to be derived by adjusting the available parameters.

The insulin-kinetics model that we developed is, to the authors knowledge, the first insulin-kinetics model that has been explicitly designed to include the effects of exercise. This was done by modeling the effects of exercise-induced capillary recruitment on two processes: insulin absorption from the subcutaneous injection site and insulin delivery from the blood to skeletal muscle. Understanding how these two rates change during exercise is critically important because they determine insulin concentration, and thus directly affect rates of glucose uptake, potentially causing hypoglycemia.

We have preliminarily validated the insulin-kinetics model by comparing predictions with data from two cohorts of T1D subjects, one resting and one exercising. The results compare favorably, and also agree with direct measurements of insulin absorption and delivery rates during exercise from literature.

The glucose-dynamics model, similarly to the insulin-model, also included for the first time the effects of exercise-induced capillary recruitment on glucose delivery rate to skeletal muscle. The predictions showed that glucose delivery rates to skeletal muscle increase drastically during exercise, which is consistent with trends seen in the literature. Additionally, we included direct measurements of glucose fluxes, $Ra_{meal}$ and $EGP$, from collaborators. This is a significant advantage in our model because we do not need to model the complex, uncertain processes of meal digestion and endogenous glucose production.

Using the measured flux inputs in the glucose-dynamics model, we preliminarily validated the model on two cohorts of healthy subjects (non-diabetic), one resting and one exercising. There is strong agreement between model predictions and the data, providing some confidence that we have modeled the various exercise-effects correctly, at least for healthy subjects. As an added contribution, we used the measured $EGP$ data to validate a new model of $EGP$ that depends on insulin, glucose, and exercise duration and intensity.

To fulfill the original objective of this dissertation, we coupled the insulin-kinetics model with the glucose-dynamics model, for application to T1D subjects. Coupling the models was straightforward, but some significant parameter adjustments needed to be made to account for insulin-resistance in T1D subjects. After making necessary adjustments, we tested the

model by comparing predictions to measured data from two cohorts of T1D subjects, one resting and one exercising. In the resting subject, there was good agreement between model predictions and measurements. However, in the exercising subject, the effect of exercise on glucose uptake in the skeletal muscle was significantly overestimated resulting in poor predictions. This was likely because we did not model the saturable nature of glucose uptake. We venture to say that we have preliminarily validated the T1D model for the resting case, but work still needs to be done to improve model predictions during exercise.

Even though the T1D model predictions were poor during exercise, we still gained significant insight into insulin-glucose dynamics by performing several test cases. These test cases show that in the postprandial state (i.e. after a meal) the timing of exercise, not just the intensity, is crucial to avoiding hypoglycemia. Tests like these help shed light on how best to dose insulin to avoid hypoglycemia.

This significant modeling effort provides a means to understand the interplay between several complex glucoregulatory processes. More importantly, this model can potentially be used in a model predictive control algorithm in the artificial pancreas to more safely dose insulin when exercise is involved. When these devices inevitably become available, the life of the person with T1D will be markedly improved, and will be one of the greatest medical and engineering achievements in modern times.

## 6.2 Model Insights

In Chapter 5, 10 test cases were simulated. These provided some significant insights into insulin-glucose dynamics during exercise. We showed that the timing of exercise with respect to a meal matters. Earlier exercise is predicted to lead to less hypoglycemia than late exercise. This can be explained by the observation that $Ra_{meal}$, which accounts for a significant portion of glucose infused into the CS following a meal because of $EGP$ suppression, is diminished as more time is put between the meal ingestion and exercise. Because of this $Ra_{meal}$ cannot act as a buffer to hypoglycemia.

We also predicted that intense exercise leads to less hypoglycemia than light exercise. This occurred because $EGP$ responds more rapidly and to a greater magnitude, for more intense exercise. Anecdotal evidence supports this prediction. Persons with T1D often experience hyperglycemia during intense exercise periods because of the rapid release of glucagon, which we have modeled indirectly through our variable $L$. On the other hand, it is a common occurrence for those with T1D to experience hypoglycemia during a light walk, perhaps because their $EGP$ response is muted because it is only 'light' exercise.

Next, capillary recruitment, which was a novel part of our model, was shown to have a significant effect on glucose uptake and production, and may be critically important to accurately predicting $G$ during exercise. Results also indicated that insulin-resistance may be partly explained by a lack of capillary recruitment. By running a test case where we shut off capillary recruitment we essentially limited the rate that glucose and insulin can move between compartments. In doing this we reduced the concentration of glucose and insulin in

the skeletal muscle compartment, and because uptake is proportional to both, uptake was significantly reduced.

The model also provides an interesting insight about the natural limits on insulin absorption from subcutaneous tissue. If we assume, as we did in Chapter 2, that absorption is driven by pure diffusion then $PS_a^I$, the permeability surface area of the capillaries to insulin, may represent a hard upper-limit on the absorption rate. This is because even if hexameric dissociation occurs instantaneously upon injection, $PS_a^I$ would still provide resistance to transport. Because our model does not include hexameric dissociation, it may represent the upper limit of the insulin absorption rate. Thus, there may be little room for the design of faster absorbing insulin, at least if injected into subcutaneous tissue.

In regard to these model insights, it must be stressed that our interpretation is through the lens of the developed model. For example, it has been postulated in the literature that capillary recruitment may be an important factor in insulin-resistance. Our model corroborates this theory, but doesn't confirm it. Many more experiments would need to be carried out to validate/invalidate our hypotheses.

## 6.3 Limitations and Future Work

As with all models, there are limitations to the accuracy and robustness of our model.

Despite its importance, the liver is poorly understood in regards to its ability to take up and provide glucose ($EGP$). This stems partly from the uncertainly of local glucose and insulin concentrations in the liver, which are known to affect $EGP$ and liver glucose uptake. However, the larger problem is that experiments on humans that isolate the effects of the liver are highly invasive and thus data cannot be easily obtained. Liver uptake during exercise is even less understood, and creating a liver model for the purposes of this dissertation would have required significant effort. For this reason, we adopted a liver model from Sorensen [64] that was derived for healthy patients. However, because of the importance of the liver, future work must include a T1D specific liver model.

Next, the coupled T1D insulin-glucose model does not accurately predict the drop in glucose associated with exercise. This may be because the effect of saturability of glucose uptake was not included in the model. In future work, the effect of saturability, as well as the effect of synergistic effects of insulin and exercise, should be added to the model.

Both liver and skeletal muscle glucose uptake may also have 'uptake hysteresis,' the phenomenon of insulin sensitivity decreasing in time after a meal. This effect has been shown in the literature, but it is likely unimportant for modeling the acute effects of exercise, and hence is low priority in future work. A related concept is insulin-resistance in T1D patients. We used data from the literature to quantify this effect when adjusting our insulin-sensitivity parameters, $\mathrm{r}_{liv}^G$ and $\mathrm{r}_{SM_{ins}}^G$, for application of the model to T1D subjects. However, additional work needs to be done to accurately quantify this effect because it is crucial to glucose predictions in our model.

Insulin and glucose delivery rates to skeletal muscle, though accurate during rest, do not agree with findings in literature during exercise. This is a weakness of the diffusion model that we have used and may be remedied by including the heterogeneity of the capillary bed as proposed by Renkin [38]. However, the glucose delivery rate seems to be fairly unimportant in comparison to other phenomena, and thus the benefit of this addition is not clear. It is considered lower priority in future work.

Most importantly, more data is needed to validate and refine the model, as the small patient cohorts used for testing in this dissertation are insufficient. A larger dataset could also provide insight into the magnitude of intra/interpatient variability with respect to acute exercise effects.

# Bibliography


[1] M. D. Breton, "Physical activity-the major unaccounted impediment to closed loop control.," *Journal of diabetes science and technology*, vol. 2, no. 1, pp. 169–174, Jan. 2008.

[2] R. Basu, M. L. Johnson, Y. C. Kudva, and A. Basu, "Exercise, hypoglycemia, and type 1 diabetes.," *Diabetes technology & therapeutics*, vol. 16, no. 6, pp. 331–337, Jun. 2014. DOI: 10.1089/dia.2014.0097.

[3] CDC, *National Diabetes Statistics Report*, 2014.

[4] J. D. R. Foundation, *Type 1 Diabetes Facts*, 2017. (visited on 08/03/2017).

[5] L. Li, X. Li, W. Zhou, and J. L. Messina, "Acute psychological stress results in the rapid development of insulin resistance.," *The Journal of endocrinology*, vol. 217, no. 2, pp. 175–184, May 2013. DOI: 10.1530/JOE-12-0559.

[6] L. Hinshaw, C. Dalla Man, D. K. Nandy, A. Saad, A. E. Bharucha, J. A. Levine, R. A. Rizza, R. Basu, R. E. Carter, C. Cobelli, Y. C. Kudva, and A. Basu, "Diurnal pattern of insulin action in type 1 diabetes: implications for a closed-loop system.," *Diabetes*, vol. 62, no. 7, pp. 2223–2229, Jul. 2013. DOI: 10.2337/db12-1759.

[7] A. Saad, C. Dalla Man, D. K. Nandy, J. A. Levine, A. E. Bharucha, R. A. Rizza, R. Basu, R. E. Carter, C. Cobelli, Y. C. Kudva, and A. Basu, "Diurnal pattern to insulin secretion and insulin action in healthy individuals.," *Diabetes*, vol. 61, no. 11, pp. 2691–2700, Nov. 2012. DOI: 10.2337/db11-1478.

[8] J. O. Holloszy, "Exercise-induced increase in muscle insulin sensitivity.," *Journal of applied physiology (Bethesda, Md. : 1985)*, vol. 99, no. 1, pp. 338–343, Jul. 2005. DOI: 10.1152/japplphysiol.00123.2005.

[9] C. Frosig, A. J. Rose, J. T. Treebak, B. Kiens, E. A. Richter, and J. F. P. Wojtaszewski, "Effects of endurance exercise training on insulin signaling in human skeletal muscle: interactions at the level of phosphatidylinositol 3-kinase, Akt, and AS160.," *Diabetes*, vol. 56, no. 8, pp. 2093–2102, Aug. 2007. DOI: 10.2337/db06-1698.

[10] J. F. Brun, R. Guintrand-Hugret, C. Boegner, O. Bouix, and A. Orsetti, "Influence of short-term submaximal exercise on parameters of glucose assimilation analyzed with the minimal model.," *Metabolism: clinical and experimental*, vol. 44, no. 7, pp. 833–840, Jul. 1995.

[11] D. Araújo-Vilar, E. Osifo, M. Kirk, D. A. García-Estévez, J. Cabezas-Cerrato, and T. D. R. Hockaday, "Influence of moderate physical exercise on insulin-mediated and non—insulin-mediated glucose uptake in healthy subjects," *Metabolism*, vol. 46, no. 2, pp. 203 –209, 1997, ISSN: 0026-0495. DOI: http://dx.doi.org/10.1016/S0026-0495(97)90303-6.

[12] M. Clinic, *Diseases and Conditions*, 2017. (visited on 08/04/2017).

[13] J. S. Freeman, "Insulin Analog Therapy: Improving the Match With Physiologic Insulin Secretion," *The Journal of the American Osteopathic Association*, vol. 109, no. 1, pp. 26–36, Jan. 2009, ISSN: 0098-6151. DOI: 10.7556/jaoa.2009.109.1.26.

[14] Medtronic, *Multiple Daily Injection Therapy*, 2017. (visited on 08/04/2017).

[15] University of California San Francisco, *Type 1 Diabetes*, 2017. (visited on 08/04/2017).

[16] I. Diabetes, *What is an insulin pump and how does it help*, 2017. (visited on 08/04/2017).

[17] N. S. Larson and J. E. Pinsker, "The role of continuous glucose monitoring in the care of children with type 1 diabetes," *International Journal of Pediatric Endocrinology*, vol. 2013, no. 1, p. 8, 2013, ISSN: 1687-9848 1687-9856. DOI: 10.1186/1687-9856-2013-8.

[18] U. R. Strips, *Urine Reagent Strips*, Aug. 2017. (visited on 08/08/2017).

[19] Medicalrojak, *Sulfonylureas and Ischemic Preconditioning?*, 8/8/17. (visited on 08/08/2017).

[20] Dexcom, *Dexcom launches world's first continuous diabetic monitoring solution with 24x7 remote monitoring anywhere using Nordic Bluetooth Smart wireless technology*, Aug. 2017.

[21] T. J. D. R. F. C. G. M. S. Group, "Continuous Glucose Monitoring and Intensive Treatment of Type 1 Diabetes," *New England Journal of Medicine*, vol. 359, no. 14, pp. 1464–1476, 2008. DOI: 10.1056/NEJMoa0805017.

[22] "The Effect of Continuous Glucose Monitoring in Well-Controlled Type 1 Diabetes," *Diabetes Care*, vol. 32, no. 8, pp. 1378–1383, 2009, ISSN: 0149-5992. DOI: 10.2337/dc09-0108.

[23] M. Clinic, *Artificial Pancreas*, Aug. 2017. (visited on 08/08/2017).

[24] A. C. van Bon, E. Verbitskiy, G. von Basum, J. B. L. Hoekstra, and J. H. DeVries, "Exercise in closed-loop control: a major hurdle.," *Journal of diabetes science and technology*, vol. 5, no. 6, pp. 1337–1341, Nov. 2011.

[25] E. Smalley, "Medtronic automated insulin delivery device gets FDA nod," *Nature Biotechnology*, vol. 34, p. 1220, Dec. 2016.

[26] B. P. Kovatchev, E. Renard, C. Cobelli, H. C. Zisser, P. Keith-Hynes, S. M. Anderson, S. A. Brown, D. R. Chernavvsky, M. D. Breton, L. B. Mize, A. Farret, J. Place, D. Bruttomesso, S. Del Favero, F. Boscari, S. Galasso, A. Avogaro, L. Magni, F. Di Palma, C. Toffanin, M. Messori, E. Dassau, and F. J. Doyle, "Safety of Outpatient Closed-Loop Control: First Randomized Crossover Trials of a Wearable Artificial Pancreas," *Diabetes Care*, vol. 37, no. 7, pp. 1789–1796, 2014, ISSN: 0149-5992. DOI: 10.2337/dc13-2076.

[27] S. J. Russell, F. H. El-Khatib, M. Sinha, K. L. Magyar, K. McKeon, L. G. Goergen, C. Balliro, M. A. Hillard, D. M. Nathan, and E. R. Damiano, "Outpatient glycemic control with a bionic pancreas in type 1 diabetes.," *The New England journal of medicine*, vol. 371, no. 4, pp. 313–325, Jul. 2014. DOI: 10.1056/NEJMoa1314474.

[28] R. Hovorka, J. M. Allen, D. Elleri, L. J. Chassin, J. Harris, D. Xing, C. Kollman, T. Hovorka, A. M. F. Larsen, M. Nodale, A. De Palma, M. E. Wilinska, C. L. Acerini, and D. B. Dunger, "Manual closed-loop insulin delivery in children and adolescents with type 1 diabetes: a phase 2 randomised crossover trial.," *Lancet*, vol. 375, no. 9716, pp. 743–751, Feb. 2010. DOI: 10.1016/S0140-6736(09)61998-X.

[29] R. A. Harvey, E. Dassau, W. C. Bevier, D. E. Seborg, L. Jovanovic, F. J. r. Doyle, and H. C. Zisser, "Clinical evaluation of an automated artificial pancreas using zone-model predictive control and health monitoring system.," *Diabetes technology & therapeutics*, vol. 16, no. 6, pp. 348–357, Jun. 2014. DOI: 10.1089/dia.2013.0231.

[30] A. D. Association, *Exercise and Type 1 Diabetes*, 2013.

[31] S. Kalra, J. J. Mukherjee, S. Venkataraman, G. Bantwal, S. Shaikh, B. Saboo, A. K. Das, and A. Ramachandran, "Hypoglycemia: The neglected complication," *Indian Journal of Endocrinology and Metabolism*, vol. 17, no. 5, pp. 819–834, 2013 Sep-Oct, ISSN: 2230-8210 2230-9500. DOI: 10.4103/2230-8210.117219.

[32] M. J. MacDonald, "Postexercise late-onset hypoglycemia in insulin-dependent diabetic patients.," *Diabetes care*, vol. 10, no. 5, pp. 584–588, 1987 Sep-Oct.

[33] A. Maran, P. Pavan, B. Bonsembiante, E. Brugin, A. Ermolao, A. Avogaro, and M. Zaccaria, "Continuous glucose monitoring reveals delayed nocturnal hypoglycemia after intermittent high-intensity exercise in nontrained patients with type 1 diabetes.," *Diabetes technology & therapeutics*, vol. 12, no. 10, pp. 763–768, Oct. 2010. DOI: 10.1089/dia.2010.0038.

[34] diaTribe, *Medtronic MiniMed 670G Trial Results: 44% Reduction in Hypoglycemia, 0.5% A1c Improvement*, Jun. 2016.

[35] G. Ahlborg and P. Felig, "Lactate and Glucose Exchange across the Forearm, Legs, and Splanchnic Bed during and after Prolonged Leg Exercise," *Journal of Clinical Investigation*, vol. 69, no. 1, pp. 45–54, Jan. 1982, ISSN: 0021-9738.

[36] D. H. Wasserman, "Four grams of glucose.," *American journal of physiology. Endocrinology and metabolism*, vol. 296, no. 1, E11–21, Jan. 2009, ISSN: 0193-1849 0193-1849. DOI: 10.1152/ajpendo.90563.2008.

[37] E. M. Renkin, "Multiple pathways of capillary permeability.," *Circulation Research*, vol. 41, no. 6, pp. 735–743, 1977, ISSN: 0009-7330. DOI: 10.1161/01.RES.41.6.735.

[38] E. M. Renkin, "B. W. Zweifach Award lecture. Regulation of the microcirculation.," *Microvascular research*, vol. 30, no. 3, pp. 251–263, Nov. 1985, ISSN: 0026-2862 0026-2862.

[39] G. Ahlborg, P. Felig, L. Hagenfeldt, R. Hendler, and J. Wahren, "Substrate turnover during prolonged exercise in man. Splanchnic and leg metabolism of glucose, free fatty acids, and amino acids.," *The Journal of clinical investigation*, vol. 53, no. 4, pp. 1080–1090, Apr. 1974, ISSN: 0021-9738 0021-9738. DOI: 10.1172/JCI107645.

[40] R. A. DeFronzo, E. Ferrannini, Y. Sato, P. Felig, and J. Wahren, "Synergistic interaction between exercise and insulin on peripheral glucose uptake.," *Journal of Clinical Investigation*, vol. 68, no. 6, pp. 1468–1474, Dec. 1981, ISSN: 0021-9738.

[41] E. Fernqvist, B. Linde, J. Östman, and R. Gunnarsson, "Effects of physical exercise on insulin absorption in insulin-dependent diabetics. A comparison between human and porcine insulin," *Clinical Physiology*, vol. 6, no. 6, pp. 489–497, Dec. 1986, ISSN: 1365-2281. DOI: 10.1111/j.1475-097X.1986.tb00782.x.

[42] V. A. Koivisto and P. Felig, "Effects of Leg Exercise on Insulin Absorption in Diabetic Patients," *New England Journal of Medicine*, vol. 298, no. 2, pp. 79–83, 1978. DOI: 10.1056/NEJM197801122980205.

[43] A. C. Inyard, L. H. Clerk, M. A. Vincent, and E. J. Barrett, "Contraction Stimulates Nitric Oxide–Independent Microvascular Recruitment and Increases Muscle Insulin Uptake," *Diabetes*, vol. 56, no. 9, pp. 2194–2200, 2007, ISSN: 0012-1797. DOI: 10.2337/db07-0020.

[44] R. N. Bergman, Y. J. Yang, I. D. Hope, and M. Ader, "The role of the transcapillary insulin transport in the efficiency of insulin action: studies with glucose clamps and the minimal model.," *Hormone and metabolic research. Supplement series*, vol. 24, pp. 49–56, 1990, ISSN: 0170-5903 0170-5903.

[45] R. A. DeFronzo, E. Ferrannini, K. G. M. M. Alberti, P. Zimmet, and G. Alberti, *International Textbook of Diabetes Mellitus, 2 Volume Set*. John Wiley & Sons, 2015, vol. 1.

[46] R. Basu, B. Di Camillo, G. Toffolo, A. Basu, P. Shah, A. Vella, R. Rizza, and C. Cobelli, "Use of a novel triple-tracer approach to assess postprandial glucose metabolism.," *American journal of physiology. Endocrinology and metabolism*, vol. 284, no. 1, Jan. 2003. DOI: 10.1152/ajpendo.00190.2001.

[47] R. Steele, J. S. Wall, R. C. de Bodo, and N. Altszuler, "Measurement of Size and Turnover Rate of Body Glucose Pool by the Isotope Dilution Method," *American Journal of Physiology – Legacy Content*, vol. 187, no. 1, pp. 15–24, 1956, ISSN: 0002-9513.

[48] R. Steele, C. Bjerknes, I. Rathgeb, and N. Altszuler, "Glucose Uptake and Production During the Oral Glucose Tolerance Test," *Diabetes*, vol. 17, no. 7, pp. 415–421, Jul. 1968. DOI: 10.2337/diab.17.7.415.

[49] A. Vella and R. A. Rizza, "Application of Isotopic Techniques Using Constant Specific Activity or Enrichment to the Study of Carbohydrate Metabolism," *Diabetes*, vol. 58, no. 10, pp. 2168–2174, Oct. 2009. DOI: 10.2337/db09-0318.

[50] G. Toffolo, R. Basu, C. Dalla Man, R. Rizza, and C. Cobelli, "Assessment of postprandial glucose metabolism: conventional dual- vs. triple-tracer method.," *American journal of physiology. Endocrinology and metabolism*, vol. 291, no. 4, E800–806, Oct. 2006. DOI: 10.1152/ajpendo.00461.2005.

[51] R. Steele, "Influences of glucose loading and of injected insulin on hepatic glucose output.," *Annals of the New York Academy of Sciences*, vol. 82, pp. 420–430, Sep. 1959.

[52] C. Cobelli, D. Foster, and G. Toffolo, *Tracer Kinetics in Biomedical Research*. Springer Science & Business Media, 2000, vol. 1.

[53] R. R. Wolfe and D. L. Chinkes, *Isotope Tracers in Metabolic Research: Principles and Practice of Kinetic Analysis*, 2nd ed. John Wiley & Sons, 2005.

[54] L. Hinshaw, M. Schiavon, A. Mallad, C. D. Man, R. Basu, A. E. Bharucha, C. Cobelli, R. E. Carter, A. Basu, and Y. C. Kudva, "Effects of delayed gastric emptying on postprandial glucose kinetics, insulin sensitivity, and beta-cell function.," *American journal of physiology. Endocrinology and metabolism*, vol. 307, no. 6, Sep. 2014. DOI: 10.1152/ajpendo.00199.2014.

[55] R. N. Bergman, "Lilly lecture 1989. Toward physiological understanding of glucose tolerance. Minimal-model approach.," *Diabetes*, vol. 38, no. 12, pp. 1512–1527, Dec. 1989.

[56] C. Dalla Man, A. Caumo, and C. Cobelli, "The oral glucose minimal model: estimation of insulin sensitivity from a meal test.," *IEEE transactions on bio-medical engineering*, vol. 49, no. 5, pp. 419–429, May 2002. DOI: 10.1109/10.995680.

[57] G. M. Steil, B. Clark, S. Kanderian, and K. Rebrin, "Modeling insulin action for development of a closed-loop artificial pancreas.," *Diabetes technology & therapeutics*, vol. 7, no. 1, Feb. 2005. DOI: 10.1089/dia.2005.7.94.

[58] A. Roy and R. S. Parker, "Dynamic modeling of exercise effects on plasma glucose and insulin levels.," *Journal of diabetes science and technology*, vol. 1, no. 3, pp. 338–347, May 2007.

[59] C. Dalla Man, R. A. Rizza, and C. Cobelli, "Meal simulation model of the glucose-insulin system.," *IEEE transactions on bio-medical engineering*, vol. 54, no. 10, pp. 1740–1749, Oct. 2007. DOI: 10.1109/TBME.2007.893506.

[60] C. Dalla Man, D. M. Raimondo, R. A. Rizza, and C. Cobelli, "GIM, simulation software of meal glucose-insulin model.," *Journal of diabetes science and technology*, vol. 1, no. 3, pp. 323–330, May 2007.

[61] C. D. Man, M. D. Breton, and C. Cobelli, "Physical activity into the meal glucose-insulin model of type 1 diabetes: in silico studies.," *Journal of diabetes science and technology*, vol. 3, no. 1, Jan. 2009.

[62] B. P. Kovatchev, M. Breton, C. D. Man, and C. Cobelli, "In Silico Preclinical Trials: A Proof of Concept in Closed-Loop Control of Type 1 Diabetes," *Journal of diabetes science and technology (Online)*, vol. 3, no. 1, pp. 44–55, Jan. 2009, ISSN: 1932-2968.

[63] C. D. Man, F. Micheletto, D. Lv, M. Breton, B. Kovatchev, and C. Cobelli, "The UVA/PADOVA Type 1 Diabetes Simulator: New Features.," *Journal of diabetes science and technology*, vol. 8, no. 1, Jan. 2014. DOI: 10.1177/1932296813514502.

[64] J. Sorensen, "A Physiologic Model of Glucose Metabolism in Man and Its use to Design and Assess Improved Insulin Therapies for Diabetes," PhD thesis, Massachusetts Institute of Technology, 1985.

[65] P. J. Lenart and R. S. Parker, "Modeling Exercise Effects in Type 1 Diabetic Patients," *IFAC Proceedings Volumes*, vol. 35, no. 1, pp. 247 –252, 2002, 15th IFAC World Congress, ISSN: 1474-6670. DOI: https://doi.org/10.3182/20020721-6-ES-1901.01350.

[66] N. Kalant, T. Leibovici, I. Rohan, and K. McNeil, "Effect of exercise on glucose and insulin utilization in the forearm.," *Metabolism: clinical and experimental*, vol. 27, no. 3, pp. 333–340, 1978 Mar, ISSN: 0026-0495 0026-0495. pmid: 628354.

[67] P. G. Jacobs, J. El Youssef, R. Reddy, N. Resalat, D. Branigan, J. Condon, N. Preiser, K. Ramsey, M. Jones, C. Edwards, K. Kuehl, J. Leitschuh, U. Rajhbeharrysingh, and J. R. Castle, "Randomized trial of a dual-hormone artificial pancreas with dosing adjustment during exercise compared with no adjustment and sensor-augmented pump therapy.," *Diabetes, obesity & metabolism*, vol. 18, no. 11, pp. 1110–1119, 2016 Nov, ISSN: 1463-1326 1462-8902. DOI: 10.1111/dom.12707. pmid: 27333970.

[68] P. G. Jacobs, N. Resalat, J. El Youssef, R. Reddy, D. Branigan, N. Preiser, J. Condon, and J. Castle, "Incorporating an Exercise Detection, Grading, and Hormone Dosing Algorithm Into the Artificial Pancreas Using Accelerometry and Heart Rate.," *Journal of diabetes science and technology*, vol. 9, no. 6, pp. 1175–1184, 2015 Oct 5, ISSN: 1932-2968 1932-2968. DOI: 10.1177/1932296815609371. pmid: 26438720.

[69] R. Hovorka, V. Canonico, L. J. Chassin, U. Haueter, M. Massi-Benedetti, M. O. Federici, T. R. Pieber, H. C. Schaller, L. Schaupp, T. Vering, and M. E. Wilinska, "Nonlinear model predictive control of glucose concentration in subjects with type 1 diabetes," *Physiological Measurement*, vol. 25, no. 4, p. 905, 2004.

[70] C. Castillo, C. Bogardus, R. Bergman, P. Thuillez, and S. Lillioja, "Interstitial insulin concentrations determine glucose uptake rates but not insulin resistance in lean and obese men.," *Journal of Clinical Investigation*, vol. 93, no. 1, pp. 10–16, Jan. 1994, ISSN: 0021-9738.

[71] K. Kolendorf, J. Bojsen, and S. L. Nielsen, "Adipose tissue blood flow and insulin disappearance from subcutaneous tissue.," *Clinical pharmacology and therapeutics*, vol. 25, no. 5 Pt 1, pp. 598–604, May 1979, ISSN: 0009-9236 0009-9236.

[72] E. Ferrannini, B. Linde, and O. Faber, "Effect of bicycle exercise on insulin absorption and subcutaneous blood flow in the normal subject.," *Clinical physiology (Oxford, England)*, vol. 2, no. 1, Feb. 1982.

[73] L. Zhao, W. Chai, Z. Fu, Z. Dong, K. W. Aylor, E. J. Barrett, W. Cao, and Z. Liu, "Globular Adiponectin Enhances Muscle Insulin Action via Microvascular Recruitment and Increased Insulin DeliveryNovelty and Significance," *Circulation Research*, vol. 112, no. 9, pp. 1263–1271, 2013, ISSN: 0009-7330. DOI: 10.1161/CIRCRESAHA.111.300388.

[74] N. Wang, W. Chai, L. Zhao, L. Tao, W. Cao, and Z. Liu, "Losartan increases muscle insulin delivery and rescues insulintextquoterights metabolic action during lipid infusion via microvascular recruitment," *American Journal of Physiology - Endocrinology and Metabolism*, vol. 304, no. 5, E538–E545, 2013, ISSN: 0193-1849. DOI: 10.1152/ajpendo.00537.2012.

[75] P. Hildebrandt, P. Sejrsen, S. L. Nielsen, K. Birch, and L. Sestoft, "Diffusion and polymerization determines the insulin absorption from subcutaneous tissue in diabetic patients," *Scandinavian Journal of Clinical and Laboratory Investigation*, vol. 45, no. 8, pp. 685–690, 1985. DOI: 10.1080/00365518509155280.

[76] P. Hildebrandt and K. Birch, "Basal Rate Subcutaneous Insulin Infusion: Absorption Kinetics and Relation to Local Blood Flow," *Diabetic Medicine*, vol. 5, no. 5, pp. 434–440, 1988, ISSN: 1464-5491. DOI: 10.1111/j.1464-5491.1988.tb01023.x.

[77] J. P. Vora, A. Burch, J. R. Peters, and D. R. Owens, "Relationship between absorption of radiolabeled soluble insulin, subcutaneous blood flow, and anthropometry.," *Diabetes care*, vol. 15, no. 11, pp. 1484–1493, Nov. 1992, ISSN: 0149-5992 0149-5992.

[78] G. Nucci and C. Cobelli, "Models of subcutaneous insulin kinetics. A critical review.," *Computer methods and programs in biomedicine*, vol. 62, no. 3, pp. 249–257, Jul. 2000.

[79] E. M. Renkin, "Transport of potassium-42 from blood to tissue in isolated mammalian skeletal muscles.," *The American journal of physiology*, vol. 197, pp. 1205–1210, Dec. 1959, ISSN: 0002-9513 0002-9513.

[80] R. L. Fournier, *Basic Transport Phenomena in Biomedical Engineering*. CRC Press, 2011.

[81] C. Cobelli, A. Mari, and E. Ferrannini, "On linearity of insulin kinetics.," *The American journal of physiology*, vol. 251, no. 2 Pt 1, E247–250, Aug. 1986, ISSN: 0002-9513 0002-9513.

[82] L. G. Leal, *Advanced transport phenomena: fluid mechanics and convective transport processes*. Cambridge University Press, 2007.

[83] L. R. Williams and R. W. Leggett, "Reference values for resting blood flow to organs of man," *Clinical Physics and Physiological Measurement*, vol. 10, no. 3, p. 187, 1989.

[84] B. Saltin, "Capacity of blood flow delivery to exercising skeletal muscle in humans.," *The American journal of cardiology*, vol. 62, no. 8, 30E–35E, Sep. 1988, ISSN: 0002-9149 0002-9149.

[85] P. Hasgall, F Di Gebbari, C Baumgartner, E Neufeld, M. Gosselin, D Payne, A Klingenböck, and N Kuster, "IT'IS Database for thermal and electromagnetic parameters of biological tissues," vol. 3.0, Sep. 2015. DOI: 10.13099/VIP21000-03-0.

[86] J. Bülow and J. Madsen, "Adipose tissue blood flow during prolonged, heavy exercise," *Pflügers Archiv*, vol. 363, no. 3, pp. 231–234, 1976, ISSN: 1432-2013. DOI: 10.1007/BF00594606.

[87] J. Bulow and J. Madsen, "Human adipose tissue blood flow during prolonged exercise II.," *Pflugers Archiv : European journal of physiology*, vol. 376, no. 1, pp. 41–45, Aug. 1978, ISSN: 0031-6768 0031-6768.

[88] J. Bulow, "Human adipose tissue blood flow during prolonged exercise, III. Effect of beta-adrenergic blockade, nicotinic acid and glucose infusion.," *Scandinavian journal of clinical and laboratory investigation*, vol. 41, no. 4, pp. 415–424, Jun. 1981, ISSN: 0036-5513 0036-5513.

[89] M. G. Clark, S. Rattigan, E. J. Barrett, and M. A. Vincent, "Point:Counterpoint: There is/is not capillary recruitment in active skeletal muscle during exercise," *Journal of Applied Physiology*, vol. 104, no. 3, pp. 889–891, 2008, ISSN: 8750-7587. DOI: 10.1152/japplphysiol.00779.2007.

[90] E. A. Richter, "Glucose Utilization," in *Comprehensive Physiology*, John Wiley Sons, Inc., 2010, ISBN: 978-0-470-65071-4.

[91] E. M. Renkin, O. Hudlicka, and R. M. Sheehan, "Influence of metabolic vasodilatation on blood-tissue diffusion in skeletal muscle.," *The American journal of physiology*, vol. 211, no. 1, pp. 87–98, Jul. 1966, ISSN: 0002-9513 0002-9513.

[92] D. Dawson, M. A. Vincent, E. J. Barrett, S. Kaul, A. Clark, H. Leong-Poi, and J. R. Lindner, "Vascular recruitment in skeletal muscle during exercise and hyperinsulinemia assessed by contrast ultrasound.," *American journal of physiology. Endocrinology and metabolism*, vol. 282, no. 3, E714–720, Mar. 2002, ISSN: 0193-1849 0193-1849. DOI: 10.1152/ajpendo.00373.2001.

[93] M. Coggins, J. Lindner, S. Rattigan, L. Jahn, E. Fasy, S. Kaul, and E. Barrett, "Physiologic hyperinsulinemia enhances human skeletal muscle perfusion by capillary recruitment.," *Diabetes*, vol. 50, no. 12, pp. 2682–2690, Dec. 2001, ISSN: 0012-1797 0012-1797.

[94] L. Womack, D. Peters, E. J. Barrett, S. Kaul, W. Price, and J. R. Lindner, "Abnormal skeletal muscle capillary recruitment during exercise in patients with type 2 diabetes mellitus and microvascular complications.," *Journal of the American College of Cardiology*, vol. 53, no. 23, pp. 2175–2183, Jun. 2009, ISSN: 1558-3597 0735-1097. DOI: 10.1016/j.jacc.2009.02.042.

[95] J. T. Belcik, B. P. Davidson, T. Foster, Y. Qi, Y. Zhao, D. Peters, and J. R. Lindner, "Contrast-Enhanced Ultrasound Assessment of Impaired Adipose Tissue and Muscle Perfusion in Insulin-resistant Mice," *Circulation. Cardiovascular imaging*, vol. 8, no. 4, 2015 Apr, ISSN: 1941-9651 1942-0080. DOI: 10.1161/CIRCIMAGING.114.002684. pmid: 25855669.

[96] L. Tobin, L. Simonsen, and J. Bulow, "Real-time contrast-enhanced ultrasound determination of microvascular blood volume in abdominal subcutaneous adipose tissue in man. Evidence for adipose tissue capillary recruitment.," *Clinical physiology and functional imaging*, vol. 30, no. 6, pp. 447–452, Nov. 2010, ISSN: 1475-097X 1475-0961. DOI: 10.1111/j.1475-097X.2010.00964.x.

[97] K. A. Sjøberg, S. Rattigan, N. Hiscock, E. A. Richter, and B. Kiens, "A new method to study changes in microvascular blood volume in muscle and adipose tissue: real-time imaging in humans and rat," *American Journal of Physiology - Heart and Circulatory Physiology*, vol. 301, no. 2, H450–H458, 2011, ISSN: 0363-6135. DOI: 10.1152/ajpheart.01174.2010.

[98] C. R. Honig, C. L. Odoroff, and J. L. Frierson, "Capillary recruitment in exercise: rate, extent, uniformity, and relation to blood flow.," *The American journal of physiology*, vol. 238, no. 1, H31–42, Jan. 1980, ISSN: 0002-9513 0002-9513.

[99] M. A. Vincent, L. H. Clerk, J. R. Lindner, W. J. Price, L. A. Jahn, H. Leong-Poi, and E. J. Barrett, "Mixed meal and light exercise each recruit muscle capillaries in healthy humans.," *American journal of physiology. Endocrinology and metabolism*, vol. 290, no. 6, E1191–1197, Jun. 2006, ISSN: 0193-1849 0193-1849. DOI: 10.1152/ajpendo.00497.2005.

[100] M. A. Vincent, D. Dawson, A. D. H. Clark, J. R. Lindner, S. Rattigan, M. G. Clark, and E. J. Barrett, "Skeletal muscle microvascular recruitment by physiological hyperinsulinemia precedes increases in total blood flow.," *Diabetes*, vol. 51, no. 1, pp. 42–48, Jan. 2002, ISSN: 0012-1797 0012-1797.

[101] S. Gudbjörnsdóttir, M. Sjöstrand, L. Strindberg, J. Wahren, and P. Lönnroth, "Direct Measurements of the Permeability Surface Area for Insulin and Glucose in Human Skeletal Muscle," *The Journal of Clinical Endocrinology & Metabolism*, vol. 88, no. 10, pp. 4559–4564, 2003. DOI: 10.1210/jc.2003-030434.

[102] S. Gudbjornsdottir, M. Sjostrand, L. Strindberg, and P. Lonnroth, "Decreased muscle capillary permeability surface area in type 2 diabetic subjects.," *The Journal of clinical endocrinology and metabolism*, vol. 90, no. 2, pp. 1078–1082, Feb. 2005, ISSN: 0021-972X 0021-972X. DOI: 10.1210/jc.2004-0947.

[103] T. Khazaeinia, A. A. Ramsey, and Y. K. Tam, "The effects of exercise on the pharmacokinetics of drugs.," *Journal of pharmacy & pharmaceutical sciences : a publication of the Canadian Society for Pharmaceutical Sciences, Societe canadienne des sciences pharmaceutiques*, vol. 3, no. 3, pp. 292–302, 2000 Sep-Dec, ISSN: 1482-1826 1482-1826.

[104] A. Guyton and J. Hall, *Textbook of Medical Physiology*, 11th. Elsevier Saunders, 2006, ISBN: 0-7216-0240-1.

[105] P. De Feo, G. Perriello, M. M. Ventura, F. Calcinaro, G. Basta, C. Lolli, C. Cruciani, A. Dell'Olio, F. Santeusanio, and P. Brunetti, "Studies on overnight insulin requirements and metabolic clearance rate of insulin in normal and diabetic man: relevance to the pathogenesis of the dawn phenomenon.," *Diabetologia*, vol. 29, no. 8, pp. 475–480, Aug. 1986, ISSN: 0012-186X 0012-186X.

[106] B. Thorsteinsson, S. Fugleberg, and C. Binder, "Insulin Clearance from Plasma in Type I (Insulin-Dependent) Diabetic Patients: Influence of Glycaemic Level," *Pharmacology Toxicology*, vol. 62, no. 4, pp. 206–209, 1988, ISSN: 1600-0773. DOI: 10.1111/j.1600-0773.1988.tb01873.x.

[107] B. Thorsteinsson, S. Fugleberg, B. Feldt-Rasmussen1, K. Ellemann, O. O. Andersen, and C. Binder, "Kinetic Models for Insulin Disappearance from Plasma in Type I Diabetic Patients," *Pharmacology Toxicology*, vol. 60, no. 2, pp. 90–95, 1987, ISSN: 1600-0773. DOI: 10.1111/j.1600-0773.1987.tb01502.x.

[108] M. A. Kurauti, R. Freitas-Dias, S. M. Ferreira, J. F. Vettorazzi, T. R. Nardelli, H. N. Araujo, G. J. Santos, E. M. Carneiro, A. C. Boschero, L. F. Rezende, and J. M. Costa-Júnior, "Acute Exercise Improves Insulin Clearance and Increases the Expression of Insulin-Degrading Enzyme in the Liver and Skeletal Muscle of Swiss Mice," *PLOS ONE*, vol. 11, no. 7, pp. 1–16, Jul. 2016. DOI: 10.1371/journal.pone.0160239.

[109] J. A. Tuominen, P. Ebeling, and V. A. Koivisto, "Exercise increases insulin clearance in healthy man and insulin-dependent diabetes mellitus patients," *Clinical Physiology*, vol. 17, no. 1, pp. 19–30, Jan. 1997, ISSN: 1365-2281. DOI: 10.1046/j.1365-2281.1997.01717.x.

[110] A. Holmäng, K. Mimura, and P. Lönnroth, "Involuntary leg movements affect interstitial nutrient gradients and blood flow in rat skeletal muscle," *Journal of Applied Physiology*, vol. 92, no. 3, pp. 982–988, 2002, ISSN: 8750-7587. DOI: 10.1152/japplphysiol.01194.2000.

[111] M. Sjöstrand, A. Holmäng, and P. Lönnroth, "Measurement of interstitial insulin in human muscle," *American Journal of Physiology - Endocrinology and Metabolism*, vol. 276, no. 1, E151–E154, 1999, ISSN: 0193-1849.

[112] P.-A. E. Jansson, J. P. Fowelin, H. P. Von Schenck, U. P. Smith, and P. N. Lönnroth, "Measurement by Microdialysis of the Insulin Concentration in Subcutaneous Interstitial Fluid: Importance of the Endothelial Barrier for Insulin," *Diabetes*, vol. 42, no. 10, pp. 1469–1473, 1993, ISSN: 0012-1797. DOI: 10.2337/diab.42.10.1469.

[113] M. Schiavon, L. Hinshaw, A. Mallad, C. Dalla Man, G. Sparacino, M. Johnson, R. Carter, R. Basu, Y. Kudva, C. Cobelli, and A. Basu, "Postprandial glucose fluxes and insulin sensitivity during exercise: a study in healthy individuals.," *American journal of physiology. Endocrinology and metabolism*, vol. 305, no. 4, E557–566, Aug. 2013. DOI: 10.1152/ajpendo.00182.2013.

[114] E. M. Eggleston, L. A. Jahn, and E. J. Barrett, "Hyperinsulinemia Rapidly Increases Human Muscle Microvascular Perfusion but Fails to Increase Muscle Insulin Clearance," *Diabetes*, vol. 56, no. 12, pp. 2958–2963, 2007, ISSN: 0012-1797. DOI: 10.2337/db07-0670.

[115] L. A. Jakobsen, A. Jensen, L. E. Larsen, M. R. Sørensen, H. C. Hoeck, L. Arendt-Nielsen, and P. Gazerani, "Effect of cutaneous blood flow on absorption of insulin: a methodological study in healthy male volunteers," *International Journal of Physiology, Pathophysiology and Pharmacology*, vol. 3, no. 4, pp. 257–265, 2011, ISSN: 1944-8171.

[116] E. E. C. Engwerda, C. J. Tack, and B. E. de Galan, "Pharmacokinetic and Pharmacodynamic Variability of Insulin When Administered by Jet Injection.," *Journal of diabetes science and technology*, p. 1 932 296 817 699 638, Mar. 2017, ISSN: 1932-2968 1932-2968. DOI: 10.1177/1932296817699638.

[117] I. Raz, G. Bitton, D. Feldman, T. Alon, A. Pfutzner, and W. V. Tamborlane, "Improved Postprandial Glucose Control Using the InsuPad Device in Insulin-Treated Type 2 Diabetes: Injection Site Warming to Improve Glycemic Control," *Journal of Diabetes Science and Technology*, vol. 9, no. 3, pp. 639–643, May 2015, ISSN: 1932-2968. DOI: 10.1177/1932296815578881.

[118] S. A. Charman, D. N. McLennan, G. A. Edwards, and C. J. H. Porter, "Lymphatic Absorption Is a Significant Contributor to the Subcutaneous Bioavailability of Insulin in a Sheep Model," *Pharmaceutical Research*, vol. 18, no. 11, pp. 1620–1626, 2001, ISSN: 1573-904X. DOI: 10.1023/A:1013046918190.

[119] P. Felig, J. Wahren, and R. Hendler, "Influence of Oral Glucose Ingestion on Splanchnic Glucose and Gluconeogenic Substrate Metabolism in Man," *Diabetes*, vol. 24, no. 5, pp. 468–475, 1975, ISSN: 0012-1797. DOI: 10.2337/diab.24.5.468.

[120] E. Ferrannini, J. Wahren, P. Felig, and R. A. DeFronzo, "The role of fractional glucose extraction in the regulation of splanchnic glucose metabolism in normal and diabetic man," *Metabolism*, vol. 29, no. 1, pp. 28 –35, 1980, ISSN: 0026-0495. DOI: http://dx.doi.org/10.1016/0026-0495(80)90094-3.

[121] E. A. Richter and M. Hargreaves, "Exercise, GLUT4, and skeletal muscle glucose uptake.," *Physiological reviews*, vol. 93, no. 3, pp. 993–1017, Jul. 2013, ISSN: 1522-1210 0031-9333. DOI: 10.1152/physrev.00038.2012.

[122] J. M. Ren, C. F. Semenkovich, E. A. Gulve, J. Gao, and J. O. Holloszy, "Exercise induces rapid increases in GLUT4 expression, glucose transport capacity, and insulin-stimulated glycogen storage in muscle.," *The Journal of biological chemistry*, vol. 269, no. 20, pp. 14 396–14 401, May 1994, ISSN: 0021-9258 0021-9258.

[123] A. J. Rose and E. A. Richter, "Skeletal muscle glucose uptake during exercise: how is it regulated?," *Physiology (Bethesda, Md.)*, vol. 20, pp. 260–270, Aug. 2005, ISSN: 1548-9213 1548-9221. DOI: 10.1152/physiol.00012.2005.

[124] H. Yki-Järvinen, A. A. Young, C. Lamkin, and J. E. Foley, "Kinetics of glucose disposal in whole body and across the forearm in man.," *Journal of Clinical Investigation*, vol. 79, no. 6, pp. 1713–1719, Jun. 1987, ISSN: 0021-9738.

[125] R. N. Bergman, Y. Z. Ider, C. R. Bowden, and C. Cobelli, "Quantitative estimation of insulin sensitivity.," *The American journal of physiology*, vol. 236, no. 6, E667–677, Jun. 1979.

[126] C. Cobelli, C. Dalla Man, G. Toffolo, R. Basu, A. Vella, and R. Rizza, "The Oral Minimal Model Method," *Diabetes*, vol. 63, no. 4, pp. 1203–1213, 2014. DOI: 10.2337/db13-1198.

[127] C. Dalla Man, A. Caumo, R. Basu, R. Rizza, G. Toffolo, and C. Cobelli, "Minimal model estimation of glucose absorption and insulin sensitivity from oral test: validation with a tracer method.," *American journal of physiology. Endocrinology and metabolism*, vol. 287, no. 4, E637–643, Oct. 2004. DOI: 10.1152/ajpendo.00319.2003.

[128] A. D. Baron, G. Brechtel, P. Wallace, and S. V. Edelman, "Rates and tissue sites of non-insulin- and insulin-mediated glucose uptake in humans.," *The American journal of physiology*, vol. 255, no. 6 Pt 1, E769–774, Dec. 1988, ISSN: 0002-9513 0002-9513.

[129] B. Nielsen, G Savard, E. Richter, M. Hargreaves, and B. Saltin, "Muscle blood flow and muscle metabolism during exercise and heat stress," *Journal of applied physiology*, vol. 69, no. 3, pp. 1040–1046, 1990.

[130] A. Katz, S. Broberg, K. Sahlin, and J. Wahren, "Leg glucose uptake during maximal dynamic exercise in humans," *American Journal of Physiology - Endocrinology and Metabolism*, vol. 251, no. 1, E65–E70, 1986.

[131] J. Radziuk, T. J. McDonald, D. Rubenstein, and J. Dupre, "Initial splanchnic extraction of ingested glucose in normal man," *Metabolism*, vol. 27, no. 6, pp. 657 –669, 1978, ISSN: 0026-0495. DOI: http://dx.doi.org/10.1016/0026-0495(78)90003-3.

[132] G. Ahlborg and J. Wahren, "Brain substrate utilization during prolonged exercise.," *Scandinavian journal of clinical and laboratory investigation*, vol. 29, no. 4, pp. 397–402, 1972, ISSN: 1502-7686 0036-5513.

[133] C. Dalla Man, K. E. Yarasheski, A. Caumo, H. Robertson, G. Toffolo, K. S. Polonsky, and C. Cobelli, "Insulin sensitivity by oral glucose minimal models: validation against clamp.," *American journal of physiology. Endocrinology and metabolism*, vol. 289, no. 6, E954–959, Dec. 2005. DOI: 10.1152/ajpendo.00076.2005.

[134] P. Aarnio, T. Lauritsen, and F. Dela, "Insulin Secretion and Glucose Kinetics During Exercise With and Without Pharmacological $a1$- and $a2$-Receptor Blockade," *Diabetes*, vol. 50, no. 8, pp. 1834–1843, 2001, ISSN: 0012-1797. DOI: 10.2337/diabetes.50.8.1834.

[135] R. A. Rizza, G. Toffolo, and C. Cobelli, "Accurate Measurement of Postprandial Glucose Turnover: Why Is It Difficult and How Can It Be Done (Relatively) Simply?," *Diabetes*, vol. 65, no. 5, pp. 1133–1145, 2016, ISSN: 0012-1797. DOI: 10.2337/db15-1166.

[136] R. DeFronzo, D. Simonson, and E. Ferrannini, "Hepatic and peripheral insulin resistance: A common feature of Type 2 (non-insulin-dependent) and Type 1 (insulin-dependent) diabetes mellitus," *Diabetologia*, vol. 23, no. 4, pp. 313–319, 1982, ISSN: 0012-186X. DOI: 10.1007/BF00253736.

[137] H. S. Lew and Y. C. Fung, "The motion of the plasma between the red cells in the bolus flow.," *Biorheology*, vol. 6, no. 2, pp. 109–119, Aug. 1969, ISSN: 0006-355X 0006-355X.

[138] J. P. Keener and J. Sneyd, *Mathematical Physiology*. Springer, 2009, vol. 1.

[139] L. Smaje, B. W. Zweifach, and M. Intaglietta, "Micropressures and capillary filtration coefficients in single vessels of the cremaster muscle of the rat," *Microvascular Research*, vol. 2, no. 1, pp. 96 –110, 1970, ISSN: 0026-2862. DOI: http://dx.doi.org/10.1016/0026-2862(70)90055-5.

[140] O. A. Larsen, N. A. Lassen, and F. Quaade, "Blood Flow through Human Adipose Tissue Determined with Radioactive Xenon," *Acta Physiologica Scandinavica*, vol. 66, no. 3, pp. 337–345, Mar. 1966, ISSN: 1365-201X. DOI: 10.1111/j.1748-1716.1966.tb03208.x.

[141] S. S. KETY, "The Theory and Applications of the Exchange of Inert Gas at the Lungs and Tissues," *Pharmacological Reviews*, vol. 3, no. 1, pp. 1–41, 1951, ISSN: 0031-6997.

[142] R. Chen, F.-C. Fan, S Kim, K. Jan, S. Usami, and S Chien, "Tissue-blood partition coefficient for xenon: temperature and hematocrit dependence," *Journal of Applied Physiology*, vol. 49, no. 2, pp. 178–183, 1980.

# Appendix A

# Insulin Absorption Modeling

Note that the nomenclature in this appendix is different than that employed in the body of the dissertation.

## A.1 Application of Divergence Theorem

By application of the divergence theorem the following expression is exactly zero

$$D_{ISF} \int_{V_s} \nabla^2 c \; dV = D_s \int_S \nabla c \cdot n \; dS = 0 \tag{A.1}$$

This is because $\nabla c$ is zero by application of boundary condition $\frac{\partial c}{\partial r} = 0$ on the boundary.

## A.2 Simplifying the Convection-Diffusion Equation for a Capillary

In the full BVP describing insulin absorption in a capillary, $D_b$ is the diffusion coefficient of insulin in blood plasma, $U$ is the plasma flow velocity in the axial direction $x$, $R$ is the radius of the vessel, $L$ is the length of the vessel, and $P$ is the permeability of the vessel wall

$$U\frac{\partial b}{\partial x} = D_b\Big(\frac{1}{\rho}\frac{\partial}{\partial \rho}\Big(\rho\frac{\partial b}{\partial \rho}\Big) + \frac{\partial^2 b}{\partial x^2}\Big) \tag{A.2}$$

subject to

$$b = I \text{ at } x = 0 \text{ for } \rho = [0, R] \tag{A.3}$$

$$\frac{\partial b}{\partial \rho} = 0 \text{ at } \rho = 0 \tag{A.4}$$

$$q = P(c - b) \text{ at } \rho = R. \tag{A.5}$$

Permeability $P$ relates flux at the wall to the concentrations on each side of the wall. $c$ is the concentration in the subcutaneous (SC) ISF that surrounds the capillary and $I$ in the concentration in the circulatory system (CS) domain, which we assume is equal to the concentration at the inlet. We also assume that there is no significant accumulation of insulin in the capillary, and so $\frac{\partial b}{\partial t} = 0$. In general $b(\rho, x, I(t), c(r,t))$, but we will simplify the problem to allow us to solve for $b$ as only a function of $x$.

The first simplification that will be make is to hold $I(t)$ and $c(r,t)$ fixed when solving for $b$. We can do this because the difference in timescales is large; $b$ changes on the timescale of blood traversing the capillary domain ($\sim$ 1 second), $c$ changes on the timescale of permeation through the capillary wall ($\sim$ 1 hour). $I$ changes on the same timescale as $c$. The difference in lengthscales is also large; $b$ changes on the lengthscale of a capillary ($\sim$ 1 mm) while $c$ changes on the lengthscale of the SC ISF domain ($\sim$ 1 cm). We can thus evaluate $b$ locally, holding boundary conditions at a fixed $r$ and $t$. Thus $b(\rho, x, I(t), c(r,t)) \approx b(\rho, x)$.

Even with the first simplification, the convection-diffusion equation that describes the drug absorption in the SC capillary domain is still a PDE. This linear PDE could be solved in a relatively simple manner (both an analytical and a numerical solution are shown in Appendix C.1), but we prefer to work with ODEs when possible for their simplicity. We will simply the PDE to an ODE through scaling of terms by non-dimensionalization.

We non-dimensionalize Equation 2.16 with substitution of variables $\check{b} = b/\bar{c}$, $\check{c} = c/\bar{c}$, $\check{x} = x/L$, and $\check{\rho} = \rho/R$. $\bar{c}$ is the average concentration in the ISF.

$$\frac{\partial \check{b}}{\partial \check{x}} = \frac{D_b}{UR}\Big(\frac{L}{R}\,\frac{1}{\check{\rho}}\frac{\partial}{\partial \check{\rho}}\Big(\check{\rho}\frac{\partial \check{b}}{\partial \check{\rho}}\Big) + \frac{R}{L}\,\frac{\partial^2 \check{b}}{\partial \check{x}^2}\Big) \tag{A.6}$$

subject to

$$\check{b} = \frac{I}{\bar{c}} \text{ at } \check{x} = 0 \text{ for } \check{\rho} = [0,1] \tag{A.7}$$

$$\frac{\partial \check{b}}{\partial \check{\rho}} = 0 \text{ at } \check{\rho} = 0 \tag{A.8}$$

$$\check{q} = \frac{P \cdot R}{D_b}(\check{c} - \check{b}) \text{ at } \check{\rho} = 1 \tag{A.9}$$

The last BC was derived through utilization of expression $q = D_b\frac{\partial b}{\partial \rho} = \frac{D_b \bar{c}}{R}\frac{\partial \check{b}}{\partial \check{\rho}}$.

We have assumed uniform flow for the velocity field $U$. This is a valid assumption because typically in capillaries, single red blood cells (RBCs) form plugs every few cell lengths [137] with a resulting flow field that is nearly uniform in the cross section.

Now examining the non-dimensionalized Equation A.6 we see that the magnitude of each term is dependent on the Péclet number $Pe = UR/D_b$ and the aspect ratio $AR = L/R$. Capillaries are much longer than they are wide and thus the second term on the RHS is much smaller than the first, and we eliminate it. We now integrate Equation A.6 over the

capillary cross section

$$\frac{\partial}{\partial \check{x}} \int_A \check{b}\ dA = \Big(\frac{D_b}{UR}\frac{L}{R}\Big) \int_A \frac{1}{\check{\rho}} \frac{\partial}{\partial \check{\rho}} \Big(\check{\rho} \frac{\partial \check{b}}{\partial \check{\rho}}\Big)\ dA. \tag{A.10}$$

Now, utilizing the divergence theorem, we convert the area integral to a line integral on the boundary and apply BC A.9

$$\int_A \frac{1}{\check{\rho}} \frac{\partial}{\partial \check{\rho}} \Big(\check{\rho}\Big) \frac{\partial \check{b}}{\partial \check{\rho}} dA = \int_s \frac{\partial \check{b}}{\partial \check{\rho}} \cdot n\ ds = \frac{P \cdot R}{D_b} \int_s (\check{c} - \check{b})\ ds. \tag{A.11}$$

Plugging into Equation A.10 we obtain

$$\frac{\partial}{\partial \check{x}} \int_A \check{b}\ dA = \Big(\frac{PRL}{UR^2}\Big) \int_s (\check{c} - \check{b})\ ds. \tag{A.12}$$

Per the previous argument, $\check{c}$ is fixed. Additionally, since $\check{b}$ is axially symmetric, it does not vary along the capillary perimeter curve $s$ and can be evaluated at the wall and pulled out of the integral. The integral over $s$ is then $\int_0^{2\pi} \check{\rho}\ d\theta = 2\pi$ and we have

$$\frac{\partial}{\partial \check{x}} \int_A \check{b}\ dA = \Big(\frac{P2\pi RL}{UR^2}\Big)(\check{c} - \check{b}|_{wall}). \tag{A.13}$$

The last step before we can convert the integral equation to an ODE is to evaluate how $\check{b}$ varies along the cross-section $A$. We will show with scaling arguments that $\check{b}(\check{\rho}, \check{x}) \approx \check{b}(\check{x})$. To show this approximation is reasonable we need to show that the concentration boundary layer of $\check{b}$ is 'large'. This would imply that the concentration gradient in the $\check{\rho}$ direction, from the wall to the axial centerline, is small and hence $\check{b}$ is only weakly dependent on $\check{\rho}$.

We start by estimating the size of the coefficient $Pe^{-1} \cdot AR$ in Equation A.10. $D_b$ has previously been approximated as $O(10^{-6})$ cm$^2$/s in water [138, p.54][75], $U$ as $O(10^{-1})$ cm/s [138, p.476], and $R$ as $3 \cdot 10^{-4}$ cm [138, p.476], resulting in $Pe \sim 30$. This means that downstream convective transport occurs more quickly than than radial diffusive transport. However, considering that the $AR \sim 200$ [139, rat muscle], the diffusion distance is very small in comparison to the convection distance. This is confirmed by the value of the product $Pe^{-1} \cdot AR$ which is only $\sim 6$; diffusion to the capillary centerline has occurred when the plasma has traversed only 1/6 of the capillary length, a relatively 'rapid' diffusion. Furthermore, $Pe$ is likely overestimated due to unaccounted phenomena. The dispersive effects of shear and circulation in the flow due to the presence of RBCs can greatly increase the rate of diffusion to the center line [137]. We thus comfortably assume that diffusion of insulin to the centerline occurs quickly compared to the downstream convection and we make a low $Pe$ argument. It follows that the concentration boundary layer is 'large' and that the concentration $\check{b}$ is not strongly dependent on $\check{\rho}$. This scaling allows us to approximate $\check{b}(\check{\rho}, \check{x}) \approx \check{b}(\check{x})$.

We utilize the approximation by treating $\check{b}$ as a constant in the cross section in Equation A.13. Thus $\check{b}$ is pulled out of the integral on the LHS and $\check{b}|_{wall} \approx \check{b}$. Noting $\int_A dA = \pi$ the result is

$$\frac{d\check{b}}{d\check{x}} = \Big(\frac{P2\pi RL}{U\pi R^2}\Big)(\check{c} - \check{b}) \tag{A.14}$$

Now we examine the single dimensionless parameter that governs the system. The product $P2\pi RL$ is the permeability surface area ($PS$). $U\pi R^2$ is the volume flow rate ($Q$). Because we have a ratio of these two quantities, we may express each of these as specific (per-unit volume) properties, which are measurable and have units of $\mathrm{mL}_b/\mathrm{min}/\mathrm{mL}_{tiss}$. The solution to Equation A.14 subject to boundary condition A.7 is (details in Appendix A.3)

$$\check{b}(\check{x}, r, t) = \frac{c(r,t)}{\bar{c}} - (\frac{c(r,t)}{\bar{c}} - \frac{I(t)}{\bar{c}})e^{-\frac{PS}{Q}\check{x}} \tag{A.15}$$

Remember, $r$ and $t$ were arbitrarily fixed when solving for $\check{b}$ locally, but $\check{b}$ is a field variable that depends on time and the location in the ISF, and so depends on $t$ and $r$ globally. Thus, the solution is valid for all $r$, $t$ and $\check{x}$ from 0 to 1. The general dimensional form of the solution A.15 is

$$b(x, r, t) = c(r,t) - (c(r,t) - I(t))e^{-\frac{PS}{Q}\frac{x}{L}} \tag{A.16}$$

## A.3 Solution to ODE Governing Capillary Domain

Here, we solve Equation 2.20.

$$\frac{db}{dx} = \Big(\frac{P2\pi RL}{U\pi R^2}\Big)\frac{1}{L}(c - b). \tag{A.17}$$

$$b = I \text{ at } x = 0 \tag{A.18}$$

The homogeneous solution is

$$b_h = A \cdot e^{-\frac{PS}{Q}\frac{x}{L}} \tag{A.19}$$

The particular solution is then

$$b_p = B(x) \cdot e^{-\frac{PS}{Q}\frac{x}{L}} \tag{A.20}$$

Plugging the particular solution into Equation A.17 we get

$$\frac{dB(x)}{dx} = \frac{PS}{Q}\frac{1}{L}ce^{\frac{PS}{Q}\frac{x}{L}} \tag{A.21}$$

Now, because we would like to know the solution at each point in time, we use a convolution integral to solve for $B(x)$

$$\int_0^x \frac{dB(x)}{dx}\, dx = \frac{PS}{Q}\frac{1}{L}c\int_0^x e^{\frac{PS}{Q}\frac{x}{L}}\, dx \tag{A.22}$$

$$B(x) = c(e^{\frac{PS}{Q}\frac{x}{L}} - 1) \tag{A.23}$$

We hold $c$ fixed due to separation of length scales between the capillary and ISF domain. The particular solution is

$$b_p = c(1 - e^{-\frac{PS}{Q}\frac{x}{L}}) \tag{A.24}$$

and the general solution is

$$b_g = b_h + b_p \tag{A.25}$$

$$b_g = A \cdot e^{-\frac{PS}{Q}\frac{x}{L}} + c(1 - e^{-\frac{PS}{Q}\frac{x}{L}}) \tag{A.26}$$

and applying the boundary condition A.18 we get the final form of the solution (dropping subscript $g$)

$$b = c(r,t) - (c(r,t) - I(t))e^{-\frac{PS}{Q}\frac{x}{L}} \tag{A.27}$$

## A.4 Measuring Tissue Perfusion Rate $Q$ in Adipose Tissue

The measurement of tissue perfusion rate $Q$ in the adipose tissue was first described by Larson in 1966[140]. The calculations are simple and straight forward and only require one time-series measurement - the tracer mass that is present in the subcutaneous compartment. This is typically measured as counts per minute (cpm) of a radioactive tracer such as Xenon ($Xe^{133}$). $Xe^{133}$ is chosen because it is an inert gas, and thus its transfer from one solvent to the other obeys Henry's law[141]. Additionally, it readily moves into the bloodstream with little hindrance from the capillary wall. The combination of these two phenomena allows for the quantification of the $Xe^{133}$ partition coefficient, $\lambda$, in various tissues of the body. We leverage this knowledge to measure blood flow in various tissues.

Consider an injection of $Xe^{133}$ into the subcutaneous tissue. It has a concentration of $\mathcal{X}_s$ [cpm per $g_{tiss}$] and it slowly diffuses into the bloodstream where it has a concentration of $\mathcal{X}_b$ [cpm per $ml_b$]. If we assume that the system is in equilibrium, then we can describe the difference in concentration with the simple relation

$$\mathcal{X}_s = \lambda \mathcal{X}_b \tag{A.28}$$

where $\lambda$ is the partition coefficient between the concentration in the subcutaneous space and the blood space, which has been previously reported in several studies [140, 142]. $\lambda$ does depend on hematocrit slightly, but if we assume that the subject has a near average hematocrit, we use the $\lambda$ value calculated for a typical 40% hematocrit [140]. This equilibrium assumption is valid when we consider that $Xe^{133}$ has a large diffusion coefficient, meaning that we are not rate limited by diffusion, but rather blood flow. This is equivalent to saying that transfer from the tissue to the blood occurs rapidly, and reaches the equilibrium described by Equation A.28 before blood leaves the region. Thus we can determine blood flow $Q$ by only knowing the rate of disappearance of $Xe^{133}$ from the subcutaneous space. To obtain this relation, we apply Fick's principle for extraction of $Xe^{133}$ from the subcutaneous tissue

$$\frac{d\mathcal{X}_s}{dt} = Q(\mathcal{X}_{b_a} - \mathcal{X}_{b_v}) \tag{A.29}$$

where $\mathcal{X}_{b_a}$ is the arterial (upstream) concentration in the blood and $\mathcal{X}_{b_v}$ is the venous (downstream) concentration in the blood. Considering that upon leaving the microcirculation, a substance becomes greatly diluted throughout the body, we can assume that $\mathcal{X}_{b_a} \approx 0$. Plugging A.28 into A.29, and setting $\mathcal{X}_{b_v} = \mathcal{X}_b$ (because of rapid equilibration) we get

$$\frac{d\mathcal{X}_s}{dt} = \frac{-Q}{\lambda} \cdot \mathcal{X}_s \tag{A.30}$$

$$Q = -\lambda \frac{d\ln(\mathcal{X}_s)}{dt} [\mathrm{ml}_b/\mathrm{min}/\mathrm{g}_{tiss}] \tag{A.31}$$

$$\tag{A.32}$$

$\mathcal{X}_s$ is measured using a scintillation counter and eventually the term $\frac{d\ln(\mathcal{X}_s)}{dt}$ reaches a constant value. At this point $Q$ can be calculated reliably.

It is customary to express $Q$ as per 100 $\mathrm{g}_{tiss}$, to do this, simply multiply by 100. Also, because $Q$ is typically expressed per $\mathrm{g}_{tiss}$, we often need to convert to per $\mathrm{ml}_{tiss}$. A typical conversion can be made with $\rho_{tiss}$=0.911 $\mathrm{g}_{tiss}/\mathrm{ml}_{tiss}$ for subcutaneous tissue or $\rho_{tiss}$=1.09 $\mathrm{g}_{tiss}/\mathrm{ml}_{tiss}$ for muscle[85]. In this work we have assumed $\rho_{tiss}$=1 $\mathrm{g}_{tiss}/\mathrm{ml}_{tiss}$ for simplicity.

## A.5 Measuring Permeability Surface Area, $PS$

The capillary permeability surface area ($PS$) that is used as a parameter in the insulin model was measured by Gudbjornsdottir [101], and ranges between 0.4 to 0.6 $\mathrm{ml}_{blood}/\mathrm{min}/100\mathrm{g}_{tiss}$. To make this measurement, a microdialysis technique was utilized, and a model for capillary mass transfer was assumed. Coincidentally, the model they assumed is the same capillary mass-transfer model that we derived in Chapter 2 and solved in Appendix A.3. The difference is that in their case, they are evaluating movement of solute from the plasma to the interstitial fluid, opposite to the present model. However, even with the differing sign, the solutions are

identical

$$b = c(r,t) - (c(r,t) - I(t))e^{-\frac{PS}{Q}\frac{x}{L}} \tag{A.33}$$

We can evaluate the difference in $b$ from the inlet $b|_i$ to the exit $b|_e$ as

$$b|_i - b|_e = I - c + (c - I)e^{-\frac{PS}{Q}} \tag{A.34}$$

$$I - V = I - c + (c - I)e^{-\frac{PS}{Q}}. \tag{A.35}$$

We solve for $PS$

$$PS = -Q \cdot \ln(\frac{V - c}{I - c}) \tag{A.36}$$

where $b|_i = I$ is the plasma insulin concentration at the arterial end of the capillary bed, $b|_e = V$ is the plasma insulin concentration at the venous end of the capillary bed. $c$ is the concentration of insulin in the subcutaneous space. To estimate $PS$, one needs to measure $I$, $V$, and $c$ using microdialysis catheters and $Q$, the plasma flow rate (i.e. 60 % of blood flow rate), using the method described in Appendix A.4 or equivalent.

If microdialysis catheters are properly placed, $I$ and $V$ can be measured. However, we must assume that $c$ is uniform in concentration. At pseudo-steady state this is a good assumption, as the insulin has had time to equilibrate and mix in the ISF compartment. The $PS$ measurements used in our model were taken at steady state by [101].

Lastly, it is worth noting that we are modeling diffusion in both the delivery (plasma to ISF) and the absorption direction (ISF to plasma). $PS$ measurements were taken in the delivery direction. In pure diffusion, mass-transfer is isotropic, but this may not be the case in capillaries, as active transport, facilitated diffusion, or pressure differences may have an effect. However, given the size of the insulin molecule, pure diffusion should be a good assumption, so bi-directional flux should be the case and $PS$ measurements should be valid.

## A.6 Healthy vs. T1D Insulin Response with Exercise

Here we have simulated the interstitial fluid insulin concentration $I_{ISF}$ (same as $S$ from insulin chapter) using measured plasma $I(t)$ as an input. There is a 75 minute bout of exercise from minute 120 to 195. Accounting for the enhanced delivery rate $k_d^I$, you can see that the T1D patient has an increase in $I_{ISF}$ during the exercise period, rather than a decrease in $I_{ISF}$ as in the healthy patient. When insulin comes from endogenous sources, the body can suppress insulin output during exercise, so as to prevent hypoglycemia. This is a demonstration of how the dynamics of insulin are fundamentally different when insulin is injected subcutaneously rather than coming from endogenous sources.

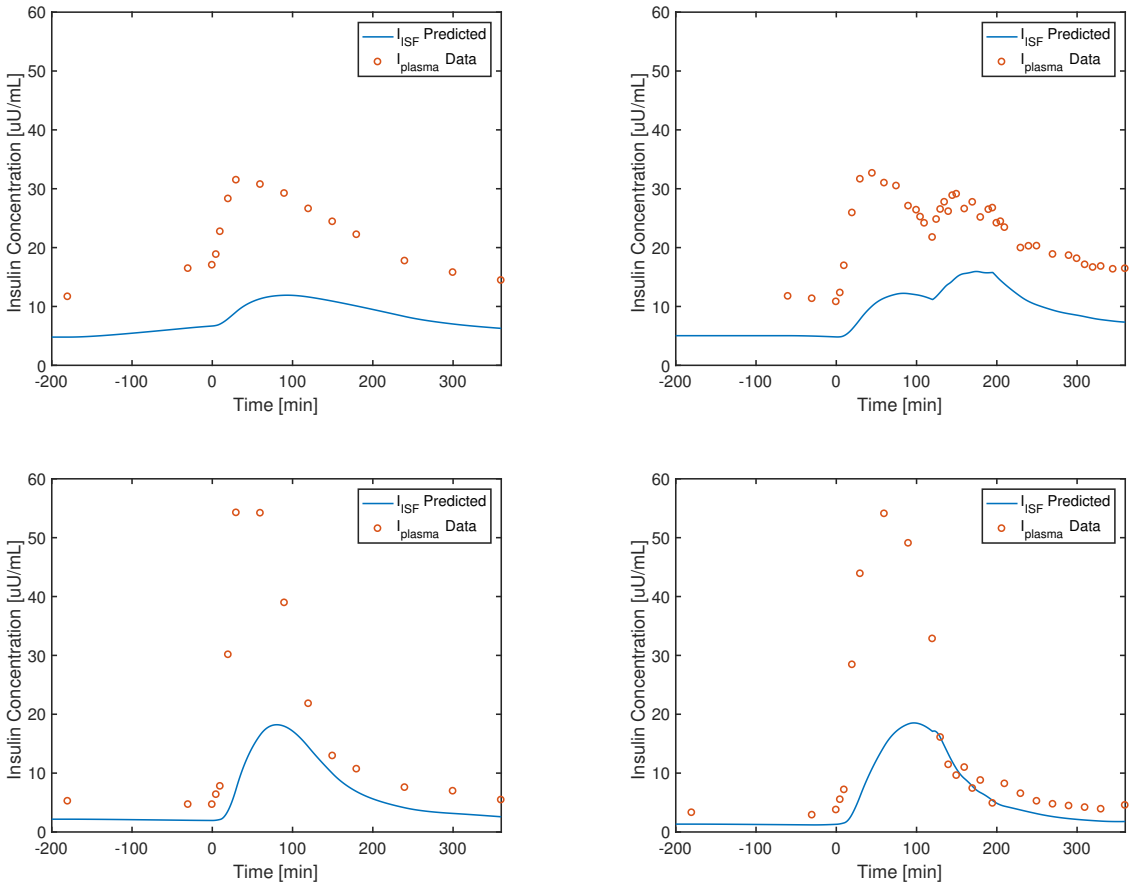


Figure A.1: Predicted interstitial fluid insulin concentration $I_{ISF}$ based on measured $I_{plasma}$ input. Notice that the only case where there is a rise in insulin concentration during exercise is with the T1D patient. No such rise in $I_{ISF}$ is present in the exercising healthy patient. Because $I_{ISF}$ is directly proportional to glucose uptake in the periphery, this is profound result. When insulin is produced endogenously, its release can immediately be suppressed so as not to cause hypoglycemia during exercise, unlike in the T1D patients. (top left) Average T1D patient at rest. (top right) Average T1D patient with exercise from t=120-195 min.(bottom left) Average healthy patient at rest. (bottom right) Average healthy patient with exercise from t=120-195 min. Not that the saw tooth pattern is exactly the opposite in the healthy patient SM insulin than in the diabetic patient SM insulin.

## A.7 Insulin Absorption Rate and Delivery Rate Dependence on Tissue Perfusion Rate

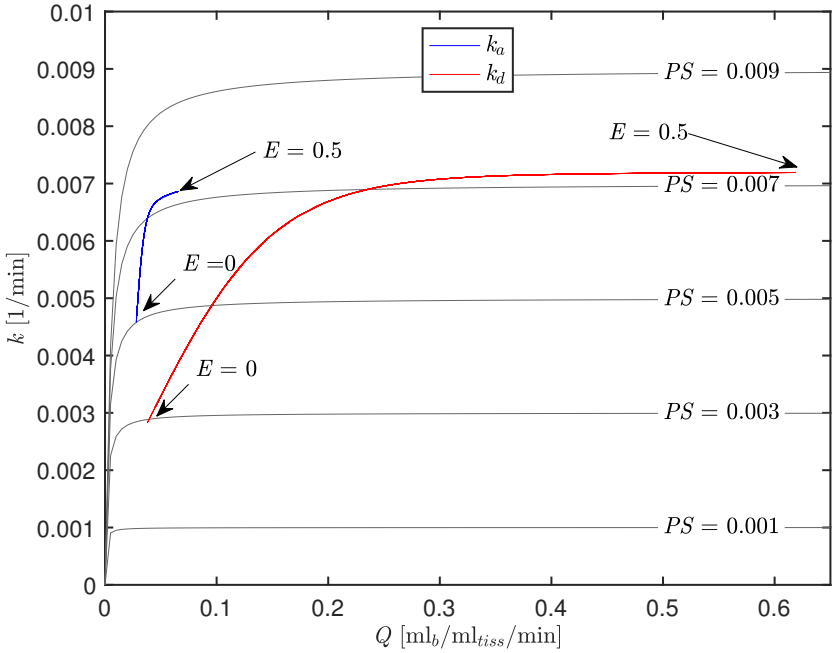


Figure A.2: Absorption/Delivery rate constant dependence on perfusion rate $Q$. The plateau shows that these processes are surface area dependent.

# Appendix B

# A Direct Approach to Assessing Insulin Sensitivity in the Oral Minimal Model

This appendix includes a manuscript that summarizes an alternative method for explicitly calculating insulin sensitivity in the Oral Minimal Model.

# A Direct Approach to Assessing Insulin Sensitivity in the Oral Minimal Model

Spencer T. Frank[1*], Ling Hinshaw[2*], Matthew Johnson[2], Rickey Carter[3], Rita Basu[2], Andrew J. Szeri[1**4], and Ananda Basu[2]

***Abstract*—*Background and Objective:*** **Insulin sensitivity (SI) is a useful index for studying insulin resistance in relation to diabetes. We introduce and validate a direct approach to calculating SI in the oral minimal model.** ***Methods:*** **Using a direct approach an explicit formula for[1] calculating SI is derived. Utilizing data from two experimental protocols SI is calculated and the results are compared to gold-standard SI calculations of Hinshaw and Cobelli. Three arguments for agreement of the two methods are made: (i) Pearson correlation, (ii) discriminative validation and (iii) Spearman rank-ordering correlation.** ***Results:*** **The average insulin sensitivities for the explicit method and the method of Cobelli and co-authors respectively, are 20.0 $\pm$ 2 and 19.0 $\pm$ 2 * 10-4 dL/kg/min per µU/mL for dataset A (A), and 10.3 $\pm$ 0.6 and 8.1 $\pm$ 0.5 * 10-4 dL/kg/min per µU/mL for dataset B (B). The Pearson correlation coefficient, indicating agreement for the two methods, is r = 0.93 (A) and r = 0.92 (B). The Spearman rank-ordering coefficient is rs = 0.93 (A) and rs = 0.91 (B). Additionally, each method has comparable discriminative power as indicated by the area under the curve for a receiving operator characteristic (0.69 vs. 0.67).** ***Conclusion:*** **Agreement between the two methods is excellent for calculating SI in healthy subjects. Moreover, the explicit formula provides a direct interpretation of SI that is mathematically straightforward. With this approach, if rate of meal appearance measurements are available, the important index of SI is more easily assessed in healthy subjects.**

***Keywords*** **—Insulin Sensitivity, Oral Minimal Model, Glucose Kinetics, Mixed Meal Tolerance Test, Diabetes**

SI – Insulin Sensitivity

This work was supported by the National Science Foundation Graduate Research Fellowship Program (S.F.). Studies supported by NIH grants DK 085516 to A.B. , DK 094331 to A.B. and DK 029953 to R.B.

1 Department of Mechanical Engineering, University of California, Berkeley, California 94720, USA
2 Division of Endocrinology, Mayo Clinic, Rochester, MN 55905, USA
3 Division of Biomedical Statistics and Informatics, Mayo Clinic, Rochester, MN 55905, USA
4 Present affiliation: Department of Mechanical Engineering, University of British Columbia, Vancouver, BC V6T 1Z4, Canada
* S. Frank and L. Hinshaw contributed equally to this work
** Corresponding Author: A. Szeri, (email: andrew.szeri@ubc.ca)

## 1. Introduction

THE insulin sensitivity index (SI), which represents insulin's ability to promote whole body glucose uptake and simultaneously suppress endogenous glucose production (EGP), is a very useful proxy for estimating insulin needs in humans[1]. Since the cardinal work of Bergman and Cobelli[2], in which the quantification of SI was first described, the index has been used to great effect, providing insights into how insulin needs change diurnally[3], after exercise[4], and with various hormonal interventions[5]. Additionally, SI has been used to determine the state of a subject's insulin resistance and glucose tolerance, and in turn their risk of developing type 2 diabetes[6]. More recently, SI has been used to improve next generation artificial pancreas control algorithms, allowing the controller to adjust to changes in insulin needs[7]. For its multitude of uses, it is important to be able to quantify SI accurately. One of the hurdles to calculating SI accurately is that a specialized mathematical technique called optimization is needed. For this reason it would be useful to simplify the calculation of SI. This paper focuses on reducing the mathematical complexity typically required to calculate SI.

SI is calculated by fitting a model of insulin-glucose dynamics, the Oral Minimal Model (OMM)[2], [8] to experimental measurements of insulin, glucose, and if available (though not always required), glucose fluxes[2], [6]. The experimental data is obtained from one of several types of glucose tolerance tests: an intravenous glucose tolerance test (IVGTT)[9], an oral glucose tolerance test (OGTT)[10], or a mixed meal tolerance test (MMTT)[8]. In these tests, the idea is to challenge an individual with a glucose load and then observe the dynamic response of insulin and glucose over several hours. This dynamic response is then mathematically interpreted through the OMM to determine SI. A high SI indicates that the individual is effective at utilizing insulin to control glucose concentrations, i.e. glucose tolerant[6] or insulin sensitive. A low SI indicates that the individual does not make effective use of insulin in controlling glucose concentrations (as is typical in type 2 diabetes[11]) i.e. glucose intolerant or insulin resistant.

Unfortunately, there are various technical challenges in accurately obtaining SI from a glucose tolerance test. These manifest themselves into two groups: The first is obtaining accurate measures of glucose flux during the glucose challenge test (some methods do exist for obtaining SI without measuring glucose fluxes[12], [13], but these are mathematically involved and/or have other drawbacks). The technical challenge of measuring glucose fluxes has been largely overcome through advanced isotope dilution techniques that make use of one, two, or three isotopic tracers to obtain increasingly more accurate model-independent[14] measurements of the rates of meal glucose

appearance ($Ra_{meal}$) and glucose disappearance ($R_d$)[14]–[17]. This is done by minimizing changes in the specific activity (SA)[14].

The second challenge is mathematical. The essence of this challenge lies in the difficulty of mathematically fitting the experimental data to a model of insulin-glucose dynamics, such as the OMM, in order to obtain the parameters that make up SI. Indeed, the fact that the OMM is a nonlinear model makes determining SI difficult and is not a trivial mathematical optimization problem.

The present work takes a direct approach to calculating SI so that researchers without access to specialized optimization software can calculate SI straight from experimental measurements. As will be shown, the presented formula is directly derived from the well-studied OMM, and under well-understood conditions provides a highly accurate approximation of SI. The formula requires a measurement of $Ra_{meal}$, far from an easy task[18], but if post-prandial glucose metabolism is already being studied then $Ra_{meal}$ should be an available measurement. This formula would thus be useful in studies of healthy subjects such as [3], [5], [19].

Two datasets (A) and (B) will be used in this study. Each dataset will be used to validate the explicit formula for calculating SI ($SI_{exp}$). The calculated $SI_{exp}$ is compared to previously published values of SI from Hinshaw, Saad and Cobelli ($SI_{Cob}$)[3], [5] that are considered the gold standard. In addition, a previously published method for explicitly calculating SI ($SI_{Caumo}$) from only glucose and insulin measurements[12] will be compared to $SI_{Cob}$. The three methods of calculating SI are compared in three ways: (i) directly through their overall Pearson correlation, (ii) through discriminant validation, and (iii) through Spearman rank-ordering. As will be seen, each of these comparisons show strong agreement between $SI_{exp}$ and $SI_{Cob}$, and somewhat weaker agreement between $SI_{Caumo}$ and $SI_{Cob}$.

This paper is organized as follows: First, a brief description of the OMM is presented to inform the reader what each aspect of the OMM represents. Next, the direct approach to calculating SI is derived with note of the specific assumptions made and their implications on calculation accuracy. The new formula is validated on the two datasets by comparing the resulting $SI_{exp}$ to previously published values of $SI_{Cob}$ and also showing how $SI_{exp}$ typically gives a more accurate result than $SI_{Caumo}$. Lastly, there will be a brief discussion on the strengths and weaknesses of the explicit method with emphasis on how the formula allows for clear and direct interpretation of SI.

## 2. MATERIALS AND METHODS

### *2.1. Subjects and Protocol*

The original subjects were enrolled in a Mayo Clinic Institutional Review Board approved protocol. The data to be analyzed is published in part in Hinshaw and Cobelli[5] (A) and in Saad and Cobelli[3] (B). (A) was of 12 subjects, each undergoing a control test and intervention test to provide paired data for a total of 24 samples. (B) was of 18 subjects, each undergoing three tests at different times of day, for a total of 54 samples. One of the main differences between (A) and (B) is that (A) consisted of a 75g carbohydrate meal and (B) only 50g. Though it is necessary to describe the datasets herein, the objective of this study is to only utilize the data for validation. It is therefore beyond the scope of this work to comment on scientific interpretations and conclusions.

In brief, eligible subjects reported to the Clinical Research Unit of Mayo Clinic in Rochester, MN at 4pm. Demographics and specifics of each protocol are listed in [3] and [5]. A mixed meal (10kcal/kg, 55% carbohydrates, 15% protein, 30% fat) was consumed at approximately 5 PM. No other food was provided until the next morning. An intravenous cannula was inserted into a forearm vein at ~ 8 PM for glucose tracer infusions.

The following morning (day 2), a triple tracer approach was performed as previously reported in [11], [15], [20]. At ~ 6 AM, a cannula was inserted into a hand vein of the contralateral arm for drawing of arterialized venous blood periodically throughout the study for measurements of glucose, glucose tracers, insulin, c-peptide and glucagon concentrations.

At ~7 AM (t=0 min) of day 2 subjects had a mixed meal containing 75 grams of dextrose (A) or 50 grams of dextrose (B) labeled with [1-$^{13}$C] glucose. Blood was frequently sampled from 3 hours before the meal to 6 hours after the meal for measurement of tracer-to-tracee ratios, glucose, and insulin. With the first bite of the meal at time=0, an infusion of [6-$^{3}$H] glucose was started and the rate varied to mimic the anticipated systemic rate of $Ra_{meal}$ for the next 6 hours[15]. At ~1 PM, all infusions were discontinued, the cannulae were removed and the subject was provided lunch.

### *2.2. Analytical Methods*

Insulin was measured with a 2-site electrochemiluminescence immunoenzymatic assay by DxI automated system (Beckman Instruments, Chaska, MN). C-peptide was measured by the Cobas e411 (Roche Diagnostics, Indianapolis, IN) using a 2 site electrochemiluminescence immunometric assay. Glucagon was measured with a direct, double

antibody radioimmunoassay (Linco Research, St. Charles, MO). Plasma samples were placed on ice, centrifuged and then separated and stored at -80ºC until assay. Plasma glucose concentration was measured using a glucose oxidase method (YSI, Inc., Yellow Springs, OH). Plasma [6-$^{3}$H] glucose SA was measured by liquid scintillation counting as described in [11]. Plasma enrichment of [1-$^{13}$C] glucose was measured using GCMS (Thermoquest, San Jose, CA) as described in [15]. Plasma glucose and insulin concentrations are shown for both datasets in Fig. 1(a,b,d,e).

*2.3. Estimation of Fluxes*

Fasting and postprandial rates of glucose turnover were calculated as described in [15] using the triple-tracer technique. The systemically infused [6-$^{3}$H] glucose was used to trace the systemic rate of appearance of [1-$^{13}$C] glucose contained in the meal. SA(t) (Specific activity i.e. ratio of plasma concentration of [6-$^{3}$H] glucose to [1-$^{13}$C] glucose) was used to calculate $Ra_{13C}$, the rate of appearance of ingested [1-$^{13}$C] glucose[17],

$$Ra_{13C}(t) = \frac{INF_{3H}(t)}{SA(t)} - \frac{p \cdot V_d \cdot G_{13C}(t)}{SA(t)} \cdot \frac{d\,SA(t)}{dt}, \quad (1)$$

where $INF_{3H}$ is the infusion rate of [6-$^{3}$H] glucose, $G_{13C}$ is the plasma concentration of [1-$^{13}$C] glucose, $V_d$ is the volume of distribution per body weight (fixed to 200 mL/kg$_{BW}$) times the subject's bodyweight, and p is the pool fraction, 0.65. The total rate of appearance of meal glucose can be calculated as

$$Ra_{meal}(t) = Ra_{13C}(t) \cdot \left(1 + \frac{1}{TTR_{meal}}\right), \quad (2)$$

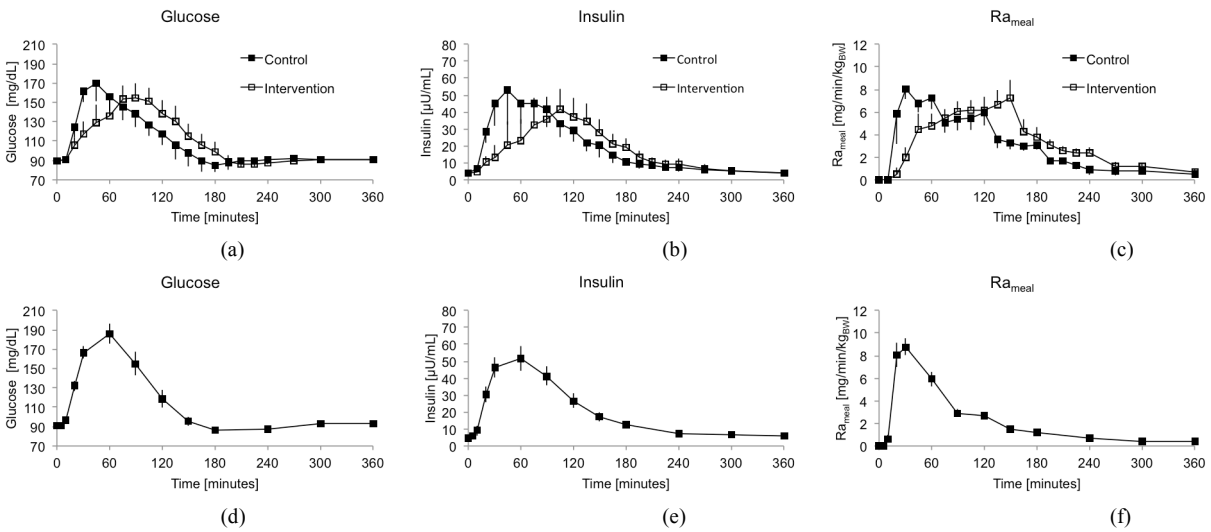


Fig. 1. *Measured Inputs and Outputs*. Average measured glucose concentration (a,d), insulin concentration (b,e), and calculated $Ra_{meal}$ (c,f) vs. time for (A) (a,b,c) and (B) (d,e,f). 95% confidence interval are shown as error bars. Dataset (A) is a paired study with each subject undergoing a control and intervention test, and will be used for discriminative validation of the explicit method. Both datasets (A) and (B) will we used for validation through a Pearson and Spearman correlation analysis.

where $TTR_{meal}$ is the ratio of [1-$^{13}$C] glucose to unlabeled glucose in the meal. $Ra_{meal}$ is shown in Fig. 1(c,f).

Even though the data presented utilizes a triple-tracer protocol, the measurement of $Ra_{meal}$ using the dual-tracer method would be similar if the systemic tracer is infused to mimic the absorption of the ingested glucose. Thus the methodology described in this paper is equally useful for dual-tracer and triple-tracer techniques.

### *2.4. Statistics*

Statistics are presented (with noted exceptions where standard deviation (SD) is used) as the sample mean $\pm$ standard error of the mean (SEM). In the figures 95% confidence intervals (CI) of SEM are used. A student's t-test was used for statistical analysis.

## *3. Theory and Calculation*

### *3.1. The Oral Minimal Model – A Brief Description*

The oral minimal model (OMM)[6] is a model of insulin-glucose dynamics that can be used to assess a patient's SI from a glucose tolerance test. It is a nonlinear lumped parameter model of whole body glucose metabolism, and is made up of two equations. Equation (3) is a single compartment model that governs insulin action (X). X can be thought of as a variable rate constant (1/min are the units) that describes the ability of insulin to promote glucose uptake and suppress glucose production. Equation (4) is a single compartment model that governs glucose dynamics in plasma. The equations and their initial conditions (unperturbed insulin and glucose concentrations) are

$$\frac{dX}{dt} = -p_2 X + p_3 (I - I_b) \qquad X(0) = 0 \quad , (3)$$

$$\frac{dG}{dt} = -S_G (G - G_b) - XG + \frac{Ra_{meal}}{V} \qquad G(0) = G_b \quad , (4)$$

where the variables are X and glucose concentration in plasma (G). The inputs are the measured insulin concentration in plasma (I) and the rate of meal appearance ($Ra_{meal}$). The constants are basal glucose concentration ($G_b$) in plasma, basal insulin concentration ($I_b$) in plasma, glucose effectiveness ($S_G$), i.e. the ability of glucose itself to promote glucose uptake and suppress its own production per volume of distribution (here set to a population average value of $S_G$=0.014 1/min[8]), and V is the volume of distribution of glucose in the body (here set to a population average value of V=1.7 dL/$kg_{BW}$ [8]). The parameters $p_2$ and $p_3$ are also treated as constants, however they are unknown and to-be-determined. The ratio of $p_3$ to $p_2$ times the volume of distribution V, define whole-body SI

$$S_I = \frac{p_3}{p_2} V \quad . (5)$$

The units of SI are dL/kg/min per μU/mL. The parameter can be defined as the insulin action per unit insulin concentration. A more specific SI definition will be presented in the discussion. It is the objective of this paper to provide a simplified means of calculating SI by a direct approach.

### *3.2. Method 1: Previously Published Values of SI via Cobelli's Method ($SI_{Cob}$)*

Cobelli and co-authors have published and validated $SI_{Cob}$ values in a number of studies[2], [3], [8], [12], [13]. Thus the values of SI obtained by Cobelli ($SI_{Cob}$) are considered the standard and will be used to validate the $SI_{exp}$ that is calculated using the explicit formula derived in this paper. The values of $SI_{Cob}$ presented here come from two previously published studies[3], [5].

Cobelli and co-authors use a nonlinear least squares optimization procedure to obtain $SI_{Cob}$. Additionally, Cobelli

preprocesses the data prior to the optimization procedure, using deconvolution and other techniques ([21], [22]) to correct for measurement errors that result from the rapid change in glucose flux at the beginning of a meal. This rapid change often results in moderate overestimation of $Ra_{meal}$. In these cases the fraction of absorbed glucose (integral of $Ra_{meal}$ over the total ingested glucose) is greater than one, which is not possible. Cobelli and co-authors correct for this overestimation and as such $SI_{Cob}$ is typically lower than the resulting SI if the data were not preprocessed. The data used in this study to calculate $SI_{exp}$ was not preprocessed and as such their values are systematically higher than $SI_{Cob}$, as will be shown.

### *3.3. Method 2: SI obtained via Direct Approach ($SI_{exp}$, i.e. Explicit Method)*

An explicit formula to calculate SI, we call $SI_{exp}$, is now derived. The benefit of this formula is $SI_{exp}$ can be calculated directly from experimental measurements, with no need for optimization techniques.

The following derivation follows work presented by Caumo et al.[12], but rather than making an assumption about the form of $Ra_{meal}$ as Caumo et al. did, we have assumed that measurements for $Ra_{meal}$ are available. For brevity, the details of the derivation are in the appendix. Here, only the main steps will be demonstrated.

We start by integrating (3) from time 0 to the final time $t_f$

$$X(t_f) - X(0) = -\int_0^{t_f} p_2 X(t)\,dt + \int_0^{t_f} p_3 (I(t) - I_b)\,dt \,. \quad (6)$$

We apply the initial condition X(0)=0 and then assume that $p_2$ and $p_3$ are constants in time (as is typical). Multiplying our equation by V, we can then algebraically rearrange to obtain an expression for full body SI as

$$SI = \frac{\dfrac{V \cdot X(t_f)}{p_2} + V\int_0^{t_f} X(t)\,dt}{\int_0^{t_f} \Delta I(t)\,dt} \,, \quad (7)$$

where $\Delta I(t) = I(t) - I_b$. Now, in order to make use of this expression we need to be able to evaluate the integral of *X*. To this end we rearrange (4) as

$$XG = \frac{Ra_{meal}}{V} - S_G(G - G_b) - \frac{dG}{dt} \quad . \quad (8)$$

Then dividing through by G (which never goes to 0), and integrating the expression in time from 0 to $t_f$ yields

$$\int_0^{t_f} X dt = \int_0^{t_f} \frac{Ra_{meal}}{V \cdot G} dt - \int_0^{t_f} \frac{S_G \Delta G}{G} dt - \int_0^{t_f} \frac{1}{G} \frac{dG}{dt} dt \quad , (9)$$

where $\Delta G = G(t) - G_b$. This expression for the integral of X is then substituted into (7). We assume that $S_G$ and V are constant in time, then after algebraically rearranging the resulting equation we obtain

$$SI = \frac{\frac{V \cdot X(t_f)}{p_2} + \int_0^{t_f} \frac{Ra_{meal}}{G} \, dt - V \cdot S_G \int_0^{t_f} \frac{\Delta G}{G} \, dt - V \cdot \ln \frac{G(t_f)}{G(0)}}{\int_0^{t_f} \Delta I \, dt} \quad . \quad (10)$$

The last part of the derivation is to find an expression for the unknown $X(t_f)$, to do this we solve (3) using the method of variation of parameters (see appendix for details). The solution to (3) evaluated at the final time $t_f$ is

$$X(t_f) = p_3 \int_0^{t_f} e^{p_2(t - t_f)} \Delta I \, dt \quad (11)$$

Finally, we can substitute (11) into (10), and algebraically solve for SI to obtain the expression

$$SI = \frac{\int_0^{t_f} \frac{Ra_{meal}}{G} \, dt - V \cdot S_G \int_0^{t_f} \frac{\Delta G}{G} \, dt - V \cdot \ln \frac{G(t_f)}{G(0)}}{\int_0^{t_f} \Delta I \, dt - \int_0^{t_f} e^{p_2(t - t_f)} \Delta I \, dt} \quad . \quad (12)$$

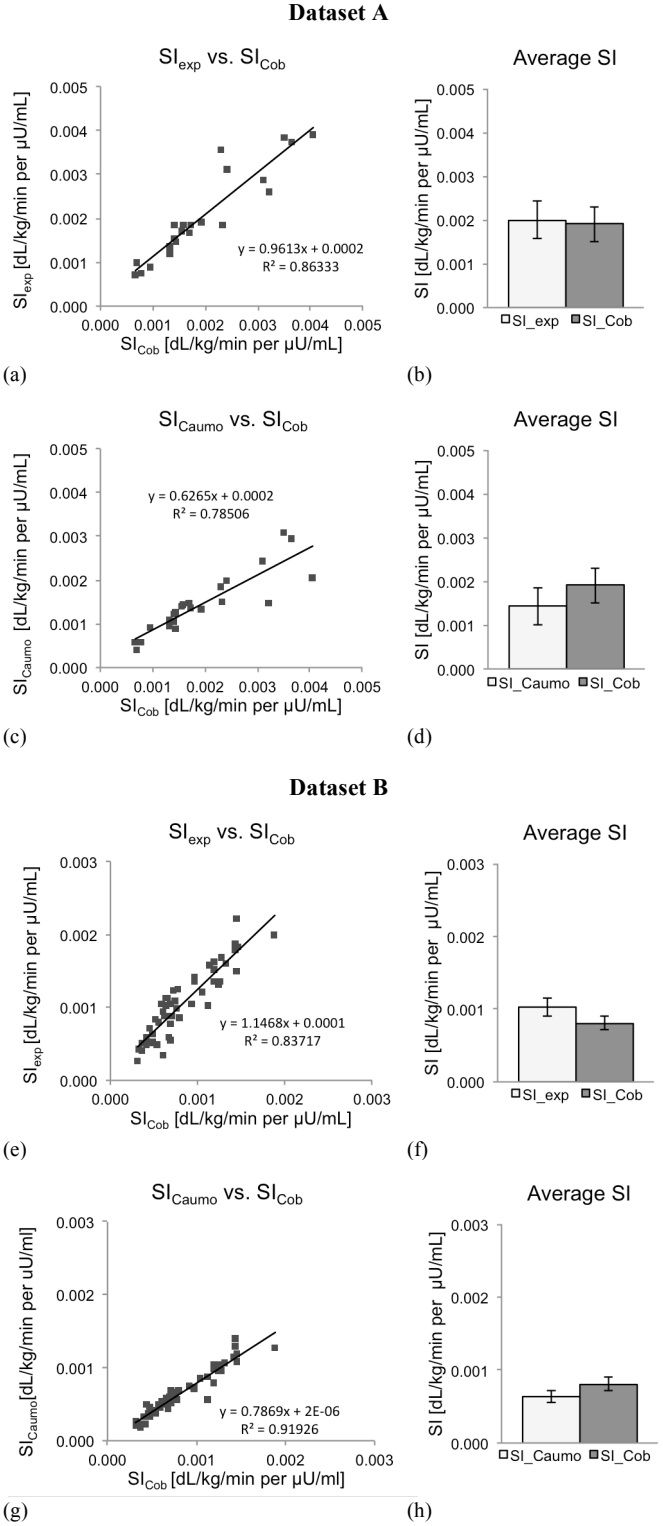


Fig. 2. *SI Comparisons for the Various Methods.* Comparison of $SI_{exp}$ to the published values of $SI_{Cob}$ from [3] and [5] for (A) (a,b) and (B) (e,f), and comparison to calculated $SI_{Caumo}$ for (A) (c,d) and (B) (g,h). The average SI for each method is plotted with the standard deviation indicated. 95% CIs are shown. Of note is that $SI_{exp}$ agrees better with $SI_{Cob}$ for dataset (A) (a slope near 1 and high $R^2$), but $SI_{Caumo}$ has a higher correlation with $SI_{Cob}$ in dataset (B). The slope for $SI_{Caumo}$ is 0.63 and 0.78, indicating significant

At this point, we have yet to make any approximations, and as such our expression is exact for determining SI. However, in order to obtain an *explicit* expression for SI - that is an expression that can calculate SI from measured, known values only - it is necessary to make some assumptions about the only unknown parameter, $p_2$. In the appendix, it is shown that for typical values of $p_2$, the second term in the denominator of (12) is typically small compared to the first term. Physiologically this is the case because insulin is no longer active in the system 6 hours after meal ingestion. With this argument we neglect the second term and obtain the fully explicit definition for SI, which we call $SI_{exp,}$

$$SI_{\exp} = \frac{\int_0^{t_f} \frac{Ra_{meal}}{G}\, dt - V \cdot S_G \int_0^{t_f} \frac{\Delta G}{G}\, dt - V \cdot \ln \frac{G(t_f)}{G(0)}}{\int_0^{t_f} \Delta I\, dt} \quad (13)$$

A second approximation further simplifies the expression; given that in healthy subjects glucose levels are nearly the same at the beginning and the end of the test, $G(t_f) \approx G(0)$ and $\ln(G(t_f)/G(0)) \approx \ln(1) = 0$. Thus we may neglect the third term in the numerator of (13)

$$SI_{\exp} = \frac{\int_0^{t_f} \frac{Ra_{meal}}{G} dt - V \cdot S_G \int_0^{t_f} \frac{\Delta G}{G} dt}{\int_0^{t_f} \Delta I\ dt} \quad (14)$$

Equation (14) allows for SI to be calculated only from known, measured values. This is an alternative convenient method for calculating SI, not requiring mathematical optimization techniques or computer solutions to differential equations. To calculate SI one needs to only carry out three integrals of the measured data. This can be done using the trapezoidal or midpoint rule (see worked example in supplementary material referenced in appendix).

In using this simplified formula, it is necessary to understand the potential for error. In Appendix C an error formula is derived to estimate the upper bound of the error from the true value of SI (12). It is shown that for typical parameter values, the error incurred through this approximate formula is less than 10%. However the error will be small only under specific conditions and assumptions, namely:

1. 6 hours of observation are allotted after the ingestion of the meal. This ensures that G(t) and X(t) return to basal prior to the cessation of the study. (i.e. G returns to $G_b$ and X returns to 0)
2. Subjects are healthy (non-diabetic) individuals.
3. Subjects are not undergoing significant physical activity during the test.
4. Mixed meal contains $\leq$ 75g carbohydrates with similar composition as [3], [5].

If these conditions and assumptions are not met, the explicit formula may not be accurate.

### 3.4. Method 3: SI obtained via Caumo Method ($SI_{Caumo}$)

An explicit formulation for calculating SI was derived by Caumo ([12] Equation VII). This formula has the benefit of not requiring the measurement of $Ra_{meal}$. Rather a form for $Ra_{meal}$ is assumed, and it depends only on glucose. This assumption makes the measurement of SI very easy, as the difficult, expensive, and time-consuming tracer methodology to measure $Ra_{meal}$ is avoided.

However, there is a drawback to the Caumo method; calculation of SI can be skewed because the measured $Ra_{meal}$ is not closely approximated by the assumed form given by Equation III in [12]. The consequences of this will be discussed in the Results and Discussion sections.

## 4. RESULTS

In order to validate $SI_{exp}$, three arguments are made in what follows. First, overall agreement is indicated with simple linear regression plots. Next, discriminative validation between the control and intervention group of dataset (A) is carried out by comparing the receiver operating characteristic (ROC) curve of the three methods. Lastly, a rank-ordering of the resulting SI is plotted to indicate that the explicit method preserves rank-order compared to Cobelli's method.

### 4.1. Pearson Correlation of the Methods

$SI_{exp}$ is calculated using the explicit formula Equation (14) derived in the Section 3.3. for the 24 samples in (A) and for the 54 samples in (B). $SI_{Caumo}$ is calculated as described by Equation VII in [12]. The resulting SI values from these three methods are compared in Fig. 2, with the statistics shown in Table I.

From Fig. 2 it can be seen that the agreement between $SI_{exp}$ and $SI_{Cob}$ is strong indicated by a high correlation coefficient, r = 0.93 (A) and r = 0.92 (B). The coefficient of determination values are $R^2 = 0.86$ (A) and $R^2 = 0.84$ (B). The slope of each regression is m = 0.96 (A) and m = 1.15 (B). However, there are a few samples that show large discrepancy in Fig. 2a, and upon further examination this was found to be due to overestimation of $Ra_{meal}$. This observation will further explored in the discussion.

TABLE I
STATISTICS OF SI FOR THE THREE METHODS

| | Dataset A | | | Dataset B | | |
|---|---|---|---|---|---|---|
| | $SI_{exp}$ | $SI_{Cob}$ | $SI_{Caumo}$ | $SI_{exp}$ | $SI_{Cob}$ | $SI_{Caumo}$ |
| Mean SI | 20.0 | 19.0 | 14.3 | 10.3 | 8.1 | 6.4 |
| Standard Deviation (SD) | 10.0 | 9.6 | 6.8 | 4.7 | 3.8 | 3.1 |
| Coefficient of Variation (CV) | 0.50 | 0.51 | 0.48 | 0.46 | 0.46 | 0.48 |
| Standard Error of Mean (SEM) | 2 | 2 | 1.4 | 0.6 | 0.5 | 0.4 |

Units of all quantities are $10^{-4}$ dL/kg/min per μU/mL (CV excepted)

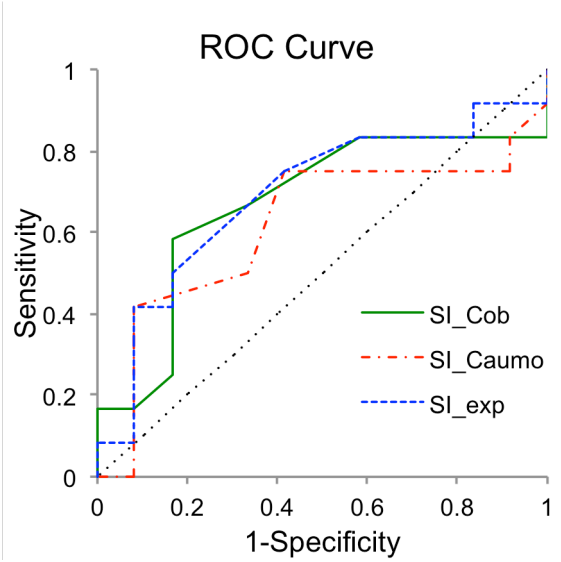


Fig. 3. *Receiver Operator Characteristic (ROC) Curves.* ROC curves for each method applied to dataset (A) as a test to discriminate between a control and intervention subject, based only on the magnitude of SI. The AUCs of the Cobelli, Caumo, and explicit methods are 0.67, 0.61, and 0.69, respectively. Notice the AUC of the Cobelli and explicit methods are very close, and significantly greater than the Caumo method, indicating superior discriminative power. The diagonal dotted line represents a random test.

In comparing $SI_{Caumo}$ to $SI_{Cob}$ we see that there is a strong correlation with an r = 0.89 (A) and r = 0.96 (B) and $R^2$ = 0.79 (A) and $R^2$ = 0.92 (B). However, for each dataset the slope of the linear regression is only m = 0.63 (A) and m = 0.78 (B), indicating that although the correlation between the two methods is strong, the overall agreement is still weak in comparison to the slope obtained from comparing $SI_{exp}$ which is closer to 1 for both datasets.

### *4.2. Discriminative Validation*

Dataset (A) is made up of a control and intervention group. To test the ability of each method to discriminate between control and intervention subjects the receiving operator characteristic (ROC) curves are plotted in Fig. 3. The curves of the three methods follow a similar trajectory, and importantly are both well above the diagonal line; this demonstrates that there is indeed a discernable difference from the control to the intervention group, consistent with the conclusions in [5]. To quantify discriminative power, the area under the curve (AUC) of the ROC curve is calculated. The AUC is 0.69 for $SI_{exp}$, 0.67 for $SI_{Cob}$, and 0.61 for $SI_{Caumo}$. The discriminative powers of $SI_{exp}$ and $SI_{Cob}$ are similar, and both are superior to $SI_{Caumo}$.

### *4.3. Rank-Ordering*

The rank-ordering of SI for only $SI_{exp}$ and $SI_{Cob}$ is shown in Fig. 4, along with the squared Spearman rank-ordering coefficient, $R_s^2$. There is a high Spearman correlation with each dataset, $r_s$ = 0.93 (A) and $r_s$ = 0.91 (B). The squared Spearman coefficient of determination is $R_s^2$ = 0.87 (A) and $R_s^2$ = 0.82 (B), indicating that the rank-ordering is mostly preserved regardless of the method used. This ranking provides further evidence of the validity of $SI_{exp}$.

## 5. DISCUSSION

A direct approach was used to reduce the complexity typically necessary to calculate SI. Because this is a new alternative method of calculation it is necessary to validate $SI_{exp}$ vs. the gold standard of calculating SI ($SI_{Cob}$). In

addition we have compared $SI_{Caumo}$, a method similar to $SI_{exp}$, to $SI_{Cob}$ in order to show how $SI_{exp}$ is an improvement over $SI_{Caumo}$.

A summary of the resulting statistics is shown in Table I. From this table it is clear that $SI_{exp}$ and $SI_{Cob}$ produce values of SI that are in high agreement. For (A) $SI_{exp} = 20 \pm 2 \bullet 10^{-4}$ dL/kg/min per μU/mL and $SI_{Cob} = 19 \pm 2 \bullet 10^{-4}$ dL/kg/min per μU/mL, with CVs of 0.50 and 0.51, respectively. (B) shows similar agreement; $SI_{exp} = 10.3 \pm 0.6 \bullet 10^{-4}$ dL/kg/min per μU/mL and $SI_{Cob} = 8.3 \pm 0.5 \bullet 10^{-4}$ dL/kg/min per μU/mL, with both CVs = 0.46. This agreement is further indicated by a high Pearson correlation coefficient of r = 0.93 (A) and r = 0.92 (B) and also the slope is close to 1 for both datasets.

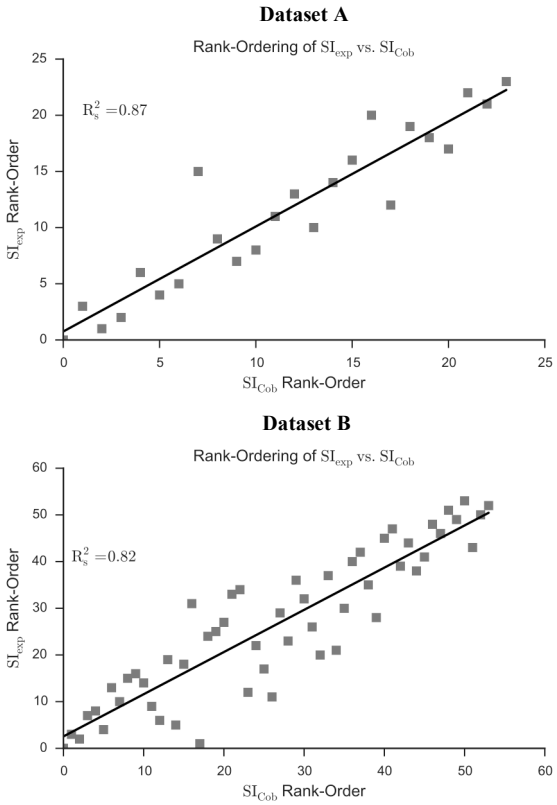


Fig. 4. *Rank-ordering Comparison of the Cobelli and Explicit Methods for Both Datasets*. The Spearman rank-ordered correlation coefficient is $r_s = 0.93$ (A) and $r_s = 0.91$ (B), their squared values are shown above. The strong correlation indicates that rank-ordering is mostly preserved for the explicit method ($SI_{exp}$) as compared to Cobelli's method ($SI_{Cob}$), further validating the explicit method.

$SI_{Caumo}$ produces values of SI that have questionable accuracy compared to $SI_{Cob}$. Though, $SI_{Caumo}$ has a high correlation with $SI_{Cob}$ at r = 0.89 and r = 0.96 for (A) and (B), respectively (Fig. 2c and 2g), the slope of the linear regression is less than 0.8 for both of these datasets, and only 0.63 for (A) indicating a significant underestimation of SI.

The rank-ordering (Fig. 4) for $SI_{Cob}$ and $SI_{exp}$ paints a similar picture, with a Spearman correlation coefficient of $r_s = 0.93$ (A) and $r_s = 0.91$ (B). This indicates that rank-ordering is mostly preserved when $SI_{exp}$ is use in place of $SI_{Cob}$.

To validate further we performed a discriminative analysis of each method using the control and intervention groups in (A). The most commonly used plot for analyzing discriminative power is the receiver operator characteristic (ROC) curve. The curves for the three methods are shown in Fig. 3. Each ROC curve represents the tradeoff between true positive rate (or sensitivity) and false positive rate (1-specificity). In the case of our dataset, each curve conveys the ability of a particular method to discriminate between a subject from the control group and a subject from the intervention group. The curves can be compared to the dotted diagonal line, which indicates the

discriminative power of random guessing, i.e. a useless test. Because the three methods fall above the diagonal line, they all possess discriminative power over random guessing, as is expected. The AUCs of each of the methods are 0.69 and 0.67 for $SI_{exp}$ and $SI_{Cob}$, respectively. The AUC of $SI_{Caumo}$ is only 0.61, a significant decrease from the other two methods.

Given that the explicit and Cobelli methods exhibits similar values of SI, similar discriminative power, and similar rank-ordering, we may conclude that these two methods are can be interchanged as a means to calculate SI in healthy subjects. Because $SI_{Caumo}$ has inferior agreement with $SI_{Cob}$ compared to $SI_{exp}$ and has lower discriminative power, we can further conclude that $SI_{exp}$ is superior to $SI_{Caumo}$. One of the potential reasons that $SI_{Caumo}$ gives inferior results is because the assumed $Ra_{meal}$ waveform from Equation III in [12]. This waveform does not capture the blunted $Ra_{meal}$ that is present in larger meals (75g) as in dataset (A) (shown in Fig. 1a).

The explicit formula has been shown to give accurate values of SI; however, the formula should not be used blindly. There are a few important assumptions made for it to be valid. The most important assumption is that X falls back to nearly 0 prior to the termination of the test. Because we do not calculate X(t) when using the explicit formula, we have no way of knowing with certainty that this will always be the case, however under the same conditions of the data presented, the error should be similarly small as the results obtained here. The specific conditions of the MMTT datasets were as follows: (i) 6 hours of observation were allotted after the ingestion of the meal, (ii) Subjects were healthy individuals, (iii) Subjects were not undergoing significant physical activity during the test, (iv) Mixed meal contained $\leq$ 75g carbohydrates and consists of 10kcal/kg, 55% carbohydrates, 15% protein, 30% fat as per [3], [5]. For meals of small size with a lower fat or protein content, the formula should also be valid, assuming that the rate of digestion is as fast or faster than the 75g mixed meal administered here. A minimum of two tracers[16] should be utilized in the measurement of $Ra_{meal}$ to ensure accuracy, as SI is very sensitive to this measurement. In general, this explicit formula would be useful in studies of healthy subjects such as [3], [5], [19].

Until further validation is performed, the explicit formula is discouraged from being used for tests other than MMTT. Validation work would need to be carried out before the formula could be used for an Oral Glucose Tolerance Test (OGTT). Additionally, it is expected that the formula would be less accurate if it were used with data from a diabetic subject, as typically glucose and insulin levels do not fall back to basal as quickly as in healthy subjects. This observation may invalidate the assumption that X returns to 0 prior to the cessation of the observation. Conveniently, if one wishes to check for the potential of error given insulin concentration measurements, an

equation for estimating error is in the appendix (A22). This formula may be used as guidance as to whether error incurred from the use of the explicit method will be significant.

Even though there is strong agreement between $SI_{exp}$ and $SI_{Cob}$, it is worth mentioning that some samples do show a discrepancy and on average $SI_{exp}$ is higher than $SI_{Cob}$, especially in (B). This discrepancy can be attributed largely to the lack of data preprocessing; not having to do with the method of calculating SI or a violation of assumptions (returning to basal), but rather with a change in the input data. $Ra_{meal}$ is often overestimated even when great care is taken and multiple tracers are used in an attempt to measure fluxes as accurately as possible[15]. The overestimation is due to an imperfect tracer clamp, which results in non-constant specific activity of tracers[14]. The error is apparent when looking at f, the fraction of ingested glucose that is actually absorbed[8]. f is defined as the integral of $Ra_{meal}$ during the test, divided by the meal dose. For (A), $f = 1.02 \pm 0.18$ (SD). In (B) f was much greater, with $f = 1.15 \pm 0.19$ (SD). Because f can not possibly be more than 1 (and typically $f \approx 0.9$ is thought to be true[8], [23]), this indicates that in many samples $Ra_{meal}$ was overestimated. For these cases preprocessing[21], [22] the data to correct for overestimation would increase the accuracy of quantifying SI. This likely explains the discrepancies seen between $SI_{exp}$ and $SI_{Cob}$. Particularly in (B), f is on average 28% greater than a nominal f of 0.9. This directly explains why $SI_{exp}$ is 25% larger than $SI_{Cob}$. In fact when using nonlinear least-squares optimization to calculate SI (not-shown) without data preprocessing, there was almost perfect agreement ($R^2 = 0.98$) with $SI_{exp}$ confirming that the discrepancies are due to data preprocessing rather than error incurred from approximations made in the explicit method.

Although there may be a benefit in preprocessing data to correct for overestimation of glucose fluxes (and other measurements), the objective of this study is to provide a formula that reduces the complexity of calculating SI. It would thus be beyond the scope of this study to introduce complex data preprocessing techniques on the inputs. Undoubtedly preprocessing may help reduce measurement error and researchers are encouraged to minimize the error of the inputs (G, I, $Ra_{meal}$) before utilizing the formula.

There are some clear benefits to utilizing the formula, yet there are also some weaknesses. First, if glucose absorption or X is slow in a given test, then assumptions may be violated, introducing error. This type of error would not be as large when using optimization methods (as in $SI_{Cob}$). Additionally, if the actual value of the parameters $p_2$ and $p_3$ are desired, rather than just their ratio (i.e. SI), they cannot be acquired from the explicit method. Still, if proper care is taken to ensure that assumptions are not violated, and if the actual value of $p_2$ and $p_3$ are not needed,

then the explicit formula provides a means to assess SI that is mathematically direct and highly accurate.

There are also indirect benefits of using the explicit method, particularly with regard to interpreting the meaning of the index SI. When looking at the OMM, it is not immediately clear what the parameters $p_2$ and $p_3$ mean, and why the ratio of them is important enough to give a name, insulin sensitivity. In our algebraic manipulations, we have expressed the definition of SI in a very direct form, allowing for direct interpretation. To facilitate this interpretation, it is illustrative to consider again (7) (with the first term neglected), and multiply it by $1/t_f$

$$SI_{\exp} = \frac{V\dfrac{1}{t_f}\displaystyle\int_0^{t_f} X(t)\,dt}{\dfrac{1}{t_f}\displaystyle\int_0^{t_f} \Delta I\,dt} \quad .(15)$$

Equation (15) illustrates mathematically the definition of $SI_{exp}$ – it is the time-averaged X divided by the time-averaged plasma insulin concentration above baseline. More succinctly, it is the total effect of insulin over the total amount of insulin above basal, for a particular meal.

We may obtain further understanding of the meaning of SI by re-examining the glucose dynamics (8). Because the OMM glucose dynamics define the insulin effect (XG) to be linearly proportional to the glucose concentration, we may divide through by glucose concentration to obtain the insulin effect per unit glucose concentration, i.e. the well-known 'insulin action (X)'

$$X = \frac{1}{G}\left(\frac{Ra_{meal}}{V} - S_G(G - G_b) - \frac{dG}{dt}\right) \quad (16)$$

By integrating this equation over the total meal duration we obtain the 'total insulin action'

$$\int_0^{t_f} X\,dt = \int_0^{t_f} \frac{1}{G}\left(\frac{Ra_{meal}}{V} - S_G(G - G_b)\right)dt \quad (17)$$

Finally, substituting into (15) we get (identical to (14))

$$SI_{\exp} = \frac{\frac{1}{t_f}\int_0^{t_f} \frac{1}{G}\left(Ra_{meal} - S_G \cdot V \cdot \Delta G\right) dt}{\frac{1}{t_f}\int_0^{t_f} \Delta I \; dt} \quad . \quad (18)$$

This definition precisely states that SI is equal to the time-averaged exogenous glucose absorbed per unit glucose minus the glucose effectiveness per unit glucose all divided by the time-averaged insulin concentration above baseline. This interpretation is consistent with the definition of SI from the literature, and as defined in Section 3.1. This direct interpretation is an added benefit of our explicit expression of SI.

## 6. CONCLUSION

A direct approach that yields an explicit formula (14) to calculate insulin sensitivity is derived and validated. We have shown that for two datasets consisting of healthy subjects undergoing a mixed meal tolerance test the explicit formula gives accurate results that are comparable with gold-standard published values of insulin sensitivity. Additionally, we have shown that the explicit method is superior to a comparable explicit method of calculation previously published. To prevent pitfalls of utilizing the explicit formula it is important that care is taken to ensure certain assumptions are valid during the test; typically 360 minutes of observation are required after the ingestion of a meal. In summary, the explicit formula clearly interprets insulin sensitivity and provides an accurate and direct alternative calculation method for healthy subjects undergoing glucose tolerance tests.

## APPENDIX

### *A. Example Calculation and Matlab Script*

An example calculation and Matlab Script for calculation of $SI_{exp}$ via Equation (14) can be found at the repository: TBD

### *B. Detailed Derivation of $SI_{exp}$*

The Oral Minimal Model (OMM) is

$$\frac{dX}{dt} = -p_2 X + p_3(I - I_b) \qquad X(0) = 0 \quad , \quad \text{(A1)}$$

$$\frac{dG}{dt} = -S_G(G - G_b) - XG + \frac{Ra_{meal}}{V} \qquad G(0) = G_b \quad . \quad \text{(A2)}$$

We start with the insulin action equation (A1) of the OMM and integrate it from time 0 to the final time ($t_f$):

$$\int_0^{t_f} \frac{dX}{dt} dt = \int_0^{t_f} -p_2 X + p_3 (I - I_b) dt \quad , \tag{A3}$$

$$X(t_f) - X(t_0) = \int_0^{t_f} -p_2 X + p_3 (I - I_b) dt \quad . \tag{A4}$$

We set $X(t_0)$ to 0 (as defined by the initial condition X(0)=0) and assume that $p_2$ and $p_3$ are constants in time (as is typically assumed), and rewrite this equation as

$$X(t_f) = -p_2 \int_0^{t_f} X + p_3 \int_0^{t_f} \Delta I \, dt \quad , \tag{A5}$$

where $\Delta I = I(t) - I_b$. A rearrangement yields

$$\frac{p_3}{p_2} = \frac{\frac{X(t_f)}{p_2} + \int_0^{t_f} X \, dt}{\int_0^{t_f} \Delta I \, dt} \quad . \tag{A6}$$

Finally, we multiply (A6) by the volume of distribution V to obtain an expression for SI in terms of V, X, $p_2$, and $\Delta I$,

$$SI = \frac{p_3}{p_2} V = \frac{\frac{V \cdot X(t_f)}{p_2} + V \int_0^{t_f} X \, dt}{\int_0^{t_f} \Delta I \, dt} \quad . \tag{A7}$$

Now, in order to make use of this expression we need to be able to evaluate the integral of X. To this end we rearrange our glucose equation (A2)

$$XG = \frac{Ra_{meal}}{V} - S_G (G - G_b) - \frac{dG}{dt} \quad . \tag{A8}$$

Then we divide through by G (which never goes to 0), and integrate the expression from 0 to $t_f$ to obtain

$$\int_0^{t_f} X dt = \int_0^{t_f} \frac{Ra_{meal}}{V \cdot G} dt - \int_0^{t_f} \frac{S_G \Delta G}{G} dt - \int_0^{t_f} \frac{1}{G} \frac{dG}{dt} dt \quad . \tag{A9}$$

Note that $\Delta G = G(t) - G_b$. Now we have an expression for the integral of X and can substitute it into our expression SI in (A7). Also, we assume that V and $S_G$ are constant in time, and utilize the identity $1/G \, dG/dt = d \ln(G)/dt$ where ln is the natural logarithm. The resulting expression is

$$SI = \frac{\frac{V \cdot X(t_f)}{p_2} + \int_0^{t_f} \frac{Ra_{meal}}{G} \, dt - V \cdot S_G \int_0^{t_f} \frac{\Delta G}{G} \, dt - V \cdot \ln \frac{G(t_f)}{G(0)}}{\int_0^{t_f} \Delta I \, dt} \quad . \tag{A10}$$

The next part of the derivation is to find an expression for $X(t_f)$. To do this we solve the differential equation (A1) using the method of variation of parameters. To start we obtain the homogenous solution. We find this solution by setting the forcing function $I-I_b$ to zero and finding the exponential solution that satisfies the homogenous differential equation, namely

$$X_h = A e^{-p_2 t} \quad , \tag{A11}$$

where A is a yet to be determined coefficient. With the homogenous solution in hand, we can now use variation of parameters to find the particular solution. Our proposed particular solution is

$$X_p = e^{-p_2 t} \cdot u(t) \quad . \tag{A12}$$

We substitute the particular solution into (A1) to obtain a first order differential equation in u:

$$\dot{u} = p_3 e^{p_2 t}(I(t) - I_b), \tag{A13}$$

which can be integrated to yield u(t):

$$u = p_3 \int_0^t e^{p_2 \tau} \Delta I \, d\tau, \tag{A18}$$

where $\tau$ is a dummy variable of time. Now we have our homogenous and particular solution. Adding them together we obtain the general solution

$$X(t) = A e^{-p_2 t} + e^{-p_2 t} p_3 \int_0^t e^{p_2 \tau} \Delta I \, d\tau. \tag{A14}$$

We can now apply the boundary condition X(0)=0 to show that A=0. The final solution for X is

$$X(t) = e^{-p_2 t} p_3 \int_0^t e^{p_2 \tau} \Delta I \, d\tau. \tag{A15}$$

The expression for SI in (A10) takes the final value of X, $X(t_f)$. To this end we evaluate (A15) to obtain $X(t_f)$

$$X(t_f) = p_3 \int_0^{t_f} e^{p_2 (t - t_f)} \Delta I \, dt. \tag{A16}$$

Note we have switched from the dummy variable $\tau$ back to t. Finally, we can substitute (A16) into (A10), and solve for SI again to get the expression

$$SI = \frac{\int_0^{t_f} \frac{Ra_{meal}}{G} \, dt - V \cdot S_G \int_0^{t_f} \frac{\Delta G}{G} \, dt - V \cdot \ln \frac{G(t_f)}{G(0)}}{\int_0^{t_f} \Delta I \, dt - \int_0^{t_f} e^{p_2 (t - t_f)} \Delta I \, dt}. \tag{A17}$$

At this point, we have yet to make any approximation (with the exception of assuming that our parameters, $p_1$, $p_2$, $S_G$, and V are constant in time, as is typical), and as such our expression is exact for determining SI. However, in order to obtain an *explicit* expression for SI (i.e. an expression that can calculate SI from measured, known values only) it is necessary to make some assumptions about the only unknown, $p_2$. The function inside of the integral in the denominator of (A17) can be rewritten to be

$$\int_0^{t_f} \left(1 - e^{p_2 (t - t_f)}\right) \Delta I \, dt. \tag{A18}$$

In most cases, $\Delta I$ is small about two hours after meal ingestion. Correspondingly, for typical values of $p_2$ (i.e. 0.02) the quantity in parentheses can be shown to be almost constant for these same two hours. Thus the argument can be made that the exponential term contributes little to the integral. With this, we neglect the second term and obtain the fully explicit equation for SI

$$SI = \frac{\int_0^{t_f} \frac{Ra_{meal}}{G} \, dt - V \cdot S_G \int_0^{t_f} \frac{\Delta G}{G} \, dt - V \cdot \ln \frac{G(t_f)}{G(0)}}{\int_0^{t_f} \Delta I \, dt}. \tag{A19}$$

A second approximation further simplifies the expression; given that in healthy subjects glucose levels are nearly the same at the beginning and the end of the test, $G(t_f) \approx G(0)$ and $\ln(G(t_f)/G(0)) \approx \ln(1) = 0$. We may neglect the third term in the numerator of (A19) to obtain the final expression for $SI_{exp}$

$$SI_{\exp} = \frac{\int_0^{t_f} \frac{Ra_{meal}}{G} dt - V \cdot S_G \int_0^{t_f} \frac{\Delta G}{G} dt}{\int_0^{t_f} \Delta I \; dt} \quad . \tag{A20}$$

*C. Error Estimate of $SI_{exp}$*

Equation (A20) is the approximate value of the true value of SI expressed by (A17). It would be convenient to estimate the error incurred from the approximation. To do this we evaluate the percentage error, E, based on the formula

$$\%E = \frac{SI - SI_{\exp}}{SI} \cdot 100 \quad , \tag{A21}$$

where SI is the true value of SI and $SI_{exp}$ is approximate. We substitute in Eq. (A20) and (A17) (neglecting the third term in the numerator) and obtain the expression

$$\%E = \frac{\int_0^{t_f} e^{p_2(t-t_f)} \Delta I \; dt}{\int_0^{t_f} \Delta I \; dt} \cdot 100 \quad . \tag{A22}$$

With (A22) we can directly calculate the error made when approximating SI with $SI_{exp}$. Typically $p_2$ ranges from 0.01 to 0.10 1/min (found from optimization - not shown). We can obtain an estimate for the *upper bound* of the error by choosing a $p_2$ on the low end, say $p_2$=0.01 1/min, because a lower $p_2$ will lead to the largest error. For (A) and (B) the upper bound error was calculated with (A22) and found to be less than 20%(A) and 18%(B) for all subjects, with an average of 10%(A) and 9%(A). Upon using optimization to determine the *actual* values of $p_2$ the actual error for each subject was calculated by plugging in $p_2$ to (A22). It was found to be less than 8%(A) and 22%(B) for all subjects (only 2 of the 54 samples were above 10%) and 3%(A) and 4%(B) on average. Thus using (A22) with a low $p_2$ = 0.01 1/min tends to give a very conservative estimate of upper bound error.


## ACKNOWLEDGMENT

This work was supported by the National Science Foundation Graduate Research Fellowship Program (S.F.). Studies supported by NIH grants DK 085516 to A.B. , DK 094331 to A.B. and DK 029953 to R.B. Thank you to A. Jbaily for insightful comments on the manuscript.


## CONFLICT OF INTEREST STATEMENT

We declare no conflict of interest.

## REFERENCES


[1] C. Cobelli, C. Dalla Man, G. Toffolo, R. Basu, A. Vella, and R. Rizza, "The Oral Minimal Model Method," *Diabetes*, vol. 63, no. 4, pp. 1203–1213, 2014.

[2] R. N. Bergman, Y. Z. Ider, C. R. Bowden, and C. Cobelli, "Quantitative estimation of insulin sensitivity.," *Am. J. Physiol.*, vol. 236, no. 6, pp. E667-677, Jun. 1979.

[3] A. Saad *et al.*, "Diurnal pattern to insulin secretion and insulin action in healthy individuals.," *Diabetes*, vol. 61, no. 11, pp. 2691–2700, Nov. 2012.

[4] J. F. Brun, R. Guintrand-Hugret, C. Boegner, O. Bouix, and A. Orsetti, "Influence of short-term submaximal exercise on parameters of glucose assimilation analyzed with the minimal model.," *Metabolism.*, vol. 44, no. 7, pp. 833–840, Jul. 1995.

[5] L. Hinshaw *et al.*, "Effects of delayed gastric emptying on postprandial glucose kinetics, insulin sensitivity, and beta-cell function.," *Am. J. Physiol. Endocrinol. Metab.*, vol. 307, no. 6, Sep. 2014.

[6] R. N. Bergman, "Lilly lecture 1989. Toward physiological understanding of glucose tolerance. Minimal-model approach.," *Diabetes*, vol. 38, no. 12, pp. 1512–1527, Dec. 1989.

[7] G. M. Steil, B. Clark, S. Kanderian, and K. Rebrin, "Modeling insulin action for development of a closed-loop artificial pancreas.," *Diabetes Technol. Ther.*, vol. 7, no. 1, Feb. 2005.

[8] C. Dalla Man, A. Caumo, and C. Cobelli, "The oral glucose minimal model: estimation of insulin sensitivity from a meal test.," *IEEE Trans. Biomed. Eng.*, vol. 49, no. 5, pp. 419–429, May 2002.

[9] R. N. Bergman, L. S. Phillips, and C. Cobelli, "Physiologic evaluation of factors controlling glucose tolerance in man: measurement of insulin sensitivity and beta-cell glucose sensitivity from the response to intravenous glucose.," *J. Clin. Invest.*, vol. 68, no. 6, pp. 1456–1467, Dec. 1981.

[10] C. Dalla Man *et al.*, "Insulin sensitivity by oral glucose minimal models: validation against clamp.," *Am. J. Physiol. Endocrinol. Metab.*, vol. 289, no. 6, pp. E954-959, Dec. 2005.

[11] A. Basu, C. Dalla Man, R. Basu, G. Toffolo, C. Cobelli, and R. A. Rizza, "Effects of type 2 diabetes on insulin secretion, insulin action, glucose effectiveness, and postprandial glucose metabolism.," *Diabetes Care*, vol. 32, no. 5, pp. 866–872, May 2009.

[12] A. Caumo, R. N. Bergman, and C. Cobelli, "Insulin Sensitivity from Meal Tolerance Tests in Normal Subjects: A Minimal Model Index," *J. Clin. Endocrinol. Metab.*, vol. 85, no. 11, pp. 4396–4402, 2000.

[13] C. Dalla Man, A. Caumo, R. Basu, R. Rizza, G. Toffolo, and C. Cobelli, "Minimal model estimation of glucose absorption and insulin sensitivity from oral test: validation with a tracer method.," *Am. J. Physiol. Endocrinol. Metab.*, vol. 287, no. 4, pp. E637-643, Oct. 2004.

[14] A. Vella and R. A. Rizza, "Application of Isotopic Techniques Using Constant Specific Activity or Enrichment to the Study of Carbohydrate Metabolism," *Diabetes*, vol. 58, no. 10, pp. 2168–2174, Oct. 2009.

[15] R. Basu *et al.*, "Use of a novel triple-tracer approach to assess postprandial glucose metabolism.," *Am. J. Physiol. Endocrinol. Metab.*, vol. 284, no. 1, Jan. 2003.

[16] G. Toffolo, R. Basu, C. Dalla Man, R. Rizza, and C. Cobelli, "Assessment of postprandial glucose metabolism: conventional dual- vs. triple-tracer method.," *Am. J. Physiol. Endocrinol. Metab.*, vol. 291, no. 4, pp. E800-806, Oct. 2006.

[17] R. STEELE, "Influences of glucose loading and of injected insulin on hepatic glucose output.," *Ann. N. Y. Acad. Sci.*, vol. 82, pp. 420–430, Sep. 1959.

[18] R. A. Rizza, G. Toffolo, and C. Cobelli, "Accurate Measurement of Postprandial Glucose Turnover: Why Is It Difficult and How Can It Be Done (Relatively) Simply?," *Diabetes*, vol. 65, no. 5, pp. 1133–1145, 2016.

[19] R. Basu *et al.*, "Effects of age and sex on postprandial glucose metabolism: differences in glucose turnover, insulin secretion, insulin action, and hepatic insulin extraction.," *Diabetes*, vol. 55, no. 7, pp. 2001–2014, Jul. 2006.

[20] L. Hinshaw *et al.*, "Diurnal pattern of insulin action in type 1 diabetes: implications for a closed-loop system.," *Diabetes*, vol. 62, no. 7, pp. 2223–2229, Jul. 2013.

[21] G. D. Nicolao, G. Sparacino, and C. Cobelli, "Nonparametric input estimation in physiological systems: Problems, methods, and case studies," *Automatica*, vol. 33, no. 5, pp. 851–870, 1997.

[22] G. Sparacino, G. Pillonetto, M. Capello, G. De Nicolao, and C. Cobelli, "WINSTODEC: a stochastic deconvolution interactive program for physiological and pharmacokinetic systems.," *Comput. Methods Programs Biomed.*, vol. 67, no. 1, Jan. 2002.

[23] M. Schiavon, C. Dalla Man, Y. C. Kudva, A. Basu, and C. Cobelli, "Quantitative estimation of insulin sensitivity in type 1 diabetic subjects wearing a sensor-augmented insulin pump.," *Diabetes Care*, vol. 37, no. 5, pp. 1216–1223, May 2014.

# Appendix C

# Mathematical Derivations

## C.1 Analytical Solution to Spherical Diffusion Equation

This Appendix provides an analytical solution to the insulin absorption problem that was solved in Chapter 2. Though this analytical solution was not employed in the model derivation, it is a good academic exercise and hence is included here. Note that the nomenclature in this appendix is different than that employed in the body of the dissertation.

### C.1.1 Problem Definition

Insulin is injected into the subcutaneous tissue at a prepared insulin concentration $c_{pre}$ and then spreads according to diffusion coefficient $D_s$ and slowly absorbs into the bloodstream dependent on the rate constant $k$ . Mathematically the concentration of insulin in the subcutaneous tissue $c$ is described by

$$\frac{\partial c}{\partial t} = D_b \nabla^2 c - kc \tag{C.1}$$

subject to

$$c(0, r) = c_{pre}\ H(a - r) \tag{C.2}$$

$$c \to 0 \text{ as } r \to \infty \tag{C.3}$$

$$\frac{\partial c}{\partial r} \to 0 \text{ as } r \to \infty \tag{C.4}$$

Where the initial concentration is a top hat profile with magnitude $c_{pre}$ and $a$ is the dose ($d$) radius found from the relationship $d = c_{pre} 4/3\pi a^3$.

Though in other chapters of this dissertation is was shown that the insulin absorption rate is not dependent on the spreading rate of insulin in the subcutaneous space, we have still developed an analytical solution to the spherical heat equation as an academic exercise. This solution was confirmed with a numerical solution to the same equation.

### C.1.2 Mathematical Formulation

The spherical diffusion equation with a sink term in an infinite domain, with constant diffusivity $\alpha$, can be written as

$$\frac{\partial u}{\partial t} + ku = \alpha^2 \nabla^2 u. \tag{C.5}$$

In an infinite domain the boundary condition on the solution $u$ is

$$u \to 0 \text{ as } r \to \infty \tag{C.6}$$

$$u = 1 \quad \text{for} \quad r \in \left[0, a\right] \quad \text{and} \quad 0 \quad \text{elsewhere.} \tag{C.7}$$

### C.1.3 Transform Method

We will solve C.5 using a Hankel transform, modified for spherical symmetry. The spherical Hankel transform is defined as follows

$$\tilde{f}\{s\} = \mathcal{H}\{f(r)\} \equiv \int_0^\infty r^2 f(r) \mathcal{J}_o(sr) dr \tag{C.8}$$

$$f\{r\} = \mathcal{H}^{-1}\{\tilde{f}(s)\} \equiv \int_0^\infty s^2 \tilde{f}(s) \mathcal{J}_o(sr) ds. \tag{C.9}$$

Where $\mathcal{J}_o$ is the zeroth order spherical bessel function, i.e. the *sinc* function.
Next, by assuming spherical symmetry of C.5, the laplacian operator simplfies to

$$\nabla^2 = \frac{1}{r^2} \frac{\partial}{\partial r} r^2 \frac{\partial}{\partial r}. \tag{C.10}$$

It can be shown (see appendix for details) that by applying C.8 to C.10 we get

$$\mathcal{H}\{\nabla^2 u\} = -s^2 \tilde{u} \tag{C.11}$$

By applying this transformation to C.5 we reduce our partial differential equation to an ordinary differential equation in time.

$$\frac{\partial \tilde{u}}{\partial t} + (k + \alpha^2 s^2)\tilde{u} = 0 \tag{C.12}$$

Which is easily solved by the exponential function

$$\tilde{u}(s,t) = \tilde{A}(s) e^{-(k+\alpha^2 s^2)t} \tag{C.13}$$

To find $\tilde{A}(s)$ we need to calculate its transform

$$\tilde{A}\{s\} = \int_0^\infty r^2 A(r) \mathcal{J}_o(sr) dr \tag{C.14}$$

Where $A(r) = H(a-r)$ is the Heaviside step function that is 1 at $r < a$ and 0 for $r > a$, consistent with the initial condition C.7. Plugging in and using integration by parts, our expression for $\tilde{A}(s)$ becomes

$$\tilde{A}\{s\} = \int_0^\infty r^2 H(a-r) \mathcal{J}_o(sr) dr = \frac{1}{s} \int_0^a r sin(sr) dr \tag{C.15}$$

$$= \frac{1}{s}\Big[\frac{-rcos(sr)}{s}\Big|_0^a + \frac{1}{s}\int_0^a cos(sr) dr\Big] \tag{C.16}$$

$$= \frac{1}{s^2}\Big[ - acos(sa) + \frac{sin(sa)}{s}\Big]. \tag{C.17}$$

Thus our solution in frequency space is

$$\tilde{u}(s,t) = \frac{1}{s^2}\Big[ - acos(sa) + \frac{sin(sa)}{s}\Big] e^{-(k+\alpha^2 s^2)t}. \tag{C.18}$$

We may convert back to physical space through the inverse Hankel Transform C.9

$$u(r,t) = \int_0^\infty \Big[ - acos(sa) + \frac{sin(sa)}{s}\Big] e^{-(k+\alpha^2 s^2)t} \mathcal{J}_o(sr) ds. \tag{C.19}$$

This integral can be solved numerically.

### Solution Validation

To validate our analytical solution, we will compare it to the numerical solution using a forward time centered space (FTCS) numerical scheme. This numerical scheme is simply derived and is applied to C.5 to obtain

$$u_i^{n+1} = u_i^n + \Delta t\Big[\frac{\alpha^2}{(\Delta r)^2}\big(u_{i+1}^n - 2u_i^n + u_{i-1}^n\big) + \frac{2\alpha^2}{\Delta r}\frac{u_{i+1}^n - u_i^n}{r_i} - cu_i^n\Big]. \tag{C.20}$$

The index $n$ is the index for time, and the index $i$ is the index for space (radial coordinate).

Using a stable timestep that satisfies the CFL condition, we simulate the diffusion process subject to the boundary conditions defined in C.6 and C.7 using C.20. This numerical solution is compared to the analytical solution in Figure C.1 and C.2.

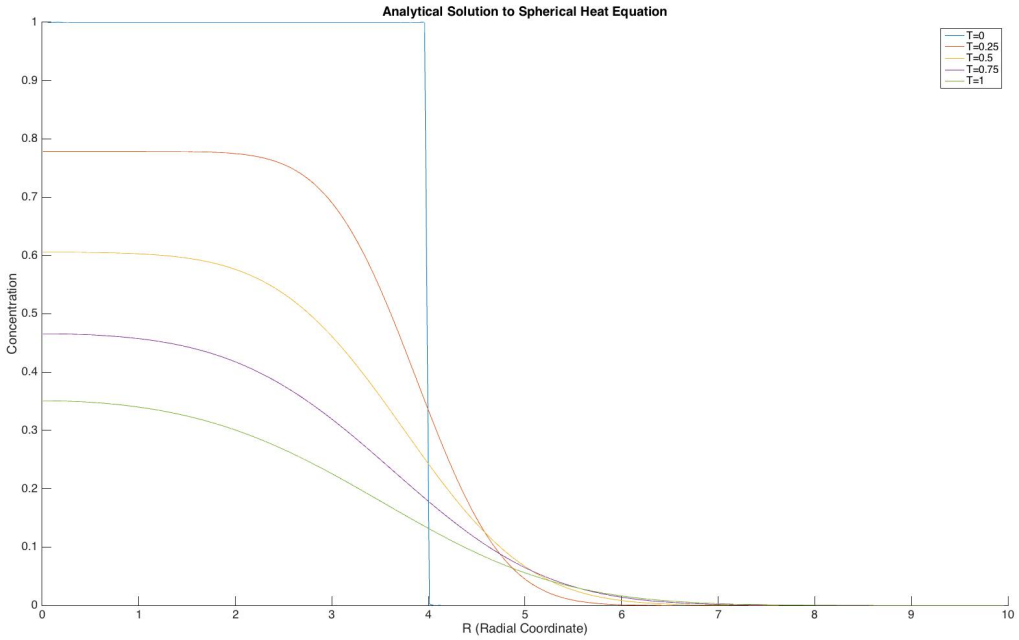


Figure C.1: Analytical solution to spherical diffusion equation.

### C.1.4 Transform Details

Our goal is to show that

$$\mathcal{H}\{\nabla^2 y\} = -s^2 \tilde{y}. \tag{C.21}$$

We start by applying the spherical Hankel transform C.8 to the spherically symmetric laplace operator C.10 and integrating by parts

$$\begin{aligned}
\mathcal{H}\{\nabla^2 y\} &= \int_0^\infty r^2 \frac{1}{r^2}\frac{\partial}{\partial r} r^2 \frac{\partial y}{\partial r} \mathcal{J}_o(sr) dr && \text{(C.22)}\\
&= \int_0^\infty \frac{\partial}{\partial r} r^2 \frac{\partial y}{\partial r} \mathcal{J}_o(sr) dr && \text{(C.23)}\\
&= \mathcal{J}_o(sr) r^2 \frac{\partial y}{\partial r}\Big|_0^\infty - \int_0^\infty r^2 \frac{\partial y}{\partial r}\frac{\partial}{\partial r}\mathcal{J}_o(sr) dr && \text{(C.24)}\\
&= 0 - \left[ y r^2 \frac{\partial}{\partial r}\mathcal{J}_o(sr)\Big|_0^\infty - \int_0^\infty y\Big(2r\frac{\partial}{\partial r}\mathcal{J}_o(sr) + r^2\frac{\partial^2}{\partial r^2}\mathcal{J}_o(sr)\Big) dr\right] && \text{(C.25)}\\
&= -0 + \int_0^\infty y\Big(2r\frac{\partial}{\partial r}\mathcal{J}_o(sr) + r^2\frac{\partial^2}{\partial r^2}\mathcal{J}_o(sr)\Big) dr\Big] && \text{(C.26)}
\end{aligned}$$

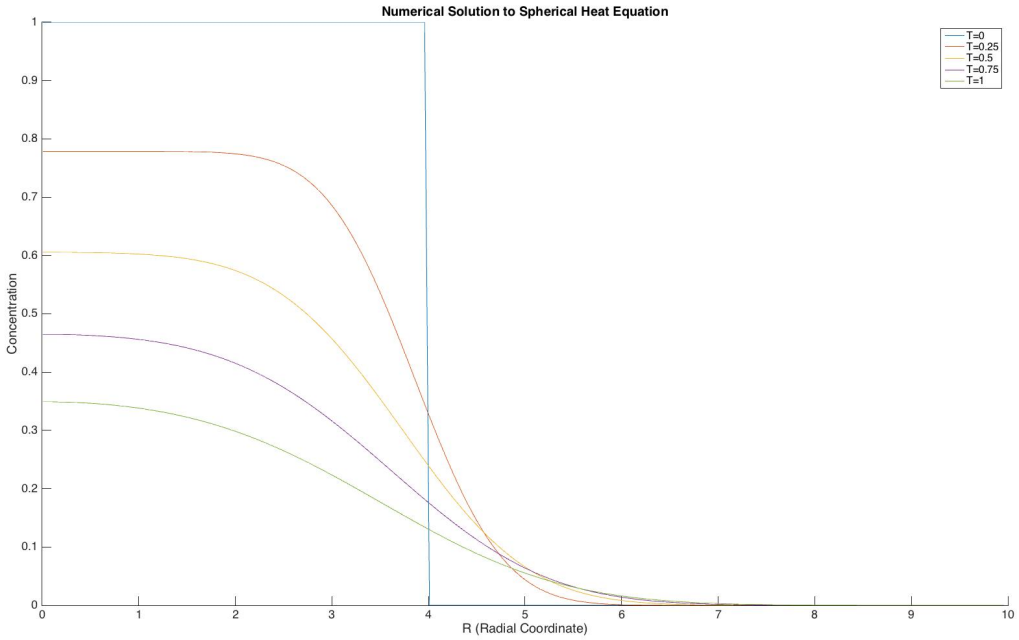


Figure C.2: Numerical solution to spherical diffusion equation.

and by using separation of variables on C.5 one obtains the zeroth order spherical bessel equation

$$r^2\frac{d^2R(sr)}{dr^2} + 2r\frac{dR(sr)}{dr} + s^2r^2R(sr) = 0 \tag{C.27}$$

which is exactly satisfied by the zeroth order spherical bessel function $R(sr) = \mathcal{J}_o(sr)$ yielding the relation

$$r^2\frac{d^2\mathcal{J}_o(sr)}{dr^2} + 2r\frac{d\mathcal{J}_o(sr)}{dr} = -s^2r^2\mathcal{J}_o(sr) \tag{C.28}$$

and thus C.26 can be rewritten as

$$\mathcal{H}\{\nabla^2 y\} = \int_0^\infty y\Big(2r\frac{\partial}{\partial r}\mathcal{J}_o(sr) + r^2\frac{\partial^2}{\partial r^2}\mathcal{J}_o(sr)\Big)dr \tag{C.29}$$

$$\mathcal{H}\{\nabla^2 y\} = \int_0^\infty y\Big(-s^2r^2\mathcal{J}_o(sr)\Big)dr \tag{C.30}$$

$$\mathcal{H}\{\nabla^2 y\} = -s^2\int_0^\infty yr^2\mathcal{J}_o(sr)dr \tag{C.31}$$

$$\mathcal{H}\{\nabla^2 y\} = -s^2\tilde{y}. \tag{C.32}$$

Note that we have assumed that $y \to 0$ with $1/r^2$ as $r \to \infty$, which allowed us to eliminate the boundary terms in integration by parts. This is a reasonable assumption because of the spherical nature of diffusion.

Figure C.3: The author (center) and his wonderful labmates, AJ (left) and Claire (right), during their walk to UC Berkeley campus on a brisk morning.